

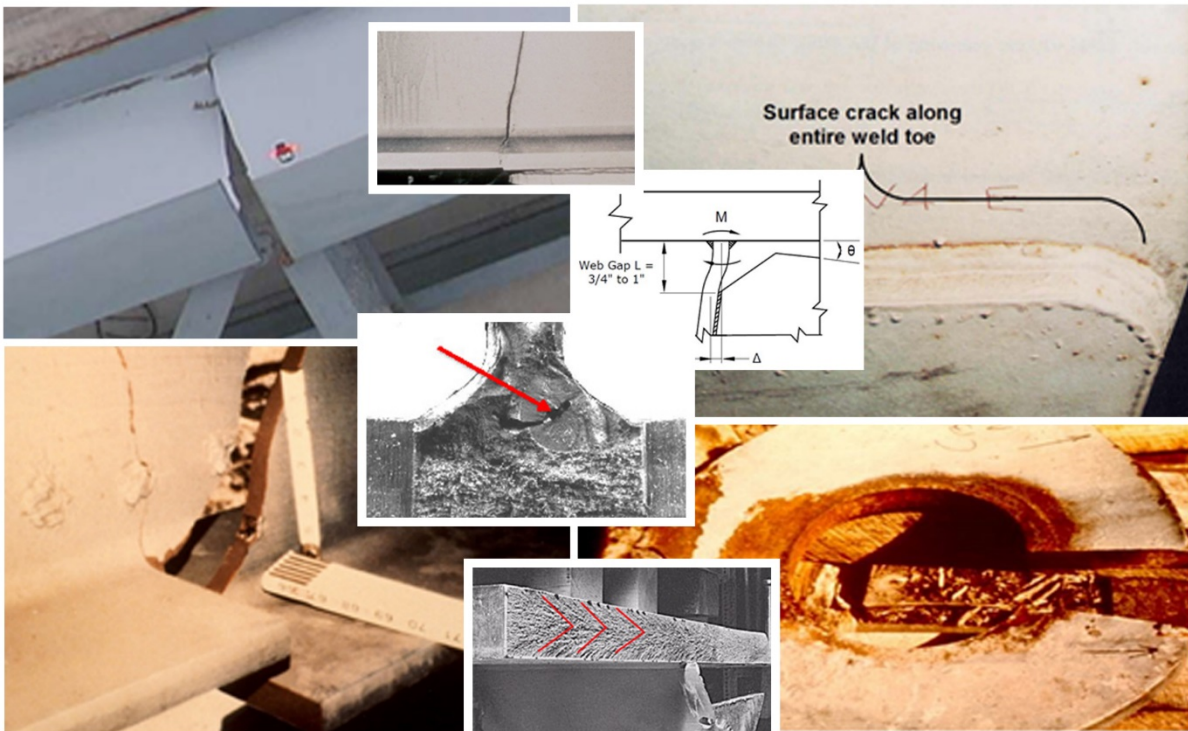


U.S. Department of Transportation
Federal Highway Administration

Publication No. FHWA-NHI-16-016
December 2016

NHI Course No. 130122

Design and Evaluation of Steel Bridges for Fatigue and Fracture



REFERENCE MANUAL



FOREWORD

This Manual covers a full range of topics related to fatigue and fracture in steel bridges, including analysis, design, evaluation, repair, and retrofit. The information presented is intended to expound and complement the same topics covered in AASHTO's LRFD Bridge Design Specifications and Manual for Bridge Evaluation. The hard and competent work of the Michael Baker International and the authors, Francesco M. Russo, Ph.D., P.E., Dennis R. Mertz, Ph.D., P.E., Karl H. Frank, Ph.D., P.E., Kenneth E. Wilson, P.E., S.E., in producing this Manual is gratefully acknowledged.

The contributions and constructive review comments received during the preparation of the handbook from many bridge engineering professionals across the country are very much appreciated. In particular, I would like to recognize the contributions of Matt Farrar of the Idaho Transportation Department, Greg Perfetti and David Snoke of the North Carolina Department of Transportation and John Hastings of the Tennessee Department of Transportation.

Finally, I would like to single out and again recognize Dennis Mertz who passed away prior to the publication of this Manual. Dennis was a colleague, mentor and friend to many across the nation in the bridge design and construction industry. His knowledge, counsel, industry and wit will be missed.

A handwritten signature in black ink, appearing to read 'J. Hartmann', with a long horizontal flourish extending to the right.

Joseph L. Hartmann, Ph.D., P.E.
Director, Office of Bridges and Structures

Notice

This document is disseminated under the sponsorship of the U.S. Department of Transportation (USDOT) in the interest of information exchange. The U.S. Government assumes no liability for the use of the information contained in this document.

The U.S. Government does not endorse products or manufacturers. Trademarks or manufacturers' names appear in this report only because they are considered essential to the objective of the document.

Quality Assurance Statement

The Federal Highway Administration (FHWA) provides high-quality information to serve Government, industry, and the public in a manner that promotes public understanding. Standards and policies are used to ensure and maximize the quality, objectivity, utility, and integrity of its information. FHWA periodically reviews quality issues and adjusts its programs and processes to ensure continuous quality improvement.

Technical Report Documentation Page

1. Report No. FHWA-NHI-16-016	2. Government Accession No.	3. Recipient's Catalog No. FHWA-NHI-16-016		
4. Title and Subtitle Design and Evaluation of Steel Bridges for Fatigue and Fracture – Reference Manual		5. Report Date December 2016		
		6. Performing Organization Code FHWA/DTS-NHI-1		
7. Author (s) Francesco M. Russo, Ph.D., P.E., Dennis R. Mertz, Ph.D., P.E., Karl H. Frank, Ph.D., P.E., Kenneth E. Wilson, P.E., S.E.		8. Performing Organization Report No. MBRM143222		
		9. Performing Organization Name and Address Michael Baker International Airside Business Park, 100 Airside Drive Moon Township, PA 15108		10. Work Unit No. (TRAIS)
12. Sponsoring Agency Name and Address Federal Highway Administration National Highway Institute (HNHI-10) 1310 North Courthouse Road Arlington, VA 22201		11. Contract or Grant No. DTFH61-11-D-00046		
		13. Type of Report and Period Covered Final Submission October 2014 – December 2016		14. Sponsoring Agency Code FHWA
15. Supplementary Notes FHWA Contracting Officer's Representative: Melonie Barrington, P.E., PMP FHWA Technical Manager: Brian M. Kozy, Ph.D., P.E. Michael Baker Principal Investigator: Mary P. Rosick, P.E. Michael Baker Project Manager: Kenneth E. Wilson, P.E., S.E., PMP				
16. Abstract This Manual explains the relevant issues related to fatigue and fracture in steel bridges, including analysis, design, evaluation, repair, and retrofit. Chapter 1 provides an introduction to fatigue and fracture, as well as an introduction to the Reference Manual. Chapter 2 begins with a discussion of cracking in steel structures, including crack behavior, sources of discontinuities in steel structures, the nature of stresses affecting fatigue and fracture, and brittle and ductile behavior in steel. Chapter 3 provides the basics of fracture mechanics, covering such topics as fracture control, evaluation of fatigue cracking, and fracture mechanics as a quantitative tool. Chapter 4 describes fatigue behavior, including discontinuities and stress concentrations, the influence of production and fabrication on fatigue, testing as the basis for design limits, and environmental effects. Chapter 5 describes analysis for fatigue, and it provides information for both approximate and refined analysis methods, including local-stress analysis. Chapter 6 addresses the fatigue design approach as presented in the <i>AASHTO LRFD Bridge Design Specifications</i> , and it explains the fundamental fatigue limit state equation, the various AASHTO fatigue detail categories, the differences between finite life and infinite life, and the computation of fatigue stress range and factored nominal resistance, including a step-by-step design example for fatigue. Chapter 7 describes fracture control, including design, fabrication, and inspection, and it covers such topics as redundancy, constraint-induced fracture, and the Total Fracture Control Plan. Chapter 8 addresses the AASHTO fatigue-evaluation approach, including remaining fatigue life evaluation, estimates of fatigue life based on the <i>AASHTO Manual for Bridge Evaluation</i> , and remaining fatigue life for “negative remaining life” bridge details. Chapter 9 describes assessment, repair, and retrofit of structures, and it provides a description of several common fatigue details, general repair and retrofit strategies, as well as constraint-induced fracture, over-height vehicle collisions, and fitness-for-service analysis. Finally, Chapter 10 covers non-welded components such as built-up members, bolts and rods, and reinforcement of concrete. In addition, Appendix A describes fatigue calibration based on the SHRP2 Project R19B.				
17. Key Words Fatigue, Fracture, Cracking, Fracture Control Plan, Loads, Resistance, Analysis, Design, Evaluation, Retrofit, Repair, Stress Range, Residual Stress, Cycles, Brittle, Ductile, Toughness, Discontinuity, Weld, Fatigue Details, Fatigue Life, Finite Life, Infinite Life		18. Distribution Statement This report is available to the public from the NHI Bookstore at http://www.nhi.fhwa.dot.gov/training/nhistore.aspx		
19. Security Classif. (of this report) Unclassified	20. Security Classif. (of this page) Unclassified	21. No. of Pages 310	22. Price	

SI* (MODERN METRIC) CONVERSION FACTORS

APPROXIMATE CONVERSIONS TO SI UNITS

Symbol	When You Know	Multiply By	To Find	Symbol
LENGTH				
in	inches	25.4	millimeters	mm
ft	feet	0.305	meters	m
yd	yards	0.914	meters	m
mi	miles	1.61	kilometers	km
AREA				
in ²	square inches	645.2	square millimeters	mm ²
ft ²	square feet	0.093	square meters	m ²
yd ²	square yard	0.836	square meters	m ²
ac	acres	0.405	hectares	ha
mi ²	square miles	2.59	square kilometers	km ²
VOLUME				
fl oz	fluid ounces	29.57	milliliters	mL
gal	gallons	3.785	liters	L
ft ³	cubic feet	0.028	cubic meters	m ³
yd ³	cubic yards	0.765	cubic meters	m ³
NOTE: volumes greater than 1000 L shall be shown in m ³				
MASS				
oz	ounces	28.35	grams	g
lb	pounds	0.454	kilograms	kg
T	short tons (2000 lb)	0.907	megagrams (or "metric ton")	Mg (or "t")
TEMPERATURE (exact degrees)				
°F	Fahrenheit	5 (F-32)/9 or (F-32)/1.8	Celsius	°C
ILLUMINATION				
fc	foot-candles	10.76	lux	lx
fl	foot-Lamberts	3.426	candela/m ²	cd/m ²
FORCE and PRESSURE or STRESS				
lbf	poundforce	4.45	newtons	N
lbf/in ²	poundforce per square inch	6.89	kilopascals	kPa

APPROXIMATE CONVERSIONS FROM SI UNITS

Symbol	When You Know	Multiply By	To Find	Symbol
LENGTH				
mm	millimeters	0.039	inches	in
m	meters	3.28	feet	ft
m	meters	1.09	yards	yd
km	kilometers	0.621	miles	mi
AREA				
mm ²	square millimeters	0.0016	square inches	in ²
m ²	square meters	10.764	square feet	ft ²
m ²	square meters	1.195	square yards	yd ²
ha	hectares	2.47	acres	ac
km ²	square kilometers	0.386	square miles	mi ²
VOLUME				
mL	milliliters	0.034	fluid ounces	fl oz
L	liters	0.264	gallons	gal
m ³	cubic meters	35.314	cubic feet	ft ³
m ³	cubic meters	1.307	cubic yards	yd ³
MASS				
g	grams	0.035	ounces	oz
kg	kilograms	2.202	pounds	lb
Mg (or "t")	megagrams (or "metric ton")	1.103	short tons (2000 lb)	T
TEMPERATURE (exact degrees)				
°C	Celsius	1.8C+32	Fahrenheit	°F
ILLUMINATION				
lx	lux	0.0929	foot-candles	fc
cd/m ²	candela/m ²	0.2919	foot-Lamberts	fl
FORCE and PRESSURE or STRESS				
N	newtons	0.225	poundforce	lbf
kPa	kilopascals	0.145	poundforce per square inch	lbf/in ²

* SI is the symbol for the International System of Units. Appropriate rounding should be made to comply with Section 4 of ASTM E380. (Revised March 2003)

Table of Contents

Chapter 1	Background and Organization of the Manual	1.1
Section 1.1	Introduction	1.1
1.1.1	Historical Perspective	1.1
1.1.2	Evolution of Fatigue and Fracture Design, Evaluation, and Inspection Approaches	1.4
Section 1.2	Scope of Reference Manual and Presentation of Major Themes	1.13
1.2.1	Physical Phenomena of Cracking	1.14
1.2.2	Fatigue Stress	1.14
1.2.3	Fatigue Resistance	1.15
1.2.4	Fatigue and Fracture Control	1.15
1.2.5	Retrofit Strategies	1.16
Chapter 2	Cracking in Steel Structures	2.1
Section 2.1	Crack Behavior	2.1
2.1.1	Necessary Conditions	2.1
2.1.2	Crack-growth Regimes	2.1
Section 2.2	Sources of Discontinuities in Steel Structures	2.4
2.2.1	Production	2.4
2.2.2	Fabrication	2.4
Section 2.3	Stress	2.8
2.3.1	Sustained Stress	2.9
2.3.2	Cyclical Stress	2.11
2.3.3	Stress Concentrations from Details	2.12
Section 2.4	Material Behavior	2.13
2.4.1	Brittle versus Ductile Behavior	2.13
2.4.2	Effects of Temperature and Strain Rates	2.17
Chapter 3	Theory	3.1
Section 3.1	General	3.1
Section 3.2	Accounting for a Crack	3.1

Section 3.3 Principles of Fracture Control	3.5
3.3.1 Material Toughness	3.5
3.3.2 Effect of Critical Crack Size upon Inspection.....	3.7
3.3.3 Assurance through CVN Toughness Requirements.....	3.8
Section 3.4 Paris' Law and Miner's Rule	3.10
Section 3.5 Fracture Mechanics as a Quantitative Tool.....	3.12
Chapter 4 Fatigue Behavior	4.1
Section 4.1 The Influence of Production and Fabrication.....	4.1
4.1.1 Materials and Processing.....	4.1
4.1.2 Discontinuities at Welded Joints	4.3
4.1.3 Weld Residual Stresses.....	4.6
4.1.4 Bolting and Riveting.....	4.12
4.1.5 Cold Bending	4.13
4.1.6 Hot Bending.....	4.14
4.1.7 Heat Straightening Repairs.....	4.15
Section 4.2 Stress Parameters Influencing Fatigue	4.16
4.2.1 Effect of Minimum Stress	4.17
4.2.2 Effect of Steel Yield Strength	4.18
4.2.3 Consideration of Variable Amplitude Fatigue Loading.....	4.19
Section 4.3 Testing as the Basis for Design Limits.....	4.23
4.3.1 Development of Design Limits for Finite Life	4.23
4.3.2 Development of Design Limits for Infinite Life	4.27
4.3.3 Testing to Establish the Fatigue Resistance of Special Elements	4.29
Section 4.4 Environmental Effects.....	4.29
4.4.1 Weathering Steel	4.30
4.4.2 Corrosion Effects on Fatigue Life	4.31
Section 4.5 Summary	4.35
Chapter 5 Analysis for Fatigue	5.1
Section 5.1 General	5.1
Section 5.2 Load-Induced vs. Distortion-Induced Fatigue.....	5.1

Section 5.3 Global Analysis	5.2
5.3.1 Approximate Analysis	5.2
5.3.2 Refined Analysis	5.9
Section 5.4 Fatigue Stress Analysis	5.10
5.4.1 Nominal-Stress Approach	5.10
5.4.2 Local-Stress Approach.....	5.11
5.4.3 Fracture-Mechanics Approach	5.17
Chapter 6 AASHTO Fatigue Design Approach	6.1
Section 6.1 General.....	6.1
6.1.1 The Fatigue Limit State.....	6.1
Section 6.2 Classification of Fatigue	6.3
Section 6.3 Load-Induced Fatigue	6.5
6.3.1 General Limit State	6.5
6.3.2 Applicability.....	6.15
6.3.3 Infinite Life – The Fatigue I Load Combination	6.15
6.3.4 Finite Life – The Fatigue II Load Combination.....	6.18
6.3.5 Calibration of the Fatigue Limit State	6.22
6.3.6 Special Details and Provisions for Other Structure Types.....	6.24
Section 6.4 Distortion-Induced Fatigue.....	6.46
Section 6.5 Step-by-Step Application of LRFD Fatigue Design.....	6.50
6.5.1 Determine Locations Requiring Fatigue Limit State Verification (Step 1)	6.50
6.5.2 Compute Force Effects (Step 2).....	6.50
6.5.3 Calculate Stress Ranges at Fatigue Details (Step 3)	6.54
6.5.4 Calculate Fatigue Resistance (Step 4).....	6.56
Section 6.6 Example Problem of Fatigue Design.....	6.57
6.6.1 Determine Locations Requiring Fatigue Limit State Verification (Step 1)	6.58
6.6.2 Compute Force Effects (Step 2).....	6.58
6.6.3 Calculate Stress Ranges at Fatigue Details (Step 3)	6.59
6.6.4 Calculate Fatigue Resistance (Step 4).....	6.59
Chapter 7 Fracture Control	7.1
Section 7.1 Historical Development of Fracture Control Practices.....	7.1

Section 7.2	Fracture Control by Design	7.4
7.2.1	Charpy V-Notch Requirements for Primary Members	7.5
7.2.2	Fracture Critical Members.....	7.7
7.2.3	Selection of Materials.....	7.11
7.2.4	Detailing to Avoid Constraint.....	7.15
Section 7.3	Fracture Control By Enhanced Fabrication.....	7.29
7.3.1	Fabrication Controls.....	7.31
Section 7.4	Fracture Control By In-Service Inspection	7.32
Chapter 8	AASHTO Fatigue-Evaluation Approach	8.1
Section 8.1	Identifying the Nature of Cracking	8.1
8.1.1	Load-Induced Fatigue.....	8.1
8.1.2	Distortion-Induced Fatigue.....	8.2
Section 8.2	Remaining Fatigue Life Evaluation	8.2
8.2.1	Estimating the Stress Range.....	8.3
Section 8.3	Estimating Fatigue Life by the MBE.....	8.6
8.3.1	Infinite-Life Check.....	8.6
8.3.2	Finite Life.....	8.7
8.3.3	Example	8.9
Section 8.4	Remaining Fatigue Life for “Negative Remaining Life” Bridge Details	
	8.10	
8.4.1	General.....	8.10
8.4.2	Fatigue Serviceability Index, Q	8.10
8.4.3	Strategies to Increase the Fatigue Serviceability Index.....	8.12
Chapter 9	Assessment, Repair, and Retrofit of Structures.....	9.1
Section 9.1	Common Fatigue Details	9.1
9.1.1	Web Gaps Associated with Out-of-Plane Bending	9.2
9.1.2	Fatigue Considerations for Welds	9.4
9.1.3	Welded Cover Plates	9.9
Section 9.2	Repair Strategies.....	9.12
9.2.1	Understand the Source of Cracking	9.12
9.2.2	Design Repair Detail.....	9.14

9.2.3	Validate Repair Detail	9.16
Section 9.3	Special Topics	9.17
9.3.1	Constraint-Induced Fracture	9.17
9.3.2	Over-Height Vehicle Collisions.....	9.17
9.3.3	Fitness-for-Service Analysis.....	9.19
Chapter 10	Non-Welded Components	10.1
Section 10.1	Built-Up Members	10.1
10.1.1	Behavior of Riveted and Bolted Connections	10.1
10.1.2	Bolted Connections with Bolts Loaded in Shear	10.2
10.1.3	Bolted Connections with Bolts Loaded in Tension.....	10.5
10.1.4	Riveted Members and Connections	10.7
Section 10.2	Anchor Rods	10.10
10.2.1	Fatigue Considerations for Anchor Rods.....	10.10
10.2.2	Stress Corrosion Cracking / Hydrogen Embrittlement	10.13
Section 10.3	Reinforcement of Concrete.....	10.14
10.3.1	Reinforcing Bars	10.15
10.3.2	Prestressing Strands.....	10.17
10.3.3	Post-Tensioning Tendons and Anchorages.....	10.20
10.3.4	Stay Cables	10.21
Appendix A	A.1	
Section A.1	General	A.1
Section A.2	Fatigue Limit State Calibration	A.2
Section A.3	Components of the Fatigue Limit State	A.2
A.3.1	Multiple Presence	A.2
A.3.2	Cycle Counting / Cycles Per Passage.....	A.3
A.3.3	Selection of Fatigue Load Factors.....	A.10
Section A.4	Calibration of the Fatigue Limit State	A.13
Glossary	G.1	
References	R.1	
Figure and Table Credits	F.1	

This page intentionally left blank

CHAPTER 1 BACKGROUND AND ORGANIZATION OF THE MANUAL

SECTION 1.1 INTRODUCTION

This Reference Manual, along with an accompanying training course, is a primary component of the Design and Evaluation of Steel Bridges for Fatigue and Fracture training program. Its objective is to provide engineers with the necessary technical information to effectively design and evaluate steel highway bridge structures for the limit states of fatigue and fracture to improve safety, economy, and longevity of infrastructures. An additional objective is to educate engineers about the history, scope, methodologies, assumptions, limitations, and application of the American Association of State Highway and Transportation Officials (AASHTO) Specifications addressing fatigue and fracture.

The learning outcomes for this Manual and training program are expected to enable students to:

- Explain the fundamentals of fatigue and fracture on steel highway structures
- Identify the various analysis methods for determining fatigue and fracture on steel highway structures
- Explain the various AASHTO methodologies as it pertains to fatigue and fracture design
- Identify the AASHTO methodology for fatigue and fracture evaluation
- Describe the various strategies for repair and retrofit of steel highway structures

This Manual is intended to be used by State DOT bridge and structures engineers and practitioners responsible for steel bridge design and evaluation, as well as engineers at all levels including designers, consultants, reviewers, maintenance and management engineers, and load raters.

1.1.1 Historical Perspective

Some of the first reports of fatigue and fracture failures in metal structures are traced back to the 1800's (Shank, 1954). With the onset of the industrial age and more widespread use of wrought iron and early steels in manufacturing, industrial, and transportation industries, steel began to be used in tension members with repeated loads. Examples of failures were reported in elements such as mine hoists, railroad bridge members, railroad car axles, as well as pressure vessels and storage tanks. Observations of cracks in truss hangers and stringer end connection angles led to investigations between the 1930's and 1960's. The earliest welded bridge fractures were reported in Germany, Belgium, and France in the 1920's and 1930's in welded vierendeel truss bridges (Barsom and Rolfe, 1999). These early fractures led to prohibitions against welding to the tension flange of girders (which we now know from experience is the cause of secondary distortion-induced fatigue cracking in structures from that era). It was not until the late 1960's that the beginnings of the modern approach to fatigue and fracture design and evaluation of bridges began to take form.

Figure 1.1.1-1 provides a chronological summary of the important developments presented in this chapter. Beginning with 1900 and continuing to the present day, thirteen key events and developments related to fatigue and fracture in steel bridges are identified on a timeline. These events include significant research findings, development of design provisions, and bridge failures, and they have shaped the current practice of design, evaluation, and inspection of steel bridges for fatigue and fracture. These key events are described in greater detail in subsequent sections of this chapter.

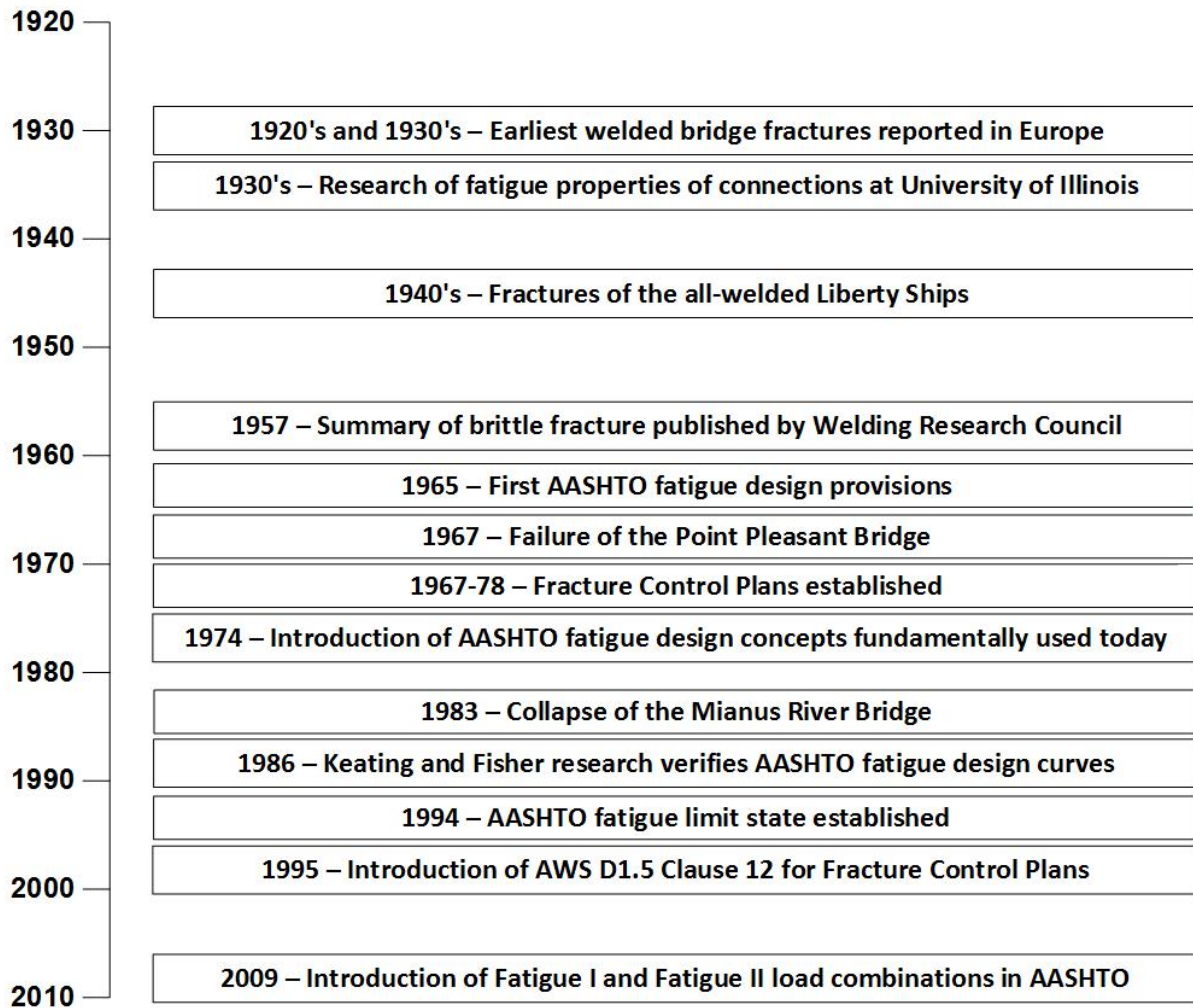


Figure 1.1.1-1 Chronological summary of important developments related to fatigue and fracture of steel bridges.

1.1.1.1 Basic Description of Fatigue and Fracture

The modern view of fatigue of welded structures is that fatigue is the process of crack extension under the application of repeated loading sufficiently large (above a threshold, which is explained later) with initiation assumed present due to some discontinuity introduced in the manufacturing of the base metal or as a consequence of fabrication. The process of fatigue crack

extension is labeled as sub critical crack growth since the process consists of incremental crack extension with each cycle of loading. The meaning of “sub critical” is that the crack can be tolerated in the member without unstable propagation and fracture.

Fracture is characterized by unstable crack extension which occurs when the energy required to extend the crack is exceeded by the energy released by an incremental extension of the crack. Fracture is the rupture in tension or rapid extension of a discontinuity (which could be a fatigue crack), leading to gross deformation, loss of function or serviceability, or complete separation of the component. The crack extends over time in a stable manner due to fatigue until it reaches its critical size, and fracture becomes the end event of a fatigue crack. This process is shown schematically in Figure 1.1.1.1-1.

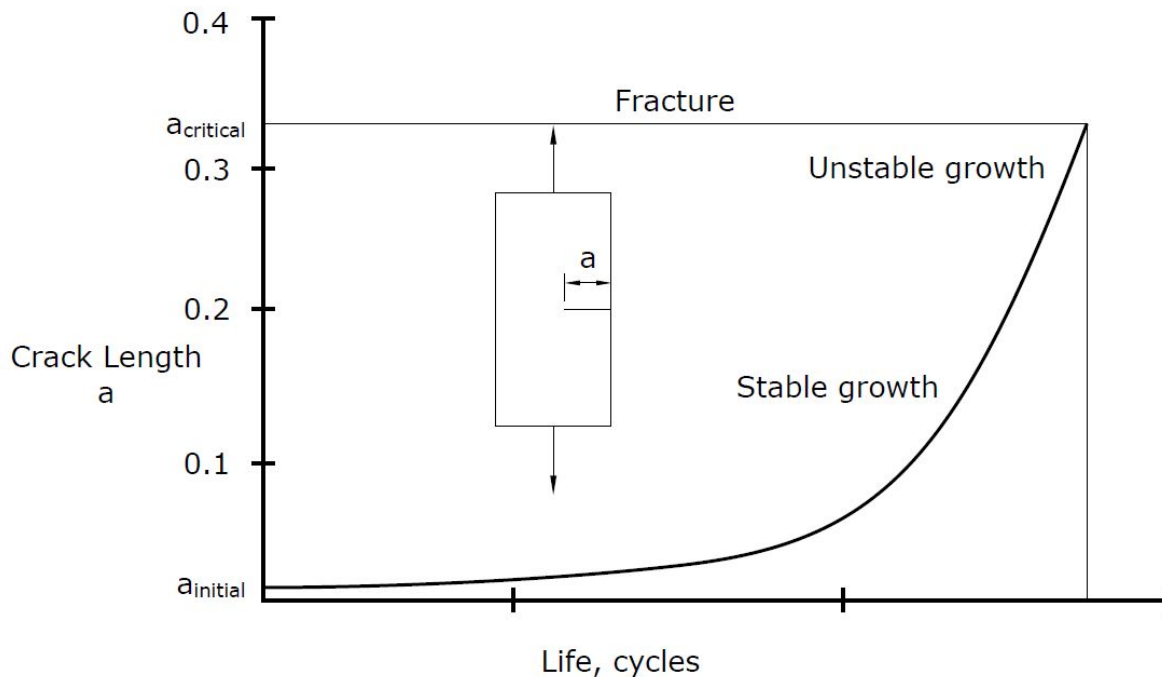


Figure 1.1.1.1-1 Fatigue crack extension from repeated load above threshold.

All structures are assumed to have a crack initiating discontinuity arising from either the manufacturing of the steel or as a result of cutting, drilling, welding, or other changes made to the member during fabrication. All steel members possess discontinuities due to fabrication and manufacturing, but these are benign as long as the stresses are kept sufficiently low. The structural engineering approach to fatigue presumes the existence of some discontinuity that serves as a potential initiation site for cracking. It acknowledges that all inspection methods have detection limits which serve to limit the initial discontinuity size, but also allows for discontinuities that cannot be identified. Inspection cannot detect all discontinuities; its purpose is to identify and reject those that could cause harm.

Fatigue details also exhibit what is referred to as threshold fatigue strength. This means that applied stress ranges below the threshold stress range theoretically do not cause crack extension. The threshold is a function of the geometry of the fatigue detail, a combination of the local stress concentration at the detail and the expected initial discontinuity. Most modern highway bridges on major roads are designed so that the stress is below the threshold which provides a structure which will confidently not exhibit fatigue crack extension.

1.1.1.2 Importance of Fatigue and Fracture in Bridge Engineering

In modern high volume interstate highways, fatigue frequently controls much of the design of welded bridge members, including both proportions and details. The large number of fully loaded trucks produces millions of cycles of fatigue loading each year. The number of trucks on an interstate highway typically exceeds 1,000 trucks per day, which produces over 27 million cycles in 75 years. In order for the bridge to survive this repeated loading, the design stress range is conservatively kept below the threshold value in most cases. The lower allowable stress ranges associated with the threshold causes the design and location of details such as splices, stiffeners, and any attachments to be controlled by fatigue. Modern bridge designs utilize weld details which have known and acceptable fatigue resistance. Vintage details such as welded cover plates are not used due to their low fatigue resistance. The designer must select the proper details based upon the expected fatigue stress.

In a flexural member, the stress range is not constant along its length. Consequently, the designer must determine the stress range at every detail that is susceptible to fatigue and assure that it is within acceptable limits. The designer needs to specify which parts of a member are subject to tension since these portions are subject to more stringent material toughness and weld inspection criteria. The goal of the design is to provide a fatigue tolerant structure which will not exhibit fatigue damage or any fracture during the service life of the structure.

1.1.2 Evolution of Fatigue and Fracture Design, Evaluation, and Inspection Approaches

1.1.2.1 Evolution of Fatigue Design

Pre-1950's steel bridges were mostly connected with rivets, and welding was used for non-structural connections, if at all. Fatigue of riveted bridges had been a concern of the railroad industry, and extensive studies of the fatigue properties of riveted and later bolted and butt welded connections were performed by Professor W.M. Wilson at the University of Illinois starting in the 1930's (Wilson and Coombe, 1939; Wilson, 1940). This work was continued by Munse and Stallmeyer with the inclusion of other welded connections. These tests were done on relatively small specimens using mechanical loading equipment.

The fifth edition of the American Association of State Highway Officials (AASHO) *Standard Specifications for Highway Bridges* (AASHO, 1949), published in 1949, contained no mention of fatigue, and welding was allowed only on low carbon steel and wrought iron used for connection of secondary members, such as stiffeners, railings, and bracing. The welding and material to be welded was to conform to *Specifications for Welded Highway and Railway*

Bridges, Design, Construction, and Repair (AWS, 1936), of the American Welding Society, first published in 1936. There were no notch toughness requirements for the base metal or weld metal, and the inspection requirements were generally visual inspection.

The seventh edition of the *AASHTO Standard Specifications for Highway Bridges* (AASHTO, 1957), published in 1957, allowed welding of a new steel, ASTM A373, which was the forerunner to ASTM A36 steel. However, it also did not contain any mention of fatigue design.

The first AASHTO fatigue design provisions were introduced in 1965. The 1965 ninth edition of the *AASHTO Standard Specifications for Highway Bridges* (AASHTO, 1965) had extensive fatigue design provisions and defined fatigue categories. The fatigue resistance was based largely on the University of Illinois work, a summary of which is contained in the Welding Research Council publication *Fatigue of Welded Steel Structures* authored by W.H. Munse (1964). A similar approach was employed in mechanical engineering components using base metal data from rotating beam specimens and fatigue notch factors. Fatigue life was thought to be dependent upon the “R” ratio, the algebraic ratio of the minimum stress (S_{min}) to the maximum stress (S_{max}), and tied to the use of a Goodman diagram, shown in Figure 1.1.2.1-1, to determine fatigue resistance. The Goodman diagram was developed based on research by J. Goodman during the early 1900’s but is no longer used today in structural engineering.

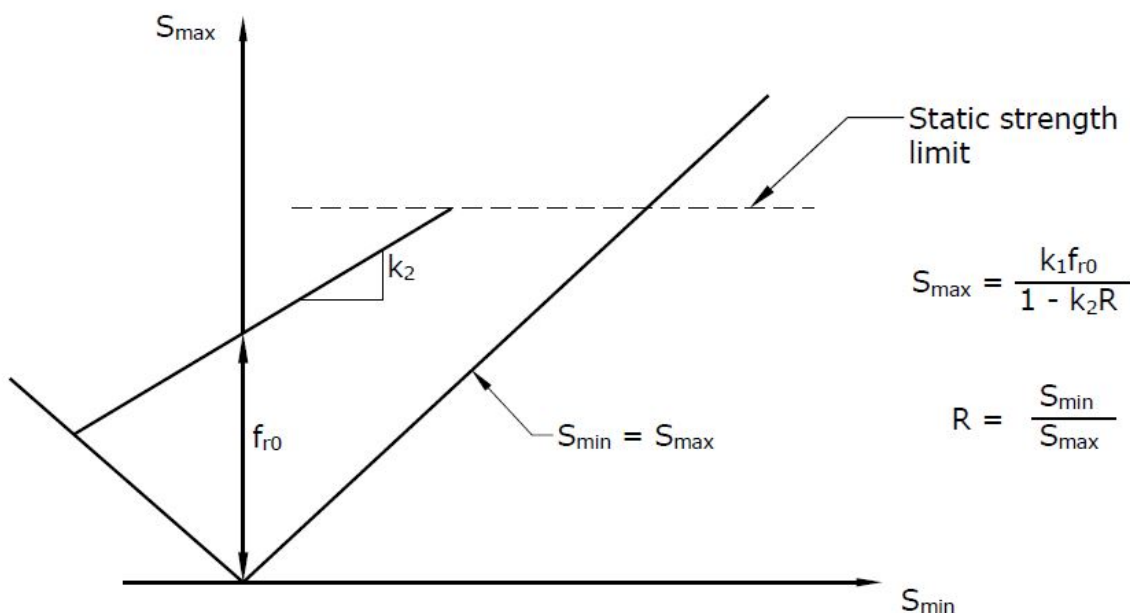


Figure 1.1.2.1-1 Goodman diagram for early determination of fatigue strength.

The allowable fatigue stress when the maximum stress is tensile was defined as:

$$F_r = \frac{k_1 f_{r0}}{1 - k_2 R}$$

Equation 1.1.2.1-1

where

$$k_1 = 1.0 + \alpha \left(\frac{F_u}{58,000} - 1 \right) \geq 1$$

F_u is the tensile strength of the material in psi, and α , referred to as alpha, is a coefficient with values defined by AASHTO varying from 0 to 1.06, depending on the type and location of material, the type of maximum stress, and the number of cycles of maximum stress.

Since the minimum tensile strength of ASTM A36 steel is 58,000 psi, the value for k_1 equals 1 for this steel and increases with higher strength steels, implying a variable fatigue resistance as a function of material tensile strength. The coefficients k_2 and f_{ro} were tabulated for each fatigue category and design life with different values if the maximum stress was tensile or compressive. A modified formula, which had the yield strength of the material as a variable, was used when the maximum stress was compressive. The coefficients were tabulated for three cyclic design lives of 100,000, 500,000, and 2,000,000 cycles, which were a function of road type and load length. The design life for an AASHTO “H” loading on a major road was 2,000,000 cycles of assumed constant amplitude loading, while a lane load on the same bridge would have a design life of 100,000 cycles. The allowable fatigue stress for a category, categorized by the S_{max} parameter, varied along the length of the girder due to the inclusion of the R-ratio, which is related to dead load and live load stresses. The design specification included ASTM A36 steel, as well as ASTM A242 (a weathering steel), ASTM A440 (a non-weldable steel), and ASTM A441 (a weldable steel with yield strength that varied with the thickness of the plate).

The tenth edition of the AASHTO *Standard Specifications for Highway Bridges* (AASHTO, 1969), published in 1969, had changes in the fatigue design specification and included ASTM A588, ASTM A572, and ASTM A514 steel. ASTM A588 for welded structures required supplemental Charpy V-notch (CVN) testing for information only. Although the CVN test was established around 1900, this was the first bridge steel to have a toughness requirement, albeit an informational one. Along with the variation in allowable fatigue stress due to the inclusion of the tensile strength in the coefficient, k_1 , there were separate fatigue categories for the high strength ASTM A514 steel. Some categories, such as Category F, had alpha equals 0 and k_2 equals 1, which gives a constant stress range independent of material strength and mean stress. This is similar to modern design approaches in that it is material-independent.

It is interesting to compare the tenth edition Category F base metal adjacent to a fillet weld and Category K ASTM A514 base metal adjacent to a transverse stiffener with a tensile maximum stress to Category C of the current *AASHTO LRFD Bridge Design Specifications* (AASHTO, 2015b); these are physically analogous details (AASHTO, 1969; AASHTO, 2015b). The comparison is shown for a design life of 500,000 cycles in Table 1.1.2.1-1. Category F is much more conservative than the present specification, while the upper end of the resistance values for Category K are comparable to the present specifications, as might be expected for a fatigue specification that is independent of material grade.

Table 1.1.2.1-1 Comparison of fatigue design stress range for a welded stiffener.

Category	Design Stress Range (ksi)
C – LRFD	20.6
F (1969)	12
K (A514) (1969)	12.7 through 21.2 for R>0

The basis for most modern fatigue design in bridges comes from work originally completed through NCHRP Project 12-7 conducted from 1966 to 1972. This research resulted in the publication of NCHRP Report 102, entitled *Effect of Weldments on the Fatigue Strength of Steel Beams* (Fisher et al., 1970) and NCHRP Report 147, entitled *Fatigue Strength of Steel Beams with Welded Stiffeners and Attachments* (Fisher et al., 1974). These studies involved the testing of 531 steel beams and girders, each having two or more details, and demonstrated that the stress range was the most significant factor in the design for fatigue. This seminal research examined rolled shapes, welded beams, groove welded splices, cover plates, and various stiffener details. The beams used in the research were small 14 inch deep sections. Later tests included larger plate girder specimens.

The fatigue strength of weldments was eventually defined in the NCHRP Project 12-7 research using an exponential relationship between stress range and fatigue life shown below:

$$N = \text{Number of Cycles to Failure} = \frac{A}{S_r^3}$$

Equation 1.1.2.1-2

where A is a constant for a given category of fatigue details and is computed based on regression analysis of test data.

This equation plots as a linear relationship on a log-log scale, as shown in Figure 1.1.2.1-2. The mean stress or minimum stress was found not to be a statistically significant parameter upon the fatigue life of the specimens. The beam specimens used in the testing program preserved the local tensile residual stress at the weld. The magnitude of the residual stress local to the weld is equal to the yield strength of the base metal. The residual stresses in the specimens were consistent with those in real details that would be applied to bridge girders. Only full-size specimens were able to capture the influence of residual stress. Smaller specimens did not lock in the residual stresses, and test results inferred a dependence on mean stress as a factor in fatigue life. The tests included steel with specified yield strengths from 36 to 100 ksi, covering the range of steels available at the time of the testing.

Tests at very low applied stress ranges have revealed that at low stress ranges, no cracking occurs (Fisher et al., 1983). This level of stress range is called the threshold stress range, S_{Rth} , and is an important characteristic of the fatigue resistance. If the stress range is below this threshold, no crack extension occurs, and the fatigue life is deemed to be infinite.

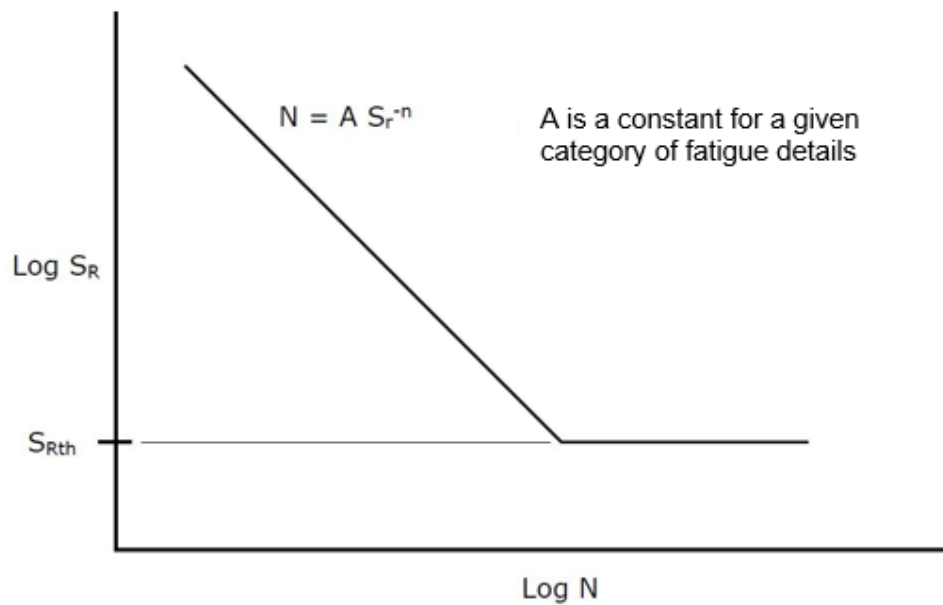


Figure 1.1.2.1-2 Fatigue S-N curve.

It was not until the 1974 interim specifications to the AASHTO *Standard Specifications for Highway Bridges* (AASHTO, 1974a) that the fatigue design concepts still fundamentally in use today were introduced to designers. In the 1974 major revisions, AASHTO adopted the stress range concept, with the stress range now being the only design variable required for fatigue. Variations in strength of materials were deemed to be immaterial to fatigue resistance. Six fatigue categories designated A through F of decreasing fatigue resistance were introduced, with members and their details grouped to specific categories. The AASHTO specifications added figures to explain the details and provided the foundation for over four decades of development of the fatigue design and evaluation specifications.

From 1974 to 1994, the AASHTO standard specifications continued to be used for the design of bridges. The AASHTO standard specifications relied on the standard design vehicle, known as HS 20, for the calculation of live load effects. The live load effects were generally computed with the same vehicle weight used for the calculation of force effects for both strength and service conditions, without adjustment. They were also computed with the same distribution factors used for the design of a bridge for both strength and service conditions (which included both single-lane and multi-lane loading, depending on the number of stress cycles). This typically resulted in the design of members for fatigue considering multiple loaded lanes on the bridge simultaneously.

Over time, as additional domestic and international data sets became available, the AASHTO fatigue design approach was re-examined and fundamentally confirmed. Keating and Fisher (Keating and Fisher, 1986) examined 1,500 test data points in addition to the fatigue test data points originally collected in the NCHRP Project 12-7 investigation. Their updated study, completed in 1986, confirmed the accuracy of the AASHTO fatigue design curves as reasonably predicting the lower bound fatigue life of an expanded population of test data. Minor adjustments were made to the slopes of the AASHTO fatigue design curves, as well as a slight adjustment in

the infinite life maximum stress range for cover-plated beams, but otherwise the original fatigue research was confirmed for its accuracy. The larger data set was used to create a new category, B', to cover certain longitudinally loaded group welded attachments. Category E' was also created to represent the fatigue strength of web attachments thicker than 1 inch.

In 1994, the *AASHTO LRFD Bridge Design Specifications* (AASHTO, 1994) were introduced. For the first time, fatigue was defined as its own limit state. The design vehicle was changed from the previous HS 20 to a new lighter-weight vehicle, 75 percent of the weight of the prior HS 20 vehicle and with an extended wheelbase. Fatigue assessments are now conducted with only a single vehicle in a single lane on the bridge and with a lower impact value than is used for design at the strength and service limit states.

In 1995, Clause 12 was added to the *Bridge Welding Code* (AWS D1.5) (AASHTO/AWS, 1995), containing requirements for fabricating fracture critical structures. This essentially replaced the *Guide Specifications for Fracture Critical Non-Redundant Steel Bridge Members*, published in 1978 by AASHTO (AASHTO, 1978), for welding and fabrication requirements. Clause 12 of the AWS D1.5 provides information related to contract documents, base metal requirements, welding processes, consumable requirements, Welding Procedure Specification (WPS), contractor requirements, thermal cutting, repair of base metal, straightening, curving, cambering, tack welds and temporary welds, preheat and interpass temperature control, postweld thermal treatments, weld inspection, and repair welding. However, it does not assign responsibility for specifying which, if any, steel bridge member or member component falls in the category of fracture critical.

In 2009, there were additional changes to the fatigue design provisions with the single fatigue load combination being replaced with Fatigue I and Fatigue II load combinations, though these effectively are the same as the prior check but stated differently. A section dealing with constraint-induced fracture was also introduced at that time.

1.1.2.2 Evolution of Fracture Control Plans and Fracture Critical Inspections

Control of Steel Construction to Avoid Brittle Failure (Shank, 1957), edited by Shank and published by the Welding Research Council in 1957, provides a summary of the understanding of brittle fracture in the 1950's. This publication also coincided with the beginning of the interstate highway construction. The monogram concentrates heavily on material properties as the cause of structural fractures and discusses fatigue in a single paragraph. It indicates the need to reduce stress concentrations for increased fatigue resistance and acknowledges that improvement in fatigue design will also reduce the risk of a brittle fracture. The coupling of fatigue and fracture was stated as:

“Moreover, the beginning of a small fatigue crack may become the focus of a brittle fracture crack even though from a strictly fatigue viewpoint the part would still have a long life.”

This statement does not focus on fatigue cracking as a root cause of subsequent brittle fracture but inversely as low toughness reducing the fatigue life. The monograph concludes with the sentence:

“This discussion serves to indicate the present limitations of our knowledge, but more important, it is meant to show that the three factors – materials, design and fabrication – all may play an important role in the ultimate performance and no one of them should be neglected at the expense of others.”

This last sentence is the heart of the fracture control plan currently used in the design of steel bridges and other structures.

The critical crack size is dependent upon the material’s fracture toughness, which also depends upon the temperature and rate of loading. The goal of the fracture control plan is to assure material that can tolerate cracks of the order of the material’s thickness at the lowest anticipated service temperature under operating stress levels. A 0.4 by 0.4 inch CVN test specimen is used to measure the notch toughness of the material, which is correlated with material fracture toughness.

Much of the knowledge of low carbon, lower strength steels and fracture came from studies of welded ship hull failures during World War II. The fractures of the all-welded Liberty Ships (see Figure 1.1.2.2-1) stimulated a large program to improve their fracture resistance. The changes included improved chemistry control and CVN toughness requirements of the base metal, improved hatch geometry to reduce stress concentrations, and the addition of a riveted crack arrest band around the ship to arrest a running crack. The work on the Liberty Ships was followed by extensive fracture testing at the Naval Research Laboratory by Pellini and his colleagues (Pellini, 1983).

The concept of a Nil Ductility Temperature (NDT) as a means of characterizing the fracture resistance of steel came from a dynamic test of a specimen containing a brittle weld with a notch. The NDT was the temperature above which the test plate could bend plastically without propagation of a brittle fracture. Pellini’s approach assumed that the cracking would occur from a locally embrittled area of the weld. If the temperature of the plate was above the NDT, the crack would not propagate outside of the locally embrittled area of the weld. Hence, the approach taken was to rely upon a base metal capable of arresting a dynamic crack. Pellini’s approach did not consider that fatigue cracks formed in sound metal could be the cause of the fracture.

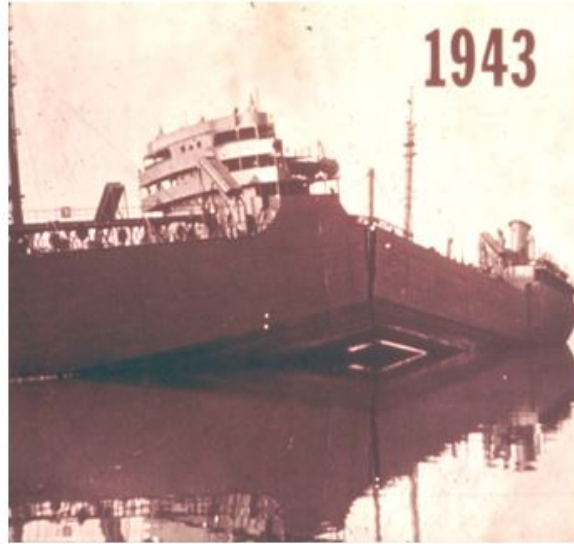


Figure 1.1.2.2-1 Liberty Ship fracture.

The collapse of the Point Pleasant Bridge in 1967 and its subsequent failure investigation marked a significant change in design and construction of steel bridges. The collapse was triggered by a brittle, unstable crack extension of a small crack in a single eyebar which formed the chain suspending the bridge. The bridge was in service for over 40 years with no apparent structural distress. The fractured eyebar is shown in Figure 1.1.2.2-2. The eyebar has been assembled with the left-hand side matched to show the extent of plastic deformation which occurred on the left-hand segment before it finally fractured. The right-hand fracture in the right side shows no evidence of any plasticity. The fracture of this side was triggered by the small cracks, 0.15 inches deep, shown in Figure 1.1.2.2-3.

The graphic difference in failure mode of the sides of the eyebar brought to the attention of the bridge engineering community that bridge steels needed to be able to tolerate cracks that might form under service load so that they may be discovered during an inspection. The smooth machined tensile coupons that were relied upon in the mill test of the material verified that material would perform in a ductile manner like the left segment of the eyebar but did not provide a measure of the material's resistance to brittle fracture. Materials that could tolerate a small crack without failure were clearly needed. This led to the implementation of the CVN requirement for bridge steels subjected to tension. The fracture toughness requirement for bridge steels was based on work in the nuclear field and verified by low temperature fracture testing of large girder specimens.

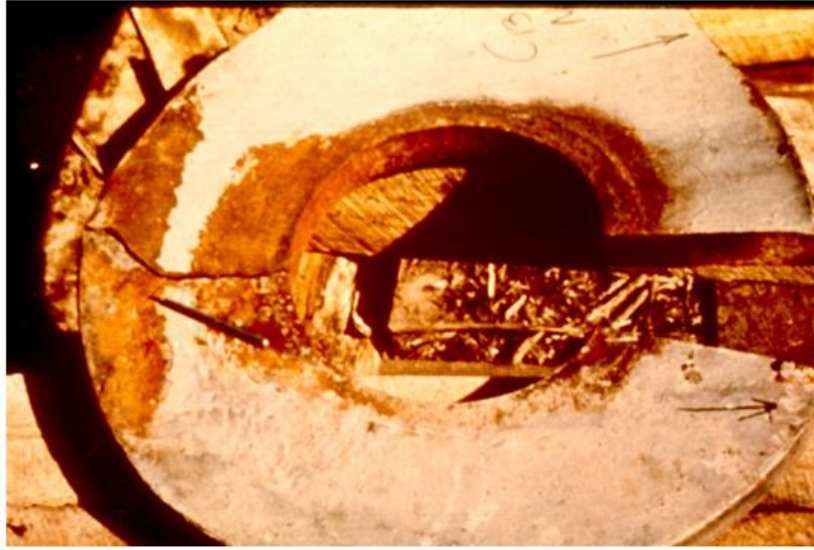


Figure 1.1.2.2-2 Fractured eyebar from the failed Point Pleasant Bridge.



Figure 1.1.2.2-3 Shallow cracks at exterior of the pin hole in the Point Pleasant Bridge.

The failure of the Point Pleasant Bridge by the fracture of a single member due to lack of redundancy, even though there were two eyebars forming the suspension chain, caused a change in the design of bridges. Clearly these members needed special consideration. These critical members were labeled as fracture critical. The required fracture toughness, fabrication inspection, and welding requirements of these members was developed as a result of the failure. These requirements, built upon a fracture mechanics understanding as espoused earlier by Shank (i.e., with materials, design, and fabrication having important roles), led to a holistic approach to providing an increase in reliability of these members.

The increased fabrication inspection requirements were implemented to reduce the probability of discontinuities and stress concentrations in these members. The higher toughness was to ensure that failure of these members would not be triggered by a small undetectable crack which might

develop during the service life of the bridge. The implementation of hands-on inspection of the fracture critical members provided further safety to ensure that any crack that developed, even with these increased material and fabrication requirements, was discovered before it became unstable.

In addition, supplemental AASHTO material specification toughness was required for ASTM A588 and ASTM A572 when it was welded but not for the higher strength ASTM A514. The 10th edition of the AASHTO *Standard Specifications for Highway Bridges* (AASHTO, 1969) included detailed welding procedures for ASTM A514 and mandatory radiograph testing of all tension butt welds. Ultrasonic inspection was not mandated. All ASTM A514 welds were to be inspected for more than 48 hours after welding to ensure any delayed cracking could be discovered.

It is also important to note that during the 1970's, the American Society for Nondestructive Testing (ASNT) standards for the various levels of inspectors were implemented. Prior to the development of these criteria, the uniformity and quality of nondestructive inspection was not controlled and was variable. The American Welding Society (AWS) followed up later with the Certified Weld Inspector Certification. These changes in the qualifications for shop inspectors greatly increased the reliability and uniformity of weld inspection. These changes ensured that weld inspectors were adequately trained and qualified, and they greatly reduced the variability in weld quality.

These requirements have proved to be successful. A national dialogue about fracture control strategy evolved during the decade following the collapse of the Point Pleasant Bridge. As a result, a Fracture Control Plan (FCP) was developed by AASHTO and AWS, and AASHTO's first *Guide Specifications for Fracture Critical Non-Redundant Steel Bridge Members* (AASHTO, 1978) was published in 1978. Since that time, no bridge built using the requirements of the AASHTO FCP has suffered any fracture.

Later defined and currently enforced, FCMs require enhanced, arms-length inspections as a result of the Mianus Bridge collapse. The AASHTO FCP, along with this more stringent in-service inspection requirement, is referred to as the Total FCP in this Manual.

SECTION 1.2 SCOPE OF REFERENCE MANUAL AND PRESENTATION OF MAJOR THEMES

This Manual covers the relevant topics related to fatigue and fracture in steel bridges, including analysis, design, evaluation, repair, and retrofit. Chapter 2 begins with a discussion of cracking in steel structures, including crack behavior, sources of discontinuities in steel structures, the nature of stresses affecting fatigue and fracture, and brittle and ductile behavior in steel. Chapter 3 provides the basics of fracture mechanics, covering such topics as fracture control, evaluation of fatigue cracking, and fracture mechanics as a quantitative tool. Chapter 4 describes fatigue behavior, including discontinuities and stress concentrations, the influence of production and fabrication on fatigue, testing as the basis for design limits, and environmental effects. Chapter 5 describes analysis for fatigue, including information for both approximate and refined analysis methods. Chapter 6 addresses the fatigue design approach as presented in the *AASHTO LRFD*

Bridge Design Specifications (AASHTO, 2015b), and it explains the fundamental fatigue limit state equation, the various AASHTO fatigue detail categories, the differences between finite life and infinite life, and the computation of fatigue stress range and factored nominal resistance, including a step-by-step design example for fatigue. Chapter 7 describes fracture control, including design, fabrication, and inspection, and it covers such topics as redundancy, constraint-induced fracture, and the Total FCP. Chapter 8 addresses the AASHTO fatigue-evaluation approach, including remaining fatigue life evaluation, estimates of fatigue life based on the *AASHTO Manual for Bridge Evaluation* (AASHTO, 2015d), and remaining fatigue life for “negative remaining life” bridge details. Chapter 9 describes assessment, repair, and retrofit of structures, and it provides a description of several common fatigue details, it describes general repair and retrofit strategies that are common to virtually all fatigue details, and it covers the special topics of constraint-induced fracture, over-height vehicle collisions, and fitness-for-service analysis. Finally, Chapter 10 covers non-welded components such as built-up members, bolts and rods, and reinforcement of concrete. In addition, Appendix A describes calibration of the Fatigue I and II load combinations based on the SHRP2 Project R19B (Modjeski and Masters, 2015).

Information in this Manual about bridge design for fatigue and fracture is based on the *AASHTO LRFD Bridge Design Specifications*, 7th Edition with 2015 Interim Revisions (referred to in this Manual as *AASHTO LRFD*) (AASHTO, 2015b). However, it should be noted that the fatigue load factors presented in this Manual are based on the 2017 edition of the *AASHTO LRFD Bridge Design Specifications*. Information about bridge evaluation for fatigue and fracture is based on the *AASHTO Manual for Bridge Evaluation*, 2nd Edition with 2015 Interim Revisions (referred to in this Manual as *MBE*) (AASHTO, 2015d).

The following sections provide a brief summary of some of the major themes presented in this Manual.

1.2.1 Physical Phenomena of Cracking

Crack growth in steel bridges requires two conditions to occur: existing discontinuities and tensile stresses normal to the discontinuities. Cyclical stresses with a tensile component can cause fatigue crack growth, while sustained tensile stress or a single stress cycle with a tensile stress component can cause fracture. The nature of this relationship is described in Chapter 3.

Crack growth can be delineated into three distinct regimes: initiation, steady-state propagation, and unstable fracture. All three of these regimes, as well as the general behavior of fatigue cracking, are described in Chapter 2.

1.2.2 Fatigue Stress

The dominant parameter for fatigue design is stress range, which can be readily computed by the design engineer for a specific bridge application. The stress range for the fatigue limit state is the algebraic difference between a maximum and minimum live load stress caused by the passage of a single fatigue design vehicle occupying a single lane. The most common cause of fatigue cracks in bridges is in-service cyclical stress range due to trucks. As such, the fatigue limit state

includes only force effects from live load and no other loads. The single truck concept was validated as part of the SHRP2 Project R19B research (Modjeski and Masters, 2015), a summary of which is provided in Appendix A.

The fatigue design vehicle is similar to the HL-93 design truck but with a constant spacing of 30.0 feet between the 32.0-kip axles. In addition to the static force effects, a 15 percent increase in the vehicle force effects is applied to account for dynamic load allowance (also known as impact).

Two load combinations, Fatigue I and Fatigue II, are defined in *AASHTO LRFD* Table 3.4.1-1 for the fatigue limit state. The Fatigue I load combination is applied to check if the detail under investigation will theoretically exhibit infinite life. When a detail cannot exhibit infinite life due to excessive stress range, the Fatigue II load combination is applied to ensure that the detail will exhibit sufficient finite life based upon the projected average daily truck traffic (ADTT) for 75 years, the design life specified in *AASHTO LRFD*.

The computation of the factored stress range for fatigue is covered in considerable detail in Chapter 6, including a step-by-step design example.

1.2.3 Fatigue Resistance

AASHTO LRFD characterizes the fatigue resistance of details based upon the testing and conclusions discussed in Chapters 4 and 6. Details are characterized into eight Detail Categories, A, B, B', C, C', D, E, and E', in order of descending fatigue resistance. Fatigue details and their respective detail categories are presented in *AASHTO LRFD* Table 6.6.1.2.3-1.

In the log-log resistance curves, the resistance is represented by a sloping line followed by a straight horizontal line. The sloping portion represents the finite life nominal resistance. These limits are established through testing and represent a 97.5 percent probability of survival in the region of finite life. For finite life, the resistance is proportional to the cube root of a detail constant, A , divided by the number of design cycles of loading, N , for that particular detail.

The straight horizontal portion of the curve represents the infinite life nominal resistance, and these resistance values are based on the constant amplitude fatigue threshold (CAFT). The region of infinite life represented by the CAFT is somewhat less certain than the finite life region, given a lesser number of long-life tests, though the Fatigue I load combination has been established to provide safe behavior for infinite life.

The computation of fatigue resistance is covered in considerable detail in Chapter 6, including a step-by-step design example.

1.2.4 Fatigue and Fracture Control

Fatigue and fracture in steel bridges must be considered during analysis and design before the bridge is constructed, as well as in evaluation for existing bridges.

Analysis is described in considerable depth in Chapter 5. For load-induced fatigue, several analysis methods are described, including both approximate analysis and refined analysis methods, the local-stress approach, and the fracture-mechanics approach.

Design based on *AASHTO LRFD* for fatigue and fracture is described in Chapters 6 and 7, respectively. For the fatigue limit state, the design stress range must not exceed the factored nominal resistance. For fracture, a three-legged stool approach is implemented, including design, fabrication (including quality control inspection), and in-service inspection as required elements of a comprehensive plan, referred to as the Total FCP.

Evaluation is described in Chapter 8. A fatigue evaluation is not routinely performed with each rating of a steel bridge, but only when the remaining fatigue life of an uncracked bridge is desired as input into operating decisions. A methodology for fatigue evaluation of steel bridges is included in the *MBE*.

1.2.5 Retrofit Strategies

If fatigue-related problems are encountered in the field (most commonly on older bridges), then a repair or retrofit strategy must be employed to rectify the problem and to help prevent additional problems. While the specifics of the repair strategy are dependent upon the nature of the detail and problem, there are several general repair and retrofit strategies that are common for virtually all fatigue details. These general strategies include understanding the source of cracking, designing the repair detail, and validating the repair detail. Although the specifics of these three steps are dependent on the unique fatigue characteristics of the bridge, each step is essential for any successful repair or retrofit strategy.

CHAPTER 2 CRACKING IN STEEL STRUCTURES

SECTION 2.1 CRACK BEHAVIOR

Cracking in steel structures can manifest as a slow, stable process of growth from repeated applications of stress or suddenly when the conditions are right. If crack growth is allowed to propagate and continue long enough, total separation/loss of the member can result when the uncracked cross section is sufficiently reduced such that the member can no longer resist the internal forces and the crack extends in an unstable mode. The unstable growth is typically in the form of brittle fracture in steel bridge members. The fatigue process can take place at stress levels (calculated on the initial section) that are substantially less than those associated with yielding under static loading conditions. The usual condition that produces fatigue cracking is the application of a large number (millions) of load cycles, with some above a “threshold.” Consequently, the types of structural engineering applications that are susceptible to fatigue cracking include dynamically loaded structures such as bridges, highway sign and lighting structures, crane-support structures, stacks and masts, and offshore structures.

2.1.1 Necessary Conditions

Crack growth in metals requires two conditions to occur: existing discontinuities and tensile stresses normal to the discontinuities. Cyclical stresses with a tensile component can cause fatigue crack growth, while sustained tensile stress or a single stress cycle with a tensile stress component can cause sudden and complete fracture.

A relationship exists between load and resistance for both fatigue and fracture. However, the parameters in this relationship vary for fatigue and fracture. For example, the load parameter to initiate fatigue is stress range, while that for fracture is total stress. The nature of this relationship is discussed further in Chapter 3.

2.1.2 Crack-growth Regimes

Crack growth can be delineated into three distinct regimes: initiation, steady-state propagation, and unstable fracture, as illustrated in Figure 2.1.2-1.

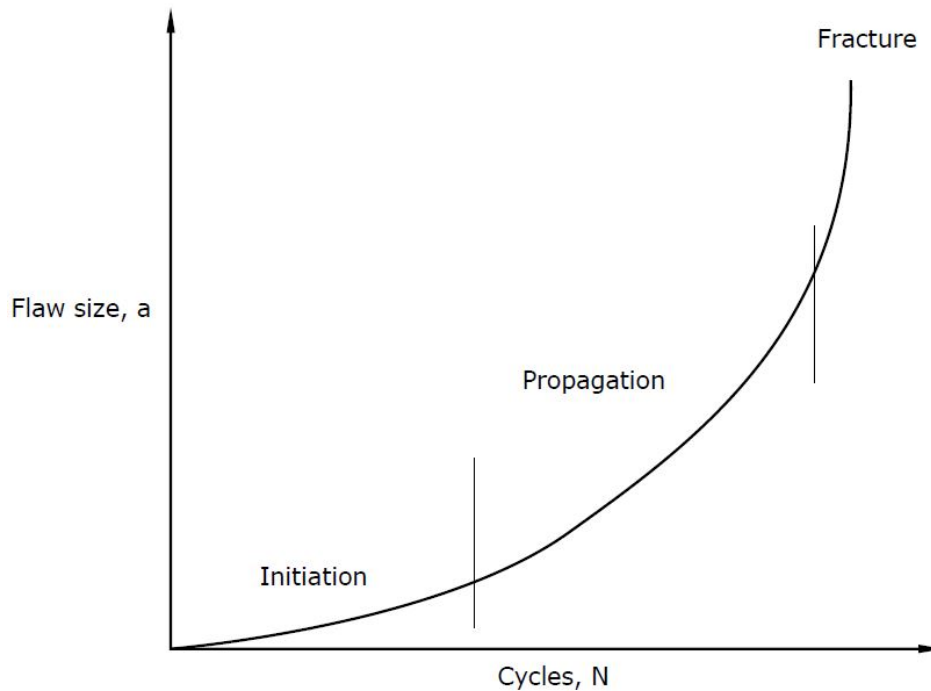


Figure 2.1.2-1 General crack-growth regimes.

2.1.2.1 Initiation

It is inevitable that discontinuities are present in fabricated steel components. These discontinuities are byproducts of steel making, as well as the various cutting, drilling, punching, and welding operations associated with the fabrication of steel bridge and structural elements. They are discussed in greater detail in Section 2.2. Given these preconditions, the engineer is responsible to control the stresses to avoid potential fatigue and subsequent brittle fracture resulting from growth of these discontinuities. The fatigue behavior of a fabricated steel engineering structure is controlled by the size, shape, and location of the discontinuities, and the stresses applied.

The initiation portion of general crack growth in which existing discontinuities are sharpened into cracks is essentially non-existent for all fabricated steel structures and can conservatively be ignored. Thus, they are assumed to be present at the start. Crack growth in bridges is delineated into only two regimes: stable fatigue cracking and unstable fracture. Figure 2.1.2.1-1 graphically illustrates crack growth in bridges.

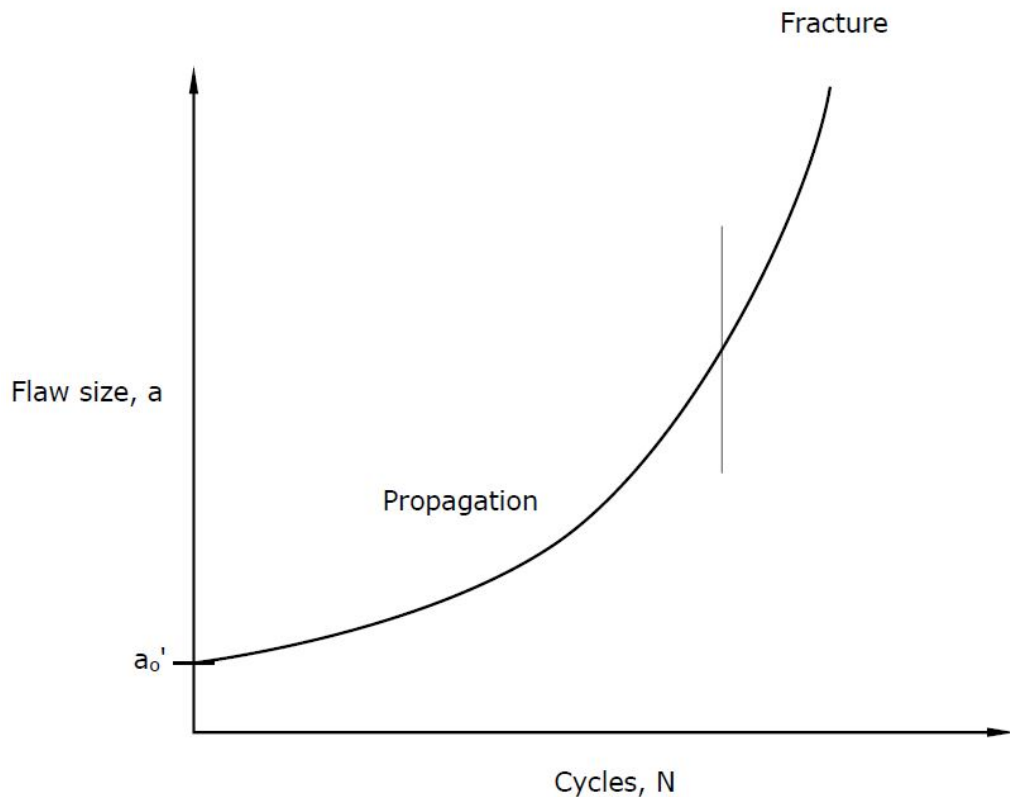


Figure 2.1.2.1-1 Crack-growth regimes for steel bridges with assumed initial discontinuity.

2.1.2.2 Propagation

The propagation regime of crack growth represents steady-state fatigue cracking that may occur when stresses above the threshold are applied. Fatigue is the propagation of microscopic cracks into macro cracks by the repeated application of tensile stress. An existing crack grows a small amount in size each time a load is applied. Growth occurs at the crack front, which is initially sharp. Even at relatively low loads, there will be a high concentration of stress at the sharp front, and plastic deformation (slip on atomic planes) therefore occurs at the crack front. Continued slip results in a blunted crack tip, and the crack grows a minute amount during this process. Upon unloading, not necessarily to zero, the crack tip again becomes sharp. The process is repeated during each load cycle and is described in detail in terms of the fracture mechanics model in Chapter 3. The rate of growth of the crack increases exponentially over time and is depicted by the nonlinear propagation region of Figure 2.1.2.1-1.

2.1.2.3 Fracture

When a critical size is achieved, the stable crack fractures in an unstable manner without an increase in stress. Fracture may be defined as rupture in tension or rapid extension of a crack, leading to gross deformation, loss of load-carrying capacity, or complete separation of the component.

Failure occurs in one of two ways. One possibility is that the steel has sufficient toughness and the fatigue crack grows to such an extent that the loss of section means the load simply can no longer be resisted by the uncracked ligament (for example, overload). In this case, failure occurs by yielding of the remaining material, or, exceptionally, by instability if the crack growth produces a grossly unsymmetrical section. In the case of yielding and a ductile failure, the critical flaw size is proportional to the yield strength. If the steel does not have sufficient toughness, the section fails by brittle fracture. In the case of a brittle failure, the critical size is proportional to the fracture toughness of the material which varies with rate of application of the load and the temperature of the material. The fracture toughness of the bridge steel is characterized by the Charpy V-notch (CVN) toughness (ASTM, 2012), discussed in detail in Section 2.4.1. Fracture is represented by the rapid extension of the crack with a limited number of additional cycles and is depicted qualitatively in Figure 2.1.2.1-1. It should be noted that in bridge structures, cracking may not necessarily lead to unstable propagation, since in many cases the limited magnitude of stress may allow the cracking to arrest, resulting in the need for either no repair or simple repair.

SECTION 2.2 SOURCES OF DISCONTINUITIES IN STEEL STRUCTURES

The discontinuities that exist in all fabricated steel structures are a consequence of the manufacturing process of the steel itself and/or the normal fabrication processes of the components.

2.2.1 Production

Discontinuities in rolled shapes and plates arise from surface and edge imperfections, irregularities in mill scale, laminations, seams, and inclusions, as well as from mechanical notches due to handling, straightening, cutting, and shearing. These irregularities are controlled by product specifications. In a rolled shape or plate away from connections and attachments, fatigue crack growth can start from one of these sources. Comparatively, the unaltered rolled shape or plate presents the most favorable fatigue life situation. However, there are not many practical cases in which a rolled shape or plate does not have some kind of attachment, connection, or other alteration, and these details have fatigue resistance less than the unaltered shape or plate. As a consequence, fatigue cracking in base metal away from details is rarely observed. As will be discussed in Chapter 6, AASHTO characterizes fatigue resistance through lettered Detail Categories A through E', Detail Category A exhibiting the highest fatigue resistance and E' the worst (AASHTO, 2015b). Unaltered rolled shapes or plates are categorized as Detail Category A.

2.2.2 Fabrication

A simple built-up section is composed of several steel plates joined together by welding. An example is a plate girder with the plates joined through fillet welding, the most common practice. Though common, there are possible discontinuities introduced. The kinds of discontinuities that can occur in a welded detail are shown pictorially in Figure 2.2.2-1. These include partial penetration and lack of fusion, porosity and inclusions, undercut or micro discontinuities at the

weld toe, and cracking or inclusions around a weld repair, at start-stop locations, or at arc strikes. Although the fabricator of the structure and those responsible for the fabrication inspection will attempt to minimize these discontinuities, it is neither practical nor economically possible to eliminate them.

In the case of a typical flange-to-web fillet weld, as shown in Figure 2.2.2-1, partial penetration is not a discontinuity and is of no concern as the applied stress is parallel to the weld. Surface discontinuities are subject to visual and magnetic-particle inspection, and can be readily identified and addressed if established workmanship criteria are not satisfied. The hidden discontinuities, such as porosity, are accepted as *AASHTO LRFD* (AASHTO, 2015b) is based upon tests of real welds with porosity discontinuities in them.

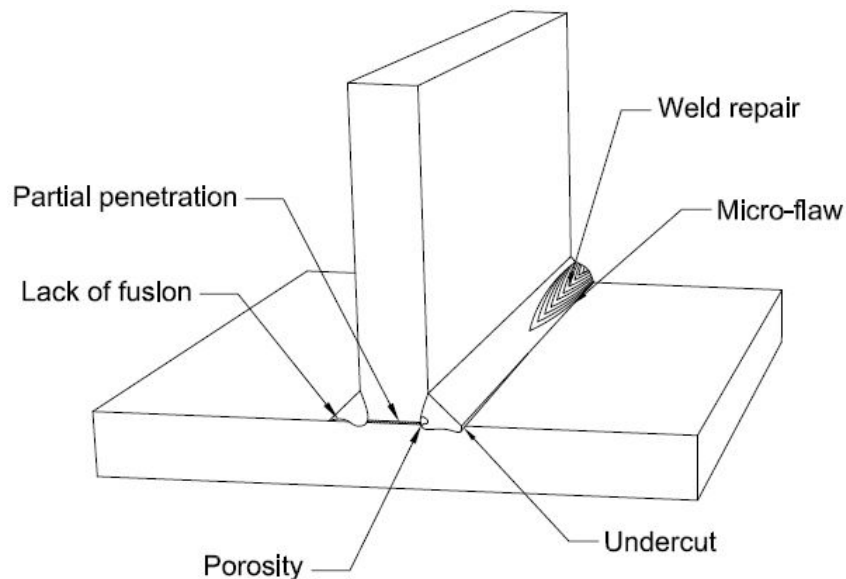


Figure 2.2.2-1 Discontinuities in a welded beam.

Test data on welded details have demonstrated that all fatigue cracks commence at some initial discontinuity in the weldment or at the weld periphery, and grow perpendicular to the applied tensile stresses. In a welded beam without attachments (simply two flange plates welded to a web), most laboratory fatigue cracks are observed to originate in the web-to-flange fillet welds at internal discontinuities such as porosity (trapped gases in the unfused area expanding and becoming trapped in the solidifying weld), incomplete fusion, or trapped slag. Figure 2.2.2-2 shows a fatigue crack that has formed from porosity (highlighted by arrow) in longitudinal submerged-arc fillet welds. These relatively large discontinuities are always present to some degree, irrespective of the welding process and techniques used during fabrication. The effect of these internal discontinuities is accounted for in the design fatigue resistance, which eliminates the need to identify them by internal inspection or remove them by repair. In other words, these internal discontinuities do not govern. Surface discontinuities in stress concentrations propagate faster and govern.

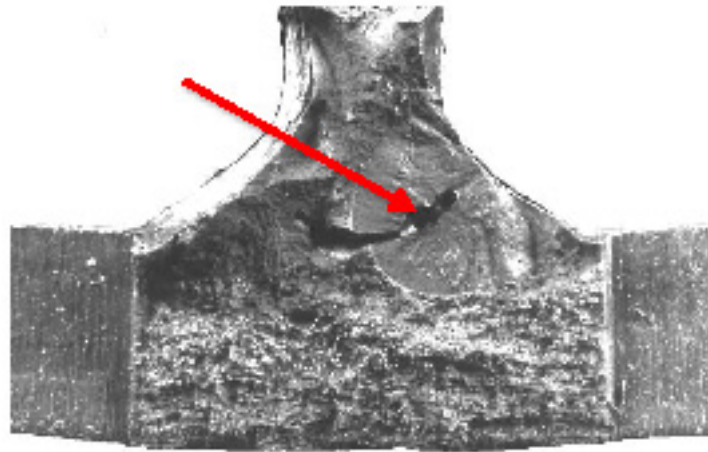


Figure 2.2.2-2 Fatigue cracks forming from internal porosity in web-to-flange connection.

Attachments, such as cover plates, gussets, stiffeners, and other components welded to a web or flange, introduce a transverse weld toe, thus forming a line of elevated residual tension where fatigue cracking can start from small, sharp discontinuities. Figure 2.2.2-3 and Figure 2.2.2-4 show a fatigue crack that has formed at a cover plate fillet weld toe. The crack surface in Figure 2.2.2-4 shows various stages of crack propagation. The first stage (1) is a surface crack growing in the flange as a semi-circle until it penetrates the far side of the flange. The second stage (2) is a through crack in the flange growing both to the right and left until it reaches the flange tip on the right. Finally, with the flange tip severed, the through crack grows toward the web on the left (3), with the rougher texture on the fracture surface suggesting more rapid propagation.

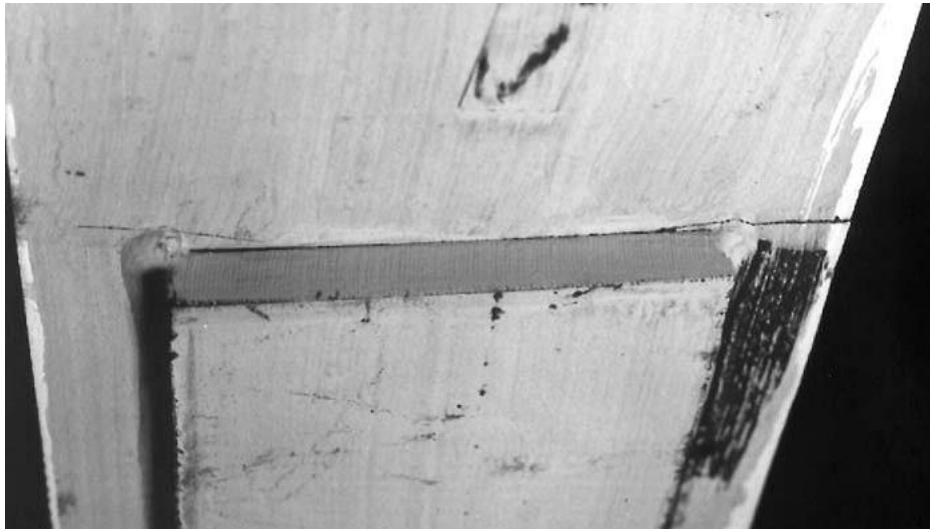


Figure 2.2.2-3 Fatigue crack at end of cover plate fillet weld toe.

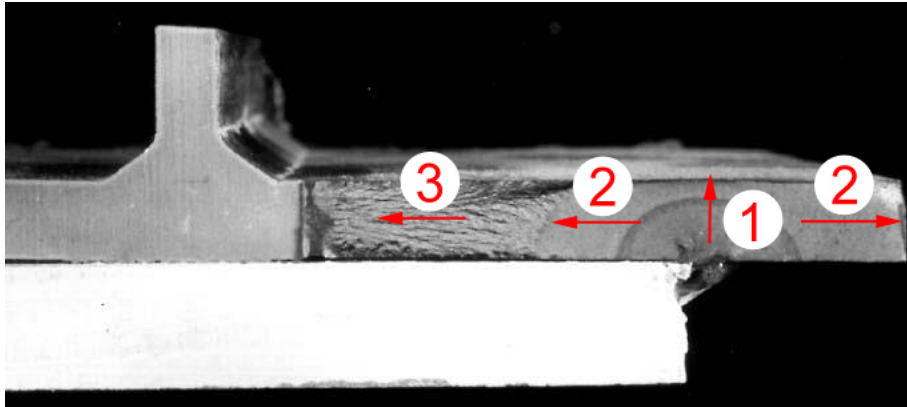


Figure 2.2.2-4 Crack surface showing fatigue crack growth (with stages of crack propagation identified).

In most cases, a discontinuity is an expected result of the type of fabrication process and has no effect on the life of the member if designed properly. For instance, the partial penetration shown in Figure 2.2.2-1 is a natural consequence of the fillet-welded connection; it is not expected that the two fillet welds will fuse in the central region of the connection. Furthermore, since the crack represented by the lack of penetration is parallel to the direction of the stress field (assuming a girder web-to-flange weld), the crack will not open under the application of stress (because the primary stress is from bending) and failure by fatigue will not occur. However, if the web plate was pulled away from the flange, then the lack of penetration would be perpendicular to the applied stress and this would be a fatigue sensitive detail.

Consider a detail involving mechanical fasteners—an I-shaped beam with a cover plate fastened to the beam flange with bolts. The discontinuity between the flange and the cover plate could be described as a discontinuity or crack, but since the discontinuity is parallel to the stress field, the "crack" does not grow and therefore its presence does not affect the fatigue performance of the member.

Mechanical details, in which holes are drilled or punched and forces are transferred by means of rivets or bolts, present a somewhat more severe fatigue resistance situation than the bare rolled shape. Drilled or sub-punched and reamed holes yield some reduction in fatigue life as compared with an unaltered member, but the difference usually is not very great due to the preloaded high-strength bolts. The disturbing effect of the hole is largely mitigated by the presence of the high local compressive stresses introduced by the bolt (Detail Category B). Punched holes give a greater reduction in fatigue resistance than do drilled or sub-punched and reamed holes because of imperfections at the hole edge arising from the punching process. In this case, the crack usually starts at the edge of the hole.

Broadly speaking, any mechanically connected detail has a higher fatigue resistance than does its equivalent welded detail. The types of discontinuities associated with weld toes transverse to the direction of stress introduced when welding have already been discussed. In addition to the fact that more discontinuities will be present when welding is used, inspection for discontinuities is more difficult than is the case when mechanically fastened details are used. Repairing

discontinuities in welded details is also difficult. Prohibiting the use of welded details in fatigue situations, however, is usually not a practical option.

The task of the structural engineer is to be able to proportion those structural members that have a potential for failure by fatigue crack growth so that they have a fatigue resistance exceeding the applied range of stress. As described in Chapter 6, this is done in the environment that some probability of failure must be accepted; in real terms, there is no structure that can be designed for zero probability of failure. The design will be carried out in the expectation that discontinuities will be present initially in all fabricated steel structures and that all such members will contain residual stresses of relatively high magnitude. A concomitant feature is that in the design process it is possible to identify the size of discontinuities that are permissible and then to use this information as the basis for both initial inspection of the structure as well as periodic inspections. This latter feature is not yet well-developed in design specifications, and the usual procedure is to accept as permissible discontinuity sizes consistent with the specifications that accompany the fabrication processes.

SECTION 2.3 STRESS

Cracking in steel structures can only occur when there are tensile stresses present. Total stress governs fracture, and fluctuation in stress, or stress range, governs fatigue. Thus, as introduced in Section 1.1.1, sustained stresses are important in the investigation of fracture, while cyclical stresses are important in the investigation of both fatigue and fracture.

Figure 2.3-1 illustrates the stresses applied to details due to dead load and live load. In addition to these applied stresses are potential residual stresses embodied within the details.

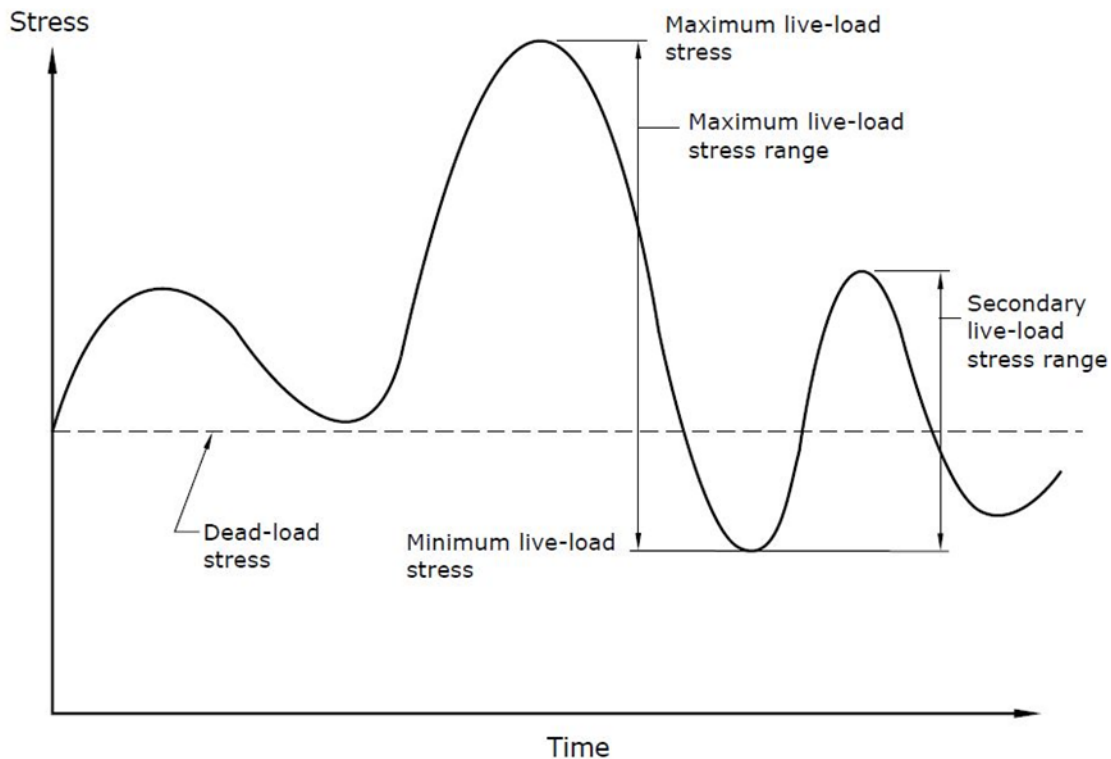


Figure 2.3-1 Typical stress versus time history for a continuous bridge.

2.3.1 Sustained Stress

2.3.1.1 Residual Stresses from Production and Fabrication

Steel structures that are fabricated by welding contain residual or "locked-in" stresses that are a consequence of the welding process. These have considerable influence on the propagation of fatigue cracks. The main effect is to significantly reduce the effects of the mean stress levels. This effect is numerically demonstrated in Section 4.2.3.2. For modern codes, this has brought about a return to the simple stress range versus cycle life model for fatigue strength suggested by Wöhler almost 150 years ago (Wöhler, 1870). Furthermore, independence of steel grade was justified by the use of a large database of laboratory results taken from tests of different steel grades produced in different countries. Code developers have taken advantage of such opportunities and, consequently, fatigue design guidelines have been greatly simplified and harmonized internationally.

Consider a weld used to join adjacent plates as shown in Figure 2.3.1.1-1. As the weld cools, it tries to contract in width and, more importantly, in length. However, since the plate and the weld must maintain compatibility of length, the relatively cooler (and thus less expanded) plate restrains the weld during the cooling and contraction process. This puts the weld and a relatively small volume of plate adjacent to the weld into tension. Conversely, the main portion of the plate is compressed by the contracting weld, thereby placing it into compression. The resulting

stresses from this process are called residual stresses. Since there are no external forces applied during this process, the equilibrium condition of the cross section must be reflected in the balance between residual tensile stress and the area over which it acts and the residual compressive stress and its associated area. The actual distribution and magnitude of the residual stress pattern depends upon such factors as the strength of the steel and the weld metal, the sequencing of the welds, the geometry of the connected parts, and the size of the weld relative to the connected parts. The important fact, however, is that the magnitude of the tensile residual stress can reach the yield strength of the material.

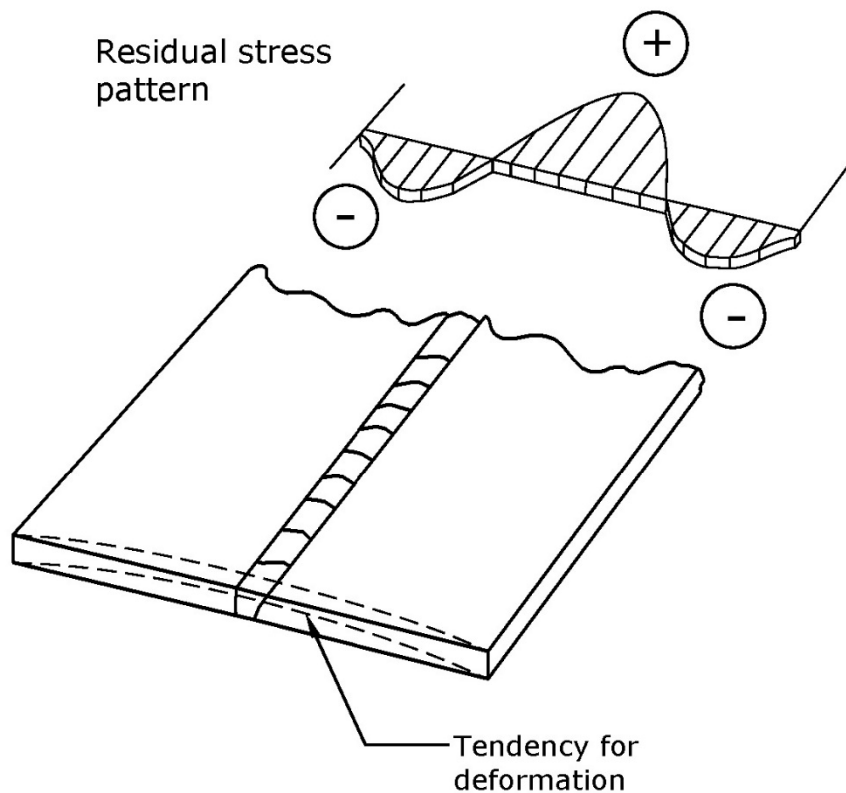


Figure 2.3.1.1-1 Residual stresses in groove-weld connected plates.

It follows, of course, that the rolled shapes or built-up members used in structural applications also contain regions of high residual tensile stress. For example, very large residual tensile stresses are present at the junction of the flange and web of a beam that has been built up by welding the component parts together. This junction is also the location of the discontinuities that are a potential source of fatigue crack growth, which means that the discontinuity is under a condition of initial stress even before load is applied. For the usual condition wherein this initial stress is at or near the yield strength, this means that stress range, rather than the maximum applied stress, the stress ratio (ratio of maximum stress to minimum stress), or some other parameter of applied stress, is the governing condition describing fatigue crack growth. The

concept of stress range is thus the fundamental characterizing parameter used to design and assess steel structures for fatigue. This is reflected in the AASHTO approach.

To summarize, in large welded structures, there are very high tensile residual stresses near potential fatigue crack sites, and their presence significantly reduces the effects of mean stress level of the applied stresses and steel grade upon crack propagation for standard weldable structural steels. As a result, it is generally agreed that stress range is the dominant stress parameter for fatigue design.

2.3.1.2 Dead-Load Stresses from Construction

Sustained dead-load stress accumulates during the construction of a bridge. Since stress due to dead load is constant and always present in the member, as illustrated by the horizontal dashed line in Figure 2.3-1, the change in stress is always simply equal to the change in stress produced by the cyclical loads, as discussed in Section 2.3.2.

As discussed in Section 2.3.1.1, the dead-load stress is not significant for fatigue as the residual tensile stress local to the weld toe is typically at or near the yield strength, making the dead-load stress inconsequential.

2.3.2 Cyclical Stress

2.3.2.1 Transportation and Handling

In a few unique cases, fatigue cracks have been discovered prior to bridges being put into service as a result of stresses induced during transportation and handling (Fisher, 1984). In a case study of the I-480 Cuyahoga River Bridge in Ohio, longitudinal fatigue cracks were observed in girder webs in the gaps at the ends of transverse stiffeners cut short of the bottom flanges, a location where cracks would not occur during service.

All of the cracks were located near the wooden blocks used to support the girders during shipment by rail. Similar girders shipped by truck were crack-free. Stiffeners were welded to both sides of the flange, and cracks were also observed in each side of the web. Vertical tie-down rods used to support the girders offered little resistance to lateral movement of the girders. Twisting of the girder flanges resting on the wooden support blocks occurred from the lateral sway of the girder due to improper blocking of the gap to prevent the distortion. Fatigue cracks were caused by large cyclical web-bending stresses in the short web gap.

2.3.2.2 In-Service Live Load

Figure 2.3-1 shows the applied stress history at a certain location in a member as a truck crosses a bridge. Shown are the maximum live-load stress, the minimum live-load stress, and the dead-load stress. In any history of stress versus time, there is one absolute maximum live-load stress and one absolute minimum live-load stress. The stress range between these two extremes is shown in the figure. (It is noteworthy that the stress range is independent of the dead-load stress,

and it has already been indicated that stress range is the dominant stress-related feature of fatigue-resistance determination.) However, there can be other "local" maximum and minimum live-load stresses. This leads to the question: how is the detail under examination for fatigue resistance influenced by these other stress variations? A method is presented in Chapter 4 that accounts for the fatigue damage that results when the cyclical loading is not applied at a constant harmonic amplitude.

Though fatigue is driven by tensile stresses, the entire stress-range excursion, tensile and compressive stress, is considered. Since local to the weld toe, the residual stress is at or near the yield strength, the superposition of residual and applied stresses produces an excursion entirely in tension. If the stress range is entirely in compression, it is not considered for fatigue, as a crack cannot grow beyond the extremely small zone of residual tensile stresses at the weld toe.

2.3.3 Stress Concentrations from Details

All elements of a fabricated steel structure contain production- or fabrication-related discontinuities, and most also include stress concentrators, such as weld toes, located at details such as attachments or connections.

At the attachment, the nominal stress (i.e., the stress in the member away from any stress concentration) becomes amplified from several sources of stress concentration, as illustrated in Figure 2.3.3-1. First, the amplification is reflected in the local structural stress (which is also commonly referred to as the hot-spot stress). AASHTO defines the local structural stress as the stress at a welded detail including all stress raising effects of a structural detail but excluding all stress concentrations due to the local weld profile itself. Second, there is the local total stress. While the local structural stress is computed using extrapolation methods, the local total stress is not based on extrapolation. Rather it is based upon an analysis which includes the weld geometry.

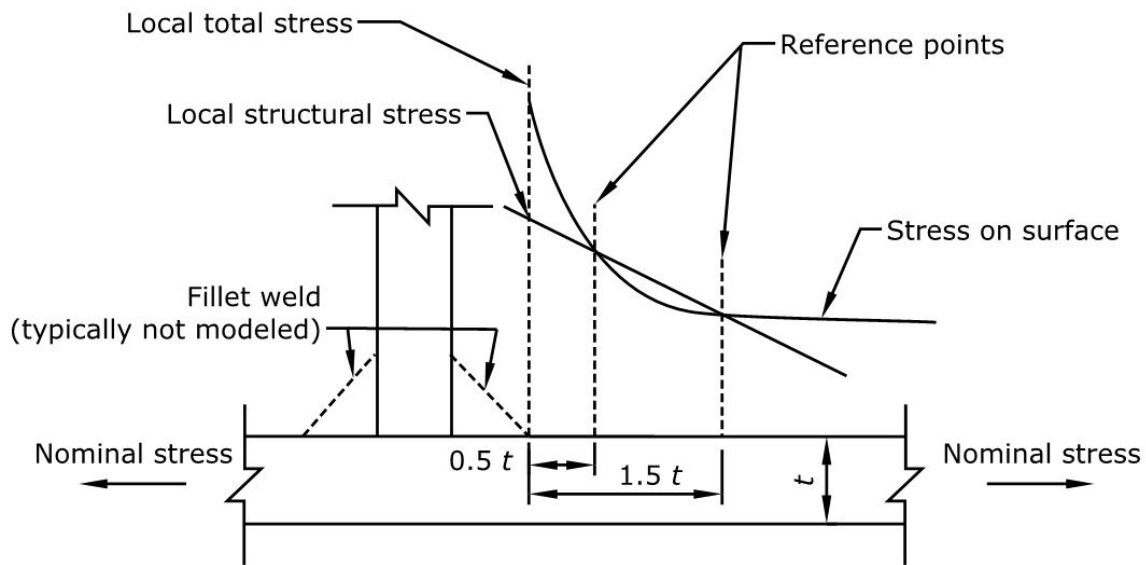


Figure 2.3.3-1 Concentration of nominal stress into local structural stress and local total stress.

SECTION 2.4 MATERIAL BEHAVIOR

2.4.1 Brittle versus Ductile Behavior

Structural steels fail in either a ductile or brittle manner, as introduced in Section 2.1.2.3, depending upon conditions such as temperature, strain rate, material toughness, and constraint. Ductile failures are typically preceded by large amounts of plastic deformation and are characterized by a failure surface oriented 45 degrees to the applied stress. Brittle failures typically occur with little or no prior plastic deformation and at extremely high speeds, approaching 7000 ft/sec in steels (Barsom and Rolfe, 1999). They are characterized by a failure surface oriented normal to the applied stress. The fracture of the Caltrans Workers Memorial Bridge (originally known as the Bryte Bend Bridge) in Sacramento, California in 1970 is shown in Figure 2.4.1-1. The failure is attributed to the low-toughness of ASTM A514 steel at a reentrant corner detail (between a transverse brace and the tension flange of the tub girder) in the presence of a weld-toe crack from fabrication and/or shipping. Note the characteristic appearance of the brittle fracture surface showing chevron marks (highlighted in the figure) in the flange pointing back to the fracture initiation site.

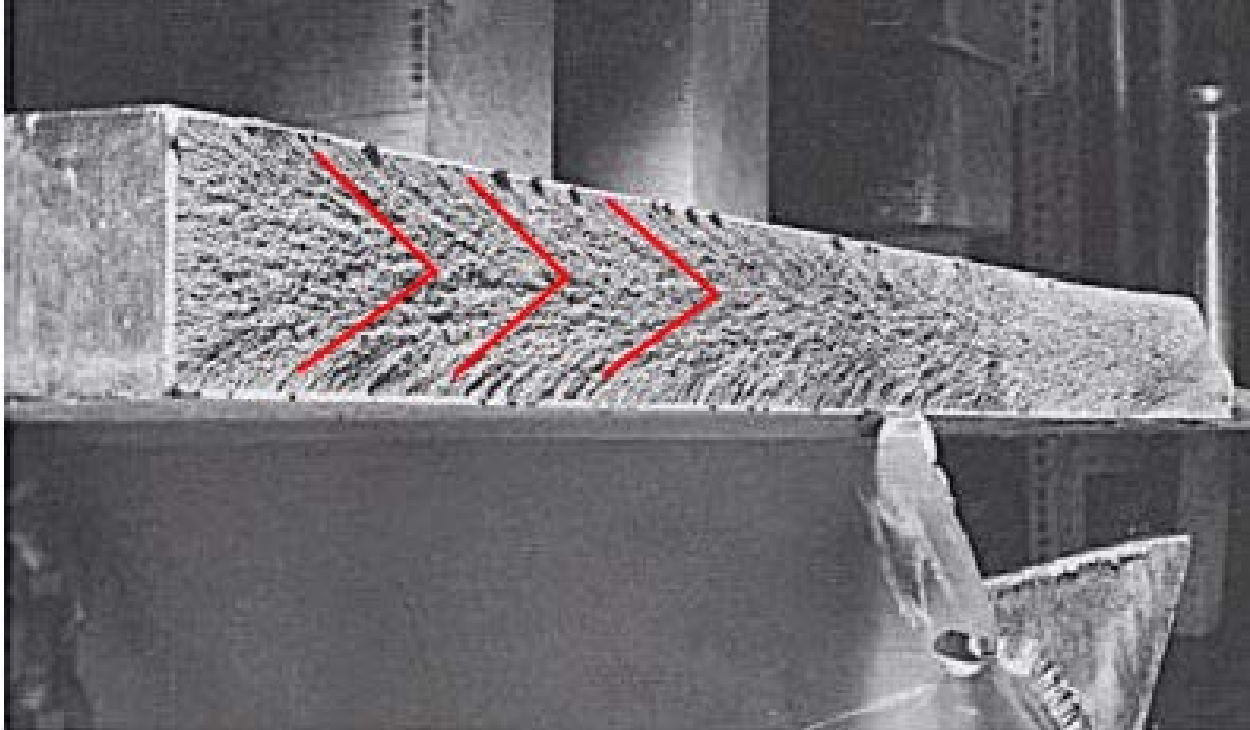


Figure 2.4.1-1 Fractured tub-girder flange from the Caltrans Workers Memorial Bridge (with chevron marks highlighted).

Brittle versus ductile behavior is influenced by fracture toughness of the material. An accurate determination of the fracture toughness is complicated, especially in most structural engineering design situations. Less sophisticated approaches are used for practical problems in structural engineering. The most widely used method for approximating the toughness quality of a steel is a procedure that was developed over 80 years ago known as the Charpy V-notch (CVN) impact test. In brief, this method measures the energy absorbed by the rapid fracture of a small bar containing a machined notch. The bar is broken by a swinging pendulum, and the absorbed energy is measured by the difference in swing height before and after fracture.

A plot of CVN absorbed energy as a function of temperature is shown in Figure 2.4.1-2. The CVN absorbed energies shown in the lower left portion of the figure are characteristic of lower levels of notch toughness or brittle behavior at low test temperatures (the lower shelf), while the CVN absorbed energies in the upper right portion at higher temperatures (the upper shelf) are characteristic of ductile behavior. The region between these two extremes is called the transition region.

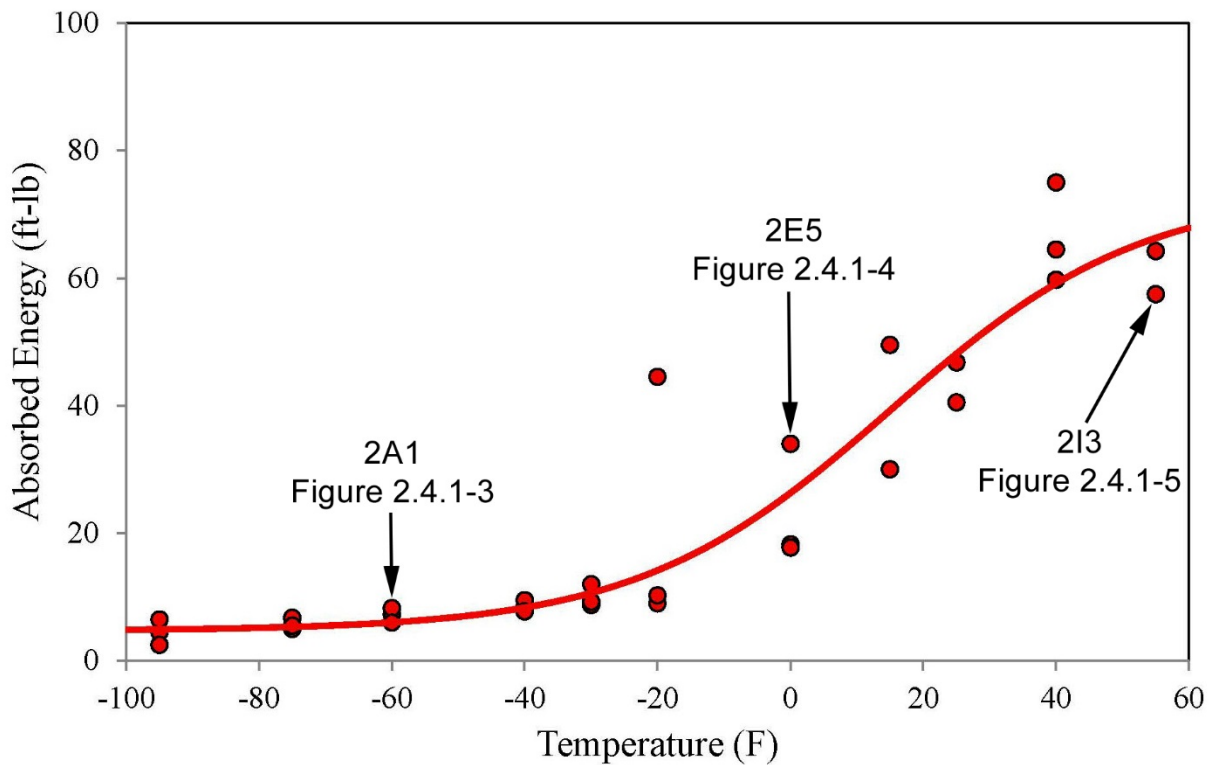


Figure 2.4.1-2 Charpy V-notch absorbed energy as a function of temperature.

The fracture surfaces of three of the Charpy V-notch specimens are called out in Figure 2.4.1-2 and shown separately in Figure 2.4.1-3, Figure 2.4.1-4, and Figure 2.4.1-5. The fracture surface on the specimen at -60°F (below the transition region) is characterized by flat fracture surfaces (brittle behavior) and no noticeable change in width at the notch. The fracture surface at 55°F (above the transition region) is characterized by shear lips (ductile behavior) and a noticeable change in width at the notch. The specimen at 0°F exemplifies the transition.

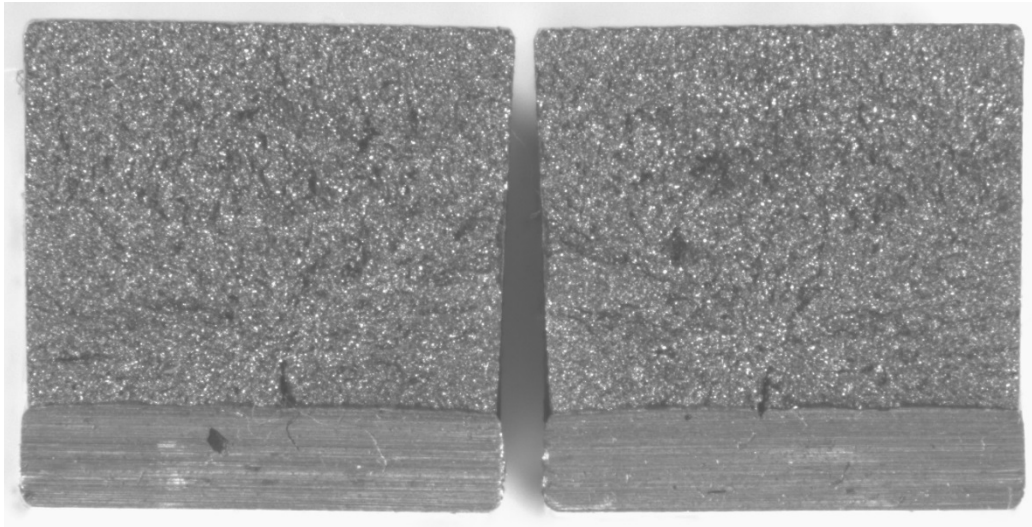


Figure 2.4.1-3 Photograph of fracture surface of Charpy V-notch Specimen 2A1 tested at lower temperature (see Figure 2.4.1-2).

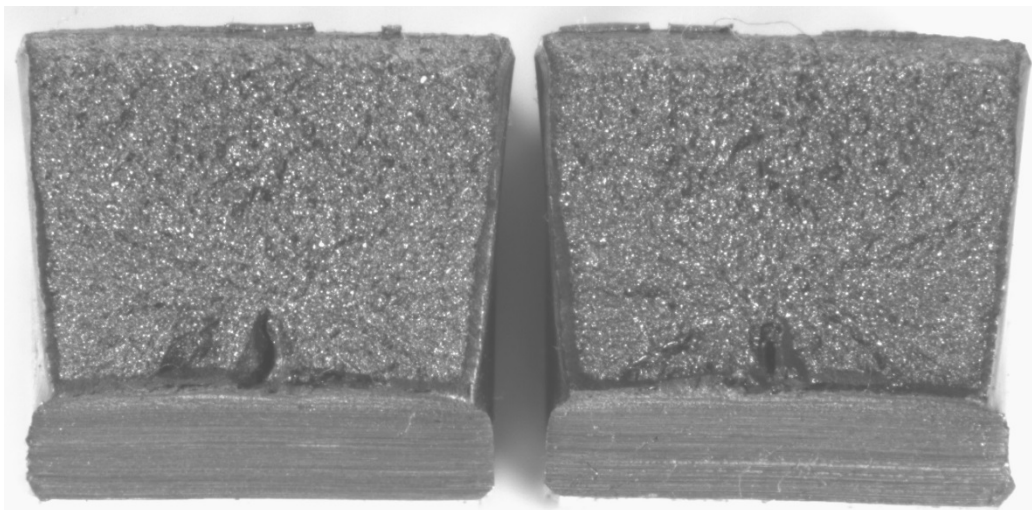


Figure 2.4.1-4 Photograph of fracture surface of Charpy V-notch Specimen 2E5 tested at the transition temperature (see Figure 2.4.1-2).

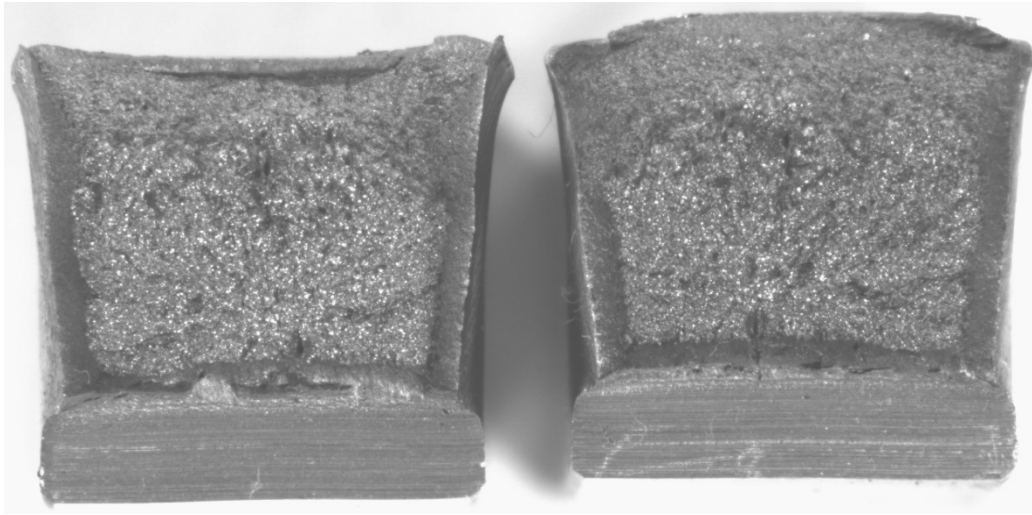


Figure 2.4.1-5 Photograph of fracture surface of Charpy V-notch Specimen 2I3 tested at higher temperature (see Figure 2.4.1-2).

Some materials other than bridge steels do not exhibit a distinct transition behavior. Other materials exhibit relatively low notch toughness at all temperatures (such as high-strength aluminum), yet others exhibit relatively high notch toughness at all temperatures (such as steels with yield strengths greater than bridge steels).

Bridges are designed to preclude fracture based upon proper material selection or, when applicable, the use of a Fracture Control Plan (FCP) per the *Bridge Welding Code* (AASHTO/AWS, 2010). A transition temperature is established as an indication of the notch toughness of a structural material. The designer selects a steel with a fracture-toughness level that is sufficiently high above the transition temperature for the intended application, as discussed in detail in Chapter 7. Thus the design for fracture is a function of material specifications and fabrication control rather than fracture mechanics analysis methods.

2.4.2 Effects of Temperature and Strain Rates

CVN tests are performed at higher, more easily achieved, temperatures than bridge service temperatures. They are also performed at greater, more easily controlled, strain rates than bridge service loadings. Fortunately, correlations between test temperature and intermediate and impact strain rates are available and are well defined. These correlations allow for the use of this common and simple test to characterize the expected in-service performance of bridge steels.

In general, the fracture toughness of steels increases with increasing temperature and decreasing strain rate. This behavior is shown schematically in Figure 2.4.2-1. The transition from brittle to ductile behavior begins at lower temperatures for specimens tested at slow loading rates, compared with specimens tested at impact loading rates used in CVN tests. The shift in transition curves between bridge loading (intermediate, with approximately 1.0 second loading to fracture) and impact (less than 0.001 second to fracture) is about 75 percent of the shift between static and impact curves.

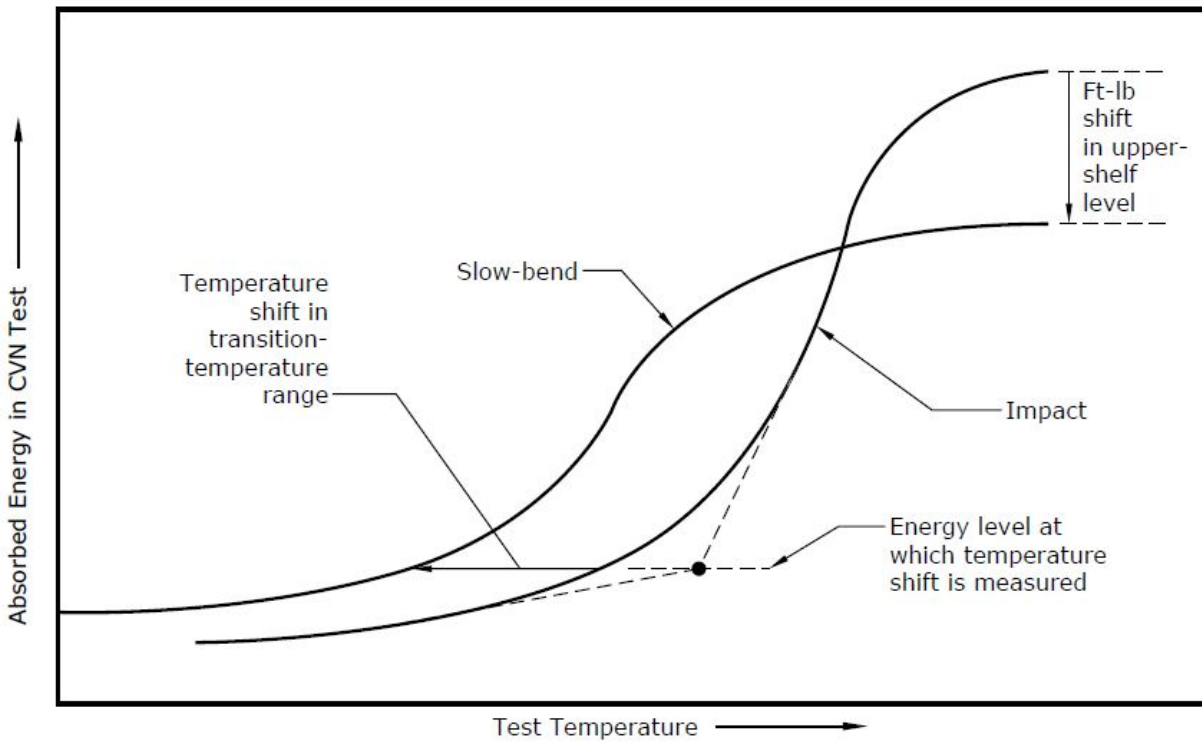


Figure 2.4.2-1 Schematic representation of the shift in temperature and upper shelf due to strain rate.

The fracture behavior of bridge steels as a function of the temperature shift based upon loading rate in conjunction with the fracture criterion and the AASHTO operating temperature zones (AASHTO, 2015b) results in the AASHTO FCP (AASHTO/AWS, 2010), discussed in detail in Chapter 7.

CHAPTER 3 THEORY

SECTION 3.1 GENERAL

Fracture mechanics provides a theoretical basis for understanding many aspects of fatigue and fracture behavior in steel structures. The use of the fracture mechanics method of analysis is relatively recent. Originally advanced to explain the rupture of glass specimens (Griffith, 1921), its introduction into the field of structural engineering practice started when it was used in the 1940's to help explain the catastrophic failure of welded ship hulls. Currently it is employed to assess the behavior of elements used in machinery, pipelines, automotive parts, spacecraft, turbine blades, and many other components.

In this chapter, basic concepts of the fracture mechanics approach are described to assist the reader in understanding crack behavior and the basis of the fatigue and fracture design rules. For those who might need to design at higher levels of sophistication, it provides the basis for further reading and self-instruction.

Only a basic level of fracture mechanics concepts is employed in this chapter. For simplicity, the discussion is limited to cases in which the loads are applied at locations remote from the crack locations and normal to the crack surfaces, the so-called Mode 1 configuration. Excellent review articles provide more detailed information (for example, see Irwin and de Wit, 1983; Rolfe, 1983; and Smith, 1978-79), and several reference books are available (Broek, 1984; Barsom and Rolfe, 1999; and Pellini, 1983). Detailed fracture mechanics application to the assessment of structures can be found in publications on fitness-for-service such as API 579-1/ASME FFS-1 (API, 2007) and BS 7910 (British Standards Institute, 2015).

SECTION 3.2 ACCOUNTING FOR A CRACK

Five cases of a loaded plate containing a crack are shown in Figure 3.2-1. It requires no knowledge of fracture mechanics to appreciate that Cases 1 through 5 are placed in order of increasing severity. Taking Case 1 as the basis for comparison, the following important fracture mechanics parameters can be identified as elements of the base case are changed:

- The influence of increasing the crack length (Case 2)
- The influence of crack location (i.e., at the edge of the plate) (Case 3)
- The addition of bending on an edge crack (Case 4)
- The presence of a stress concentration (Case 5)

Of course, the result of any of these parameters in weakening the plate will depend on the actual circumstances. The effect can be significant, however. For instance, the consequence of a sharp stress concentration in combination with a crack (Case 5) could weaken a plate to less than one-half of its uncracked strength.

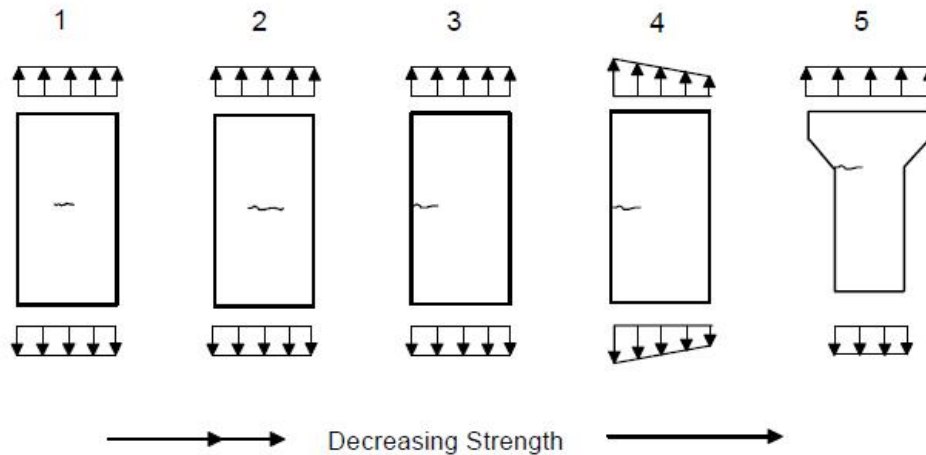


Figure 3.2-1 Five different cases of a plate containing a crack.

A magnified view of the area around a crack tip in an infinitely wide plate is shown in Figure 3.2-2. This resembles closely the conditions of Case 1 in which the crack length is small compared with the plate width. When a remote stress, σ , is applied, the crack opens a certain distance, d , and the stress that this cross-sectional area would have carried is diverted to the uncracked area of the plate. This diversion creates a high concentration of stress in the vicinity of the crack tip. For an elastic material, theoretically this stress is infinite at the crack tip which is modeled as having a sharp zero radius. In real materials, plastic zones are formed since the strain exceeds the ability of the material to behave elastically.

This process—whereby (1) an applied load causes a crack to open, (2) the crack opening relieves crack surfaces of stress, and (3) crack tip plastic straining is created—is the fundamental mechanism that weakens structures containing cracks or discontinuities. Fracture mechanics focuses on the local behavior at the crack tip. The state of stress at the crack tip controls whether the crack will advance under increase in load, producing unstable (brittle) crack extension or stable progressive extension under fatigue loading. (It should be noted that in bridge structures, cracking may not necessarily lead to unstable propagation, since in many cases the limited magnitude of stress may allow the cracking to arrest, resulting in the need for either no repair or simple repair.)

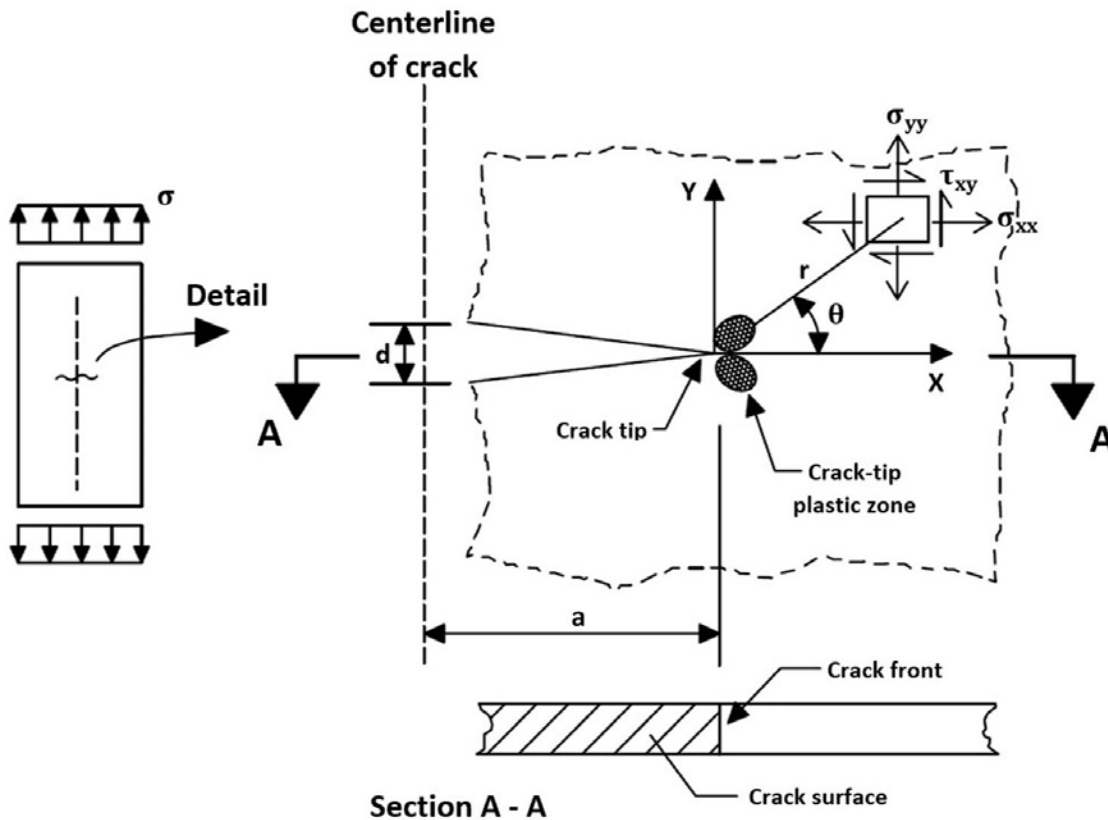


Figure 3.2-2 Crack stress field and crack characteristics in a wide plate.

If plasticity is ignored, a description of the stress field near the crack tip can be obtained. Using special stress functions, a solution containing the coordinates r and θ is developed. For the particular case of $\theta = 0$ (that is, for the stress in the y -direction), the stress is:

$$\sigma_{yy} = \frac{\sigma\sqrt{\pi a}}{\sqrt{2\pi r}}$$

Equation 3.2-1

provided that the crack length, a , is much larger than the distance from the crack tip, r , at which point the stresses are being evaluated and the crack length “ $2a$ ” is much smaller than the plate dimensions. The numerator in Equation 3.2-1 determines the gradient of the theoretical stresses as they rise to infinity when r approaches zero. This numerator is called the stress intensity factor, K , a single term characterizing the intensity of the stress at the crack tip. Thus:

$$K = \sigma\sqrt{\pi a}$$

Equation 3.2-2

The advantage of this model is that any combination of stress and crack length can be characterized by the single parameter K . Analytical solutions are available for other particular geometrical configurations and loading conditions; these are summarized in handbooks (Tada et al., 1985; Roark et al., 2012). However, many practical cases cannot be solved analytically. In such instances, the following expression is used to approximate K :

$$K = WY\sigma\sqrt{\pi a}$$

Equation 3.2-3

where Y is an expression that corrects for plate and crack geometry and W corrects for nonuniform local stress fields caused by stress concentration due to connection geometry and local residual stresses. Usually such correction factors are determined using numerical methods. However, solutions can also be found in handbooks.

As an example of the effect of crack geometry upon the stress intensity factor, the edge crack present in Cases 3 through 5 in Figure 3.2-1 produces a more severe case than the center crack in Cases 1 and 2. The crack length in the center crack is “ $2a$ ”, while the crack length in the edge crack is “ a ”. The value of Y in Equation 3.2-3 is 1.12 for an edge crack. Consequently, the ratio of the stress intensity factor of an edge crack to a center crack with equal crack lengths “ c ” and the same applied stress in a large plate is:

$$\frac{K_{edge}}{K_{center}} = \frac{1.12\sqrt{c}}{\sqrt{2}} = 1.58$$

Equation 3.2-4

A crack at an edge of a flange produces a 58 percent larger stress intensity factor at the crack tip than a similar size crack centered on the plate.

Equation 3.2-1 is based upon linear-elastic material behavior and cannot account for yielding at the crack tip. Furthermore, stress redistribution due to plasticity alters the stress field outside the crack tip plastic zone. Nevertheless, if the plastic zone is small, say less than 2 percent of the plate thickness, of the crack length, and of the uncracked ligament, then the elastic stress intensity factor (K) approach is satisfactory.

However, these limitations are violated in many practical situations. For example, an elastic-plastic analysis may be required when stress concentrations cause localized plasticity. The most common analyses either use a parameter named J , which is an expression of the change in potential energy with respect to crack length, or use a parameter called the crack tip opening displacement (CTOD). Further description of elastic-plastic analyses is available elsewhere (Barsom and Rolfe, 1999). In addition, ASTM has produced standards for determining these parameters experimentally (e.g., ASTM, 2013). These inelastic parameters can be approximately related by Equation 3.2-1. An equivalent elastic K value for plane stress can also be estimated using the following equation:

$$\frac{K^2}{E} = J = \sigma_y CTOD$$

Equation 3.2-5

where E is Young's modulus and σ_y is the effective yield strength. When plate thickness is large enough to restrict behavior to essentially two-dimensional straining (plane strain conditions), the material constant, E , is replaced by $E / (1 - \nu^2)$, where ν is Poisson's ratio. Steels with high resistance to fracture (high fracture toughness) can tolerate large inelastic strains at the crack tip before crack extension, while steels with low resistance to fracture exhibit little crack tip plasticity before fracturing.

A further restriction on K exists for small crack lengths, where all of the approaches explained above lose their validity. When the size of the crack or initial discontinuity is of the order of grain size, microstructural properties such as grain orientation influence crack growth (Lankford, 1985). Microstructural fracture mechanics models may then become necessary. These models are not yet well defined, and no generally accepted design rules are available. For the usual situation, when the crack length is greater than about five grain diameters, the models that assume an isotropic continuum (i.e., those employing K or J) are sufficiently accurate.

SECTION 3.3 PRINCIPLES OF FRACTURE CONTROL

3.3.1 Material Toughness

The collapse of the Point Pleasant Bridge from the brittle/unstable extension of a small flaw provided the impetus for the bridge engineering community to consider a new fracture control strategy which included the probable existence of a crack in a tension member. The realization of the possibility for a small crack to cause a complete fracture of a member led to the development of a fracture control plan. This plan consisted of revised fabrication, welding, and inspection standards, fracture toughness requirements for the steels and weldments, and more stringent fatigue design specifications. Later, after the collapse of the Mianus River Bridge, in-service inspection of nonredundant tension members also became more stringent.

An accurate determination of the fracture toughness is complicated, especially in most structural engineering design situations. This is primarily due to the fact that, for most designs, plane strain conditions do not dominate; conditions of essentially two-dimensional stress (plane stress) have an influence, thereby disqualifying K as a model that characterizes combinations of stress and crack length. Elastic-plastic models are needed because the stress at fracture produces a plastic zone size that exceeds the limitations cited for the validity of K specified in Section 3.2.

Less sophisticated approaches are used for practical problems in structural engineering. The most widely used method for approximating the toughness quality of a steel is a procedure that was developed in the early 1900's, the Charpy impact test, introduced in Chapter 2.

The Charpy impact test and many other similar procedures (Pellini, 1983) provide only qualitative information, because stress and crack length values cannot be assessed directly. However, correlation with fracture mechanics models is available for certain situations (Barsom

and Rolfe, 1999). For example, Charpy impact data in the lower region of the energy versus temperature response curve can be converted into dynamic plane-strain fracture toughness values, K_{I_d} , using an empirical formula. If required, the K_{I_d} values can then be converted to static plane-strain fracture toughness values, K_{I_c} . In general, such correlations are valid only for steels of low to medium strength which covers typical bridge steels. Moreover, the toughness value where conditions change from plane strain to plane stress depends upon the yield strength, crack geometry, and thickness of the element. These correlations provide an estimate for the material's resistance to crack propagation; they do not capture the resistance of a crack propagation, particularly in materials with high toughness to yield strength ratio.

At a given temperature, a given material will always exhibit higher fracture toughness for plane stress conditions than for plane strain conditions in the elastic-plastic region. Therefore, K_{I_c} and K_{I_d} are conservative first estimates of the fracture toughness. Elastic-plastic analyses, which result in less conservatism, can be used when the design problem justifies increased complexity of work.

The need for the steel to tolerate a crack which might form by fatigue from the extension of an initial small discontinuity (e.g., a tiny slag intrusion at the surface of the fusion line of a fillet weld or embedded discontinuity in a butt weld) was provided by including fracture toughness in the material specifications for tension members. The fracture toughness requirements are based upon the basic fracture mechanics relationship between applied stress, flaw size, and toughness:

$$K_{I_c} > K = WY\sigma\sqrt{\pi a}$$

Equation 3.3.1-1

where the left side of the inequality is K_{I_c} , the material's fracture toughness, and the right side is the stress intensity for the crack in the structure.

The stability of the crack as a function of the parameters of Equation 3.3.1-1 is shown in Figure 3.3.1-1. Combinations of crack size and stress level below the upper solid line have a stress intensity factor less than the fracture toughness of the material and represent stable cracks that can be tolerated in the material. The upper solid line shown in the graph is when K_{I_c} equals K , and this is the instability line similar to the limit defined by Euler buckling of a column. Combinations of stress and crack size above this line are unstable and will produce a brittle fracture. The fracture control strategy is designed to prevent the crack from reaching its critical size during the life of the structure. The level of fracture toughness specified by the Charpy V-notch energy requirements is designed to ensure that the critical crack size will be easily detectable by a close visual inspection of the bridge.

Higher strength steels require higher toughness to provide the same critical crack as a lower strength steel since the stress levels in the high strength steels are likely larger. Consequently, the toughness levels are higher for higher strength steel. Thicker components also require higher toughness due to the constraint offered by the thicker material, which limits the plasticity at the crack tip. In addition, thicker materials have larger crack sizes when the crack is visible on the surface of the plate.

The minimum toughness specified in the material specification provides the means to calculate a tension component's ability to resist brittle fracture. If the toughness is not specified, the designer does not have a basis to assure the flaw tolerance of the component. This is similar to what would occur if the yield or tensile strength was not specified; the designer would not be able to calculate the load resulting in yielding of the member.

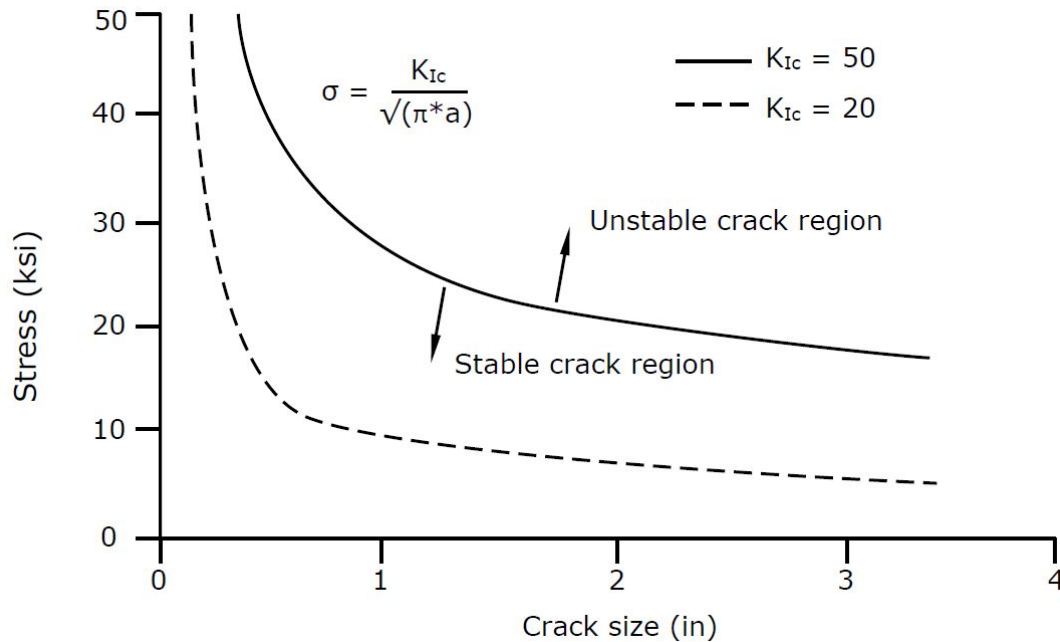


Figure 3.3.1-1 Fracture resistance as a function of toughness, stress, and crack size.

3.3.2 Effect of Critical Crack Size upon Inspection

As depicted in Figure 3.3.1-1, the critical crack size (i.e., the crack size that will trigger unstable crack propagation and fracture of the member) is a function of flaw size, applied stress, and fracture toughness. The lower dashed line in the figure represents the behavior if the toughness of the material is less. Similarly, the critical crack size for a given stress level decreases.

The eyebars in the Point Pleasant Bridge were fabricated with very low toughness steel. The critical crack depth was only approximately $\frac{1}{4}$ inch. Its companion bridge, the St. Mary's Bridge, was inspected after the collapse of the Point Pleasant Bridge to evaluate its safety. It was impossible to distinguish between cracks of this size and rust pits formed on the interior of the eyebar pin hole. Due to the low toughness or low flaw tolerance of the material, the safety of the bridge could not be reliably determined due to the inability to find these small cracks. The bridge was subsequently taken out of service and demolished.

Modern bridge steels used in tension members have toughness requirements to provide tolerable crack sizes that exceed the size crack that could frequently be missed in a field inspection. The toughness level increases with increase in yield strength since the stress level at failure in the member is controlled by the material's strength. The validity of the toughness requirements was verified in full-size girder tests performed at Lehigh University (Roberts et al., 1977c). The tests

showed that when the maximum design stress is applied to the girders at service loading rate with the specimen cooled to the lowest anticipated service temperature, fatigue cracks of the order of the plate thickness could be tolerated without producing a brittle fracture.

For bridges fabricated with toughness requirements, current in-service bridge inspection using primarily visual inspection provides adequate reliability. However, older welded bridges fabricated without toughness requirements may have much smaller critical flaw sizes and therefore may require more sensitive inspection techniques. Riveted bridges are not as critical since they do not have fatigue prone details and have inherent member redundancy.

3.3.3 Assurance through CVN Toughness Requirements

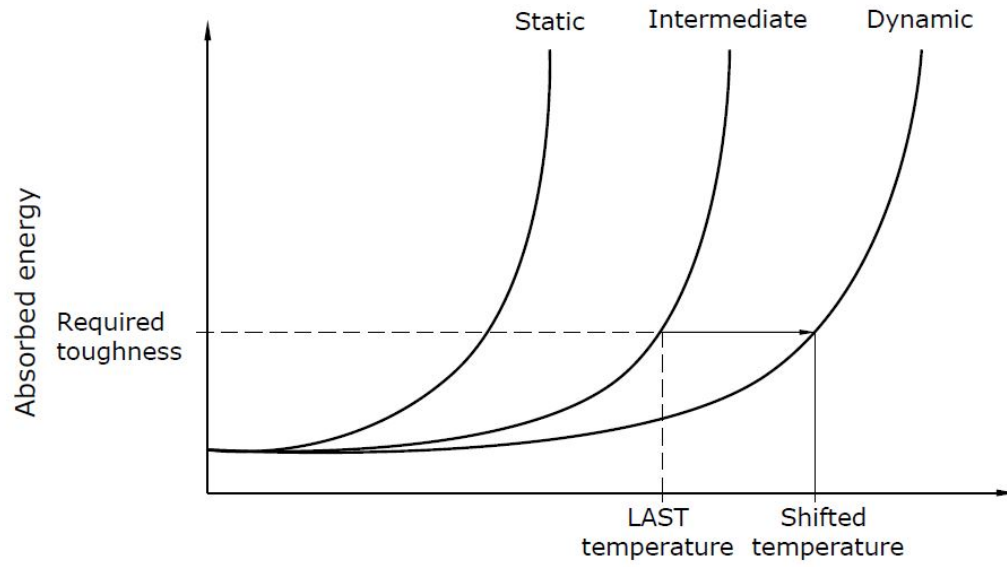
The grades of steels used in bridge structures have a complex fracture toughness behavior. The toughness of a given steel varies with the rate of loading and the temperature, as introduced in Chapter 2. Extensive tests have shown that the static and dynamic curves have similar shapes and that the difference between the two curves can be described in terms of difference in temperature, often called the temperature shift. The temperature shift for steels is inversely proportional to the yield strength, F_y , of the steel. Very high strength steels (i.e., steels with yield strengths of 150 ksi or greater) show no temperature shift; the dynamic and static curves are identical. However, for lower strength steels, the temperature shift can be estimated as:

$$T_s = 215 - 1.5F_y$$

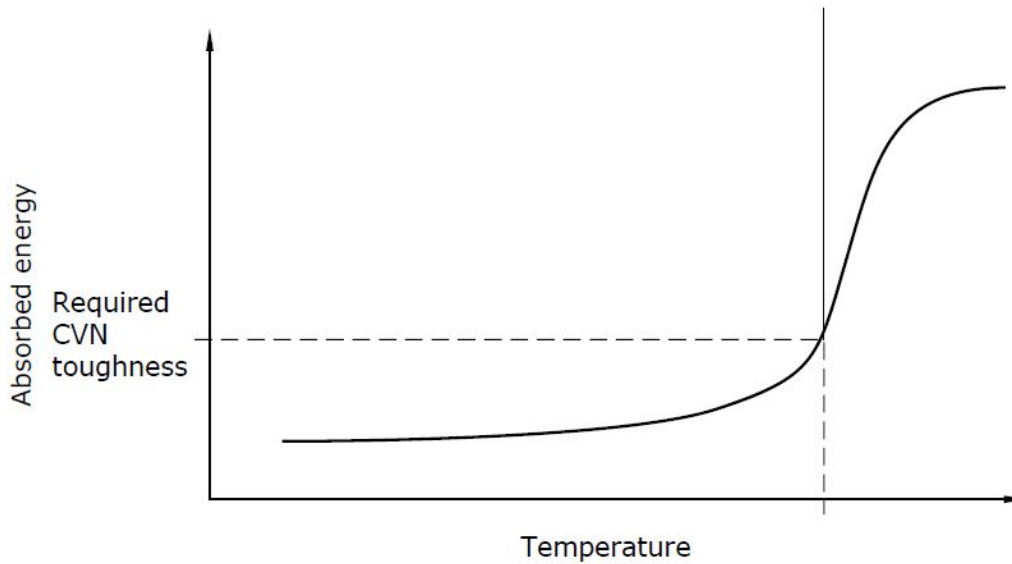
Equation 3.3.3-1

For example, a Grade 50 steel has a temperature shift of 140 °F. The Charpy V-notch (CVN) test used to measure the notch toughness of the structural steels is a dynamic test. The service loading rate of a bridge is an intermediate loading rate, 10^1 seconds. The response of the material at this intermediate loading rate is depicted by the curve between the dynamic and static curves. The difference in temperature between the dynamic and intermediate curves is approximately $0.75T_s$.

The test temperature used for the dynamic CVN temperature is the lowest anticipated service temperature (often referred to as LAST) of the structure plus $0.75T_s$. This methodology is shown in Figure 3.3.3-1. The required toughness and LAST define the point on the intermediate loading rate toughness curve in Figure 3.3.3-1a. The temperature is shifted up to the dynamic curve using the temperature shift concept and finally down to the CVN curve of Figure 3.3.3-1b to define the required CVN energy at the shifted temperature.



(a) Controlled load rate test



(b) CVN test

Figure 3.3.3-1 CVN-toughness development.

A number of correlations have been developed to relate the fracture toughness to the notch toughness measured using CVN testing. The most commonly used correlation is of the form:

$$K_{Ia} = 12.5\sqrt{CVN} \quad (\text{in units of ksi}\sqrt{\text{in.}})$$

Equation 3.3.3-2

where CVN is the impact energy in ft-lbs absorbed by the steel in a dynamic CVN test.

For example, for a 50-ksi yield strength steel ($T_s = 140$ °F) to be used in a structure with a LAST of -35 °F, the CVN test temperature can be calculated as:

$$T_{CVN} = LAST + 0.75T_s = -35 + 0.75(140) = 70$$

Equation 3.3.3-3

The required toughness for a 1-inch through crack in the center of the plate can be calculated using Equation 3.2-2, where “ a ” is the half-crack length. Assuming the maximum applied stress can be up to the yield strength:

$$K_{required} = \sigma_y \sqrt{\pi a} = 50 \sqrt{0.5\pi} = 62.7 \text{ ksi}\sqrt{\text{in}}$$

Equation 3.3.3-4

The required CVN absorbed energy can be calculated using Equation 3.3.3-2:

$$CVN = \left(\frac{K_{Ic}}{12.5} \right)^2 = \left(\frac{62.7}{12.5} \right)^2 = 25.1 \text{ ft-lb}$$

Equation 3.3.3-5

Therefore, the material requirement is that the average of three CVN specimens tested at 70 °F must exceed 25 ft-lb.

Similar calculations were used to develop the toughness requirements in ASTM A709, the bridge steel specification. It should be noted that these requirements apply only to tension members. Fracture critical members have slightly higher toughness and lower test temperature to provide enhanced flaw tolerance. The weld metal toughness requirements in AWS D1.5 are more stringent than the base metal requirements, since the weld qualification geometry used to obtain the test specimens does not match the production welds. The weld qualification tests are used to ensure that the weld metal in the structure has a toughness equal to or greater than the base metal.

SECTION 3.4 PARIS' LAW AND MINER'S RULE

Extension of cracks by fatigue is labeled stable crack propagation since the crack extends a finite distance with each load cycle. The first application of fracture mechanics to fatigue crack propagation was in the aerospace industry by Paris, Gomez, and Anderson (Paris et al., 1961). They reasoned that the extension of a crack by fatigue would be proportional to the range of stress at the crack tip. They coined a new parameter to describe this range of stress in terms of the local elastic crack tip stress, referred to as Delta (Δ) K , as shown below.

$$\Delta K = \sigma_r WY\sqrt{\pi a}$$

Equation 3.4-1

They found that the average crack extension per load cycle, (which is also the slope of the crack extension curve), could be related to the value of Delta (Δ) K by a simple power law, often referred to as the Paris power law:

$$\frac{da}{dn} = C \Delta K^n$$

Equation 3.4-2

where:

$$\frac{da}{dn} = \text{average crack extension per load cycle}$$

They also found that a value of n equal to 4 best fit their data form studies of fatigue crack growth in aluminum aircraft alloys. The value of the coefficient C is a material property. Later studies in steels found that a value of n equal to 3 gave the best fit to the data.

Later studies indicated that as the maximum stress intensity of the crack approached the fracture toughness of the material, the crack growth accelerated. The later studies also indicated that if the value of Delta (Δ) K was small, no crack extension occurred. This limiting value is often termed the crack growth threshold and is written as Delta (Δ) K_{th} .

The fatigue crack growth under random loading similar to that produced by vehicles on a bridge was found to be proportional to the effective stress range in place of the constant stress range. The effective stress range is calculated using a rainflow cycle counting algorithm and Miner's linear cumulative damage law.

Miner's linear rule for variable amplitude fatigue is:

$$\sum \frac{n_i}{N_i} = 1$$

Equation 3.4-3

where n_i is the number of cycles at stress range i and N_i is the constant amplitude fatigue life at the stress level i .

These values can be written as:

$$N_i = A \sigma_{r_i}^{-n}$$

Equation 3.4-4

and $n_i = \gamma_i T$, where T is the total number of cycles and γ_i is the fraction of the total cycles occurring at stress level i .

Substituting these values into Miner's rule yields:

$$\sum \frac{n_i}{N_i} = \sum \frac{\gamma_i T}{A \sigma_{r_i}^{-n}} = \frac{T}{A} \sum \gamma_i \sigma_{r_i}^n = 1$$

Equation 3.4-5

Rewriting the equation, the total number of fatigue cycles to failure, T , becomes:

$$T = \frac{A}{\sum \gamma_i \sigma_{r_i}^n}$$

Equation 3.4-6

Equation 3.4-6 has the same form as Equation 3.4-4, the equation for the constant amplitude fatigue life. The effective stress range, defined as the constant amplitude stress range that will produce the same fatigue life as the variable amplitude stress history, is:

$$\sigma_{re} = \left(\sum \gamma_i \sigma_{r_i}^n \right)^{1/n}$$

Equation 3.4-7

Substituting into Equation 3.4-7 a crack growth exponent of 3 for structural steels yields the following:

$$\sigma_{re} = \left(\sum \gamma_i \sigma_{r_i}^3 \right)^{1/3}$$

Equation 3.4-8

This relationship was used to relate the typical traffic vehicle spectrum of fatigue stresses into a constant level stress range which produces the same fatigue damage, which in turn becomes the fatigue design truck.

SECTION 3.5 FRACTURE MECHANICS AS A QUANTITATIVE TOOL

The basic fracture mechanics concepts can provide insight into the resistance of structures under fatigue loading. The Paris power law presented in Equation 3.4-2 provides a method to calculate the fatigue resistance of a structure. The equation may be rewritten in the following form:

$$\text{Fatigue Life} = N = \int dn = \frac{1}{C \sigma_r^3} \int_{a_i}^{a_c} (WY\sqrt{\pi a})^{-3} da$$

Equation 3.5-1

where:

- a_i = initial crack length (inches)
 a_c = critical crack length (inches)
 σ_r = stress range (ksi)
 C = crack growth constant for the material = 3.6×10^{-10} for structural steel with a crack growth exponent of $n = 3$

If the functions of W and Y are known, the fatigue life can be calculated using this equation. Normally, due to the complexity of these expressions, the integral must be evaluated numerically.

To demonstrate the use of Equation 3.5-1, it will be used to evaluate the fatigue life of a wide cracked plate with a crack length of $2a$ in the center, as shown in Figure 3.5-1. The stress is applied remotely from the crack, and the width of the plate is much larger than the crack length, $2a$. Therefore, W and Y both equal 1, allowing the integration to be performed quite simply.

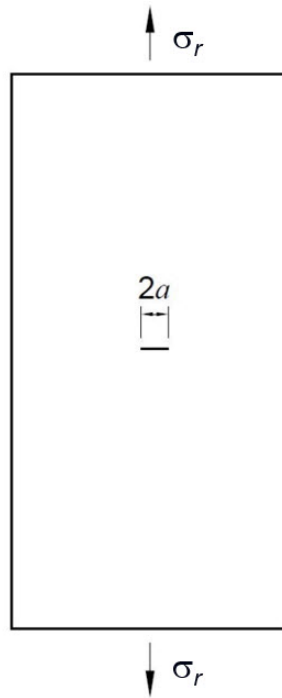


Figure 3.5-1 Wide cracked plate with a crack length of $2a$ in the center.

For this example, Equation 3.5-1 results in the following:

$$N = \frac{1}{\sigma_r^3 C \pi^{3/2}} \frac{2}{\sqrt{a_i}} \left[1 - \sqrt{a_i/a_c} \right]$$

Equation 3.5-2

The term in the parentheses provides a means of evaluating the significance of the initial flaw size to the critical flaw size. If a_i and a_c are of comparable size, the fatigue life becomes very

short. However, if the initial flaw size is controlled during fabrication through the shop inspection requirements and the critical flaw size provided by the material's fracture toughness is of the order of the plate thickness, then the term in the parentheses approaches 1 and the critical flaw size has minimal effect on the fatigue life. If a_i is much smaller than a_c , then the estimate of the fatigue life becomes:

$$N = \frac{1}{C\pi^{3/2}} \frac{2}{\sqrt{\sigma_r^6 a_i}}$$

Equation 3.5-3

The initial crack size and stress range have been placed under the radical sign to demonstrate the relative importance that each has on the fatigue life. A 10 percent reduction in the initial flaw size results in a 5 percent increase in fatigue life, while a 10 percent reduction in the stress range results in a 37 percent increase in fatigue life. As a consequence, a reduction in the design stress range is the most effective method of increasing fatigue resistance of a structure, given that the ratio a_i to a_c is small.

The more general form of the fatigue life equation, Equation 3.5-1, can be helpful in interpreting and understanding the AASHTO fatigue categories. The equation is written again as:

$$\text{Fatigue Life} = N = \int dn = \frac{1}{C\sigma_r^3} \int_{a_i}^{a_c} (WY\sqrt{\pi a})^{-3} da$$

Equation 3.5-4

The integral shown in brackets is a function of the crack and detail geometry and the initial and final crack size. For a given fatigue detail, this would be a constant if the geometry and initial flaw size are controlled. However, for practical welded bridge construction, these become random variables, although limited by the fabrication standards. Consequently, the fatigue life of replicate test specimens typically will not be a single value. The fatigue life categories in AASHTO are based upon a lower bound of the fatigue strength that consider the variability of these variables upon fatigue resistance. If A is defined as the value of the term in brackets divided by the crack growth constant, C , then fatigue life can be defined using the following simple expression:

$$\text{Fatigue Life} = N = \int dn = \frac{A}{\sigma_r^3}$$

Equation 3.5-5

Taking the logarithm of each side of the equation provides a linear log-log relationship:

$$\text{Log } N = \text{Log } A - 3 \text{Log } \sigma_r$$

Equation 3.5-6

This is the form of the AASHTO fatigue requirements. AASHTO provides the value of A for each fatigue category.

CHAPTER 4 FATIGUE BEHAVIOR

As introduced in Chapter 2, fatigue in steel structures is the process of growth of cracks under the action of repetitive tensile loads. Further, in Chapters 2 and 3, the presence of discontinuities is revealed to be one of two conditions necessary for fatigue-crack growth. The fatigue life of a component is dependent upon the applied stress range, the initial discontinuity introduced during fabrication, and local stress increase due to the joint geometry. The influence of each of these variables is discussed in this chapter.

SECTION 4.1 THE INFLUENCE OF PRODUCTION AND FABRICATION

Discontinuities exist in all fabricated steel structures as a consequence of the manufacturing process of the steel itself and/or the normal fabrication processes of the components.

The term “discontinuity” does not necessarily imply defect. A discontinuity may or may not be classified as a defect, depending upon its size and orientation in the member or connection. Discontinuities are rejectable only if they exceed the specification requirements for type, size, distribution, or location. These acceptance criteria can be found in the *AASHTO/AWS D1.5 Bridge Welding Code* for weldments (AASHTO/AWS, 2010), ASTM A6 for base metal (ASTM, 2014), and the *AASHTO LRFD Bridge Construction Specifications* (AASHTO, 2015a). All cracks detected during the shop inspection are rejectable. The shop inspection serves to ensure that any discontinuities that remain in the weld will not reduce the design fatigue resistance.

4.1.1 Materials and Processing

Discontinuities may be found in the base metal of rolled shapes and plates. Figure 4.1.1-1 illustrates representative discontinuities for a rolled beam.

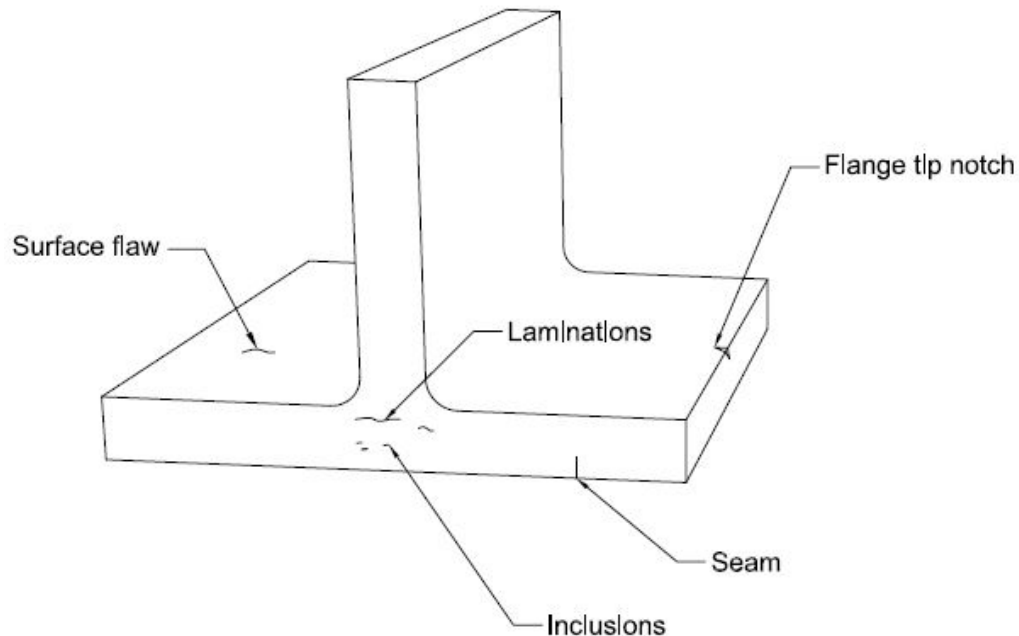


Figure 4.1.1-1 Examples of discontinuities in a rolled beam.

Seams and laps are longitudinal base-metal discontinuities in rolled shapes and plates. When located parallel to the applied stress, they are generally not considered critical. When perpendicular to the applied stresses, they can propagate as cracks. Seams and laps are surface-connected discontinuities that result from cracks in the surface of the slab or mechanical deformations caused by the manufacturing process. Rolling blunts the discontinuities such that the seam is generally not as sharp as the original slab crack.

Laminations are planar discontinuities elongated during rolling. They generally are parallel to the surfaces and are most commonly found near the mid-thickness of rolled shapes or plates. Laminations may be completely internal, or they may extend to an edge. Laminations are formed when gas voids, nonmetallics, or slab shrinkage cavities are rolled flat.

Inclusions result from nonmetallic, solid material being entrapped in slabs during the steel production process and flattened during rolling. These discontinuities sometimes appear after flame cutting the plate to size or beveling the plate in preparation for a groove weld. The AWS D1.5 specifications (AASHTO/AWS, 2010) limits the size of these planar discontinuities that may be left in place. Larger discontinuities must be either ground out or repaired by welding.

Some joint geometries can produce large through thickness stresses, such as the corner joint shown in Figure 4.1.1-2. The stress caused the shrinkage of the welds on each side of the plate and produced a tear in the center vertical plate. Figure 4.1.1-3 shows an improved detail with the weld preparation on the vertical plate which engages any discontinuities in the plates and limits the through thickness stress generated by the weld shrinkage. Other joint improvements are shown as well. This topic is further covered in Section 7.1.4.2.

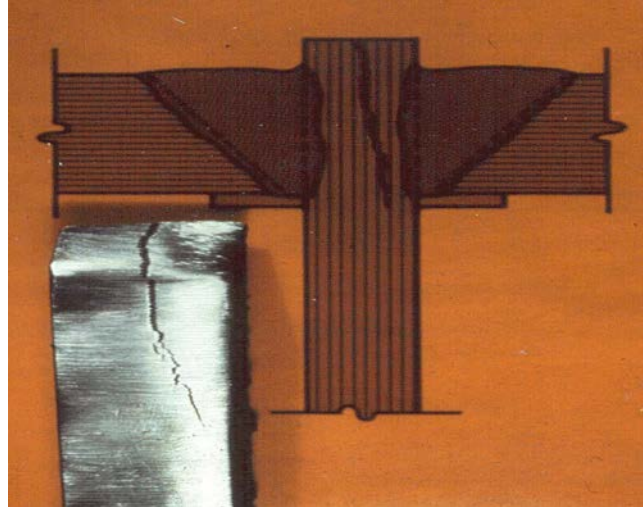


Figure 4.1.1-2 Lamellar tear due to through thickness stresses from weld shrinkage.

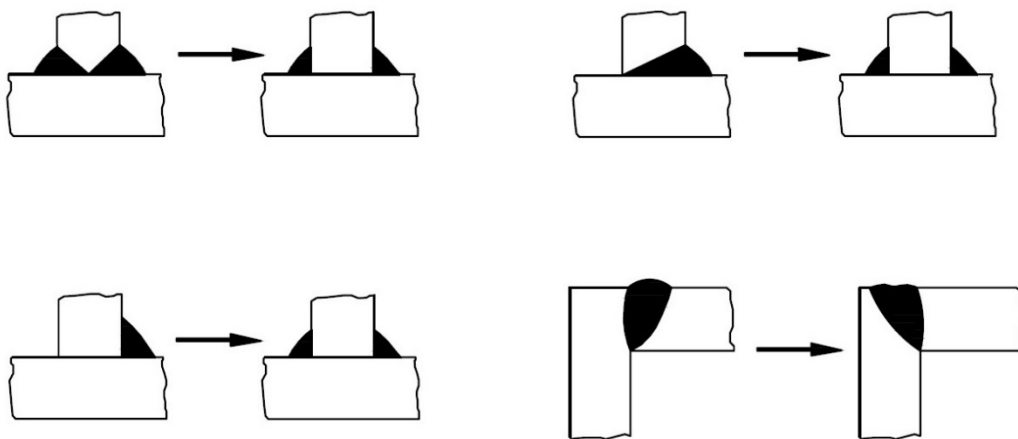


Figure 4.1.1-3 Improved weld details to reduce through thickness stresses.

4.1.2 Discontinuities at Welded Joints

At welded joints, discontinuities may be found in the weld metal or in the heat-affected zone in butt, tee, corner, and lap joint configurations. Figure 4.1.2-1 illustrates representative discontinuities for a welded beam.

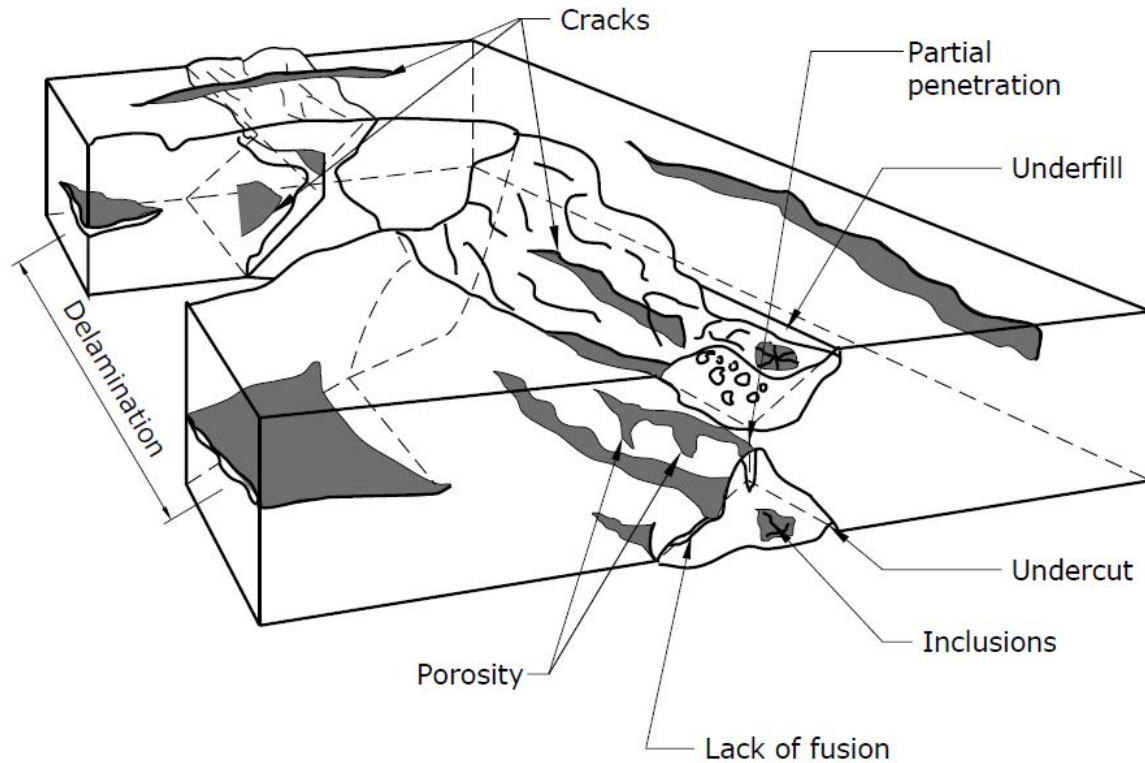


Figure 4.1.2-1 Examples of discontinuities in a welded beam.

Porosity is created when solidifying weld metal entraps gas. The discontinuity is generally spherical in shape but may be elongated. Undercut generally is the result of the molten weld metal not filling the base metal melted at the edge of the weld. It is caused by either improper technique and/or excessive weld heat. The *AWS Bridge Welding Code* requires that undercut greater than 0.01 inch must be repaired if the weld is transverse to the direction of applied stress (AASHTO/AWS, 2010). For longitudinal welds parallel to the direction of stress, such as web-to-flange welds, the allowable undercut depth is 1/32 inches. It is located at the junction of the weld and the base metal, at a fillet-weld toe (as shown in Figure 4.1.2-1), or at a groove-weld fusion line. The lack of fusion shown in the figure is the result of the fillet welds used in the connection. It is of no consequence if the applied stress is parallel with the weld. Fillet welds are commonly inspected using magnetic particle inspection which detects surface discontinuities. Internal discontinuities such as porosity are accounted for in the Category B fatigue design allowable stress ranges. However, if they are big enough, they are rejectable through the AASHTO/AWS D1.5 inspection acceptance criteria (AASHTO/AWS, 2010).

More complete descriptions of common discontinuities present in both weld and base metal can be found in *AWS Bridge Welding Code* (AASHTO/AWS, 2010).

A sample welded detail, as introduced in Figure 2.3.3-1, shows a plate under uniform stress with a longitudinal fillet-welded attachment. The nominal stress is the uniform stress away from the attachment and can be calculated using simple principles of strength of materials.

The nominal stress becomes amplified closer to the attachment from two sources of stress concentration. First, the effect of global geometry of the connection as the section changes from a plate to a tee section produces an elevated stress referred to as the local structural stress. Finally, the stress concentration due to the local geometry of the weld toe dependent upon random parameters, such as weld profile and ripples in the weld toe, elevates the local structural stress further, becoming the local total stress. The local total stress can be accurately characterized for a specific weld geometry but not for a category of details.

The effect of a variation in geometry can be understood by visualizing stress flow lines. Consider the case of a short fillet welded attachment in a flat plate, as shown in Figure 4.1.2-2. Away from the attachment, the flow lines are uniformly distributed across the width of the plate. The attachment must elongate with the plate as the plate is loaded, since the attachment is fixed to the plate by the weldment. Therefore, the attachment is stressed. As the stress “flows” into the attachment, a concentration of stress occurs at the weld toe, as shown in Figure 4.1.2-2. The amount of stress flowing into the attachment, and hence the stress concentration, is dependent on the attachment length parallel to the stress. As the length increases, more stress can flow into the attachment and the stress concentration increases. The AASHTO fatigue specifications recognize the effect of attachment length and thickness upon the local stress at the weld toe in their fatigue categories. The larger or longer the attachment, the lower the fatigue strength and corresponding fatigue category.

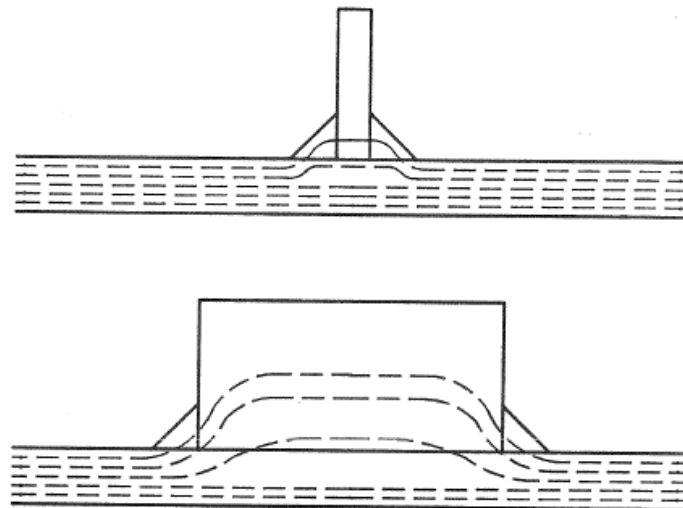


Figure 4.1.2-2 Stress flow lines in fillet-welded attachments.

As a general rule, details that involve crack growth from internal discontinuities, such as porosity, slag inclusions, cold laps, and other comparable conditions, will have a higher fatigue resistance. These discontinuities experience little or no stress concentration. Details that provide a lower fatigue resistance involve connections that experience fatigue crack growth from initial discontinuities in the weld toes and weld ends where there is a high stress concentration due to geometric conditions, as shown earlier in Figure 2.3.3-1.

The relative influence of discontinuities and the stress concentration on detail fatigue resistance is shown schematically in Figure 4.1.2-3. The fatigue resistance of detail types commonly used in bridge construction is characterized as Detail Categories A through E' (AASHTO, 2015b). The higher-resistant (greater fatigue life) details, such as Detail Category A (plain plate or rolled shape), are dominated by the initial discontinuity size and do not have large stress concentrations caused by a change in the cross section. The lower-resistant (lower fatigue life) details, such as Detail Category E', are dominated by larger stress concentrations at a weld toe with a much smaller initial discontinuity. The initial discontinuity curve peaks around Detail Category B due to the upper limit of discontinuity sizes as specified (AASHTO/AWS, 2010) for groove welded details and the acceptance of porosity in longitudinal fillet welds. The initial discontinuities in Detail Categories C through E' are the same, with small slag intrusions at the fusion line between the weld and base metal (Signes et al., 1967). The detail categories and their application in bridge design are discussed in detail in Chapter 6.

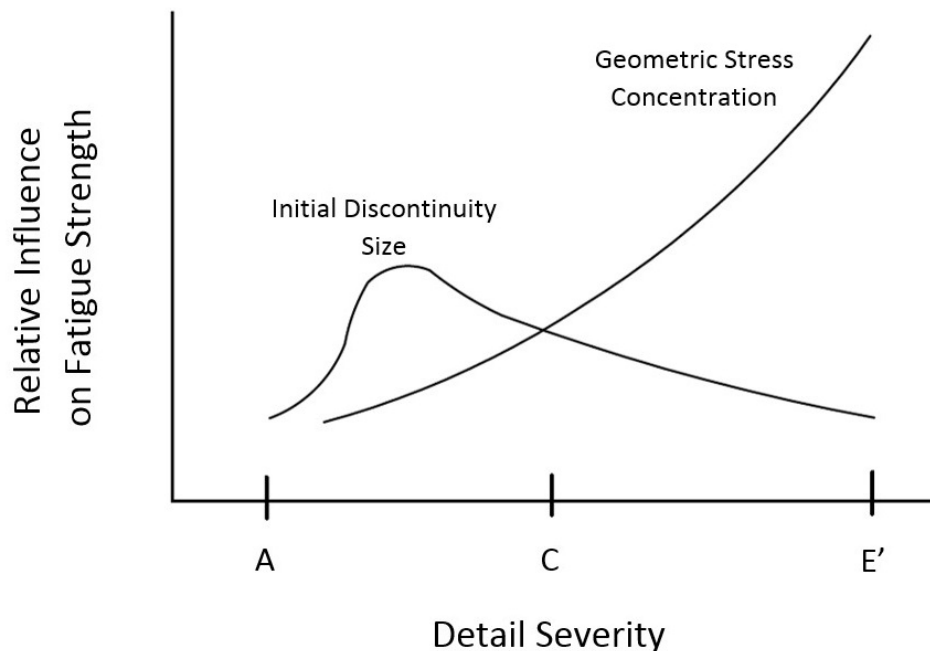


Figure 4.1.2-3 Relative influence of initial discontinuity size and stress concentration.

4.1.3 Weld Residual Stresses

4.1.3.1 Source and Magnitude

As introduced in Section 2.3.1.1, fabricated steel structures contain “residual” or “locked-in” stresses that have been introduced as a result of production and fabrication processes which cause differential cooling of the steel.

The results from residual stress measurements on beam specimens of three different steel types are plotted in Figure 4.1.3.1-1. These distributions correspond to the measured residual stresses

in the flanges of welded beam specimens and are in the longitudinal direction, parallel with the longitudinal axis of the web-to-flange fillet weld. As indicated by Figure 4.1.3.1-1, large tensile residual stresses were measured in the vicinity of the web-to-flange fillet welds. As the steel strength increased, the magnitude of the maximum tensile residual stress also increased and was near or above the yield strength for the weld metal itself. The residual stress at the tip of the flanges is also high. This residual stress at the flange tip is due to the thermal cutting of the flanges from wide plates. The quarter points of the flange are in compression. The sums of the residual tensile and compressive stresses are equal, and therefore the net internal force on the cross section is zero. The metal melted and heated during the welding and thermal cutting process will contract as it cools. The contraction of the heated area is resisted by the adjacent material which has not been heated. The differential shrinkage causes residual tensile stresses to form in the area that has been heated and compressive stresses in the unheated area.

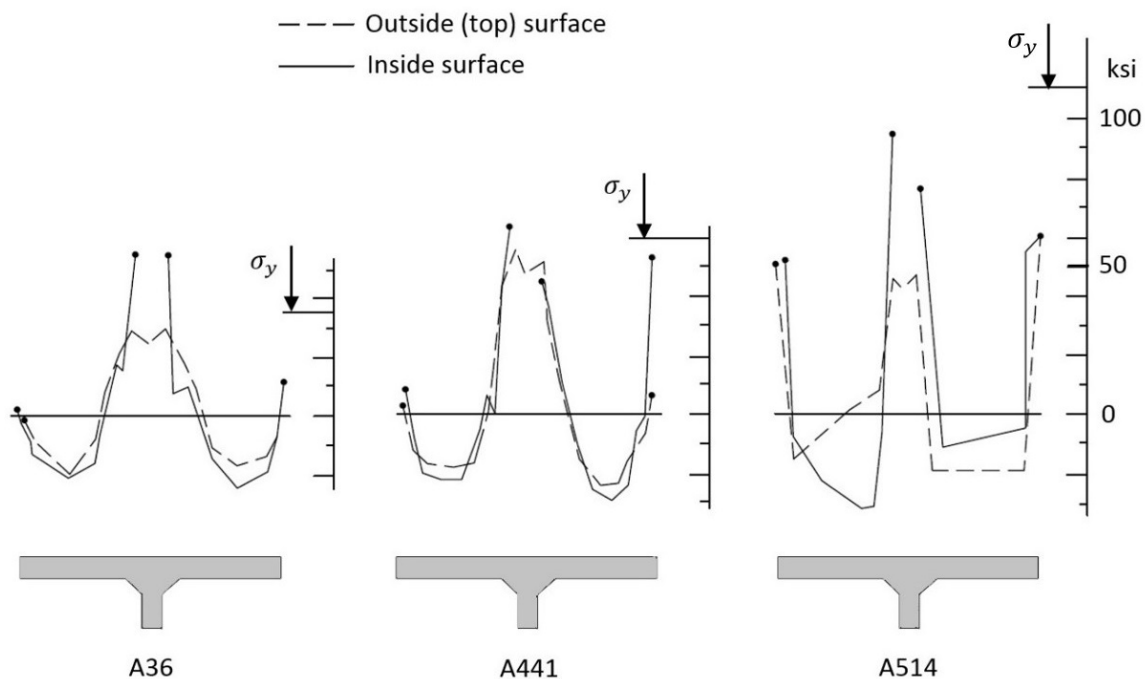


Figure 4.1.3.1-1 Residual-stress distributions in welded plate girder flanges.

For the typical condition in the vicinity of the welded fatigue detail where this initial residual stress is at or near the yield strength, stress range, rather than the maximum applied stress, the stress ratio, or some other parameter of applied stress, is the governing parameter characterizing fatigue-crack growth. The effect of the level of applied stress, the mean stress, upon fatigue life was studied in a factorial experiment using beam specimens and found to be statistically insignificant (Fisher et al., 1970). These full-size specimens used in the tests which define the fatigue life categories in the specification had the residual stresses at the details. Therefore, the effect of residual stress upon fatigue performance is incorporated into the specifications. This will be illustrated by the following numerical example.

Example

Figure 4.1.3.1-2 shows a rectangular plate and its assumed residual stress pattern. (This idealization could represent the flange of a welded beam.) This example illustrates how the local residual stress inherent in all welded structures influences the cyclic stress at a weld location.

Given:

According to the designer, the plate will be subjected to a maximum tensile stress of 31 ksi and a minimum compressive stress of 18 ksi. Calculate the net range of stress that will exist for a discontinuity at the center of the plate (cf., the junction of the web and flange of a welded beam). Compare this range of stress with the stress range that will be computed by the designer, that is, $+31 \text{ ksi} - (-18 \text{ ksi}) = 49 \text{ ksi}$. The plate has a yield strength of 44 ksi.

Solution:

Initial conditions: The pattern of residual stress is shown in Figure 4.1.3.1-2(a). It shows that the values of the initial residual stress are as high as the yield stress. Since the residual stress does not exceed the yield stress, the corresponding strains can be calculated from the elastic relationship, $\sigma = E \epsilon$, and these strains are shown in Figure 4.1.3.1-2(b). There is no force on the member, and it is noted (by inspection) that the condition $P = \int \sigma dA = 0$ is met. (This can be verified by calculation.)

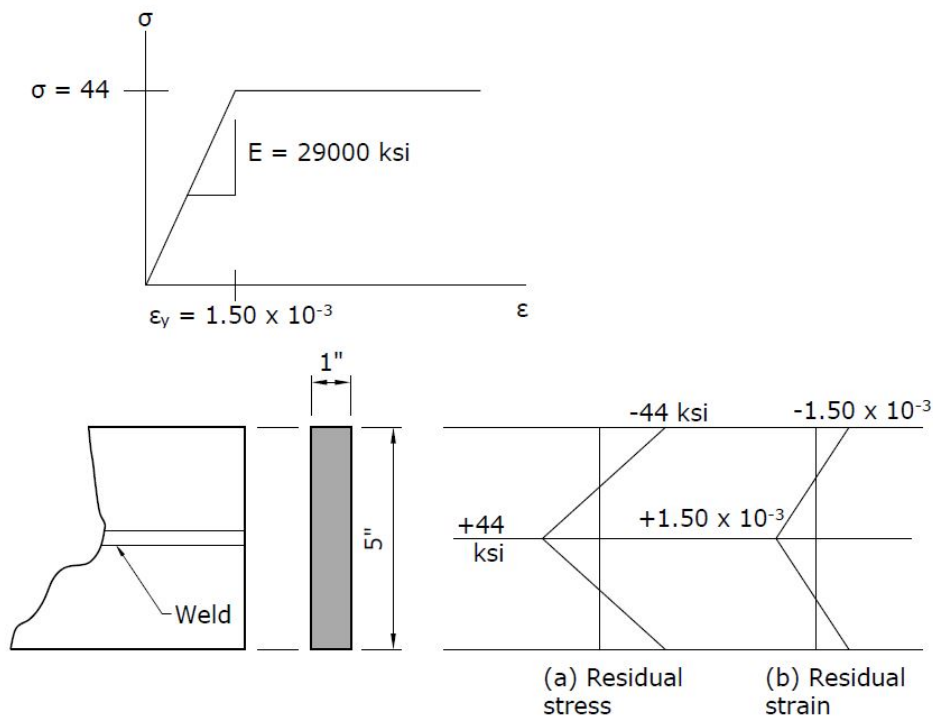


Figure 4.1.3.1-2 Initial stress condition in a welded plate.

Apply tensile force such that the design stress level is +31 ksi. This is computed as follows:

$$P = \sigma A = (31,000 \text{ psi}) (1 \text{ in} \times 5 \text{ in}) = 155,000 \text{ pounds} = 155 \text{ kips}$$

During application of this force, which is the equivalent of the imposition of a uniform tensile strain superimposed over the residual strain of Figure 4.1.3.1-2(b), not all parts of the cross section respond in the same way. Specifically, the relationship $\varepsilon = \sigma / E$ will not be valid for those regions of the resultant strain diagram where the strain is greater than the yield strain. In Figure 4.1.3.1-3, part (a) shows the residual strain (which is simply Figure 4.1.3.1-2(b) repeated), part (b) shows the strain imposed by the tensile force, part (c) shows the resultant strain, and part (d) shows the corresponding stress diagram assuming elastic – perfect plastic material behavior.

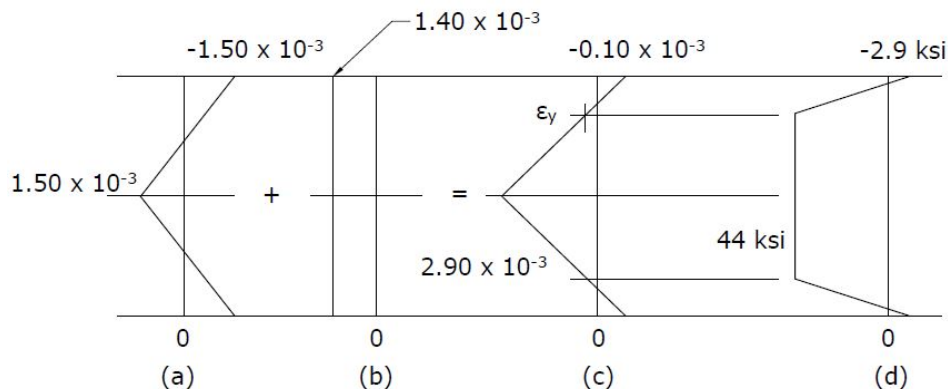


Figure 4.1.3.1-3 Superimposed strain and corresponding stress.

The value of the uniform strain corresponding to the imposition of the applied force, 1.40×10^{-3} , was determined by trial and error to satisfy the requirement that $\int \sigma dA = 155 \text{ kips}$. Iteration is required as this is now a plastic, no longer elastic, analysis. That the integral is satisfied can be confirmed by first calculating the dimensions of the stress diagram, Figure 4.1.3.1-3(d), and then calculating the force volume obtained when the stress diagram is superimposed on the cross section.

Next, apply a force producing a nominal stress of 18 ksi compression. This requires that the 155-kip force be removed and an additional force of $(-18,000 \text{ psi}) (1 \text{ in} \times 5 \text{ in}) = -90,000 \text{ pounds} = -90 \text{ kips}$ be applied. Thus, the change in force is $\Delta P = 155 \text{ kips} + 90 \text{ kips} = 245 \text{ kips}$. As before, a uniform strain must be applied of sufficient magnitude such that $\int \sigma dA = P = 90 \text{ kips}$. By iteration, this has been determined to be a strain of 1.70×10^{-3} .

Figure 4.1.3.1-4(a) shows the strains that existed at the end of the previous step. Figure 4.1.3.1-4(b) shows the uniform compressive strain that must be applied to satisfy the requirement that a compressive force of 90 kips is imposed. The resultant strains are shown in Figure 4.1.3.1-4(c).

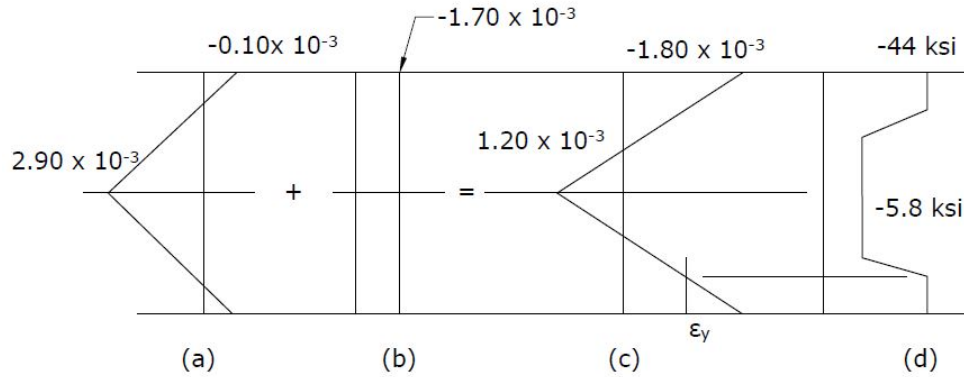


Figure 4.1.3.1-4 Additional superimposed strain and corresponding stress.

The stress values in Figure 4.1.3.1-4(d) can be explained by examining the stresses in the mid-width fiber of the cross section. As shown in Figure 4.1.3.1-5, the stress initially was 44 ksi (i.e., the yield strength). Upon initial loading of the 155-kip force, the stress remained at this value, even though the strains increased as shown in the figure. The unloading that occurred in the third step took the stresses down to 5.8 ksi compression. Thus, the actual change in stress at the mid-width fiber was from +44 ksi down to -5.8 ksi, which results in a total change of 49.8 ksi. The result is that the actual change in stress, 49.8 ksi, is nearly equal to the change in stress calculated by the designer, 49 ksi. The difference between the two values is attributable to round-off errors in the calculations. The reader can verify that the imposition of these stresses on the cross section does, in fact, produce the value of 90 kips.

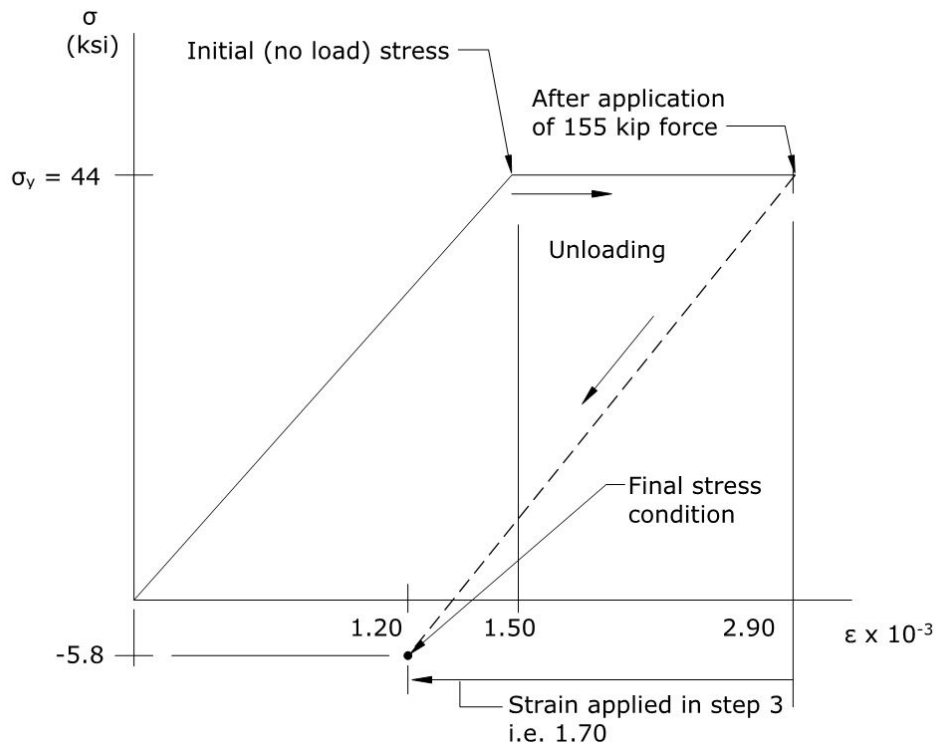


Figure 4.1.3.1-5 Stress and strain at mid-depth fiber.

Still with reference to Figure 4.1.3.1-5, it should be borne in mind that unrestricted plastic flow of the cross section cannot occur. The small zone of weld and plate that is at yield is limited to some finite value of strain because the material adjacent to it remains elastic. Hence, the stress concentration in a high residual tensile stress region is cycled to a limited strain. The magnitude of the applied stress does not change the results. If the applied loads were smaller, the yielding at the critical area of tensile residual stress would still occur and the local stress range would be elevated with a maximum stress equal to the yield stress of the material. Application of peening at the weld toe can introduce a local compressive residual stress which will increase fatigue resistance.

4.1.3.2 Effects

To summarize, in large welded structures, there are very high tensile residual stresses near fatigue crack sites, and their presence significantly reduces the effects of applied stress levels and steel grade upon crack propagation for standard weldable structural steels. As a result, it is generally agreed that stress range is the only dominant stress parameter. However, there has been a great deal of discussion regarding the best way to treat the following cases:

- The influence of compressive applied stresses
- The fatigue resistance of non-welded elements
- The fatigue resistance of stress-relieved welded elements
- The difference between results taken from testing small specimens and those taken from testing full-scale elements

Some of the differences between various codes can be traced to different interpretations of the effect of residual stresses (and other built-in stresses) upon the fatigue resistance of structural elements. A selection of approaches to these cases is described below.

Nearly all fatigue guidelines for steel structures recommend that non-welded elements, stress-relieved welded elements, and welded elements be treated in the same manner when the applied stress ranges are tensile. However, when the applied stress ranges are compressive, or partly compressive, recommendations vary. According to the AASHTO recommendations (AASHTO, 2015b), it is possible to ignore all fully compressive stress ranges. However, if a part of the stress range is tensile, then the whole stress range must be considered. European recommendations suggest that the whole stress range should be employed, regardless of whether it is completely or partially compressive, when welded elements are assessed. Eurocode 3 (EC 3) (European Committee for Standardisation, 1992) allows a reduction of the compressive stress range to 60 percent of its magnitude for non-welded and stress-relieved elements. The European Convention for Constructional Steelwork (ECCS) recommendations (European Convention for Constructional Steelwork, 1985) are the most conservative; they recommend that 100 percent of the stress range be used for all elements and all cases. It can be observed that there are no known cases of load-induced fatigue cracking in bridge structures when the cyclic stresses are totally in compression (Fisher et al., 1974).

Authors of the AASHTO provisions argue that, even if fatigue cracks start within tensile residual stress fields, under fully compressive loading, cracks will eventually stop when they propagate beyond the influence of these stresses. The developers of the EC 3 (European Committee for Standardisation, 1992) note that a crack growing from an as-welded joint in an element may be dangerous when applied stress ranges are fully compressive. Indeed, some test elements have failed due to cracks growing under fully compressive applied loading. Also, the EC 3 provisions (European Committee for Standardisation, 1992) reflect an attempt to accommodate those cases where there are no high tensile residual stresses.

For the ECCS document (European Convention for Constructional Steelwork, 1985), it was decided to provide conservative recommendations, because in most complex structures, the magnitudes of built-in stresses are unknown. Built-in stresses do not originate only from welding-related residual stresses, but they may also be caused by other effects, such as lack of fit, settlement of supports, temperature gradients, and ineffective expansion joints. Therefore, it was determined that no advantage should be given to cases in which applied stresses are in compression or in which elements contain no tensile residual stresses.

The final point in this section relates to the physical testing of fatigue specimens. Compared with elements that have no tensile residual stresses, the presence of tensile residual stress near potential crack sites in an element reduces its fatigue resistance, especially at long lives. Small test specimens may not contain the same high level of tensile residual stress found in full-scale elements. For this reason, most recent research programs have concentrated upon testing of full-scale elements in order to establish code recommendations. Therefore, results taken from tests of small specimens should be employed with caution for design assessments. However, small specimens are useful when exploring variables such as improvement procedures or use of new materials.

Test programs are sometimes used to obtain a more accurate fatigue-resistance relationship than is provided in fatigue codes. Whenever possible in these circumstances, it is desirable that the test specimen have the same dimensions as the element under consideration for the real structure.

4.1.4 Bolting and Riveting

Mechanical connection details, in which holes are drilled or punched and forces are transferred by means of rivets or bolts, present a somewhat more severe fatigue resistance situation than the bare rolled shape. This is due to the fact that the holes, if drilled or sub-punched and reamed, produce a slight reduction in fatigue resistance as compared with an unaltered member. If tensioned high-strength bolts are used, the disturbing effect of the hole is largely mitigated by the presence of the high local compressive stresses introduced by the bolt. Punched holes give a greater reduction in fatigue resistance than do drilled or sub-punched and reamed holes because of imperfections at the edge of the hole arising from the punching process. In this case, the crack usually starts at the edge of the hole.

Broadly speaking, any mechanical connection detail has a higher fatigue resistance than does its equivalent welded detail. The local stress concentration adjacent to an open hole in a large plate is 3. However, the small surface irregularities associated with the hole-making process result in good fatigue resistance of these connections. The open hole has the poorest fatigue resistance. A

preloaded connection that is loaded below its slip load will fail not at the hole but in the end of the connection where there is relatively little movement between the plates. Consequently, the fatigue strength of a connection loaded below its slip load is based upon the stress in the gross section of the plate. In a bearing connection, the failure is through the hole and the stress is calculated based on the net section.

Punching can reduce the fatigue resistance of the connection due to the small tears that occur adjacent to the hole. Punched holes have a reduced fatigue resistance and are only allowed in secondary cross-frame members.

Chapter 10 provides additional background information about the fatigue strength of riveted and bolted connections.

4.1.5 Cold Bending

In bridge construction, it is often necessary to bend structural steel to produce the required detail. Some examples include cross-frame gusset plates on skewed bridges, flanges for reduced end depth or dapped ends of girders, webs of curved girders, and flanges of cambered girders. When the required bending is performed at ambient temperature, it is referred to as cold bending. Hot bending, on the other hand, is when the steel is heated to reduce its strength and facilitate bending.

The residual bending deformation of steel is due to the inelastic strains in the steel. If the yield strength of the steel is not exceeded, the steel returns to its original shape after bending. In the stress-strain curve of Figure 4.1.5-1, the steel is loaded in the elastic region from Point A_1 to Point B with no permanent deformation or property change. Further loading beyond the yield point causes elongation to Point E. If the steel is unloaded, it returns to Point A_2 , and there is some permanent plastic deformation of the steel.

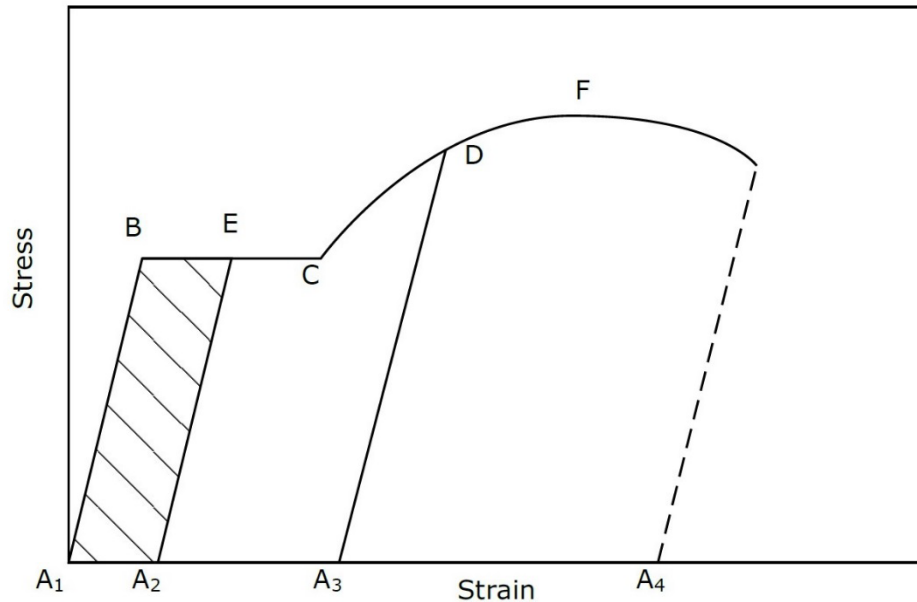


Figure 4.1.5-1 Cold-bending example.

What happens when the steel is reloaded? It now follows Path A₂-E-C-D-F, returning to follow the original stress-strain curve at Point E. A slight loss in ductility (percent elongation), represented by the cross-hatched area, results due to a shorter yield plateau.

If the steel is loaded along Path A₁-B-C-D to cause strain hardening and then unloaded to Point A₃, what happens when the steel is reloaded? It follows Path A₃-D-F. More permanent deformation results, along with changes to the steel properties, including elimination of the yield plateau, elevation of the yield strength, and greatly reduced ductility, with no effect on tensile strength.

The plastic deformation that occurs in bending increases the strength, reduces the ductility, reduces fracture toughness, and can cause surface cracking. The *AASHTO LRFD Bridge Construction Specifications*, Article 11.4.3.3 (AASHTO, 2015a) limits the radius of a bend, which limits the plastic strain introduced in the bending operation to prevent significant reductions in the steel properties. Research has indicated that cold bending is the preferred method of bending since it was found to have the least effect upon the material's properties. The minimum bend radius allowed for a main member is five times the thickness of the plate (Keating and Christian, 2012).

4.1.6 Hot Bending

Hot bending of steel reduces the bending forces but can result in reduction in the material's ductility. The temperature must be below the transformation temperature of the steel and above the blue brittle range. In order to maintain the material properties, the maximum temperature is limited to 1200 °F in the *AASHTO LRFD Bridge Construction Specifications*, Article 11.4.3.3 (AASHTO, 2015a) for rolled steel and 1100 °F for higher strength, quenched and tempered

steels. The minimum temperature should be 700 °F. Hot bending is allowed with the approval of the engineer.

Heat curving is used to bend the flanges for curved steel girders with a large radius. Tighter radius girders are fabricated with flanges cut to the desired curve. Cut curving the flanges can produce a large quantity of scrap steel, while heat curved flanges can be cut from the rectangular plates with little waste of material. The *AASHTO LRFD Bridge Construction Specifications* (AASHTO, 2015a) place limits on the girders that can be heat curved. These limits are based upon limiting the stress in the girder, particularly the web, to limit distortion and loss of strength. Heat curving is done either with V heating patterns or continuous strip heating of one side of the flange, as illustrated in Figure 4.1.6-1. The heating causes expansion of the flange on the heated side, which is resisted by compression of the flange on the unheated side. Upon cooling, the compressed unheated side of the flange forces the heated side to compress, resulting in shrinkage of the heated side of the flange and curving of the flange.

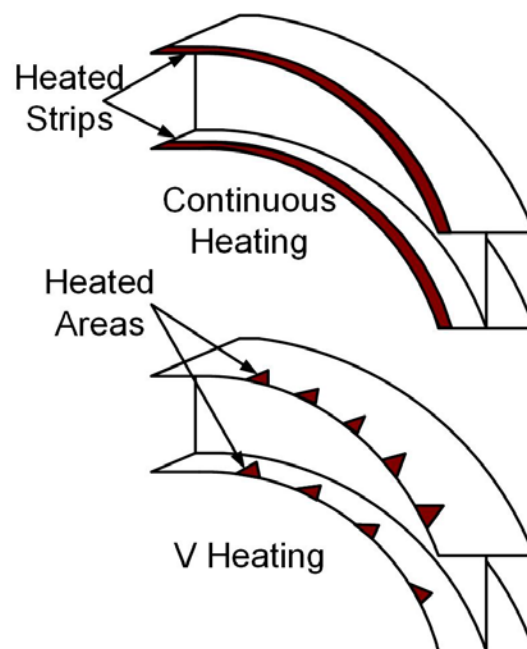


Figure 4.1.6-1 Examples of strip and v-heat curving of girder flanges.

4.1.7 Heat Straightening Repairs

Research data (Avent et al., 2000) indicate that heat straightening affects the mechanical properties of steel. Early researchers used undamaged steel and a small number of heats to conclude that property changes after cooling were minimal. However, tests on damaged and subsequently heat-straightened plates and beams indicate that some property changes may be of significance after repeated straightening or repair of members with large deformations.

The number of times a girder can be damaged and heat straightened must be considered. Changes in all the material properties become more evident with the increasing number of

damage/repair cycles. Material property changes were usually acceptable after two cycles. Thus, a condition that is safe to straighten once is usually safe to straighten a second time. The changes become significantly greater after four and eight damage/repair cycles, respectively. Based upon Avent et al. (2000), re-damaged members at the same location should not be subjected to heat straightening more than twice. NCHRP Report 604 reached the same conclusion in full-scale testing to evaluate fatigue and fracture resistance (Connor et al., 2008).

Additional information about heat straightening is provided in *Heat Straightening Repairs of Damaged Steel Bridges, A Technical Guide and Manual of Practice* (Avent and Mukai, 1998).

SECTION 4.2 STRESS PARAMETERS INFLUENCING FATIGUE

Prior to the extensive National Cooperative Highway Research Program (NCHRP) studies of fatigue resistance at Lehigh University beginning in the late 1960's, the fatigue stress limits were a function of the type of steel, the nominal stress range at the detail, and the exponent of the fatigue equation. The results of the NCHRP research (Fisher et al., 1970; Fisher et al., 1974; and Fisher et al., 1980b) are discussed in this section. Prior to this extensive research effort, the specifications of the American Association of State Highway Officials (AASHO), the precursor to AASHTO, the American Welding Society (AWS), and the American Railway Engineering Association (AREA), the precursor to AREMA, limited the applied stress to this older approach to fatigue, as described in Chapter 1.

The NCHRP-sponsored testing assessed the resistance of multiple base metal, welded, bolted, and riveted details on large scale specimens. The effect of type of loading, member size, constraint, material grade, stress range, minimum and maximum test stress levels, and fabrication quality were studied experimentally. The results led to the conclusions still used today that fatigue life is fundamentally related to the detail type and the applied stress range.

The initial NCHRP project tested over 500 full-size specimens, each with multiple attachments, so that many details could be subjected to differing stress ranges while testing a single specimen. Hundreds of additional details have been tested since in follow-up work. A photograph of one of the specimens is provided in Figure 4.2-1, and a drawing of a specimen from the NCHRP 354 long-life studies showing many different attachments is provided in Figure 4.2-2. The tests were conducted under constant amplitude test loading, meaning every stress range cycle was equal. This of course differs from real bridge loading where each passage is of a vehicle of different weight, axle spacing, speed, and lane position. The treatment of variable amplitude loading is presented in Section 4.2.3. Several observations from the test programs are presented below. These observations relate to the effect of minimum stress as compared to stress range, the effect of steel type, and the nature of the stress ranges.



Figure 4.2-1 Flexural fatigue tests conducted at Lehigh University.

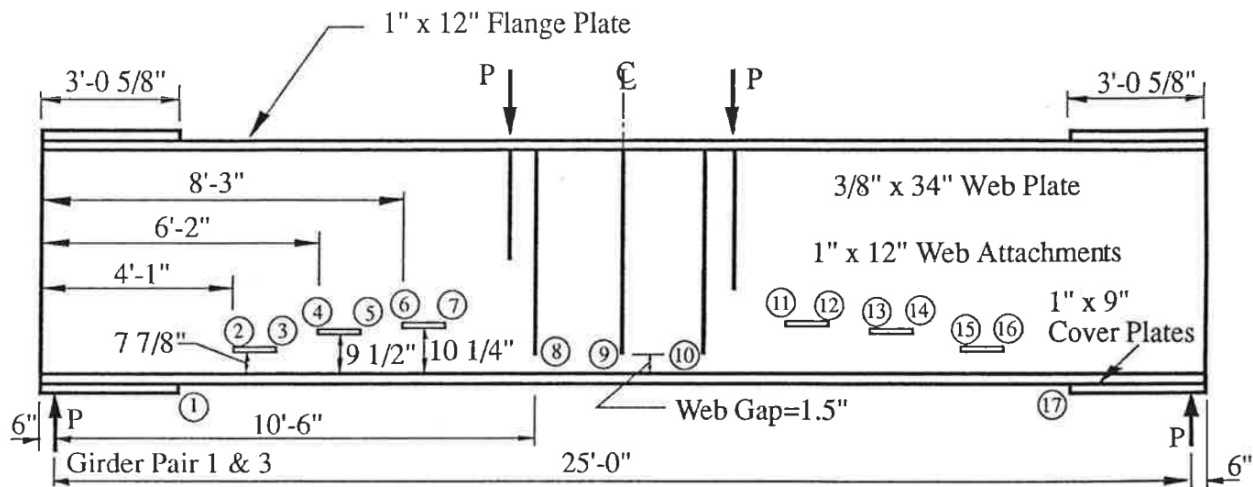


Figure 4.2-2 Sample test beam from NCHRP 354 long-life tests.

4.2.1 Effect of Minimum Stress

When a cluster of fatigue data is plotted, the level of minimum stress has very little impact on its resulting fatigue life. Details were tested in which the stress range was entirely tensile with a large minimum stress, entirely tensile with a near zero minimum stress, and in reversal with stress cycles alternating between compression and tension. The data indicate no significant difference or relationship to minimum stress and a strong correlation to total stress range when it comes to determining fatigue life.

Figure 4.2.1-1 plots the measured fatigue life for three test scenarios described above: one in which the minimum stress was 14 ksi (tensile), one in which the minimum stress was 2 ksi (tensile), and one in which the minimum stress was compressive (-10 ksi). No significant difference in fatigue life was found. This reinforces the prior discussion regarding the influence of residual stress from Section 4.1.3. In addition to the plotted points, three dashed lines are also shown in Figure 4.2.1-1. These lines represent the mean and the 95-percent confidence limits for the data (i.e., plus and minus two standard deviations from the mean). The mean and 95-percent confidence interval boundaries are commonly used in fatigue design. The significance of the lower bound (i.e., two standard deviations to the left of the mean) is that this boundary signifies the typical assumed design life in *AASHTO LRFD*.

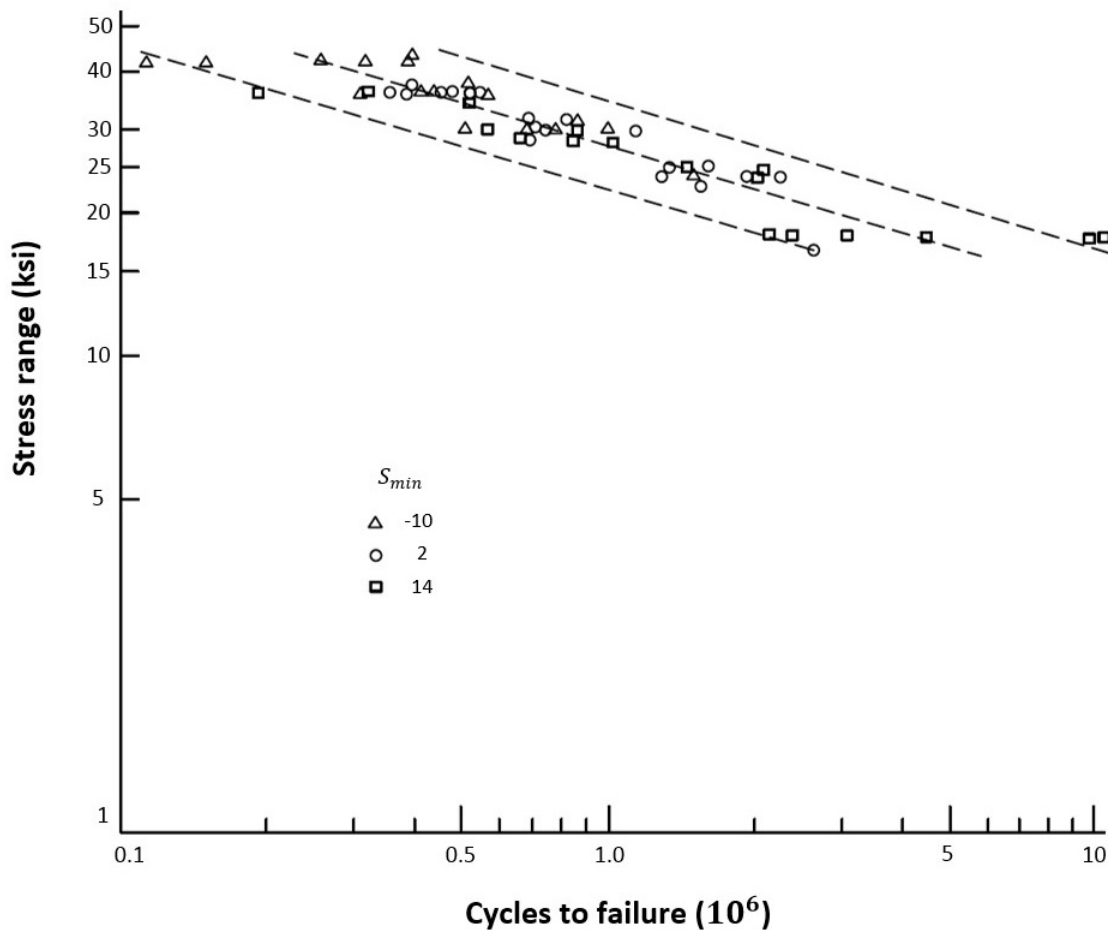


Figure 4.2.1-1 Effect of minimum stress on fatigue life.

4.2.2 Effect of Steel Yield Strength

The same types of observations were found when fatigue test data were plotted for A36, A441, and A514 steel types, as presented in Figure 4.2.2-1. The steels tested were the extreme yield strength materials used in structures at the time of the test program and still represent the extremes of yield strength for modern steel bridges. These steels have specified yield points ranging from 36 to 100 ksi. Testing of welded beams composed of each of these materials

indicated that the minimum or maximum expected fatigue life was generally the same for all grades of steel. These findings with respect to minimum stress (as presented in Section 4.2.1) and grade of steel are important in that they greatly simplify the analysis and design of steel structures for fatigue and again emphasize the point that fatigue design and evaluation can be strictly related to live load stress range and number of cycles.

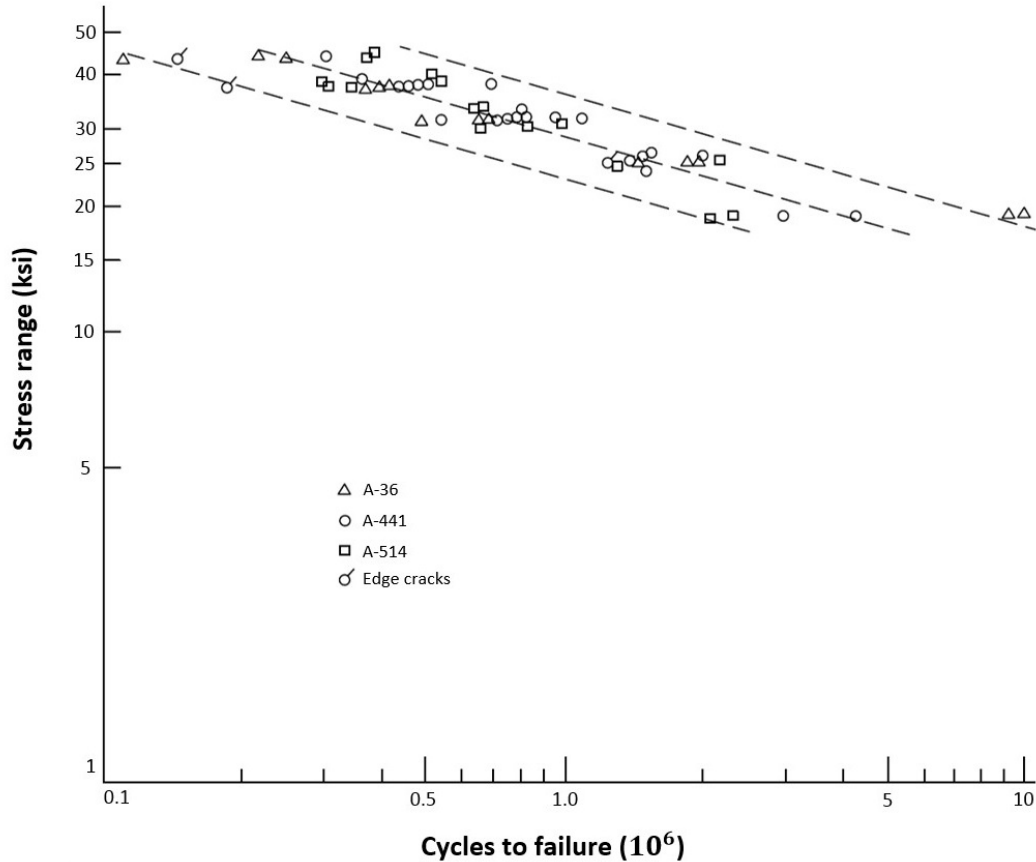


Figure 4.2.2-1 Effect of steel grade on fatigue life.

4.2.3 Consideration of Variable Amplitude Fatigue Loading

Constant amplitude fatigue is the term used to describe the behavior of an element subjected to cycles of fatigue loading of equal stress range. It is commonly the type of loading applied to specimens in a laboratory in order to determine fatigue life, such as the majority of the tests described in previous sections. It is the benchmark by which fatigue life is predicted for details, although it bears little resemblance to the actual variation of stress to which a detail will be subjected in the field. Most experimental results relate to constant amplitude behavior. There have been variable amplitude tests performed on steel structures (e.g., NCHRP 267 and 354), and the results of the constant and variable amplitude loading show that relatively simple rules can be used to establish equivalencies between the two.

Miner's rule is commonly used to estimate the effect of variable stress range that occurs in service with the constant amplitude test data used to develop the fatigue resistance in the laboratory (Miner, 1945). It was previously introduced with Equation 3.4-8. It was historically used along with truck weight survey data to define the weight of the AASHTO fatigue design truck and can also be used to provide a stress range equivalency to design or assess fatigue life when the vehicle loading is different than the *AASHTO LRFD* fatigue design truck. Equation 3.4-8, repeated herein, computes an equivalent single stress range that over a specified number of cycles produces fatigue damage equivalent to the variable amplitude loading but having the same number of cycles. In the equation, S_{re} is the equivalent stress range, S_{ri} is the stress range magnitude of an individual cycle, and γ_i is the percentage of the whole corresponding to each stress range magnitude.

$$S_{re} = \left(\sum \gamma_i S_{ri}^3 \right)^{\frac{1}{3}}$$

Equation 4.2.3-1

An example of the application of Miner's rule to compute an effective stress range is provided, along with a presentation of "damage" using the concept that fatigue damage is related to the cube of the stress range and the number of occurrences. This same procedure is discussed in Chapter 6 as it relates to the development of the fatigue design vehicle specified in *AASHTO LRFD*.

In Table 4.2.3-1, the characteristics of variable amplitude loading for a detail are presented. In first column (1) is an interval, a method used for grouping stress cycles. In this example, each interval, sometimes called a "bin," corresponds to a 1-ksi grouping. In the second column (2), the percentage of the total number of cycles corresponding to the given stress range is noted. Note that the percentages total 100 percent. In the third column (3) is the stress range measured in units of ksi. In the fourth column (4) is the cube of the stress range, as it has been found that fatigue life and hence "damage" are proportional to the cube of the stress range for welded steel. The fifth column (5) multiplies the percentage of cycles times the cube of the stress range to determine the relative damage caused by a specific stress range. Finally column six (6) computes the incremental damage from a particular range of stress. The total damage must total 100 percent.

Table 4.2.3-1 Application of Miner's rule to a variable spectrum.

(1)	(2)	(3)	(4)	(5)	(6)
Stress Interval	Percent of Vehicles, γ_i	S_{ri} , ksi	S_{ri}^3 , (ksi) ³	$\gamma_i S_{ri}^3$, (ksi) ³ (i.e., "relative damage")	Percent Damage
1	40 percent	3	27	10.80	9 percent
2	25 percent	4	64	16.00	13 percent
3	15 percent	5	125	18.75	15 percent
4	9 percent	6	216	19.44	16 percent
5	5 percent	7	343	17.15	14 percent
6	3 percent	8	512	15.36	13 percent
7	2 percent	9	729	14.58	12 percent
8	1 percent	10	1000	10.00	8 percent
	$\Sigma = 100$ percent			$\Sigma = 122.08$	$\Sigma = 100$ percent
				$S_{re} = (122.08)^{(1/3)} = 5$ ksi	

This example applies the concepts of Miner's rule to determine the effective stress range, 5 ksi, and also provides an assessment of which cycles contribute most and least to the total fatigue damage. Of note is that the stress ranges from 3 to 5 ksi constitute 80 percent of the total number of cycles but cause only 37 percent of the total damage. The highest three stress ranges, 8 to 10 ksi, only constitute 6 percent of the total number of cycles but cause an almost equal amount of damage (33 percent) as the three lowest stress ranges. This is consistent with life, or damage, being related to the cube of the stress ranges, with a small percentage of high stress ranges using up a large portion of the detail's available fatigue life.

Another example of Miner's rule is the analysis of a bridge for special traffic. Consider the design of a bridge for a mining road. The vehicle weight distribution for the loaded and unloaded trucks is given in Table 4.2.3-2 and Table 4.2.3-3, respectively. The expected number of round trips per day is 192. The calculation was made to determine the effective truck which represents the loaded and unloaded truck. The effective truck weight is 133.2 kips for the loaded trucks and 43.4 kips for the unloaded trucks.

Table 4.2.3-2 Vehicle weight distribution for loaded trucks.

Weight of Truck, W (kips)	Number of Trips per Day	γ_i (i.e., Number of Trips per Total)	$\gamma_i W^3$ (ksi) ³
110	12	0.063	83,187.5
120	35	0.182	315,000.0
130	57	0.297	652,234.4
140	71	0.370	1,014,708.3
150	17	0.089	298,828.1
Total	192	1	2,363,958.3

$$W_{re} = 133.2$$

Table 4.2.3-3 Vehicle weight distribution for unloaded trucks.

Weight of Truck, W (kips)	Number of Trips per Day	γ_i (i.e., Number of Trips per Total)	$\gamma_i W^3$ (ksi) ³
40	56	0.292	18,666.7
42	45	0.234	17,364.4
44	34	0.177	15,084.7
46	34	0.177	17,236.6
48	23	0.120	13,248.0
Total	192	1	81,600.3

$$W_{re} = 43.4$$

The effective stress range for both trucks was calculated using these effective truck weights as follows:

$$W_{effective} = (0.5 \times 133.2^3 + 0.5 \times 43.4^3)^{1/3} = 106.9 \text{ kips}$$

Equation 4.2.3-2

The effective truck load in conjunction with a dynamic load allowance can be used in the analysis of the bridge to estimate the fatigue stress range at the critical locations in the bridge. This procedure can be used as long as the number of cycles expected does not exceed the intersection of the finite life design equation and threshold stress range. This cycle limit can be found for the various details in *AASHTO LRFD* Table 6.6.1.2.3-2 for a 75-year service life. The ADTT in checking the table is the sum of the loaded and unloaded trucks (e.g., 384 in the previous example), and this value would be used as the ADTT. If a service life other than 75 years is being considered, the values in the table can be adjusted as noted in the commentary of the specification. If the number of expected cycles exceeds the limit, the design should be based on satisfying the infinite life design provisions, and the expected maximum load range of 150

kips should be used to calculate the stress at the critical details and the stress compared to the threshold stress range.

SECTION 4.3 TESTING AS THE BASIS FOR DESIGN LIMITS

4.3.1 Development of Design Limits for Finite Life

As described in previous sections, using test data first collected in earnest during the 1960's and 1970's, researchers developed best fit lines through the test data that represented the mean behavior. An example of a generic mean regression curve is provided in Figure 4.3.1-1. The fatigue data is plotted in log-log space, and the regression appears as a line. However, these lines are also frequently referred to as "curves," which is what they look like when plotted on non-log axes.

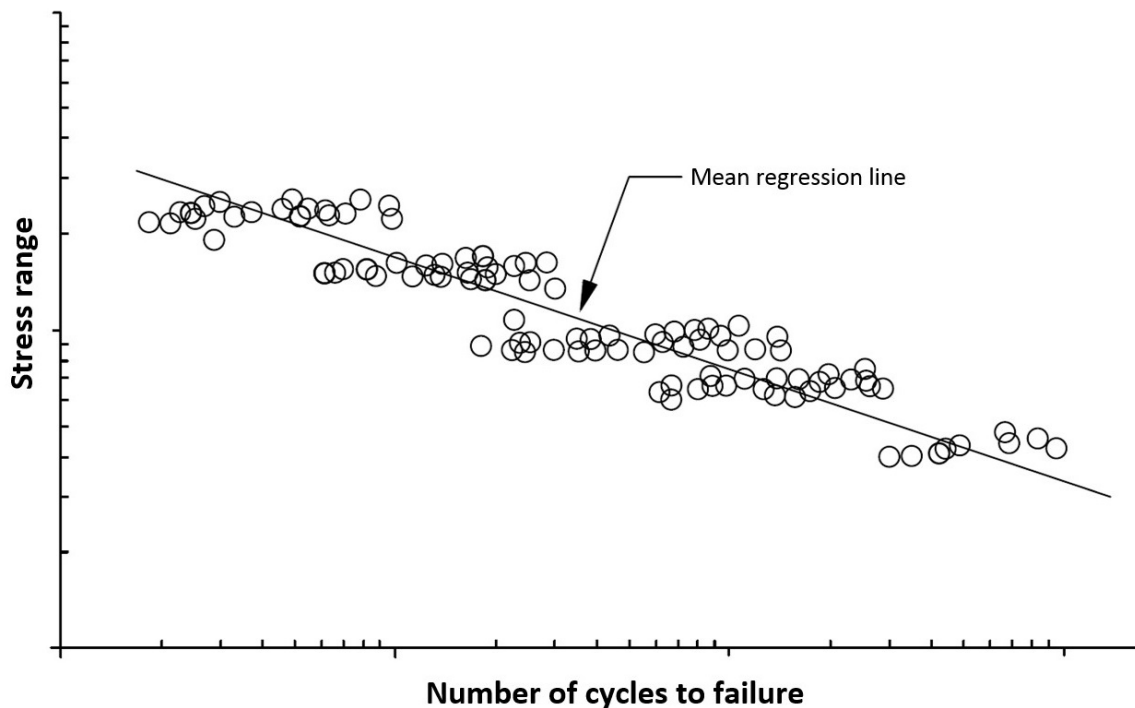


Figure 4.3.1-1 Fatigue life test data plotted on a log-log scale.

The meaning of the mean regression line as it relates to fatigue life is that the predicted life from this curve has only a 50 percent chance of being a safe prediction. For the design of new structures, this is inadequate and different standards were adopted.

For design, the curves that depict allowable (nominal) stress range versus design loading cycles have been offset two standard deviations (i.e., -2σ) to the left of the mean curve. Assuming a normal distribution, two standard deviations to each side of the mean encompasses 95 percent of the data, and the remaining tail probabilities on each side sum to 5 percent. In design, the upper tail is irrelevant because it depicts resistance far in excess of the demand, and only the lower tail

that sums to 2.5 percent is important in terms of risk. For this reason, it is said that design fatigue curves represent a 97.5-percent confidence that the fatigue life of a detail will not be exceeded during the design life of the bridge. This is the fundamental assumption historically used in the AASHTO design approach. Safety is provided (in part) through the application of these conservative bounds for fatigue life, and the corresponding “allowable” stress ranges. The statistical shift of the mean curve to the lower bound AASHTO design curves is depicted in Figure 4.3.1-2. The safety inherent in the two standard deviation shift is apparent in the difference between the mean and the design life. A more recent calibration of the fatigue limit state, which is discussed in further detail in Chapter 6 and in Appendix A, results in a different definition of safety, but the fundamental concept remains the same, namely to provide a safe lower bound prediction of fatigue life.

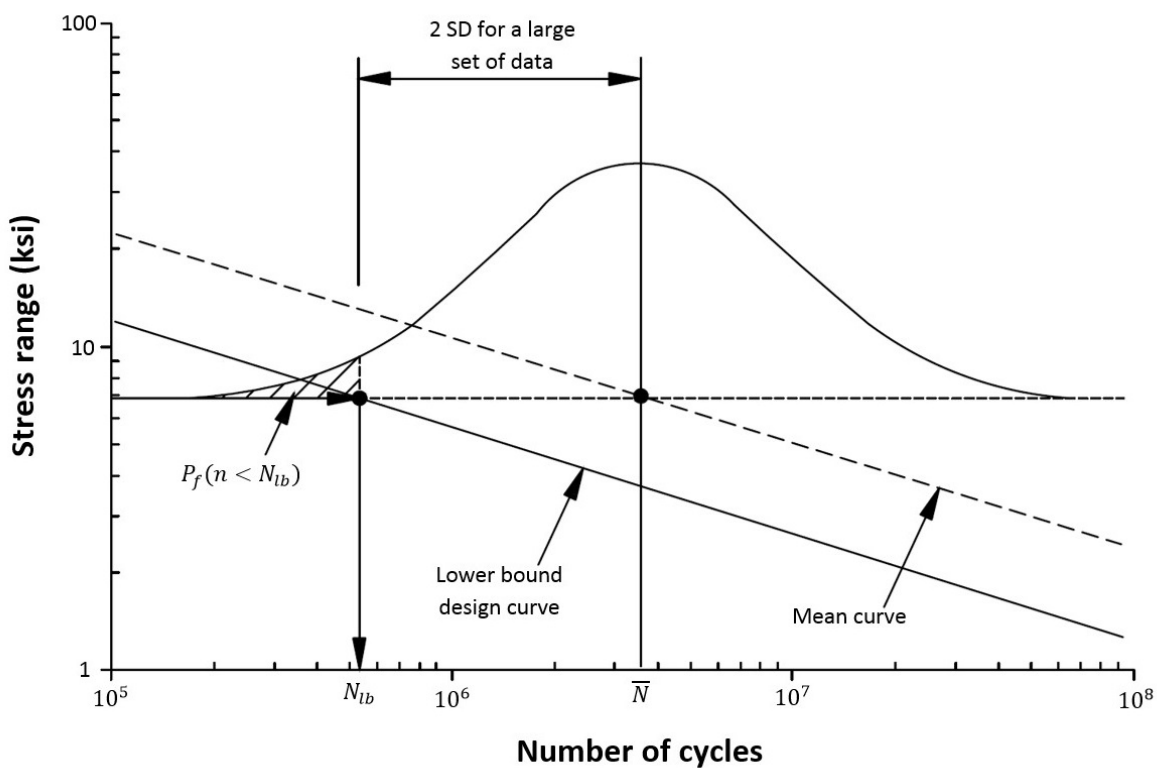


Figure 4.3.1-2 Mean and lower bound fatigue curves.

In Figure 4.3.1-2, the following terms are used:

- \bar{N} = the mean life corresponding to a specific stress range
 N_{lb} = the lower bound, or design life, for the same stress range

The shaded area represents the 2.5-percent probability of failure associated with the design life estimate.

Once the fatigue test data in the prior figures were plotted, a linear regression analysis was performed. The resulting regression equations are described by the following relationship:

$$\log N = \log A - B \log S_r$$

Equation 4.3.1-1

which is of the form of a linear equation, $y = b - mx$.

Alternatively, the relationship between the stress range, S , and number of cycles, N , is presented as:

$$N = AS_r^{-B}$$

Equation 4.3.1-2

For steel, the exponent “B” is approximately 3, and researchers have enforced a common value of 3 in all design fatigue equations. This forms the basis of the assertion that fatigue life is inversely proportional to the cube of the effective stress range.

In addition to sloping lines or curves defining the finite fatigue life behavior, an additional boundary called the constant amplitude fatigue threshold (CAFT) was established. This is discussed in Section 4.3.2. However, prior to moving on from the discussion of finite life, a brief discussion of the definition of “life” is provided in the following section.

4.3.1.1 A Definition of Finite Life

The fatigue resistance in *AASHTO LRFD* was developed through the testing of large specimens under repeated loading. The specimens were loaded until “failure” occurred, and the corresponding life of the detail and stress range were recorded. After hundreds of tests of many different types of fatigue details, a family of fatigue design curves was established.

There is no consistent definition of “failure” used by researchers. During the testing of several hundred welded and rolled steel beams, Hirt (1971) defined failure as “*generally defined in this study as an increase in midspan deflection of 0.020 inch due to fatigue cracking of the test beam.*” He also states that, “*This usually occurred when the crack had propagated through enough of the flange for net-section yielding to occur. At this stage, most of the fatigue life of the beam was exhausted. The crack generally had destroyed 15% to 75% of the flange area.*”

Figure 4.3.1.1-1 and Figure 4.3.1.1-2 are taken from the Hirt report (1971) and depict the large number of applied cycles before visible cracks were observed (using magnifying glasses and microscopes) and the much shorter duration until the section was deemed to have failed. It required 435,000 cycles before a crack that began in the weld metal propagated through the bottom flange and only an additional 32,000 before the specimen was deemed to have failed.

Several other important observations are presented in the Hirt report (Hirt, 1971). The following quotes are excerpted:

- “Most of the fatigue life of the welded beams was spent growing a crack from its initial size to a visible crack. This corresponded to growth rates below 10^{-6} in. per cycle where little information is available from crack growth studies.”
- “More than 75% of the life was spent in this region growing a crack from its initial size to a visible crack.”

There are several useful pieces of information from these statements that relate to the idea of fatigue life and failure:

- The majority of fatigue life is exhausted growing a crack from a small initial discontinuity, and crack growth rates are extremely small per cycle.
- When visible fatigue cracking is observed in the field, the majority of fatigue life has been expended.
- Significant cracking is possible with little observable change in overall member behavior, and vertical deflection increases that are observable only with instrumentation correspond to significant loss of tension flange area.

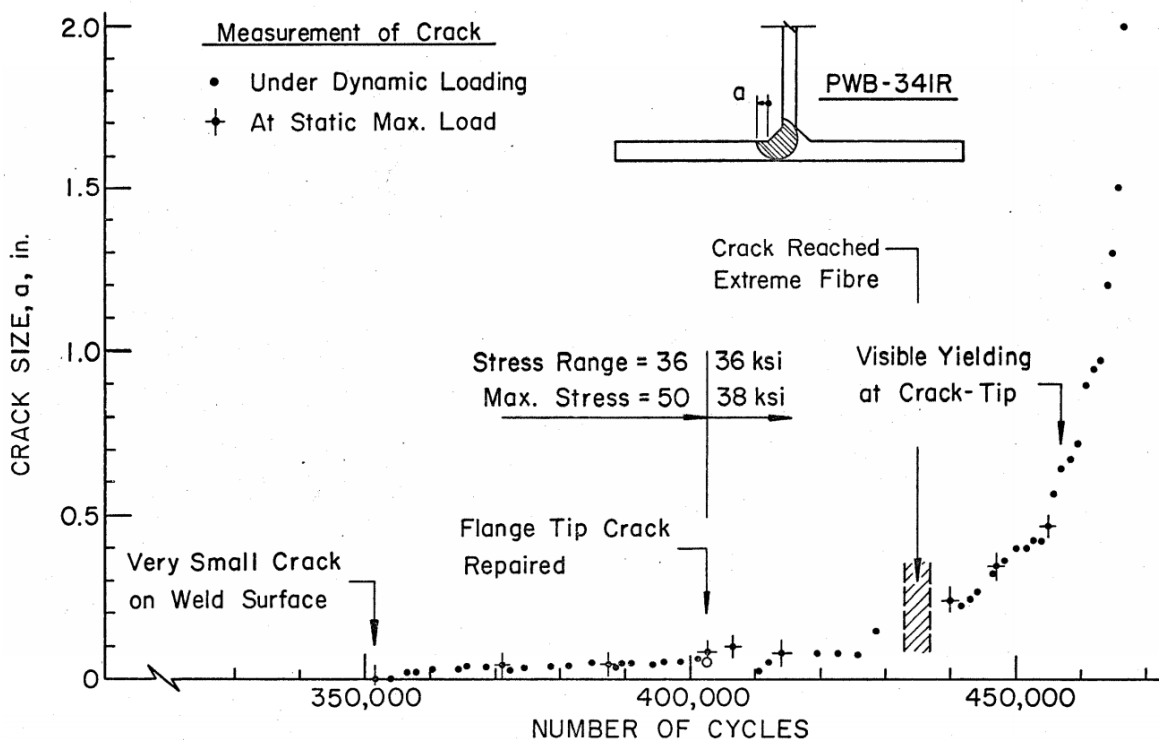


Figure 4.3.1.1-1 Crack size and growth versus number of cycles for a welded beam.

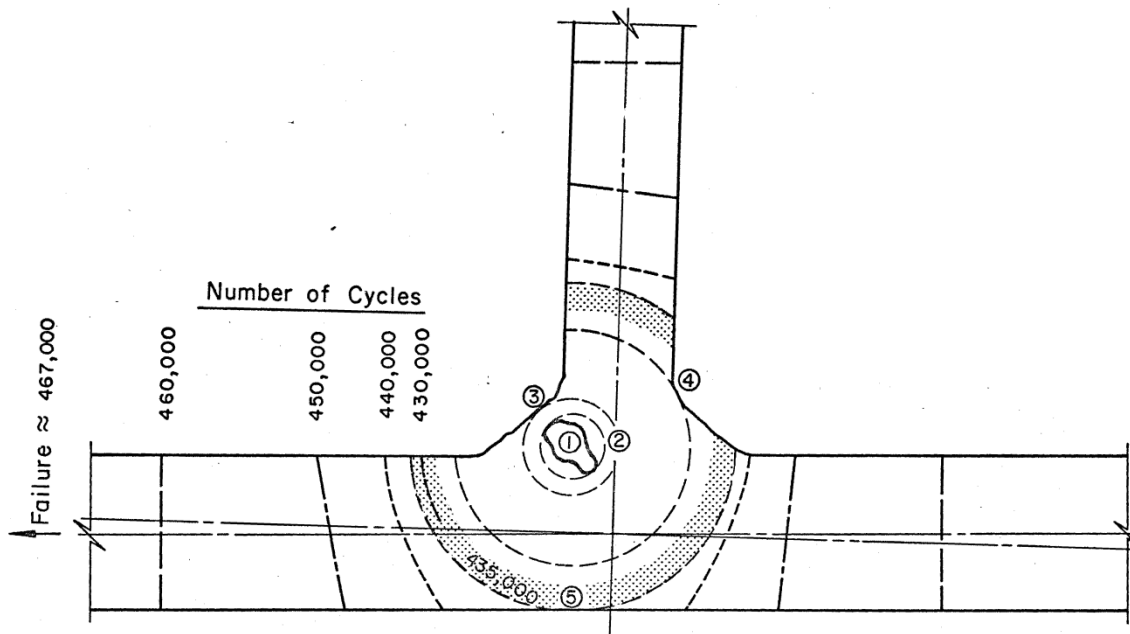


Figure 4.3.1.1-2 Number of cycles leading to failure in a steel girder.

In the NCHRP Project 12-15(5) study, the results of which are published in NCHRP Report 354 (Fisher et al., 1993), researchers studied the long life behavior of steel beams with welded transverse stiffeners, longitudinal attachments, and cover plates. For the definition of life for cracks forming at the web stiffeners and attachments, a criteria of a through-thickness crack in the web or a crack 1 inch long otherwise was established as the definition of life.

In tests to determine the fatigue performance of composite sections (Daniels and Fisher, 1968), strain gauges attached to the underside of the top flange of a composite beam were used to detect shear stud failures by examining the relative change in top flange strain over time, indicative of a loss of composite action.

As for other types of tests, additional unique definitions of failure are found. However, it is consistent that fatigue tests do not define failure as complete member failure but rather the onset of unstable propagation or significant changes in overall member behavior.

4.3.2 Development of Design Limits for Infinite Life

Research has shown that stress cycles below the constant amplitude fatigue threshold (CAFT) do not cause fatigue crack growth under constant amplitude loading. However, it is known that bridges are subjected to variable amplitude loading and may have many cycles whose magnitude is in excess of the effective stress range. Under variable amplitude loading, the stress cycles above the CAFT contribute to crack growth. The higher stress ranges cause crack extension and cause a decrease in the CAFT, with eventually all stress cycles contributing to fatigue crack growth. It is this knowledge of the decay of the CAFT limit that leads to a need to guard against

infrequent occurrences of a maximum stress range and thus guard against crack growth. Three possible scenarios are explored in Figure 4.3.2-1 to demonstrate the relationship between effective stress range, maximum stress range, crack growth, and infinite life. This figure is the foundation of the selection of the Fatigue I load factor which is discussed in greater detail in Chapter 6.

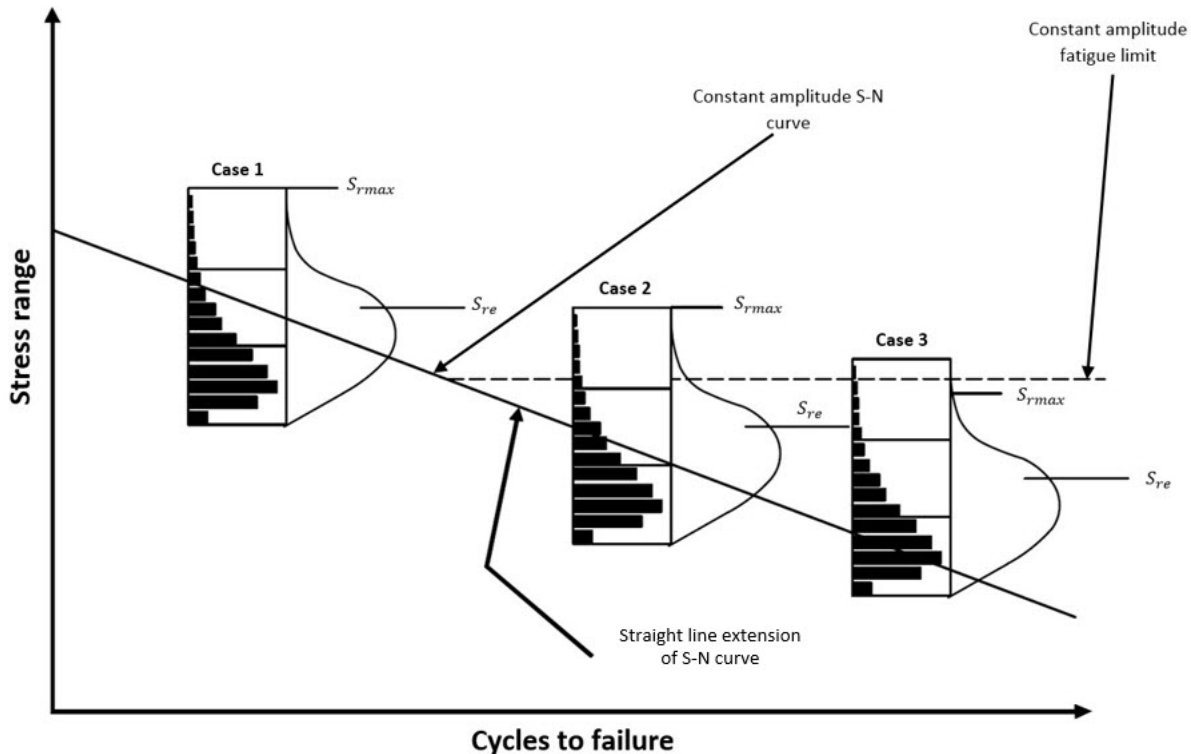


Figure 4.3.2-1 Fatigue life versus effective and maximum stress.

In Case 1, a histogram of loading is provided in which the effective stress range is relatively large. For a large effective stress range (S_{re}), the number of cycles to failure is low in a relative sense since the stress range is large. The effective stress range significantly exceeds the CAFT, and the fatigue life for a scenario such as this one is based on the finite life concepts discussed in Section 4.3.1.

In Case 2, the effective stress range is computed to be less than the CAFT which would imply infinite life. However, only when a specimen is subjected to constant amplitude loading with all cycles below the CAFT does the CAFT behavior hold true. A limited number of stress cycles above the CAFT results in crack extension, cracking will eventually progress, and the CAFT limit would be reduced to the point that all cycles, large and small, contribute to crack growth.

Case 3 is the basis for infinite life design. For infinite life, a designated maximum stress range must be below the CAFT in order for infinite life to be ensured under variable amplitude loading. Although it is not statistically possible to keep all stress cycles below the CAFT, research found that if a very small number of cycles (i.e., 0.01 percent) were in excess of the CAFT, crack growth was effectively prevented throughout the expected design life of the structure.

Examination of the histograms of random loading determined that a doubling of the effective stress range would provide this small probability of exceedance. This relationship between the load factors for finite life (effective stress) and infinite life (maximum stress) is further discussed in Chapter 6, detailing the development of the *AASHTO LRFD* design approach. Recent studies using weigh-in-motion data indicate that the relationship between the effective and maximum stress ranges is no longer the historical value of 2, assumed in the past. The maximum stress range will now be defined by a factor of approximately 2.2 using the load factors of 1.75 and 0.8 for the Fatigue I and Fatigue II load combinations, respectively, as adopted by AASHTO in 2016.

4.3.3 Testing to Establish the Fatigue Resistance of Special Elements

AASHTO LRFD does not have a codified procedure for defining the fatigue strength of special structural elements. However, procedures and test methods have been developed for some bridge hardware and components. A method of qualifying modular expansion joints through tests has been developed and is used by manufacturers of the joints to qualify them for use on bridges. Due to the complexity of these joints and the proprietary nature of their design, these joints are tested in accordance with a procedure given in NCHRP Report 402, Appendix A (Dexter et al., 1997).

Cable stay anchorage systems and the strand used in the cable stays are tested in accordance with the requirements of PTI DC45.1-12: *Recommendations for Stay Cable Design, Testing and Installation* (PTI, 2012). This specification covers other hazards such as corrosion and fire, as well as installation specifications for the products. The fatigue requirements are intended to provide a stay cable which is not susceptible to fatigue damage due to service loads. Additional details on stay cable testing are provided in Chapter 10.

Other codes have established test procedures for developing a design fatigue resistance for a new connection or equipment. Generally in the U.S., if at least 12 replicate specimens at three different stress ranges are tested to failure, the test results are evaluated and compared to the design categories in specifications. The 95-percent confidence limit for 95-percent survival of the test data should be equal to or greater than the design line for the category.

SECTION 4.4 ENVIRONMENTAL EFFECTS

In the presence of moisture and air, all steels have a potential to corrode. The rate of corrosion depends on the access to oxygen, moisture, and other contaminants, particularly road salt on the surface of the metal. As rust formation progresses, the rust forms a barrier and the rate of rusting slows down. With many common steels, the rust layers are not well adhered, at some point they fall off, and then corrosion re-initiates, this time on a reduced section.

4.4.1 Weathering Steel

With weathering steel, the oxidation process initiates in the same way, but the specific alloys produce a stable patina layer that is well adhered to the base metal and less porous than rust that forms on traditional steels. This dense patina develops under conditions of alternating wet and dry cycles to produce a protective barrier that impedes the ingress of oxygen, moisture, and pollutants. This results in a steel structure that is self-protective over time. The formation of the rust patina does result in minor pitting and surface corrosion of the steel that marginally degrades its resistance as compared to other base metals. AASHTO recognizes this distinction between the surface conditions of weathering and non-weathering steels in its treatment of fatigue categories.

For plain base metal of non-weathering steels, AASHTO designates this as Category A, the most favorable fatigue condition. A similar noncoated weathering steel structure would be assigned one lower fatigue category (i.e., Category B), acknowledging the influence of pitting on surface roughness and overall fatigue resistance. Although there is a reduction in fatigue category for weathering steel from A to B, most steel structures have bolted or welded attachments that further lower the fatigue category performance of weathering and non-weathering steels alike. This is substantiated by physical testing of cruciform joints, a typical Category C detail, and comparing those results to weathering steel fatigue data.

Figure 4.4.1-1 is taken from Fisher, Kulak, and Smith (Fisher et al., 1998) which also has a broader discussion of the impacts of corrosion on the resistance of weathering steel. It demonstrates that the geometric effect of the cruciform construction, a Category C detail, is more significant than the shift in resistance associated with weathering steel pitting.

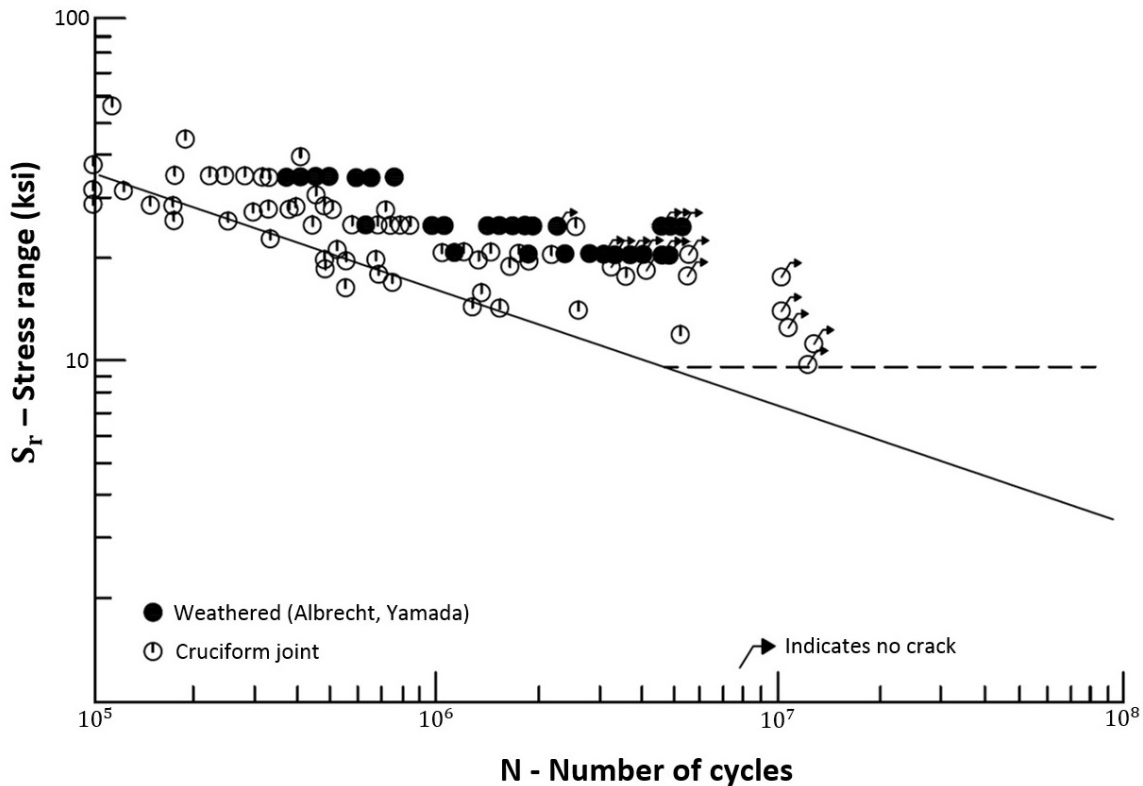


Figure 4.4.1-1 Fatigue life comparison of weathering steel and Category C cruciform joints.

4.4.2 Corrosion Effects on Fatigue Life

The effects of corrosion influence fatigue life in several ways. Corrosion, such as may be found under a leaking deck joint or at a crevice in built-up sections where debris and moisture can accumulate, results in a local reduction in cross section and a jagged or notch-like condition on the surface or edge of the member. These local corrosion effects are found frequently on older steel structures and are a consequence of many years of service, sometimes in aggressive environments. The problem is not unique to highway bridges; many steel railroad bridges have similar problems, particularly open deck railroad bridges in which the timber ties bear directly on the top flange of the longitudinal beams. Open deck railroad bridges frequently have corrosion on and around the top flanges due to the entrapment of debris or contaminants. Fisher, Kulak, and Smith (Fisher et al., 1998) comment that localized depressions on the order of 1 to 2 inches in diameter and depths on the order of 1/8 to 5/16 inches are commonly found on the top flanges of open deck steel railroad bridges. This localized corrosion is a more aggressive form of pitting that also influences the fatigue resistance of weathering steel and serves to reduce the fatigue life of the structure. Although this localized pitting is not desirable, it has been found to be not particularly detrimental since the stress concentration resulting from a pit is not particularly severe.

Corrosion may also introduce sharp notches on the surfaces or edges of structural steel members, and these notches have been found to have a more significant effect on overall fatigue life. The

influence of these notches is analogous to the stress concentration at edge cracks for which classic fracture mechanics solutions are available. An illustration of the stress concentration at the tip of a corroded edge crack is provided in Figure 4.4.2-1. These shallow cracks typically produce fatigue lives comparable to Category C and typically do not control the fatigue life estimate of the structure.

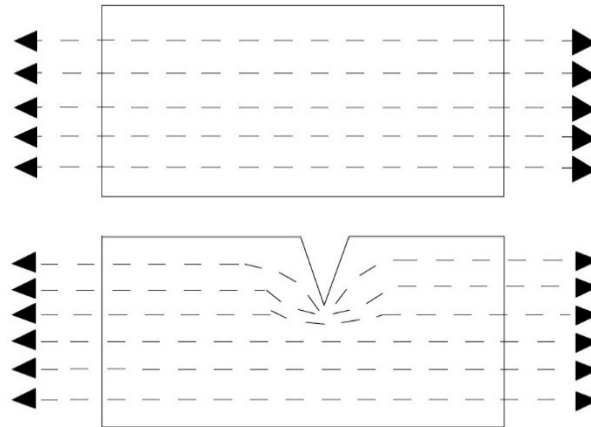


Figure 4.4.2-1 Edge notch effects on stress concentration.

Fisher et al. (1998) report that if corrosion has reduced the thickness of the structural steel elements by more than one half, fatigue cracking is likely to initiate at a notch within the corroded region rather than at a traditional net section location such as the edge of the rivet or bolt hole, even when the overall net section has been reduced in area and inertia for an approximate level of corrosion.

There are also situations in which corrosion is more or less uniform across the entire cross section. This is the case when corrosion is due to a more general source, such as high humidity, aggressive environment, or some other scenario in which the corrosive impact affects the entire member somewhat uniformly. It has been found that when corrosion is uniform throughout the cross section, the fatigue life can be reasonably estimated based on the stress ranges computed on the reduced cross section. This assumes that there are no notches or other discontinuities that would pose a more severe fatigue condition on the structure. Fisher et al. (1998) state that the effect of corrosive environment on crack growth and the effect on stress concentration has not received much attention for civil engineering applications. However, the available laboratory tests did not indicate a significant impact on stress concentration. This does not imply that the impact of corrosion on fatigue resistance is negligible, however, since the notch effect and overall increase in stress range from general corrosion must still be considered.

The influence of section loss should not be underestimated. Unprotected steel will undergo continual reduction in plate thickness over time due to the cyclical formation of corrosion products. A study of corrosion rates, as-inspected plate thicknesses, and the influence of corrosion on section property reduction was carried out by the Illinois Department of Transportation. In their report (Hahin, 1994), they present an example of an in-service bridge in the state of Illinois in which the non-weathering steel was left unpainted for 25 years. The

moment of inertia of the as-installed rolled shape was significantly reduced in that 25-year timeframe. Sketches of the as-installed and as-inspected conditions are provided in Figure 4.4.2-2.

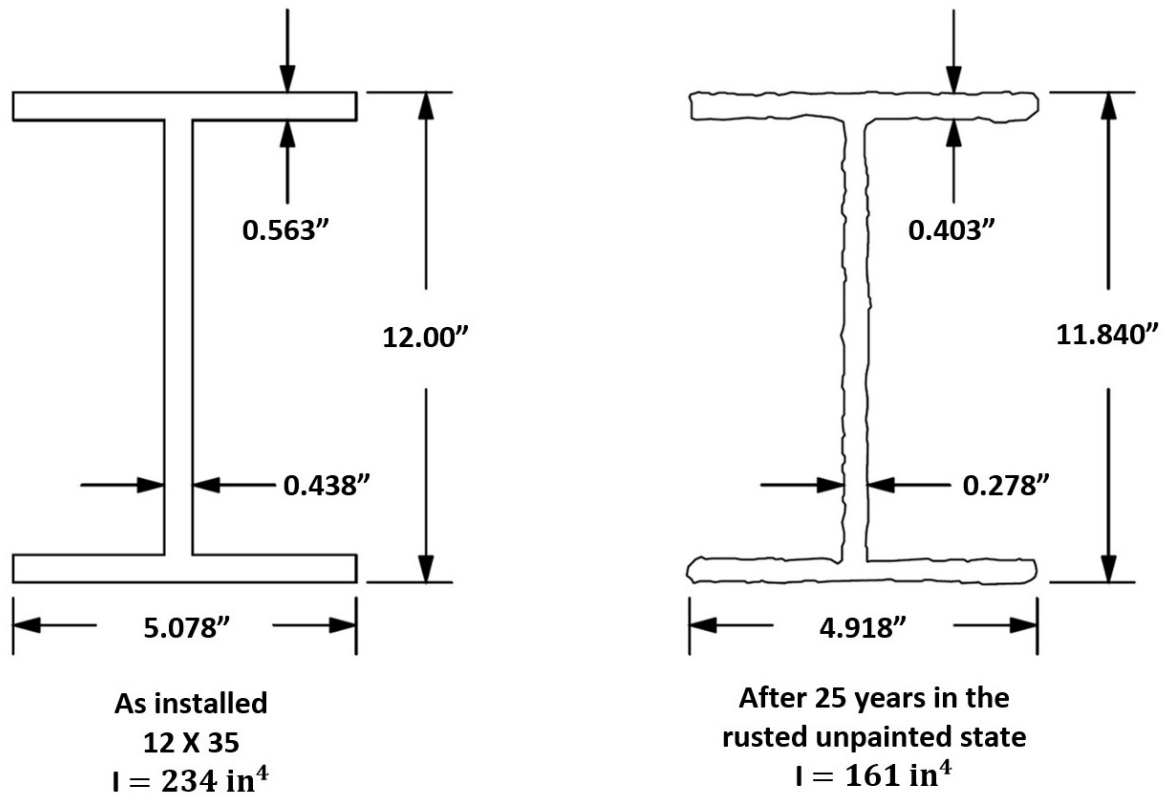


Figure 4.4.2-2 Influence of corrosion on section properties.

The computation of remaining fatigue life must recognize that the nominal stresses in the section are increased because of the reduction in section modulus, and the engineer must also consider if the Category A fatigue resistance still applies as well.

Albrecht and Lenwari (2008) report on the fatigue testing of corroded stringers removed from an abandoned streetcar trolley bridge. The bridge was constructed in 1900 and for the next 58 years carried mass transit trolleys until operation was suspended in 1958. The bridge remained albeit in an abandoned state until 1985 when the stringers were removed from the bridge and transported to the laboratory. The bridge was severely corroded at two locations: (1) on the top flange where pits formed at the intersection of the railway ties and the top flange and (2) at the top of the bottom flange where debris accumulation and trapped moisture resulted in significant corrosion over the lower 6 inches of the web and flange. When the stringers were tested in the laboratory, nine tests were performed with the stringers in their as-removed condition (i.e., with the corrosion pits on the top flange located on a compression flange). An additional 13 tests were performed with the stringers tested in the inverted position so that the severe pitting on the top flange could be loaded in tension. All of the fatigue cracks that formed during testing initiated at rust pits, indentations, mechanical seams from rolling, and notches that were formed by

corrosion over the years. Of the ten stringers tested in the normal position, six had Category A strength, two had Category B strength, and two had Category C strength. For those tested in the inverted position with the top flange rust pits now located on the tension face, nine had a Category B strength, three had a Category C strength, and one had a Category D strength. The results of all of the stringer tests are shown in the graph in Figure 4.4.2-3.

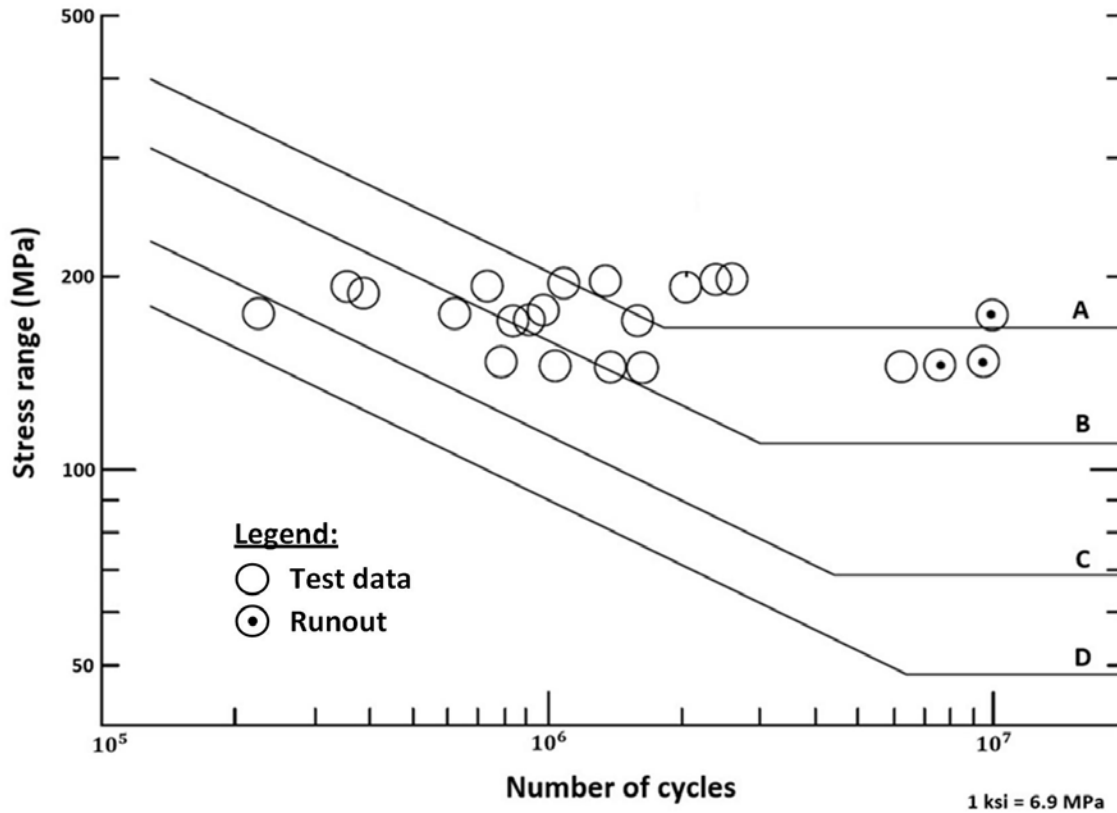


Figure 4.4.2-3 Influence of long-term corrosion on the fatigue performance of rolled shapes.

The authors conclude that corrosion clearly reduced the fatigue resistance of the trolley bridge stringers below that of the non-corroded beams. The reduction was clearly evident in the beams tested in the inverted position. The authors comment that the AASHTO S-N curve for Category A should not apply to a corroded rolled beam and that methods are available to account for the fatigue life loss due to uniform corrosion and pitting. The findings of the Albrecht study support the prior findings of Fisher, Kulak, and Smith (Fisher et al., 1998) relative to the greater influence of pitting and notch effects on reducing remaining fatigue life as compared to the overall section loss of uniform corrosion.

Although no firm guidance is available based on these studies, engineers should be aware, especially when computing the remaining fatigue life of older steel bridges, that the type of corrosion found may in fact influence the remaining fatigue life calculations, and some

consideration to evaluating the base metal as a category less than A should be given. No guidance is found in the AASHTO design specifications (AASHTO, 2015b) or in the *Manual for Bridge Evaluation* (AASHTO, 2015d) regarding the influence of corrosion on expected fatigue life.

SECTION 4.5 SUMMARY

The statistical analysis of full-scale test results of cover-plated beams, welded beams, rolled beams, and groove-welded splices revealed that stress range is the dominant stress parameter influencing fatigue resistance (Fisher et al., 1970). The use of stress range was confirmed by a minimum notch-producing detail – the rolled beams – which provide an upper boundary for fatigue resistance. Similar behavior was observed for a severe notch-producing detail – the cover-plated beams – which provide a lower boundary for fatigue resistance. The result of the analysis of variance for the three bridge steels of the day – ASTM A36, ASTM A441, and ASTM A514 (Grades 36, 50, and 100, respectively) – showed that the dominant variable at the 95-percent confidence level was stress range for each grade of steel. Minimum stress appeared to have little or no influence. Further, it was found that regardless of grade of steel, no improvement in the goodness of fit was achieved when minimum or maximum stress was included in the analysis. As noted herein, most specifications have adopted a fatigue life estimation for welded details that is dependent solely upon the stress range and connection detail. The fatigue resistance is independent of the material strength.

This page intentionally left blank

CHAPTER 5 ANALYSIS FOR FATIGUE

SECTION 5.1 GENERAL

In all fatigue designs and evaluations, a calculated or measured stress range is compared to some permissible stress range. As discussed in detail in previous chapters, stress range is the dominant stress parameter for fatigue. The processes by which these stress parameters are established ranges from the very simplistic to the extremely complex.

Three possible analytical approaches, depending on the level of refinement in the stress analysis, can be used for assessment of the fatigue limit state of a detail:

- Nominal-stress approach
- Local-stress approach
- Fracture mechanics

The difference in level of analysis is illustrated in Figure 2.3.3-1, which shows a plate under uniform stress with a longitudinal fillet-welded attachment. The nominal stress is the uniform stress away from the attachment that can be calculated using simple bending and axial load equations.

At the attachment, the nominal stress becomes amplified from several sources of stress concentration. First, the amplification is reflected in the local structural stress, or the hot-spot stress. AASHTO defines the local structural stress as the stress at a welded detail including all stress raising effects of a structural detail but excluding all stress concentrations due to the local weld profile itself.

Second, there is the local total stress. While the local structural stress is computed using extrapolation methods, the local total stress is not based on extrapolation. Rather it is dependent on random parameters, such as weld profile and ripples in the weld toe, and typically cannot be accurately characterized through analysis. Fracture mechanics can be applied to analyze qualitative aspects of the problem; however, many assumptions are required to provide meaningful quantitative results.

SECTION 5.2 LOAD-INDUCED VS. DISTORTION-INDUCED FATIGUE

Fatigue cracking is classified as either load- or distortion-induced. The assumption has been that fatigue stresses can be calculated, usually at an elementary level. The loads used are similar to those associated with the in-plane strength design of the members. In many instances, however, fatigue crack growth results from the imposition of deformations, not loads. Distortion-induced fatigue stresses are not typically quantified by analysis. Although it is possible in some of these cases to calculate a stress range, this is usually performed after the fact with very refined analysis and requires that comparison field measurements be made. Designers are not likely to be able to identify the need for such calculations in the course of their work. As will be seen, this type of fatigue crack growth results from the imposition of relatively small deformations, usually out-of-plane, in local regions of a member. These deformations are not anticipated in the design process

because they are not captured in simple distribution, or grillage analysis. The main defense against this source of cracking is proper detailing, and this, in turn, is dependent on experience.

Distortion-induced cracking is estimated to be the cause of over 90 percent of all fatigue cracking (Connor and Fisher, 2006).

SECTION 5.3 GLOBAL ANALYSIS

The analysis of bridges and structures is a mixture of science and engineering judgment. In most cases, simple models with conservative assumptions can be used to arrive at the design forces for various elements. From these design forces, specifically moments, nominal stresses are determined. For example, for straight beam bridges with small skews, beam line models with approximate distribution factors can be used to arrive at the design moments. For more complex structures or for situations where refinement offers significant benefits, a more refined analysis (e.g., grid or 3-D) might be justified.

AASHTO LRFD (AASHTO, 2015b) provides two methodologies to determine nominal stresses:

- Approximate methods as specified in *AASHTO LRFD* Article 4.6.2
- Refined methods as specified in *AASHTO LRFD* Article 4.6.3

Design and evaluation seek to estimate the performance of new and existing bridges with the least amount of effort.

Within a given design or evaluation procedure, the engineer has the option of using simplified methods that tend to be somewhat conservative or pursue a more refined approach for improved accuracy when necessary to achieve better results. It is recommended that wherever feasible, simplified analysis procedures should be applied first, before resorting to higher-level analysis methods.

Refined methods, such as finite element analysis, load testing, and site-specific live load factors, can be applied to reduce uncertainties in bridge design and evaluation, thereby achieving increased load capacities while maintaining the same target reliability level.

5.3.1 Approximate Analysis

The focus of this section is an introduction to live load distribution analysis for longitudinal and transverse members. Since the 1930's, designers have used simplified distribution factors that isolate the transverse design of a bridge from its longitudinal design. Live load distribution analysis is an integral component of typical fatigue design and evaluation of bridges.

Approximate methods of structural analysis suitable for the design and evaluation of bridges can be found in Section 4 of *AASHTO LRFD* (AASHTO, 2015b) and in Section 6A.3 of the *MBE* (AASHTO, 2015d). An approximate method of analysis can be utilized to determine the live load distribution to individual components of typical highway bridges. Live load distribution factors are dependent on multiple characteristics of each bridge.

5.3.1.1 Main Members

The cross-section type of the girders and deck influence their relative stiffnesses and therefore the load distribution. The design moment in the girder will vary with girder spacing, span length, flexural stiffness, and torsional stiffness. *AASHTO LFRD* expressions account for many parameters that were neglected previously, including skew.

The different distribution formulas are tied to the member type and load effects. The LRFD load distribution formulas are specified for exterior and interior girders, for shear and moment, and for one-lane loaded and two-or-more-lane loaded cases. The distribution factors are expressed as a fraction of full lanes.

When the bridge is analyzed for fatigue design or evaluation by approximate load distribution, as specified in *AASHTO LFRD* Article 4.6.2, the distribution factor for moment for one traffic lane should be used. As discussed earlier, the *AASHTO* fatigue methodologies are based upon a single truck at a time on the bridge, representing the worst case for accumulating fatigue damage, and nominal fatigue stresses are derived from moments.

The types of superstructures covered by the distribution-factor equations are described in *AASHTO LFRD* Table 4.6.2.2.1-1. The distribution-factor equations for moments in interior and exterior girders appear in *AASHTO LFRD* Tables 4.6.2.2.2b-1 and 4.6.2.2.2d-1, respectively. Figure 5.3.1.1-1 illustrates the cross referencing of the superstructure types with the distribution-factor equations for moment in interior girders.

Table 4.6.2.2.1-1 Common Deck Superstructures Covered in Articles 4.6.2.2.2 and 4.6.2.2.3.

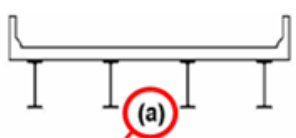
Supporting Components	Type Of Deck	Typical Cross-Section
Steel Beam	Cast-in-place concrete slab, precast concrete slab, steel grid, glued/spiked panels, stressed wood	

Table 4.6.2.2.2b-1 Distribution of Live Loads Per Lane for Moment in Interior Beams.

Type of Superstructure	Applicable Cross-Section from Table 4.6.2.2.1-1	Distribution Factors	Range of Applicability
Wood Deck on Wood or Steel Beams	a, l	See Table 4.6.2.2.2a-1	
Concrete Deck on Wood Beams	l	One Design Lane Loaded: $S/12.0$ Two or More Design Lanes Loaded: $S/10.0$	$S \leq 6.0$
Concrete Deck, Filled Grid, Partially Filled Grid, or Unfilled Grid Deck Composite with Reinforced Concrete Slab on Steel or Concrete Beams; Concrete T-Beams, T- and Double T-Sections	a, e, k and also i, j if sufficiently connected to act as a unit	One Design Lane Loaded: $0.06 + \left(\frac{S}{14}\right)^{0.4} \left(\frac{S}{L}\right)^{0.3} \left(\frac{K_g}{12.0 L t_s^3}\right)^{0.1}$ Two or More Design Lanes Loaded: $0.075 + \left(\frac{S}{9.5}\right)^{0.6} \left(\frac{S}{L}\right)^{0.2} \left(\frac{K_g}{12.0 L t_s^3}\right)^{0.1}$ use lesser of the values obtained from the equation above with $N_b = 3$ or the lever rule	$3.5 \leq S \leq 16.0$ $4.5 \leq t_s \leq 12.0$ $20 \leq L \leq 240$ $N_b \geq 4$ $10,000 \leq K_g \leq 7,000,000$ $N_b = 3$

Figure 5.3.1.1-1 Cross referencing of AASHTO LRFD tables.

A range of applicability is listed for each equation based on the parameters used in the equation. When the girder spacing exceeds the listed value in the “range of applicability” column, the specifications require the use of the lever rule or refined analysis methods. The lever rule can be conservative compared with other available methods of analysis, and the engineer might instead consider the use of refined analysis for parameters outside the “range of applicability.” The ranges of applicability for the variables involved are seen in the far right column of Figure 5.3.1.1-1.

As it turns out, an exponential distribution-factor equation is given in AASHTO LRFD Table 4.6.2.2.2b-1 for moment in interior girders with one design lane loaded, but AASHTO LRFD Table 4.6.2.2.2d-1 specifies the lever rule be used to determine moment in exterior girders with one design lane loaded. Thus, one lane loading is analyzed using the traditional lever rule to determine the fraction of live load carried by the exterior girder. A statical summation of moments is performed about one point to calculate the reaction at a second point. That reaction as a fraction of the live load is the distribution factor predicted by the lever rule method. The lever rule method conservatively predicts live load reaction on exterior beam lines. The lever rule only depends on geometry and does not account for the stiffness of the members since the assumed structural model is determinate.

The multiple presence factors of AASHTO LRFD Article 3.6.1.1.2 are not applicable for fatigue. Thus, the exponential distribution factor equation for interior girders should be divided by 1.2 as it is implicitly included in the formulation, and no multiple presence factor should be used with the lever rule for exterior girders.

Design Example

The given parameters for an approximate-analysis design example are as follows in Figure 5.3.1.1-2 through Figure 5.3.1.1-5.

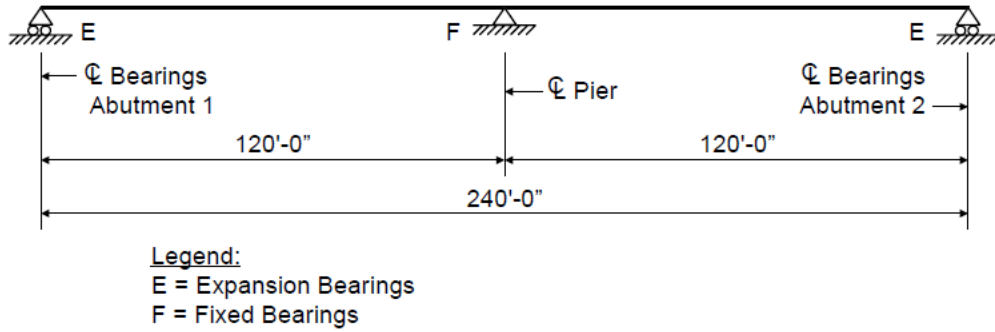


Figure 5.3.1.1-2 Girder-elevation schematic.

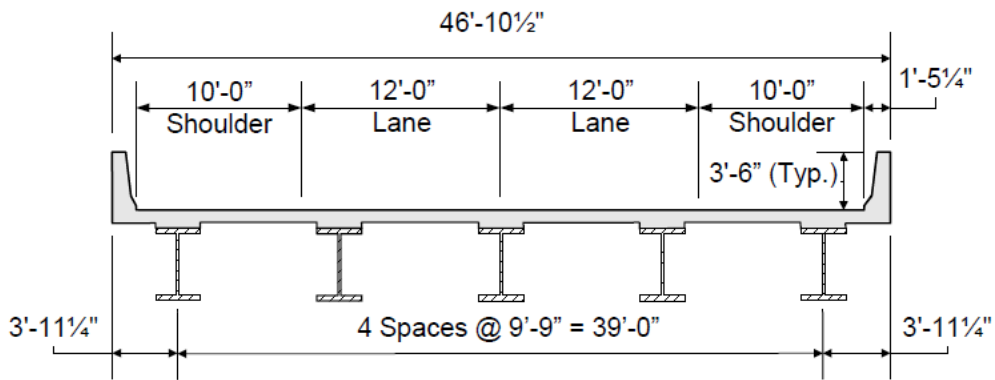


Figure 5.3.1.1-3 Bridge typical section.

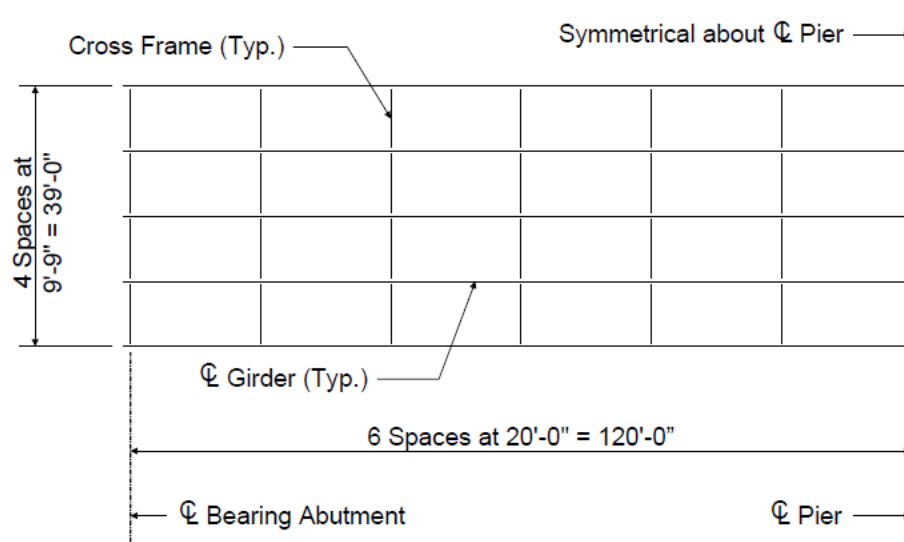


Figure 5.3.1.1-4 Bridge framing plan.

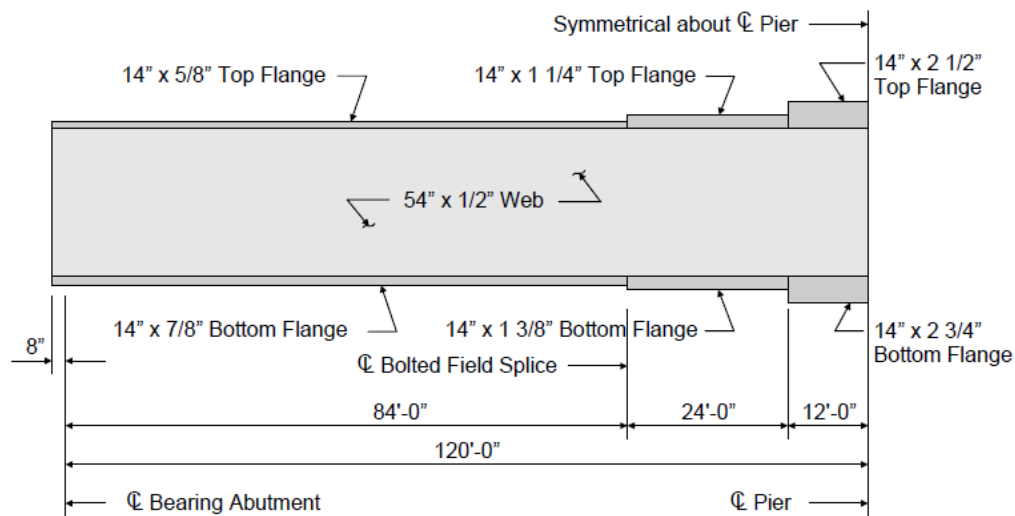


Figure 5.3.1.1-5 Girder half-elevation.

For this design example, fatigue will be checked for the fillet-welded connection of the transverse intermediate stiffeners to the girder. This detail corresponds to Illustrative Example 4.1 in *AASHTO LRFD* Table 6.6.1.2.3-1, and it is classified as Detail Category C' in *AASHTO LRFD* Table 6.6.1.2.3-1.

For this design example, the fillet-welded connection of the transverse intermediate stiffeners will be checked at the location of maximum positive moment. The fatigue detail is located at the inner fiber of the tension flange, where the transverse intermediate stiffener is welded to the

flange. However, for simplicity, the computations will conservatively compute the fatigue stress at the outer fiber of the tension flange.

The live load distribution factors for moment for an interior girder are computed as follows.

First, for interior girders, the longitudinal stiffness parameter, K_g , must be computed:

$$K_g = n \cdot (I + A \cdot e_g^2)$$

At the location of maximum positive moment:

$$\begin{aligned} n &= 8 \\ I &= 22,196 \text{ in}^4 \\ A &= 48 \text{ in}^2 \\ e_g &= 36.5 \text{ in} \end{aligned}$$

Therefore,

$$K_g = 689,150 \text{ in}^4$$

After the longitudinal stiffness parameter is computed, *AASHTO LRFD* Table 4.6.2.2.1-1 is used to find the letter corresponding with the superstructure cross section. The letter corresponding with the superstructure cross section in this design example is "a."

For one design lane loaded, the distribution of live load per lane for moment in interior beams from *AASHTO LRFD* Table 4.6.2.2.2b-1 is as follows:

$$g = 0.06 + \left(\frac{S}{14}\right)^{0.4} \left(\frac{S}{L}\right)^{0.3} \left(\frac{K_g}{12Lt_s^3}\right)^{0.1}$$

where:

$$\begin{aligned} S &= 9.75 \text{ ft} \\ L &= 120 \text{ ft} \\ t_s &= 8.0 \text{ in} \end{aligned}$$

Therefore,

$$g = 0.47 \text{ lanes per interior girder}$$

As previously described, the exponential distribution factor equation for interior girders should be divided by 1.2 as it is implicitly included in the formulation. Therefore,

$$g = 0.47/1.2 = 0.39 \text{ lanes per interior girder}$$

At the location of maximum positive moment, the range of live load plus impact moment due to the passage of the fatigue truck is given as:

$$M = 1198 \text{ k-ft per lane}$$

and

$$S_{b\text{-interior}} = 1307 \text{ in}^3$$

Therefore,

$$gM = 467 \text{ k-ft per interior girder}$$

$$f_{b\text{-interior}} = 4.29 \text{ ksi for an interior girder}$$

For one design lane loaded, the distribution of live load per lane for moment in exterior beams is computed using the lever rule, as per *AASHTO LRFD* Table 4.6.2.2.2d-1, as follows (see Figure 5.3.1.1-6):

$$g = \frac{(0.5)(4.25) + (0.5)(10.25)}{9.75}$$

$$g = 0.74 \text{ lanes per exterior girder}$$

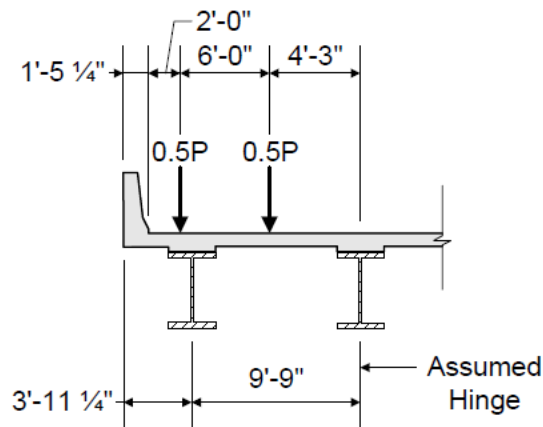


Figure 5.3.1.1-6 Schematic of the lever rule.

For the exterior beam,

$$M = 1198 \text{ k-ft per lane}$$

and

$$S_{b\text{-exterior}} = 1240 \text{ in}^3 \quad (\text{as the bridge-deck overhang is less than one-half of the})$$

girder spacing shown in Figure 5.3.1.1-6 above, the composite exterior girder is less stiff)

Therefore,

$$gM = 887 \text{ k-ft per exterior girder}$$

$$f_{b\text{-}exterior} = 8.58 \text{ ksi for an exterior girder}$$

Each of these stresses must be compared to the permissible stresses for the AASHTO Fatigue I and Fatigue II load combinations, and the appropriate checks must be satisfied. These topics are further covered in Chapter 6.

5.3.1.2 Transverse Members

LRFD distribution formulas cannot be used for transverse members spaced greater than 6 feet on center.

A lever-rule method of analysis is generally used for such members. The loading on longitudinal members is converted to live load reactions on a transverse member.

The controlling members for fatigue can include the transverse floorbeams. The current specifications assume no lateral load distribution on the floorbeams. If the floorbeam does not come into contact with the slab, the lever rule should be used to determine the moment in the floorbeam. If the floorbeam does come into contact with the slab, the load is transferred in a more complex manner. The percentage of moment taken by the floorbeam and slab will vary according to the relative stiffness of the floorbeam and slab. A more refined approach to analysis may be used to provide a more realistic assessment of the floorbeam moment.

For cases where floorbeams have been used without stringers on highway bridges, it has appeared proper to calculate the live load reaction transmitted to the floorbeam assuming the deck slab to act as a continuous beam supported by floorbeams. No transverse distribution of wheel loads is allowed unless a refined analysis is used.

5.3.2 Refined Analysis

Bridges or loading conditions for which accurate live load distribution formulas are not readily available in *AASHTO LRFD* Table 4.6.2.2.1-1 should be analyzed by refined methods of analysis. In addition, bridges that fall outside the ranges of applicability of *AASHTO LRFD* Tables 4.6.2.2.2b-1 and 4.6.2.2.2d-1 should also be analyzed by refined methods. Refined analysis may also be considered and has been used to obtain more accurate and realistic stress ranges when assessing existing structures and performing remaining fatigue life analyses.

Horizontally curved bridges should be analyzed using refined methods in order to capture (i.e., model) complex force effects (e.g., warping stresses).

A highly deteriorated structure or a structure with extensive structural repairs or retrofits may behave differently than the structure as originally designed. Refined analysis procedures may be useful for a detailed fatigue investigation of such structures.

Depending upon the elements used, a refined analysis may yield moments from which nominal stresses can be derived, or it may yield nominal stresses directly.

Where the bridge is analyzed for design by any refined method, as specified in *AASHTO LRFD* Article 4.6.3, a single design truck should be positioned transversely and longitudinally to maximize stress range at the detail under consideration, regardless of the position of traffic or design lanes on the deck.

For diaphragms or cross-frames, the range of load is determined by the passage of the fatigue design truck along the length of the bridge but in a single transverse position (i.e., one particular lane). While previous versions of the AASHTO specifications allowed for the maximum tension load to come from loading in one lane and the compression load to come from another lane, this provision is no longer applicable. It should be noted that the single truck in a single lane provision is exclusively for diaphragms and cross-frames. For orthotropic decks or box girders, no such distinction is made.

If it were assured that the traffic lanes would remain as they are indicated at the opening of the bridge throughout its entire service life, it would be more appropriate to place the truck at the center of the traffic lane that produces maximum stress range in the detail under consideration. However, because future traffic patterns on the bridge are uncertain and in the interest of minimizing the number of required calculations, the position of the truck is made independent of the location of both the traffic lanes and the design lanes.

For fatigue evaluation, it may be appropriate to assume the single truck is in a striped lane if traffic patterns on the bridge have not changed since its opening.

For detailed information about modeling and analysis using refined methods, see FHWA's *Manual of Refined Analysis* (Modjeski and Masters, 2016).

SECTION 5.4 FATIGUE STRESS ANALYSIS

5.4.1 Nominal-Stress Approach

The nominal-stress approach is the simplest way to assess the fatigue limit state at a detail and, as such, is included in design specifications from a variety of industries. This approach determines fatigue resistance and applied stress based on calculating a nominal stress near the detail being considered using simple equations for resolving bending and axial load in the member. The local stress concentrations that occur at the detail and at the notch are accounted for in the specified fatigue detail category resistance, described in Chapter 6.

5.4.2 Local-Stress Approach

The local-stress approach is similar to the nominal-stress approach, but the S-N curves in this approach are based on the range in the local structural stress, also called the hot-spot stress. To produce the S-N curves, full-scale tests are performed and the hot-spot stress ranges are either measured (i.e., strain gauges) or calculated (i.e., refined finite element models) and plotted against the cycles to failure. In effect, the stress concentration is taken out of the fatigue resistance and, instead, is accounted for in the analysis. This has the advantage of collapsing all the S-N curves for different categories into a single baseline S-N curve, but it increases the complexity of the analysis. The test data and the baseline S-N curve still include the effect of the local total stress, which may be impossible to accurately calculate and, therefore, must still be treated empirically.

5.4.2.1 Application of Local-Stress Approach

For the limited number of bridge details shown in *AASHTO LRFD* (AASHTO, 2015b), full-scale tests resulted in the characterization of their fatigue resistance. Therefore, the nominal-stress approach has been satisfactory for the bridge industry and others as well. However, for tubular structures used for ancillary sign structures, the nominal-stress approach breaks down. Fatigue resistance of tube-to-tube connections is dependent upon member and plate thickness, tube diameter, and for end plate connections, parameters such as bolt circle diameter, anchor-rod diameter, and number of anchor rods, resulting in an infinite number of possible connections. Not every possible tube-to-tube connection can be tested to define a unique S-N curve for each. Therefore, the hot-spot stress approach was developed as the only practical alternative for tubular structures (AWS, 2010 and Marshall, 1992). For bridges, the hot-spot stress approach is useful in understanding the cracking that occurs from in-plane and out-of-plane forces (e.g., orthotropic steel decks and sign structures) since out-of-plane forces are not addressed by typical bridge analysis.

5.4.2.2 Stress Components

The local-stress (or hot-spot) location is often in high strain gradient fields and, as a result, measurement of the local structural stress involves considerable uncertainty. To address this problem, guidelines have been established to extrapolate a stress concentration factor (SCF) from multiple strain gauge measurements (Zhao et al., 1999). Another simple approach is to define the hot-spot stress as the stress measured with a 1/8-inch strain gauge placed as close as practically possible to the weld toe (e.g., centered about 1/4 inch from the weld toe) (Dexter et al., 1994).

The baseline curve is sensitive to the definition of the hot-spot stress. British Standard (BS) 7608 (BSI, 1994) defines a Category T curve, along with a correction factor based on the plate thickness, and AWS (AWS, 2010) uses the X2 curve. As it turns out, these curves are similar to AASHTO Detail Category C, which is the nominal stress S-N curve associated with butt welds with reinforcement (not ground flush) in a flat uniform plate. Therefore, the hot-spot stress is equal to the nominal stress in this detail. For assessment of web gap details and other bridge details using the hot-spot approach, it is recommended that AASHTO Detail Category C be used

together with a hot-spot stress range measured or calculated $\frac{1}{4}$ inch from the weld toe (Dexter et al., 1994).

It should be noted that, although AASHTO does not explicitly classify detail categories for distortion-induced fatigue, they limit the development of web-gap stresses through improved detailing requirements. While these fatigue issues can be avoided in new bridges through the use of proper detailing, there are many thousands of in-service bridges dating back to before the mid-1970's that are susceptible to such cracking (Connor and Fisher, 2006). Research has demonstrated that distortion-induced fatigue can be classified as a Category C detail (Connor and Fisher, 2006). When the transverse stiffeners serve as diaphragm connection plates, the number of cycles to initiate distortional fatigue cracking of the web at the stiffener termination coincides with data for the AASHTO S-N curve for Category C details.

In design, the hot-spot stress approach involves the calculation of the stress concentration factor using parametric equations or finite element analysis (FEA) (AASHTO, 2015b; Connor et al., 2012; IIW, 2007; Zhao et al., 1999). However, FEA results are highly mesh dependent, since the local structural stress is often in an area of high strain gradients.

The disadvantage in the local-stress approach lies mainly in the variability between different hot-spot stress definitions and varying baseline S-N curves. Another problem involves the constant amplitude fatigue threshold (CAFT). The hot-spot approach implies that all details will have a CAFT at the same number of cycles, while full-scale fatigue tests show that the CAFT occurs at different orders of magnitude of cycles for different categories. As a result, a conservative approach is to ignore the CAFT for the hot-spot stress approach.

5.4.2.3 Model Discretization and Calibration

Stress evaluation at weld toes presents technical problems to the analyst who uses FEA, in that the angle the weld makes with the base material represents a sharp discontinuity. At that precise point, the discontinuity will cause the model to show a sharp increase in stress that is not in any way similar to the calculated stresses used to produce the fatigue database that created the widely adopted S-N curves. Thus, the concentration part of the stress that is a component of the baseline data provided in the AASHTO nominal-stress provisions must be eliminated from the assessment of the stress for such data to be of any use. It follows that for any modeling technique, there must be associated a calibration method to bring the estimated stress in line with the procedure used to evaluate stresses for the production of the database.

Finite element meshing can be accomplished using shell / plate elements or brick elements. It is the consensus of the industry at this time that shell / plate elements are adequate to characterize structures and local effects that are typically composed of relatively thin material with small effects in the through-thickness direction. This does not prohibit analysts from using brick element techniques, should they so desire, as calibration techniques are available for both.

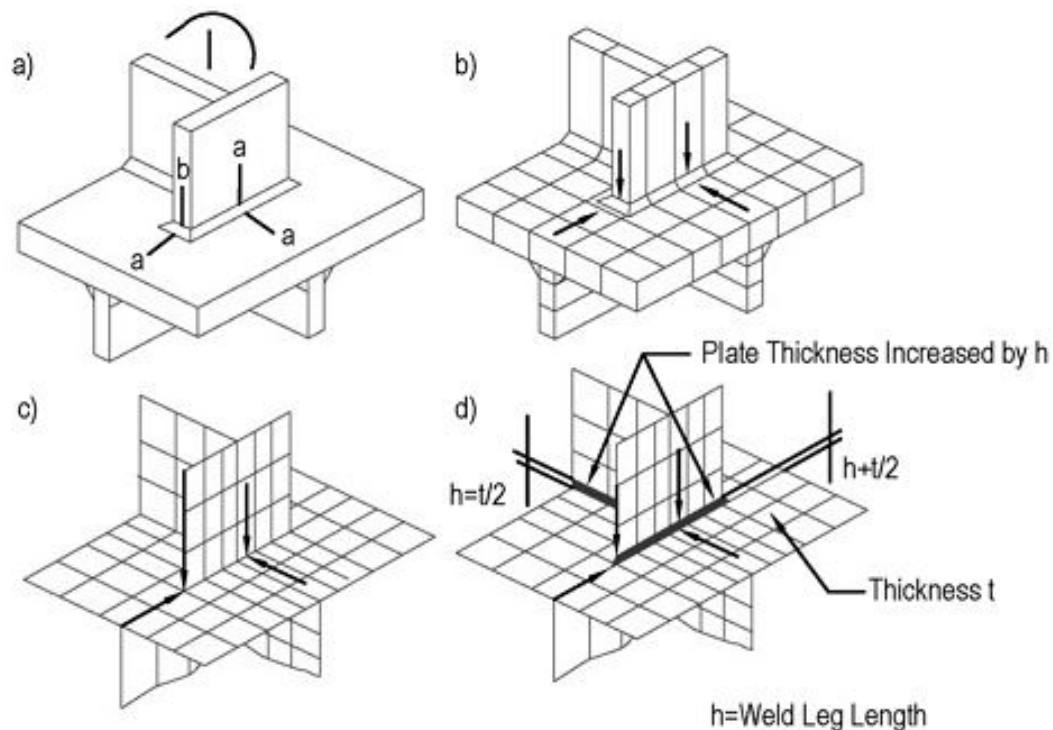
There are two accepted techniques that provide this calibration. Both use databases that are dissimilar to that adopted by AASHTO. They are the following:

- Extrapolation
- The Battelle Structural Stress (Dong and Hong, 2006)

The extrapolation method is more widely accepted and is discussed further below.

Figure 5.4.2.3-1 shows diagrams of conceptual connections for the purpose of illustrating concentrations at weld toes in abrupt transitions and in continuous fillets. In most cases, shell element sizes are standardized for determining weld toe stresses. Brick elements are often invoked at abrupt terminations.

Currently, the AASHTO specifications only apply the shell-element formulation, which is thus of interest for highway structures.



- a) Weldment prototype illustrating type "a" and "b" weld termination fatigue details
 b) Brick element model of prototype
 c) Shell element model of prototype
 d) Shell element model of prototype with plate increases at joints

Figure 5.4.2.3-1 Modeling guidance for evaluation of stress concentrations by extrapolation.

Figure 5.4.2.3-2 shows that points on the finite element are selected at an appropriate distance from the weld toe for Type "a" and Type "b" details illustrated in Figure 5.4.2.3-1 and how the stress is extrapolated to the weld toe to obtain the local structural stress.

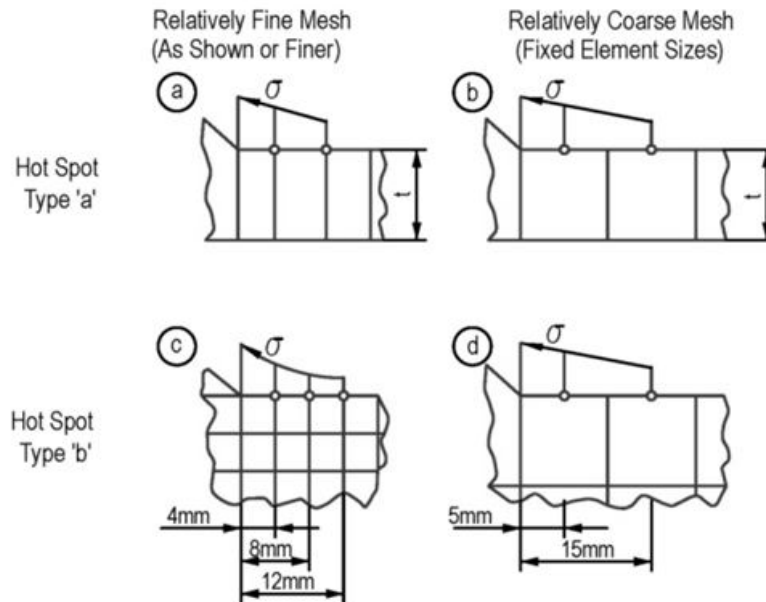


Figure 5.4.2.3-2 Stress extrapolation.

Table 5.4.2.3-1 provides a summary of appropriate mesh sizes.

Table 5.4.2.3-1 Recommended mesh sizing and extrapolation for fine and coarse meshes for analysis of stress concentration.

Type of Model and Weld Toe		Relatively Coarse Models		Relatively Fine Models	
		Type a	Type b	Type a	Type b
Element Size	Shells	$t \times t$ $\max t \times w/2$ (*)	10 x 10 mm	$\leq 0.4 t \times t$ or $\leq 0.4 t \times w/2$	$\leq 4 \times 4$ mm
	Solids	$t \times t$ $\max t \times w$	10 x 10 mm	$\leq 0.4 t \times t$ or $\leq 0.4 t \times w/2$	$\leq 4 \times 4$ mm
Extrapolation Points	Shells	0.5 t and 1.5 t mid-side points (**)	5 and 15 mm mid-side points	0.4 t and 1.0 t nodal points	4, 8, and 12 mm nodal points
	Solids	0.5 t and 1.5 t surface center	5 and 15 mm surface center	0.4 t and 1.0 t nodal points	4, 8, and 12 mm nodal points

Legend:

(*) w = longitudinal attachment thickness + 2 weld leg lengths

(**) surface center at transverse welds, if the weld below the plate is not modelled

The validity of the locations of the extrapolation points is based on the authors' affirmations that those locations give best fit to the baseline data. Other codes, such as the DNV or the AWS fatigue criteria (AWS, 2010), have alternate extrapolation criteria, indicating that for shell elements, the weld at the toe be extrapolated to the mid-plane of the shell. This is a more conservative approach, but it is accepted practice.

Again, for bridge structures, element meshes are relatively coarse, and the coarse-mesh columns of Table 5.4.2.3-1 are of concern to the bridge engineer.

The local-stress approach (or hot-spot stress approach) appears in *AASHTO LRFD* (AASHTO, 2015b), where the procedures discussed above are applied by the designer. It also appears in the *LRFD Specifications for Structural Supports for Highway Signs, Luminaires, and Traffic Signals* (AASHTO, 2015c), where these procedures have been applied for the designer, resulting in a more empirical presentation.

5.4.2.4 Example of Application of the Local-Stress Approach

Though the local-stress (or hot-spot analysis) approach is not applied for typical bridge design, the following application not only illustrates its application where appropriate (e.g., orthotropic steel bridge decks and sign structures) but also reinforces the nominal stress, local structural stress, and local total stress concepts originally introduced in Chapter 2.

In this application, a stress range of 1 ksi is applied to a cruciform specimen, symmetrical about the vertical axis, with additional welded attachments as shown in Figure 5.4.2.4-1.

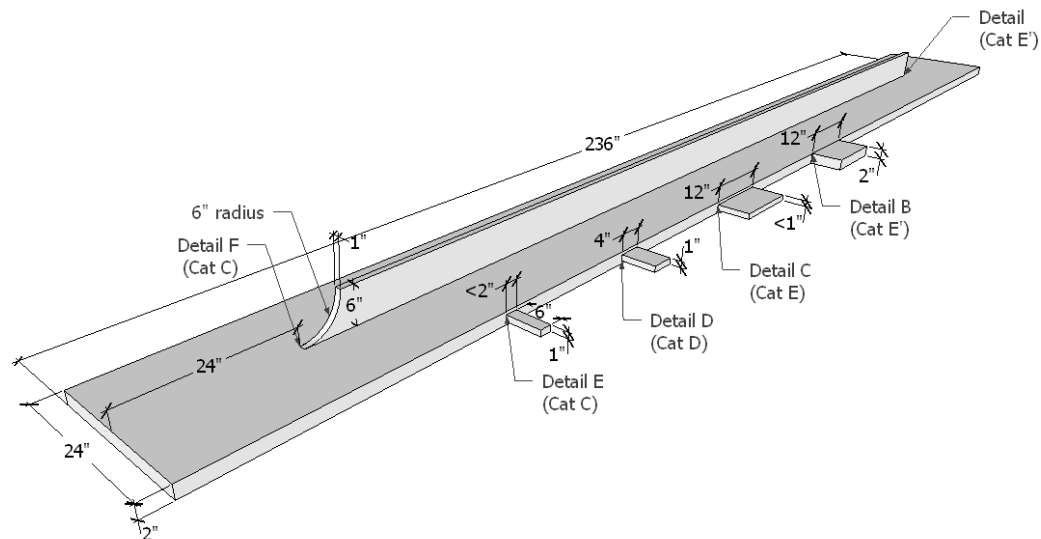


Figure 5.4.2.4-1 Cruciform specimen with attachments.

The attachments are characterized in Table 5.4.2.4-1 by length, thickness, and end treatment.

Table 5.4.2.4-1 Detail characterization.

Detail	Description
A	Long attachment with non-tapered end
B	Relatively long, medium thick attachment
C	Relatively long, medium thin attachment
D	Relatively short, medium attachment
E	Short attachment
F	Long attachment with tapered end

The specimen was modeled using the local-stress (hot-spot) approach discussed above using 8-node brick elements with dimensions of approximately 1/8 inch by 1/8 inch by 1/8 inch in the areas of interest (conforming to Type b - Relatively Fine Model requirements).

The results of the analyses in terms of calculated and extrapolated stress ranges are plotted in Figure 5.4.2.4-2 for the two longitudinal stiffener ends and Figure 5.4.2.4-3 for the four longitudinally-loaded attachments. Recall, the remote stress is a value of 1 ksi so the stress located directly at the discontinuity is the extrapolated stress, and in this case is also the stress concentration factor. For the four longitudinally-loaded attachments, the extrapolated stress increases with thickness and length. For the two longitudinal stiffener ends, the extrapolated stress decreases with the radiused end treatment. In each figure, the nominal stress, the extrapolated local structural stress, and the stress concentration factor (SCF) are illustrated.

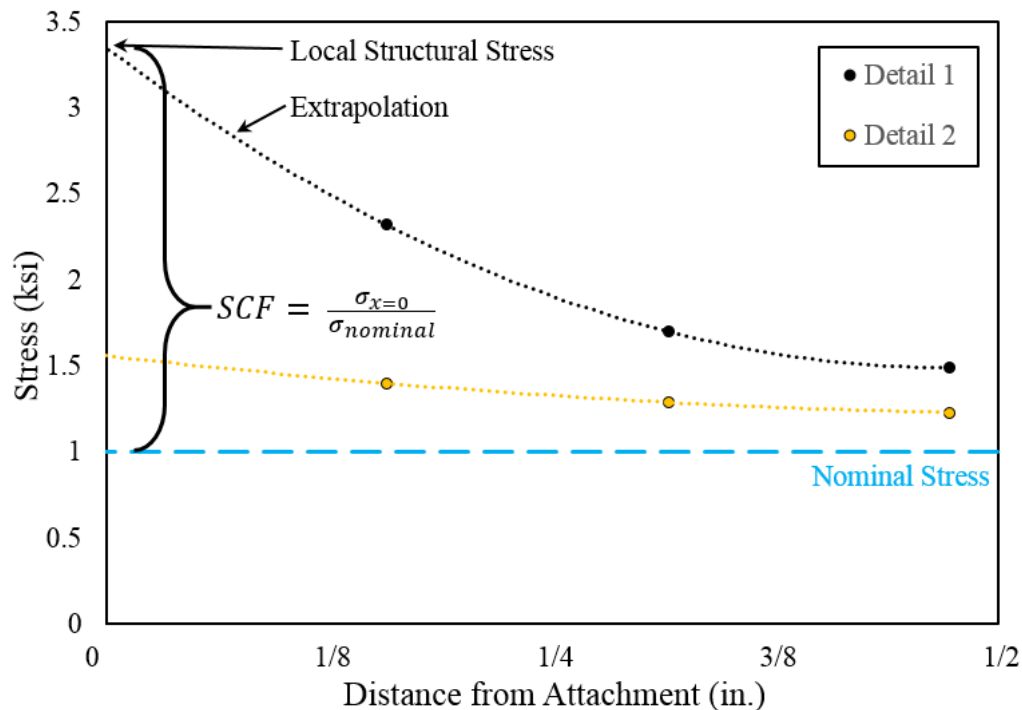


Figure 5.4.2.4-2 Extrapolated stresses at longitudinal stiffener details in Figure 5.4.2.4-1.

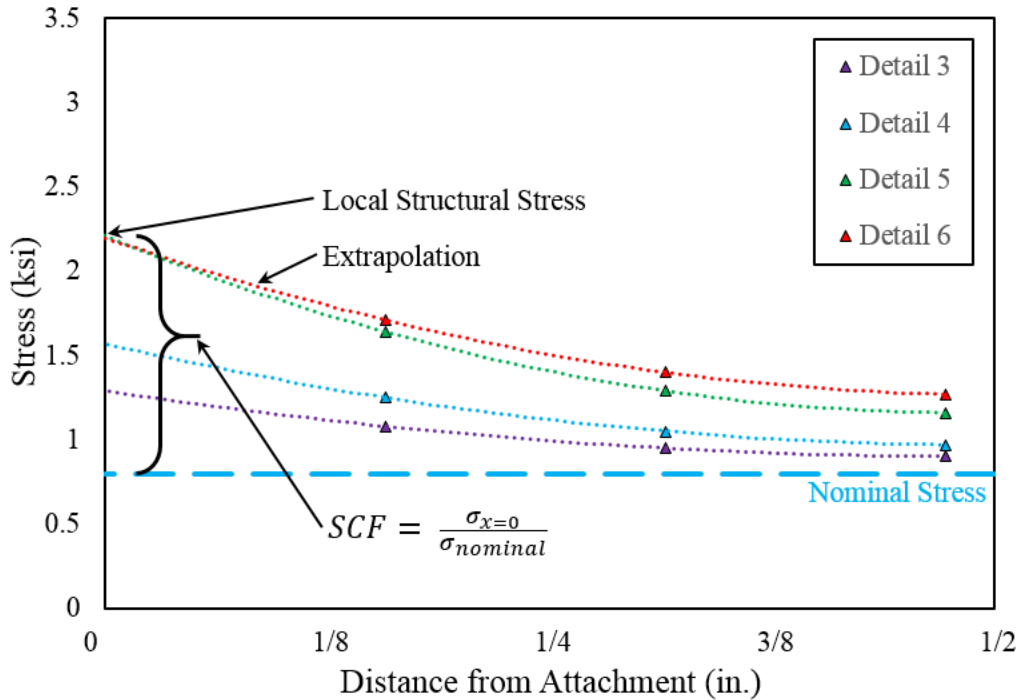


Figure 5.4.2.4-3 Extrapolated stresses at longitudinally-loaded attachments in Figure 5.4.2.4-1.

5.4.3 Fracture-Mechanics Approach

The basic concepts of the fracture-mechanics approach are described in detail in Chapter 3 to assist the reader in understanding the fatigue-and-fracture design and evaluation rules. However, the complexity of this approach is rarely warranted in design. Nevertheless, the concepts of fracture mechanics enable the designer to increase his or her qualitative understanding of structures containing sharp discontinuities. Because more parameters are explicit in fracture mechanics analyses, designers can identify more easily those parameters that influence the strength of the structure. Some examples covering the importance of discontinuities, parametric studies, and crack propagation behavior are presented in Chapter 3.

This page intentionally left blank

CHAPTER 6 AASHTO FATIGUE DESIGN APPROACH

SECTION 6.1 GENERAL

Fatigue in steel bridges is addressed in *AASHTO LRFD* by restrictions on the stress range due to live load plus impact produced by the passage of a code-specified fatigue design truck (load-induced fatigue) and by specific detailing requirements (distortion-induced fatigue). Both load-induced and distortion-induced fatigue must be considered separately during design, but they are addressed in different ways, as described in this chapter.

6.1.1 The Fatigue Limit State

Previous chapters explained that stress range is the dominant parameter for fatigue, and stress range can be readily computed by the design engineer at locations that have possibility of cracking. The design for load-induced fatigue requires that the factored stress range due to live load plus impact resulting from the passage of the fatigue design truck be less than the factored nominal resistance at every detail that is subjected to net tensile stress. The limit state is expressed mathematically as:

$$\text{Load} \leq \text{Resistance}$$

$$\gamma(\Delta f) \leq \phi(\Delta F)_n$$

Equation 6.1.1-1

The left side of the equation represents the factored stress range and is the product of a load factor, γ , and the computed stress range due to live load and impact in the member, Δf , at a detail of interest. Fatigue load factors are different from strength limit state load factors in that they are multipliers that are applied to the design truck to represent either a “maximum” (Fatigue I load combination) or “effective” (Fatigue II load combination) loading. *AASHTO LRFD* specifies a value of 1.75 for the Fatigue I load combination load factor and 0.8 for the Fatigue II load combination load factor. The right side of the equation represents the factored nominal resistance. For the fatigue limit state, the resistance factor, ϕ , is taken as 1.0 and safety is provided in the selection of the load factors and the confidence limit in the specified nominal resistance. A further discussion of recent studies and calibration of the fatigue limit state is provided in Appendix A.

Fatigue is addressed by two sets of design criteria, or load combinations, in *AASHTO LRFD*, the “Fatigue I” load combination and the “Fatigue II” load combination. These two load combinations are based upon the two distinct regimes of fatigue behavior. The Fatigue I load combination represents infinite fatigue life regime (i.e., the bridge can safely carry an infinite number of truck-load induced fatigue cycles). If this load combination is satisfied, the bridge will safely avoid cracking during a 75-year design life no matter how many constant amplitude stress cycles are applied. This is typically referred to as “infinite life.” The Fatigue II load combination represents finite fatigue life regime in which the resistance is not infinite due to the application of

higher stress ranges. If the Fatigue I load combination is not satisfied, the Fatigue II load combination may still provide adequate resistance for a projected number of stress cycles.

Both the Fatigue I and II load combinations were statistically calibrated as part of Transportation Research Board, Strategic Highway Research Project R19B (Modjeski and Masters, 2015). For the calibration of the two fatigue load combinations, the reliability index for the current design provisions (AASHTO LRFD) was computed. The term “reliability index” is a measure of safety given the statistical distributions of the load and resistance data. The reliability index is given the variable name of β . The concepts behind β are explained in Figure 6.1.1-1.

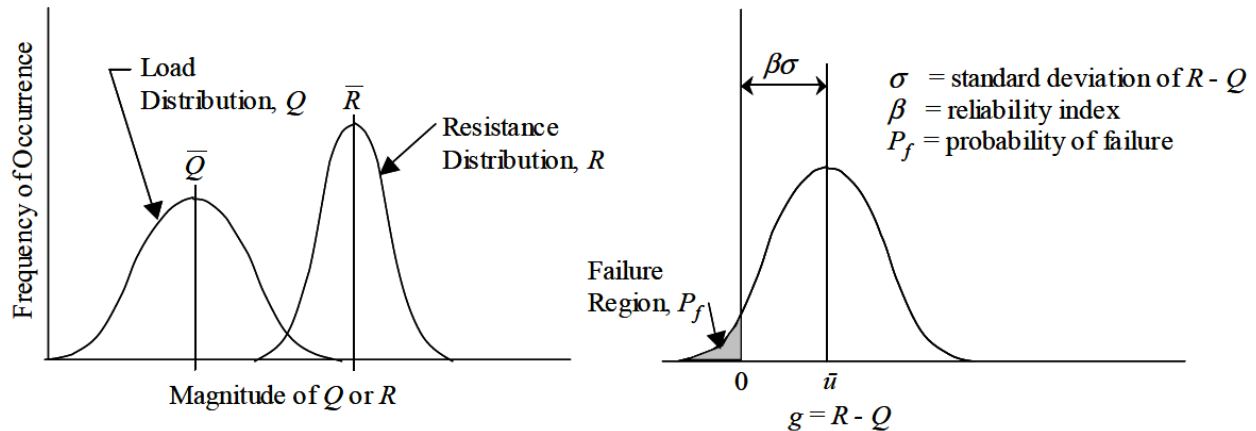


Figure 6.1.1-1 Definition of β using load and resistance statistical characteristics.

In Figure 6.1.1-1, the loads and resistances are represented by normal distribution curves. The figure includes a normal distribution curve for the loads, Q , and the resistance, R , and also presents their mean values, \bar{R} (R bar) and \bar{Q} (Q bar). The area of overlap where the extremes of the load and resistance distributions cross is considered to be failure. If a single curve is created by subtracting load from resistance (i.e., $R-Q$), the figure at the right is produced. When $R-Q$ is negative, load exceeds resistance, and the design does not satisfy the limit state objective. In order to control the number of failures, the mean of the $R-Q$ curve is offset some distance from zero, defined as β times the standard deviation, σ . A β equal to zero (no offset) indicates a 50 percent chance of failure. A β of 3.5, commonly used as a target for strength limit states, corresponds to a probability of failure of 2 in 10,000 times. The recent calibration of the fatigue limit state is based on a target β of 1.0, which corresponds well to the β found from assessing past LRFD practices. A β of 1.0 is consistent with a probability of failure of approximately 16 percent, a much larger chance the limit state will be exceeded (i.e. cracks may develop) than the accepted failure rate at the strength limit state.

Calibration of the Fatigue I load combination required that a load factor be chosen so that the maximum truck effect could be enveloped with a high degree of confidence. The maximum truck is one whose effects must be limited so that crack growth does not occur under infrequent passages. The concept of a maximum weight truck (or maximum stress range) is one which occurs a maximum of 1 in 10,000 occurrences. A load factor of 2.0, later revised to 1.75 by the R19B researchers, was suggested to account for the stress ranges of these infrequently occurring

vehicles. Similarly, calibration of the Fatigue II load combination was performed to address the accumulated damage of many millions of vehicle passages. A load factor of 0.8 was proposed to capture the cumulative force effects of millions of average or effective stress cycles. The calibration of both load combinations is discussed in this chapter, as well as in greater detail in Appendix A.

The philosophical underpinning of the AASHTO approach to fatigue design is based on the following assumptions:

- The total range of live load plus impact stress is damaging and must be considered.
- Residual stresses need not be considered.
- Only details subjected to net tensile stress need to be designed for fatigue.
- The stresses are generally calculated in composite bridges assuming the slab and girder are fully effective for both positive and negative bending moments.

SECTION 6.2 CLASSIFICATION OF FATIGUE

Two different sources of fatigue are identified in *AASHTO LRFD*: load-induced and distortion-induced fatigue.

Load-induced fatigue is defined in *AASHTO LRFD* as “*fatigue effects due to the in-plane stresses for which components and details are explicitly designed.*” Simply stated, load-induced fatigue is related to the in-plane primary stresses that are calculated from analysis. Examples of these in-plane stresses include the flexural stress in a flange or web of a steel I-girder, stress ranges in a cross-frame that result from a refined analysis, stress ranges at a shear stud to girder flange connection when designing a composite girder, stress ranges due to wind in light and sign structures, and other similar instances where engineers have results from analysis.

As described in Chapter 2, all steel structures possess initial discontinuities, stress concentrations, and residual stresses due to rolling and/or welding. Load-induced fatigue cracking is the growth of cracks from these conditions due to applied stress-range cycles from the passage of trucks, such as at the end of a cover plate end weld on the Yellow Mill Pond Bridge shown in Figure 6.2-1. This crack was detected in 1970 and is representative of cracking that occurred in some older bridges constructed when cover-plating rolled beams was a means of increasing their capacity. This type of detail is no longer used in new construction and simply illustrates a load-induced fatigue crack, a type which might still be found when inspecting older bridges. Details such as this one are not desirable for new bridges because of their poor fatigue performance.

Load-induced fatigue is controlled by the Fatigue I and II load combinations by which members are proportioned to limit stress ranges to those specified as allowable for each detail type.

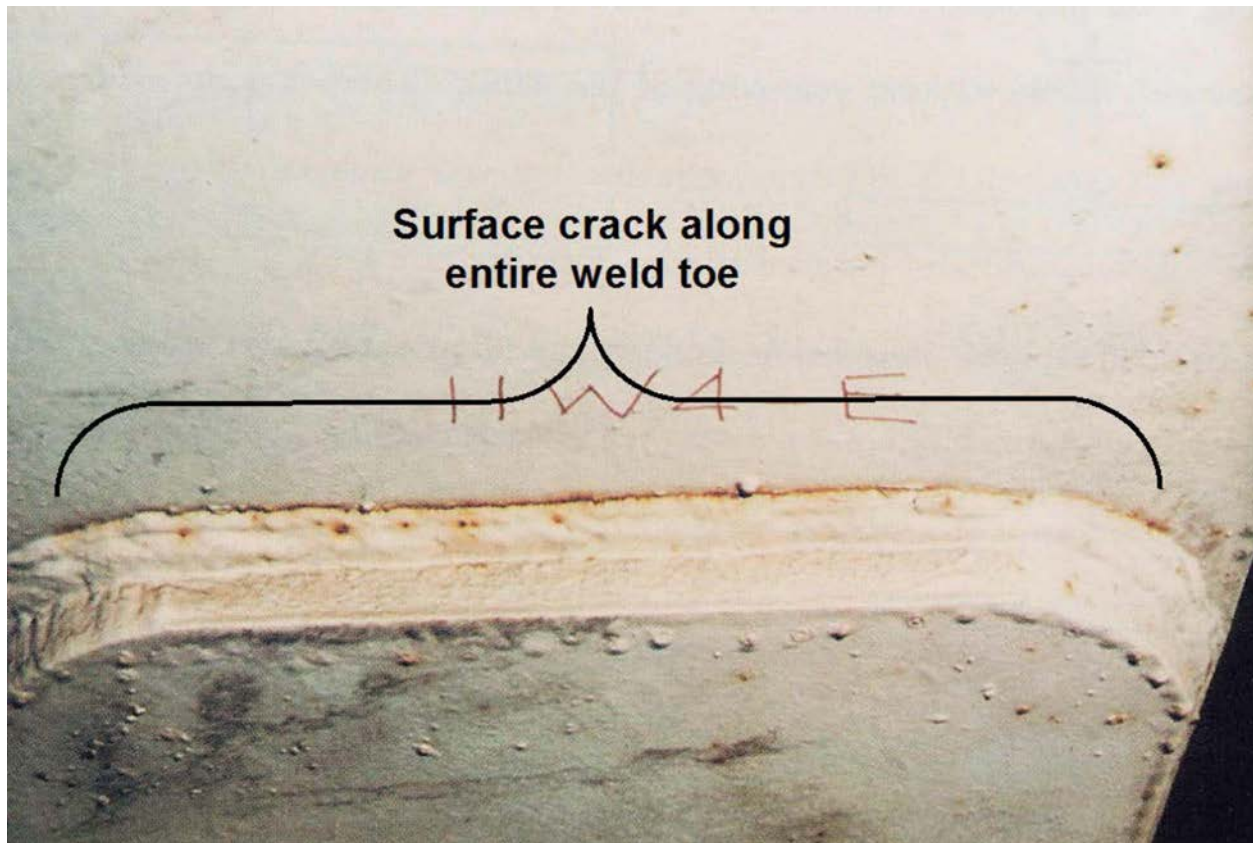


Figure 6.2-1 Cracking of a cover plate on the Yellow Mill Pond Bridge.

Distortion-induced fatigue is the designation given to cracking that arises from local out-of-plane secondary stresses not typically calculated in analysis. This type of cracking represents the majority of observed fatigue cracks that are discovered in in-service bridges. It occurs in bridges at diaphragm / cross-frame connection plates that are not positively attached to the girder flanges, at floorbeam connections to main girders, as well as in situations such as floorbeam to truss and tie girder connections. Since the mid-1980's, and dating back to the use of the *AASHTO Standard Specifications for Highway Bridges*, AASHTO has required the engineer to design new structures to prevent distortion-induced fatigue, though it remains an ongoing problem in many existing bridges (see Chapter 9 for repair and retrofit guidance). Distortion-induced cracking is prevented by providing a positive load path to transmit unintentional and intended force effects between transverse and longitudinal members. A schematic of the most common mechanism causing distortion-induced fatigue is provided in Figure 6.2-2.

Distortion-induced cracking is controlled by detailing members and connections to mitigate out-of-plane distortions, not by proportioning members to satisfy specific limit states.

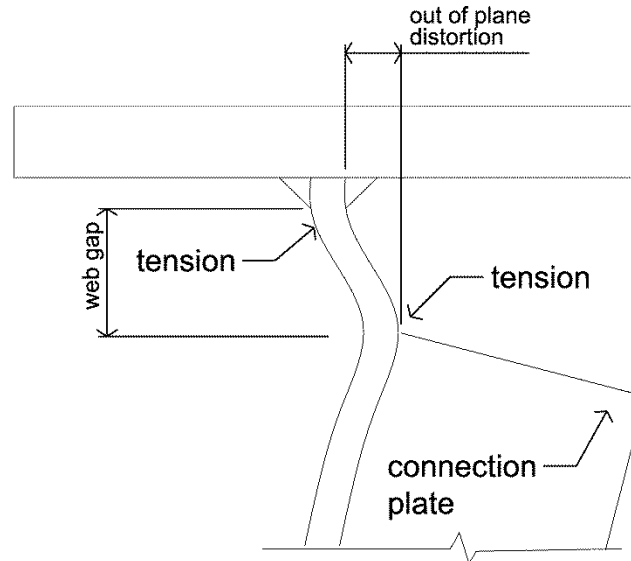


Figure 6.2-2 Common mechanism causing distortion-induced fatigue of a web gap and resulting web tensile stresses.

AASHTO designates fatigue categories to some design details that have no design nominal stress definition. Deck joints (e.g., modular joints) need to be designed by the vendor and then tested to define their fatigue acceptance, and AASHTO qualifies these by testing. Orthotropic decks also have fatigue design approaches that are codified.

SECTION 6.3 LOAD-INDUCED FATIGUE

6.3.1 General Limit State

To provide a standard definition of the load-induced fatigue limit state, *AASHTO LRFD* provides the following description in Article 1.3.2.3:

“The fatigue limit state shall be taken as restrictions on stress range as a result of a single design truck occurring at the number of expected stress range cycles.”

Furthermore, the commentary to the article states:

“The fatigue limit state is intended to limit crack growth under repetitive loads to prevent fracture during the design life of the bridge.”

With these two statements, a concise definition of the nature and intent of the limit state is provided. The purpose of the limit state check is to limit crack growth over the design life of the structure. The limit state is expressed mathematically as restrictions on cyclical stress ranges caused by the passage of a single design truck. It takes the form of Equation 6.1.1-1.

For the Fatigue I load combination, the load factor, γ , is 1.75, and for the Fatigue II load combination, γ is 0.8. For the fatigue limit state, Φ equals 1.0.

The factored force effect is on the left side of Equation 6.3.1-1, and the factored nominal resistance is on the right side, as shown in Equation 6.3.1-2.

$$\text{Factored Force Effect} \leq \text{Factored Resistance}$$

Equation 6.3.1-2

The force effect and resistance components are explored below.

6.3.1.1 Factored Force Effect

As introduced in Chapter 2 and numerically illustrated in Section 4.1.3, stress range is the dominant stress parameter for fatigue design. Further, Section 2.3.2.2 concludes that the most common cause of fatigue cracks in bridges is in-service cyclical stress range due to trucks. Therefore the fatigue limit state only considers force effects from live load and no other loads.

The Fatigue I load combination is applied to check if the detail under investigation will safely achieve infinite life. When a detail cannot provide infinite life due to the magnitude of the repeating stress range, the Fatigue II load combination is applied to ensure that the detail will exhibit sufficient finite life based upon the projected average daily truck traffic (ADTT) for 75 years, the design life specified in *AASHTO LRFD*.

The force effect for the fatigue limit state, Δf , is the live load stress range due to the passage of the fatigue load. The fatigue design vehicle is similar to the HL-93 design truck but with a constant spacing of 30.0 feet between the 32.0-kip axles, as illustrated in Figure 6.3.1.1-1. The 30-foot axle spacing is used for fatigue stress calculations to better represent the overall force effects of four- and five-axle semi-trailers that produce the majority of fatigue damage (AASHTO, 1990).

The single truck in a single lane concept was introduced with *AASHTO LRFD*. Prior to that, the *Standard Specifications for Highway Bridges* used a multi-lane distribution factor to design for fatigue, along with other differences. The single truck concept was validated as part of the SHRP2 Project R19B research (Modjeski and Masters, 2015), a summary of which is provided in Appendix A. The R19B research team evaluated millions of weigh-in-motion study records and determined there was a very small number of similar weight and configuration trucks traveling closely in the same lane or adjacent lanes and on that basis validated the prior assumption of a single truck in a single lane live load model.

The passage of the vehicle also produces a dynamic response. In addition to the static force effects, a 15 percent increase in the vehicle force effects is applied to account for dynamic load allowance, commonly called impact and abbreviated as “IM” in *AASHTO LRFD*. This is related to vehicle suspension characteristics, surface roughness of the approach and bridge pavement, and the natural frequency of the bridge.

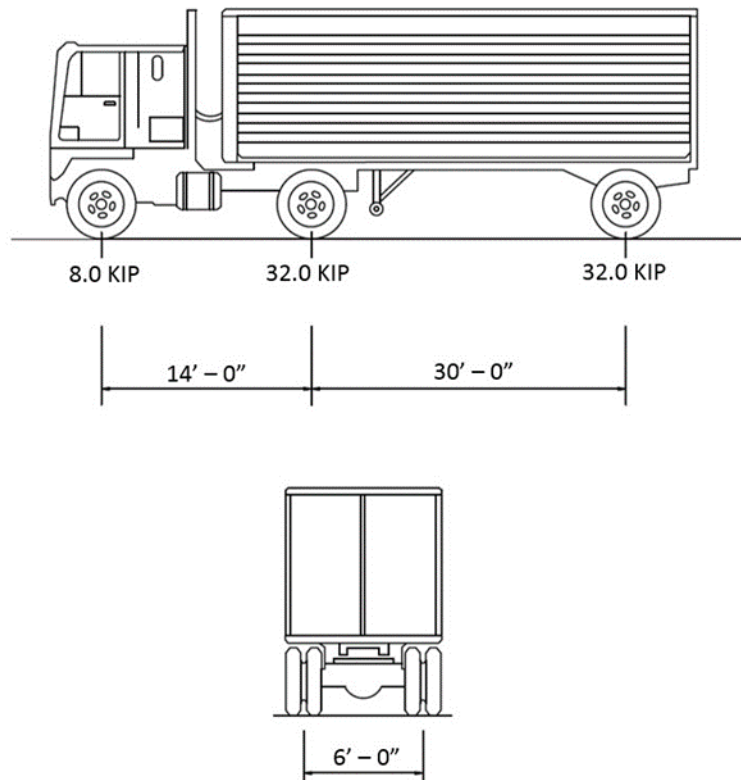


Figure 6.3.1.1-1 AASHTO fatigue design vehicle.

6.3.1.2 Factored Resistance

AASHTO LRFD specifies the design resistance of details based upon the testing and conclusions thereof discussed in Section 4.3. Details are categorized and organized into eight Detail Categories (A, B, B', C, C', D, E, and E') in order of descending fatigue resistance, which is shown graphically in Figure 6.3.1.2-1. Each piecewise continuous curve consists of a sloping portion of variable resistance followed by a straight horizontal line, representing the constant amplitude fatigue threshold (CAFT) as discussed previously in Section 4.3. All the fatigue details and their respective detail categories are presented in *AASHTO LRFD* Table 6.6.1.2.3-1. For each detail, a written description of the type of detail and orientation / type of loading is provided, along with a sketch illustrating the particular detail or application. Refer to *AASHTO LRFD* for the most current illustrations of each fatigue detail, though several examples are provided for common conditions herein. To recall, these resistance limits are established through testing and represent a 97.5 percent probability of survival in the region of finite life (sloping boundaries). The region of infinite life represented by the threshold is not statistically based, given a lesser number of long-life tests, though the Fatigue I load combination has been established to provide safe behavior for infinite life. A brief description of the detail categories is provided.

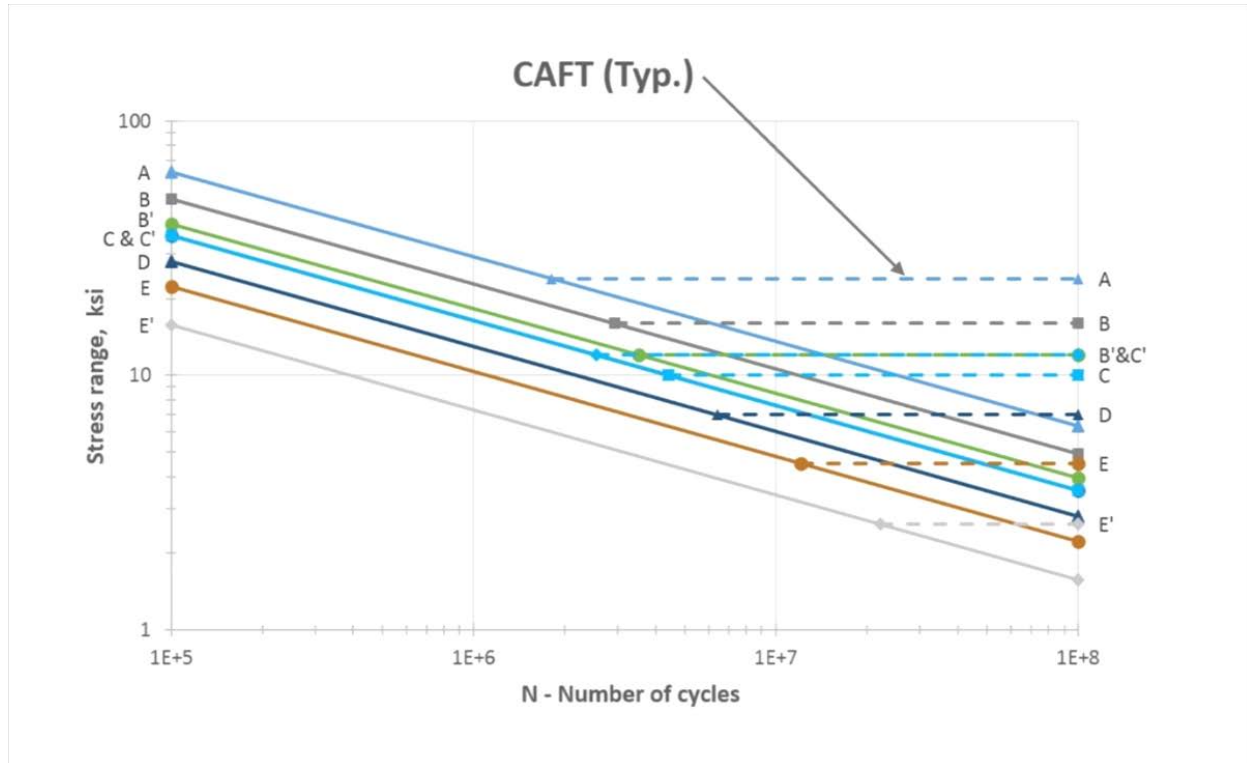


Figure 6.3.1.2-1 Nominal fatigue resistance of the detail categories specified in AASHTO LRFD.

Detail Category A – Detail Category A includes base metal (except for noncoated weathering steel) with no changes in geometry (e.g., a cope) and steel with rolled or cleaned surfaces and flame-cut edges fabricated with specific surface finish requirements. Detail Category A details represent the maximum fatigue resistance and therefore are unlikely to control the design of most steel structures since most steel members have details such as mechanical connections, welded connections, or welded attachments that reduce fatigue resistance. An example of a Detail Category A detail with illustration of potential crack initiation point is shown in Figure 6.3.1.2-2.

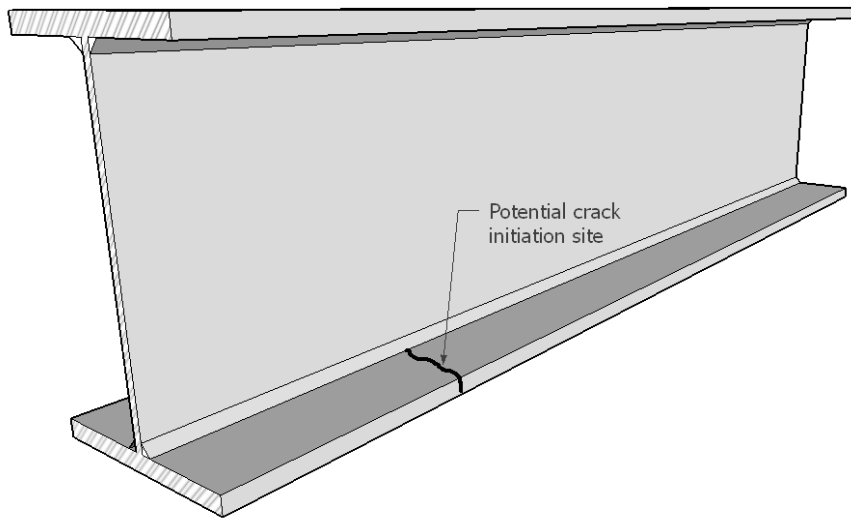


Figure 6.3.1.2-2 Detail Category A – example (base metal at edge of rolled beam).

Detail Category B – Detail Category B includes a variety of common welded details, such as longitudinally loaded built-up sections connected with fillet welds or full penetration groove welds that are welded from both sides. A common Detail Category B detail is the connection of a web and flange for a typical plate girder. Other examples of Detail Category B welded details include the side welds connecting cover plates to rolled shapes as is commonly found on older bridges, the welds throughout the length of a typical longitudinal stiffener, and full penetration butt splices with the welds ground smooth and weld soundness established by nondestructive testing (NDT). The Detail Category B designation also applies to mechanically fastened joints such as pretensioned slip critical connections, as well as bearing type connections with pretensioned high-strength bolts and standard size holes. Detail Category B also includes the base-metal fatigue resistance of noncoated weathering steel. An example of a Detail Category B detail is shown in Figure 6.3.1.2-3.

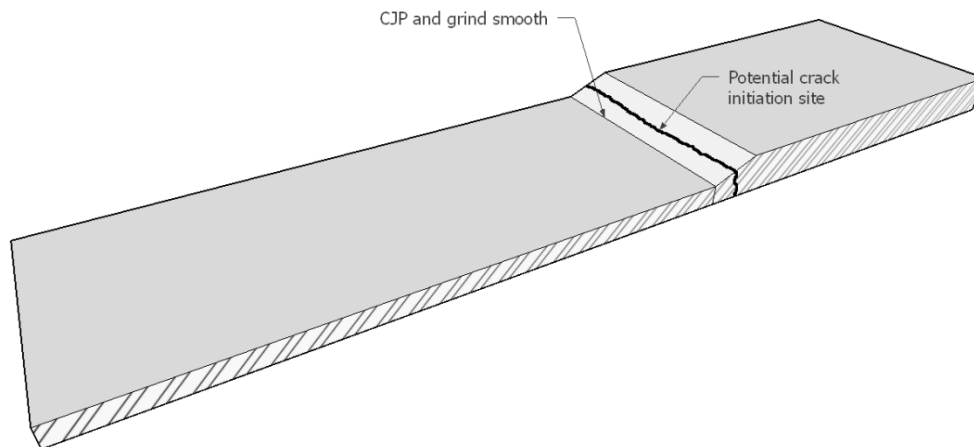


Figure 6.3.1.2-3 Detail Category B – example (full penetration groove weld).

Detail Category B' – Detail Category B' applies to built-up sections such as box members which are commonly constructed with one-sided full penetration welds with backing bars left in place after welding. The category also applies to box-shaped members with corners joined by partial penetration welds with the welds parallel to the direction of stress.

Detail Category C – Detail Category C applies to both base metal and welded connections. Examples of Detail Category C include reentrant corners, copes, cuts, blockouts, and other geometrical discontinuities that are commonly found when rolled shapes are modified to fit certain connection conditions. Detail Category C also applies to various welded details. This includes some longitudinally loaded stiffeners with radiused transitions and welds ground smooth at the end of the detail, certain transversely loaded details connected with full penetration or fillet welds, and special welds such as those used to construct elements of orthotropic deck systems. Details in Detail Category C are generally considered to be the transition between details affected primarily by discontinuities and those affected more so by stress concentration. An example of a reentrant corner crack for a Detail Category C detail is shown in Figure 6.3.1.2-4.

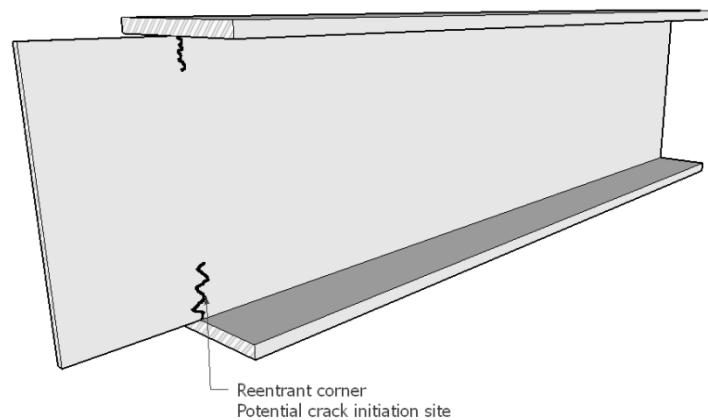


Figure 6.3.1.2-4 Detail Category C – example (reentrant corner).

Detail Category C' – Detail Category C' is a special detail category specifically reserved for checking the fatigue stress range effects in base metal at the toe of transverse stiffeners to flange fillet welds and transverse stiffener to web fillet welds. This detail category has the same fatigue life constant as Detail Category C, but it has a higher threshold stress. A transverse crack from a weld toe for a Detail Category C detail is shown in Figure 6.3.1.2-5.

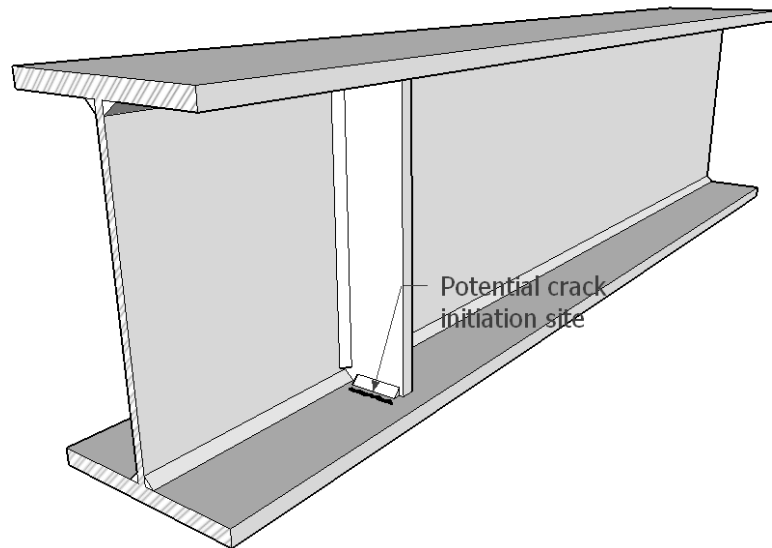


Figure 6.3.1.2-5 Detail Category C' – example (transverse stiffener).

Detail Category D – Detail Category D details are a transition between details influenced by discontinuities (A, B, B', C, and C') and those whose performance is dominated by geometry and stress concentration (D, E, and E') (see Figure 4.1.2-3). It includes both base metal, bolted joint details, and welded attachment details. Included are details such as open holes in steel sections; certain galvanized and bolted connection details; terminations of longitudinal stiffeners and gusset plates used to connect lateral bracing elements where the details have been improved by creating radiused end transitions; short longitudinal attachments without end treatment; several orthotropic deck details; and other details. Given the number of different types of details that fall in this category, Detail Category D is an example of fatigue life being related to stress concentration (in a relative sense) since base metal, bolted, and welded details are all addressed. All of these are subject to a stress concentration, be it from manufacturing such as punching of holes or from the welding of attachments to a steel element. An example of a crack from an open hole edge for a Detail Category D detail is shown in Figure 6.3.1.2-6.

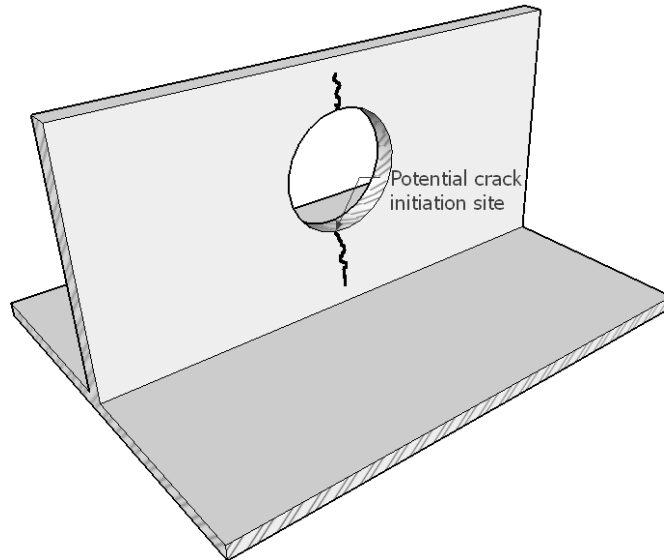


Figure 6.3.1.2-6 Detail Category D – example (open hole edge).

Detail Categories E and E' – The description of Detail Categories E and E' are grouped together as they generally apply to the same types of details. The Detail Categories E and E' details include weld and cover plate terminations, longitudinal stiffener terminations, lateral bracing connection plates, and miscellaneous welded attachments. Each one of these details is similar in that they are oriented parallel to the direction of primary stress in the member and are long enough and thick enough to draw stress out of the member with high stress concentrations at the ends of the section where the welds terminate (see Section 4.1.2). Detail Categories E and E' details also terminate abruptly, as compared to the Detail Category D details which have more gradual terminations and transitions and somewhat enhanced fatigue performance. It is this combination of high stress at the abrupt termination and the fact that the elements desire to draw load away from the basic member (due to its length and thickness) that gives rise to high local stresses and the potential for fatigue cracking. In examining the AASHTO detail categories, the engineer will notice that as elements grow longer parallel to the direction of primary stress in the member and as they grow thicker in dimension, the fatigue resistance diminishes. This observation is consistent with longer and thicker elements causing more severe stress concentrations in the base metal of the primary member as more stress is able to flow into them. See Section 4.1.2 for additional background discussion on the effect of attachment size on stress concentration. An example of cracking at the end of a cover plate for a Detail Category E / E' detail is shown in Figure 6.3.1.2-7.

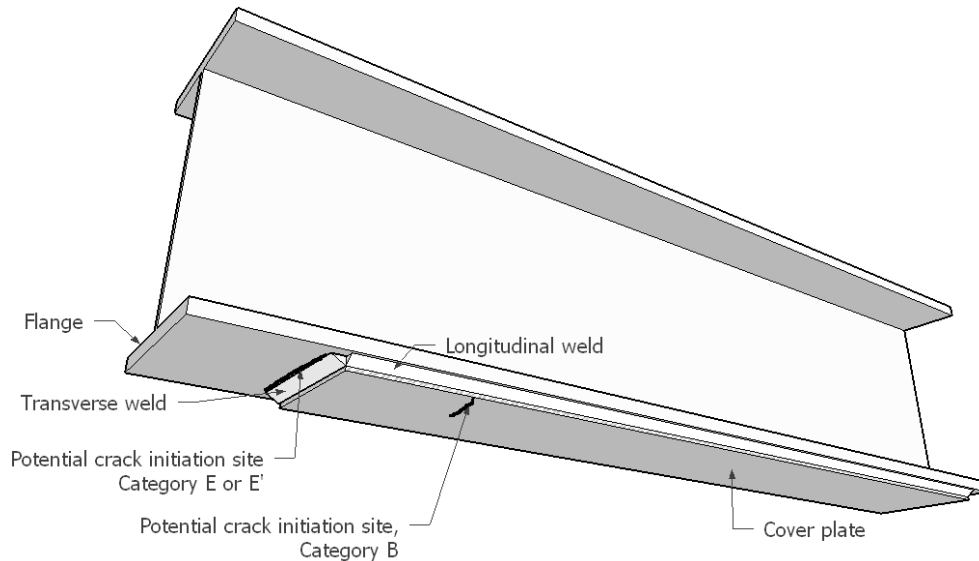


Figure 6.3.1.2-7 Detail Category E / E' – example (cover plate termination).

Regarding the various fatigue categories, it is worth noting that engineers have the freedom to modify specific design details in order to meet certain fatigue limit state requirements. An example is a longitudinal stiffener used to stiffen the web of an I-beam or box girder bridge. The most punitive fatigue category would be Category E', which is the appropriate fatigue category for a longitudinal stiffener equal to or greater than 1 inch thick and welded to the base metal with no end transition. The limits of a longitudinal stiffener are first and foremost defined by a strength requirement, yet the termination location of the stiffener is frequently related to the computed stress ranges where the engineer desires to end the stiffener. If the stress range at a desired termination point exceeds the Category E or E' allowable stresses as specified in *AASHTO LRFD*, the engineer has the opportunity to provide a radiused transition at the end of the stiffener or carry the detail longitudinally to a location on the member where it terminates in a zone of permanent compression. The effects of attachment thickness and end treatment are presented in Table 6.3.1.2-1, taken from the *AASHTO LRFD* specifications. When the stiffener terminates abruptly in a blunt end, the attachment is classified as Category E or E', depending on its thickness. With a more gradual transition, the condition at the end is improved. The improvement is without regard to attachment thickness. An example is presented in Figure 6.3.1.2-8.

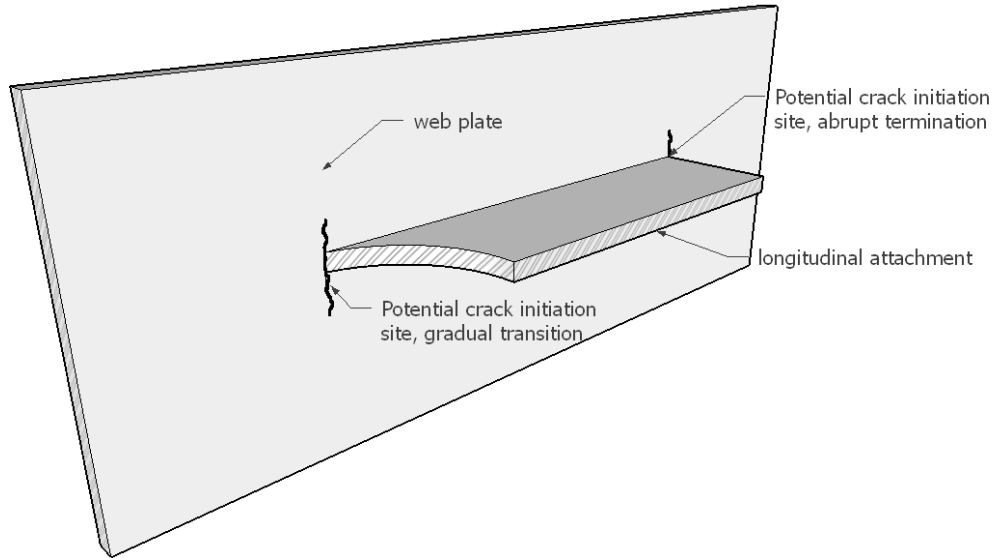


Figure 6.3.1.2-8 Improvement in detail category by end treatment.

Table 6.3.1.2-1 Variation of detail category for longitudinal stiffener terminations.

Description	Detail Category	Location of Cracking	Illustrative Figure
Base metal at the termination of longitudinal stiffener-to-web or longitudinal stiffener-to-box welds:			
With the stiffener attached by fillet welds and with no transition radius provided at the termination:			
Stiffener thickness < 1.0 in.	E	In the primary member at the end of the weld toe	See Figure 6.3.1.2-9
Stiffener thickness ≥ 1.0 in.	E'		
With the stiffener attached by welds with a transition radius, <i>R</i> , provided at the termination with the termination ground smooth:			
$R \geq 24$ in.	B	In the primary member near the point of tangency of the radius	See Figure 6.3.1.2-10
$24 \text{ in.} > R \geq 6$ in.	C		
$6 \text{ in.} > R \geq 2$ in.	D		
$2 \text{ in.} > R$	E		



Figure 6.3.1.2-9 Improvement in detail category by end treatment.

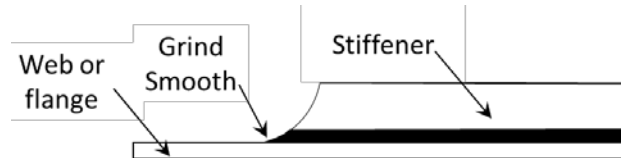


Figure 6.3.1.2-10 Improvement in detail category by end treatment.

6.3.2 Applicability

Load-induced fatigue cracks can only grow at details subjected to a net applied tensile stress. *AASHTO LRFD* Article 6.6.1.2 requires that wherever the maximum tensile live load stress due to the Fatigue I load combination exceeds the unfactored permanent compressive stress, details shall be evaluated for fatigue. If the tensile stress does not overcome the unfactored permanent load stress, net tensile loading is not available to grow a crack beyond the small zone of residual stress, even when a source of initiation is present.

6.3.3 Infinite Life – The Fatigue I Load Combination

The Fatigue I load combination controls the propagation of cracks that may occur when the maximum stress range is applied to a detail. It will control when there are higher numbers of applied stress cycles (ADTT). *AASHTO LRFD* Table 6.6.1.2.3-2 provides a table defining the equivalency between the variable amplitude fatigue life and infinite life curves shown previously in Figure 6.3.1.2-1. For the Fatigue I load combination, the loading terms are the load factor and computed stress range, respectively, and the nominal resistance is defined as the constant amplitude fatigue threshold (CAFT). Thus, the limit state equation becomes:

$$\gamma(\Delta f) \leq (\Delta F)_{TH}$$

Equation 6.3.3-1

where:

$$\begin{aligned} \gamma(\Delta f) &= \text{loading terms} \\ (\Delta F)_{TH} &= \text{nominal resistance as defined in } AASHTO LRFD \end{aligned}$$

The load effects and resistance are detailed in the following sections.

6.3.3.1 Factored Force Effect for Infinite Life

The load factor for Fatigue I, meant to preclude crack growth under the maximum stress range, is 1.75. The premise of the CAFT is that under constant amplitude loading, if all stress ranges are less than the threshold resistance, cracks will not propagate from a discontinuity. However bridges are not subject to constant amplitude loading but rather random loading with occasional large stress cycles. These larger stress cycles, even when limited to very low occurrences, can cause crack extension, and subsequent cycles of lesser stress ranges result in crack extension. Tests have determined that the number of stress cycles for these maximum stress ranges should be kept less than a 1:10,000 occurrence in order for the threshold behavior to be valid. The NCHRP 267 and 354 studies examined the long-life behavior under variable amplitude loading and tested the existence of the CAFT (Fisher, Mertz, and Zhong, 1983) and (Fisher, Nussbaumer, Keating, and Yen, 1993). Even with rates of exceedance as low as 0.05 percent, fatigue crack growth was evident in welded longitudinal web attachments and welded cover plates. Several transverse stiffeners demonstrated cracking with exceedance rates as low as 0.01 percent. The research demonstrated that the CAFT is a valid limit, but under variable amplitude loading, the number of cycles of CAFT exceedance must be severely limited. The use of a load factor of 1.75 for the infinite life check is intended to guard against, or design for, these maximum stress ranges.

In addition to the load factors normally used for fatigue, *AASHTO LRFD* has also introduced additional fatigue load factors for orthotropic decks and box girders. For orthotropic decks, because of their unique fatigue response characteristics, *AASHTO LRFD* provides a special load combination that increases the Fatigue I load factor to 2.25 when investigating fatigue at the welded rib-to-floorbeam cutout details and at the rib-to-deck welds. For box girders, *AASHTO LRFD* Article 6.11.5 introduces an additional factor of 0.75.

6.3.3.2 Factored Nominal Resistance

The resistance for an evaluation of infinite life is termed the constant amplitude fatigue threshold (CAFT) or alternately the constant amplitude fatigue limit (CAFL), with the terms commonly used interchangeably. *AASHTO* uses the acronym CAFT in its specifications. Unlike finite life tests, for which there are many tests and the statistical distribution of resistance is readily determined, infinite life tests are time consuming and expensive and more limited in number. The statistical properties of the CAFT are not well established. The CAFT is simply a straight line drawn to bound the available test data and at which point it is assumed that cracking can be prevented under constant amplitude loading. Other CAFT limits could also be drawn at different stress levels. They do not have the same precision as the finite life equations for fatigue resistance. Nevertheless they are used to design structures so that fatigue cracking is prevented over the design life.

On the resistance side of the equation, *AASHTO* expresses infinite life resistance as follows:

$$(\Delta F)_n = (\Delta F)_{TH}$$

Equation 6.3.3.2-1

with $(\Delta F)_{TH}$ provided in *AASHTO LRFD* as well as in Table 6.3.3.2-1. The values for the CAFT presented by AASHTO represent the horizontal lines in Figure 6.3.1.2-1.

Table 6.3.3.2-1 AASHTO constant amplitude fatigue threshold (CAFT) values.

Detail Category	Threshold (ksi)
A	24
B	16
B'	12
C	10
C'	12
D	7
E	4.5
E'	2.6
A325 Bolts in Axial Tension	31
A490 Bolts in Axial Tension	38

6.3.3.3 Fatigue from Shear Buckling

An additional check is required that involves shear. Because AASHTO allows for the post-buckling response of steel girder webs at the strength limit state, buckling of the web is not specifically precluded. However, since the web slenderness and stiffener spacing would allow for buckling under some load cases, a concern was expressed that the possible buckling of the web at the service and fatigue limit states be restricted. Thus, *AASHTO LRFD* requires that a check be made of web buckling under the combined effects of the unfactored dead load plus the live load resulting from the Fatigue I load combination. This check is unique from the checks for flexural or axial stress since it also involves the calculation of the accumulated dead load forces. This fatigue check is compared to a buckling capacity, and thus the total internal shear forces acting on the section are needed.

$$V_{fatigue} = 1.0(V_{DC} + V_{DW}) + 1.5V_{LL+I}$$

Equation 6.3.3.3-1

The factored shear force is equal to the unfactored shears from dead load plus the Fatigue I live load plus impact shear.

On the resistance side, the section strength is limited to the shear buckling capacity,

$$\phi V_n = C * V_p$$

Equation 6.3.3.3-2

For shear, ϕ is equal to 1, C is equal to the ratio of the shear buckling capacity to the plastic shear strength of the web and depends on web slenderness and transverse stiffener spacing, and V_p equals the plastic shear capacity of the web, taken as:

$$V_p = 0.58F_y D t_w$$

Equation 6.3.3.3-3

F_y is the yield strength of the web material, and D and t_w are the depth and thickness of the web.

6.3.4 Finite Life – The Fatigue II Load Combination

The Fatigue II load combination controls the propagation of cracks under repeating load effects over the design life of the structure. It allows for higher stress ranges but only for a finite number of cycles. It makes use of the concept of stresses produced by an “effective” truck and compares them to finite life resistance. For finite life, the limit state is expressed as:

$$\gamma(\Delta f) \leq \left(\frac{A}{N}\right)^{\frac{1}{3}}$$

Equation 6.3.4-1

The term, A , represents the detail constant, and N is the required number of design cycles for the detail. Each is described in the following sections.

6.3.4.1 Factored Force Effect for Finite Life

The load factor for Fatigue II, which was selected to represent the stresses produced by many random truck crossings, is specified as 0.8. This factor was chosen to represent the stresses produced by an effective truck and is used to assess the bridge’s finite life (i.e., the anticipated life of a detail subjected to many cycles of a repeating equal magnitude load). The finite life load factor of 0.8 is based on the SHRP2 R19B project, the results of which are described in considerable detail in Section 6.3.5 and Appendix A. The stresses produced by the fatigue design truck and the load factor, γ , are called the effective stress range.

6.3.4.2 Factored Resistance

In the region of finite life, the nominal fatigue resistance is a function of the detail category and the number of cycles. It is generally accepted that for structural steels, the life is inversely proportional to the cube of the applied stress range.

$$\text{Fatigue Life, } N \propto 1/(\Delta f)^3$$

Equation 6.3.4.2-1

A doubling of the stress range decreases the life by a factor of 8. Control of the stress range is therefore the most important factor in extending the fatigue life of a detail, as was previously discussed in Chapter 2.

AASHTO rearranges this equation into the following form and defines this as the finite life nominal resistance of a specific class of details. The allowable stress range is expressed as a function of the specific detail and the number of cycles throughout the design life of the bridge, as follows:

$$(\Delta F)_n = (A/N)^{1/3}$$

Equation 6.3.4.2-2

with A given as a detail constant and N representing the number of design cycles of loading for a particular detail. This equation plots as a straight line when the logarithms of stress and the number of cycles are used for the axes. Though plotting as a straight line, this is frequently referred to as a “curve” in this document and in the literature. Plotted on standard axes (not logarithmic axes), the equation would indeed plot as a curved line.

The AASHTO detail constants, A , needed to compute the finite life resistance are provided in Table 6.3.4.2-1.

Table 6.3.4.2-1 AASHTO detail constants for finite fatigue life.

Detail Category	Constant, A times 10^8 (ksi ³)
A	250
B	120
B'	61
C	44
C'	44
D	22
E	11
E'	3.9
A325 Bolts in Axial Tension	17.1
A490 Bolts in Axial Tension	31.5

The additional term required to compute the fatigue resistance is the number of design cycles, N , to which a detail is subjected. AASHTO specifies that the number of design cycles is:

$$N = (365)(75)n(ADTT)_{SL}$$

Equation 6.3.4.2-3

This equation computes the number of design cycles associated with the 75-year design life. The equation involves the computation of the average daily truck traffic in a single lane, $ADTT_{SL}$, as well as the number of cycles of loading per vehicle passage, n . The $ADTT_{SL}$ is an estimate of the number of trucks in a given day that will produce the effective stress range. It is computed in *AASHTO LRFD* as a function of the total truck volume and the assumed percentage of trucks that travel in the critical lane location.

The engineer must estimate the average daily truck traffic in a single design lane averaged over the life of the structure, $ADTT_{SL}$. The starting point for this estimate is the current ADTT in one direction. This is computed by taking a percentage of the ADTT for one direction of the bridge and assigning a portion of the total truck traffic to the most heavily traveled lane using the following equation:

$$ADTT_{SL} = p * ADTT$$

Equation 6.3.4.2-4

where:

p = the fraction of trucks in the most heavily traveled lane
 $ADTT$ = average daily truck traffic in one direction

To determine the ADTT in a single direction, *AASHTO LRFD* suggests that if directional split information is not available, 55 percent of the total traffic be assumed in one direction. *AASHTO LRFD* stipulates that the traffic percentage in the most heavily traveled lane, p , be taken as 100 percent for a single lane available to trucks, 85 percent for two lanes available, and 80 percent for three or more lanes available, since regardless of the number of lanes, trucks tend to bunch in specific driving locations. When determining the ADTT, consultation with the project traffic engineers is suggested in order to determine the estimated truck traffic as a percentage of the single-direction ADT. If guidance on the percentage of trucks is not available, Table 6.3.4.2-2 may be used as a guide (see *AASHTO LRFD* Article C3.6.1.4.2).

Table 6.3.4.2-2 Percentage of trucks for roadway types.

Class of Highway	Percentage of Trucks in Traffic
Rural Interstate	20 percent
Urban Interstate	15 percent
Other Rural	15 percent
Other Urban	10 percent

The number of cycles per truck passage, n , is also required. In order to understand how the number of stress cycles varies for different span arrangements, let us first consider a simple span beam with a single moving point load. The stress range at the point of interest is proportional to the algebraic difference between the live load bending moment at the point of interest with the load placed in the critical location and the live load moment with no vehicle on the bridge, which is zero. This is shown graphically in Figure 6.3.4.2-1.

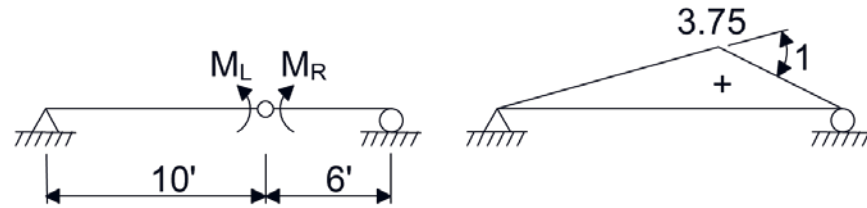


Figure 6.3.4.2-1 Influence line for bending moment in a simply supported span.

Trucks contain many axles, however, and if each axle is allowed to cross the influence line, multiple cycles may be accumulated. Considering the AASHTO fatigue design vehicle, with axle spacings of 14 feet and 30 feet, the short span depicted above is loaded and unloaded three times during the passage of one truck. For longer spans, this loading / unloading cycle is not as pronounced since the stress is more a function of the total truck than individual axle or axle grouping effects.

For a continuous span, again with a single moving unit load, the definition of stress range is still the same (i.e., the algebraic difference between the maximum and minimum live load stresses). Figure 6.3.4.2-2 presents an example of an influence line for bending at a point in the end span of a continuous bridge. The ordinates corresponding to three separate unit load placements (not three loads at the same time) are plotted as well. An engineer could use such an influence line, or more commonly a continuous beam analysis program, to determine these maximum and minimum live load moments and hence the stresses.

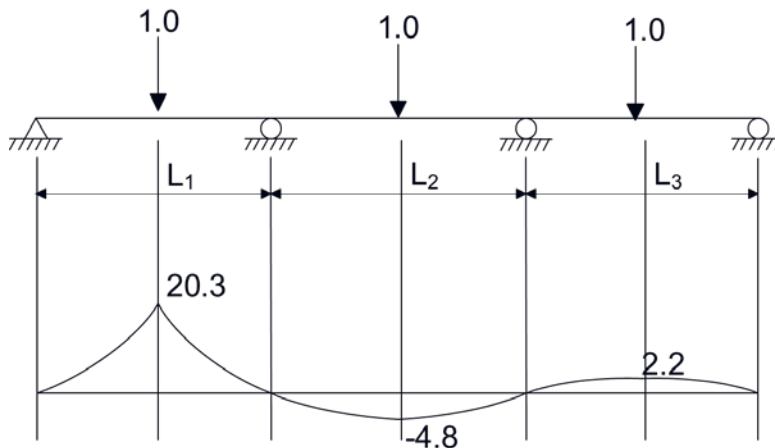


Figure 6.3.4.2-2 Influence line for bending moment in the end span of a continuous bridge.

Example time histories of stress versus time per vehicle passage are shown in Figure 6.3.4.2-3 to demonstrate the nature of actual loading histories. Shown are the larger changes in stress that correspond to the passage of design vehicles, as well as smaller oscillations that reflect the dynamic response of the bridge.

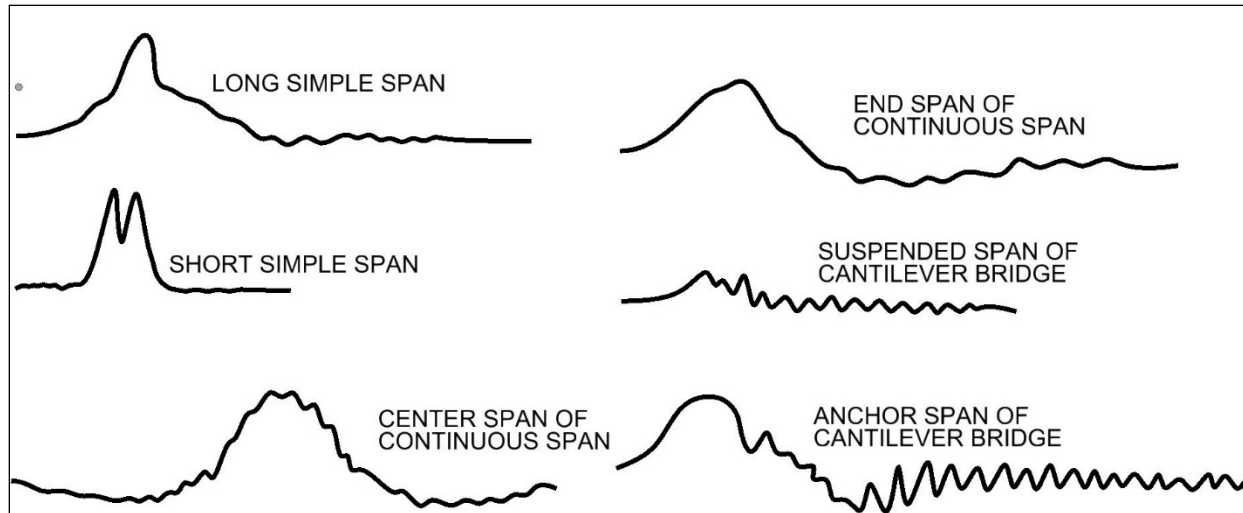


Figure 6.3.4.2-3 Time histories of stress versus vehicle passage for various bridge types.

For the short simple span, a series of cycles are produced due to individual axle crossings as shown by multiple peaks of stress. For the long simple span, the axle effect is not as pronounced, and there is essentially one longer cycle of loading, increasing then decreasing with residual vibrations afterwards. The end and center span time histories for a continuous span also follow the trend of an influence line with forces increasing or decreasing fairly uniformly with the small oscillations being due to vibration characteristics.

Cantilever / suspended (pin-and-hanger) bridges are more unique. A suspended span in a pin-and-hanger type bridge is unloaded until the load is between the hangers but vibrates even after the truck leaves the span due to the boundary conditions and due to the continued movement of the cantilever support point as the truck crosses the anchor spans. An analogous behavior is presented for the anchor span. Its behavior reflects the crossing of a truck on the anchor span but also the suspended span which it supports. Not until the truck is remote from the anchor and suspended spans does this span become fully unloaded, vibrating until the oscillations decay.

For all of the above time histories, it is the larger cycles of stress that dominate the number of equivalent cycles when the cycles are combined using techniques such as Miner's rule. Many cycles of small stress contribute very little to fatigue damage and are frequently neglected.

6.3.5 Calibration of the Fatigue Limit State

The discussion in Section 6.3.3 and Section 6.3.4 focused on the engineering approach to satisfying infinite and finite life design provisions of *AASHTO LRFD*. Within the calculations are various parameters such as load factors, resistance factors, a number of cycles per truck passage, and the premise that fatigue loading is caused by a single truck in a single lane. These assumptions were never fully calibrated like the strength limit state has been in the past. The SHRP2 Project R19B study (Modjeski and Master, 2015) included a statistical calibration of each of the fatigue load combinations, and the results are provided herein. The discussion begins with the Fatigue II load combination, for which most of the fatigue test data applies, and follows

with a discussion of the infinite life provisions of the Fatigue I load combination. A more detailed presentation of the calibration process is provided in Appendix A. These changes to the load factors are being considered for adoption in 2016.

6.3.5.1 Calibration of the Fatigue II Load Combination

The load factor for the Fatigue II load combination, the premise of single truck / single lane loading, and the “cycles-per-passage” table were studied as part of the SHRP2 Project R19B study. Researchers used weigh-in-motion (WIM) data to collect millions of records of actual truck crossings. After filtering out inaccurate data, as well as the many “under 20 kip” records, over 8 million records remained and were processed during the calibration study.

Using a series of computer models for simple and continuous bridges, the R19B team ran the millions of actual trucks over a series of simulated simple-span and two-span continuous bridges and recorded the fluctuation in moment (and hence fatigue stress range) over time. Using a cycle counting tool known as the rain flow method, they estimated the total number of cycles produced by a given number of truck crossings and computed an effective moment using Miner’s rule. More cycles than truck crossings were evident, with shorter bridges having significantly more cycles per truck than long bridges (those with spans in excess of 100 feet). Based on the bending moment simulation data and further statistical analyses by the R19B team, the current “cycles-per-passage” table is presented in Table 6.3.5.1-1.

Table 6.3.5.1-1 AASHTO cycles-per-passage table.

Longitudinal Members		n
Simple span girders		1.0
Continuous girders	Near interior support	1.5
	Elsewhere	1.0

With the new value for n , a component of the finite life resistance equation for the Fatigue II load combination was calibrated. A trial load factor of 0.8 was chosen that provides a 95 percent confidence that the load factor will envelope the bending moments and hence stresses produced by the effective truck. For the resistance data, researchers relied on a large dataset of finite life test data collected through several decades. A Monte Carlo simulation was performed to test the trial load and assumed resistance factor of 1.0 to determine if the target β of 1.0 was achieved. The outcome of the Monte Carlo simulation process validated the choice of a Fatigue II load factor of 0.8, an increase of 0.05 from the previous *AASHTO LRFD* value of 0.75. The R19B report recommended that the load factor increase was justified by the calibration process, the general upward trend in vehicle weights, and the desire to design structures for a service life possibly in excess of 75 years.

The use of a β of 1.0, consistent with a probability of failure of approximately 16 percent, is justified as follows. The target β was calibrated by first assessing the β inherent in the current *AASHTO LRFD* specification fatigue limit state. There is no evidence to believe that the existing provisions are unsafe nor unduly conservative. Using existing successful practices is a common back sight when performing calibration studies. Additionally, the assumed mean value of the

load factor used in the simulation is actually the mean plus 1.5 standard deviation value of the effective stress range load factor, so a degree of conservatism is provided on the load factor side with a design mean that is biased to the true mean. The resistance data set was truncated and only the lower tail of the resistance data was used. Data points that suggest long life or high stress resistance were purposely excluded from the curve fitting for the resistance data. However the traditional $\mu-2\sigma$ offset in the resistance models is no longer used; rather the true mean and standard deviation are used for the resistance model.

The team also used the WIM data to determine the likelihood of similarly configured trucks crossing a bridge simultaneously in adjacent lanes or following closely in the same lane. The availability of the WIM data on a per-lane basis allowed the research team to search for occasions where these side-by-side or following crossings occurred. Their conclusion is that it was rare to find two similarly loaded and configured trucks crossing the bridge at the same time. The researchers concluded that there was no need to deviate from the *AASHTO LRFD* single truck in a single lane design approach.

6.3.5.2 Calibration of the Fatigue I Load Combination

Using the same WIM data as for the Fatigue II load combination calibration, the Fatigue I load combination was calibrated. The objective of the Fatigue I load combination remains to safely provide infinite life. For each of the various WIM sites, the moment that corresponded to a 0.01 percent probability of exceedance was established as the definition of the maximum effect. This envelopes the maximum load / stress effect in order to limit the number of cycles beyond the threshold in order to prevent fatigue crack growth under infrequent overloads. This moment was then normalized to the AASHTO fatigue truck design moments to provide a ratio between these 1:10,000 occurrence moments and those predicted from application of the AASHTO design vehicle. The load factors were thus chosen to envelope all but the 1:10,000 heaviest vehicles / bending moment force effects. Similar to the Fatigue II load combination calibration, a Monte Carlo simulation process was carried out for Fatigue I with a target β of 1.0. The calibration process concluded that a load factor of 2.0 was most appropriate, a significant change from the previous 1.5 value. At the request of the AASHTO T14 subcommittee (responsible for the structural steel design provisions), the R19B team took another look at the calibration, and in August 2015, recommended moving forward with a reduced load factor of 1.75. As with the change to the Fatigue II load factor, this change was adopted based on a vote of approval in 2016.

6.3.6 Special Details and Provisions for Other Structure Types

Although the majority of this chapter focuses on main members, the design of other bridge and structural elements contain fatigue design provisions as well. This section addresses the fatigue design considerations for other important bridge structure components, including cross-frames, considerations for skewed and curved bridges, design of shear studs for composite beam bridges, fatigue aspects of modular bridge expansion joints, and fatigue design of special structures including orthotropic steel decks and highway sign and lighting structures.

6.3.6.1 Cross-Frames

The term “cross-frame” is the name commonly used to describe the truss-type bracing used to provide lateral-torsional buckling resistance to rolled and welded girders alike. The design of cross-frames must consider the fatigue effects in the members of the cross-frame as well as the effects of cross-frame loading on the design of the cross-frame connections. The design of the cross-frame and its connections is described in this section. An additional aspect of cross-frame design and detailing relates to the prevention of distortion-induced fatigue cracking in the main girders. This aspect of cross-frame detailing is addressed later in Section 6.4.

A cross-frame member is commonly welded to a gusset plate; however, end bolted connections have been used as well. The connections where the cross-frame members are attached to the gusset plates must be designed for fatigue. The accompanying photos in Figure 6.3.6.1-1 depict two cross-frames, one which uses rolled WT sections in a K-frame configuration and the other using angles in an X-frame configuration. The fatigue design approach is similar for each of these variations.



Figure 6.3.6.1-1 K-type and X-type cross-frames.

Where force effects in cross-frames or diaphragms are computed from a refined analysis, such as is commonly used in the design of curved and some skewed steel bridges, it is necessary to evaluate the fatigue stress ranges in the members and their connections. It is common that the load position producing the greatest live load tension in a member, say one of the diagonals in the cross-frames shown, is not in the same lane location transverse to the bridge as the load position producing the maximum compression load. In such cases, the effect of positioning the fatigue truck in two different transverse positions might create the largest possible range of force in these bracing members. However the loading and unloading would correspond to two unique cycles and is not from the passage of the same truck. For these reasons, in 2015, *AASHTO LRFD* clarified that the definition of the load / stress range for cross-frame members is the range of stress produced in a member by the passage of the truck in a fixed transverse portion along the length of the bridge. This implies that the approach for cross-frame fatigue is like that for main member fatigue; a truck traveling the length of the bridge, in a fixed transverse lane, is what is used to compute the range of load in the member and its connections. The refined analysis of

force and stress ranges in cross-frames need not capture the extremes when those are produced by different transverse lane locations.

To determine the fatigue stress range and resistance, *AASHTO LRFD* requires that angle and WT sections welded to a gusset plate, a common connection, be treated as a Detail Category E' weld (see Figure 6.3.6.1-2). The stress in the base metal of the cross-frame member is computed due to the range of axial force in the member. The effect of bending due to eccentricity in the connection is to be ignored. However the effect of lack of full attachment and the corresponding stress increase is accounted for through the use of a shear lag reduction factor, $U = 1 - \bar{x}/L$, which is multiplied by the gross area to represent the lack of full effectiveness due to partial attachment of members such as angles and WT sections.

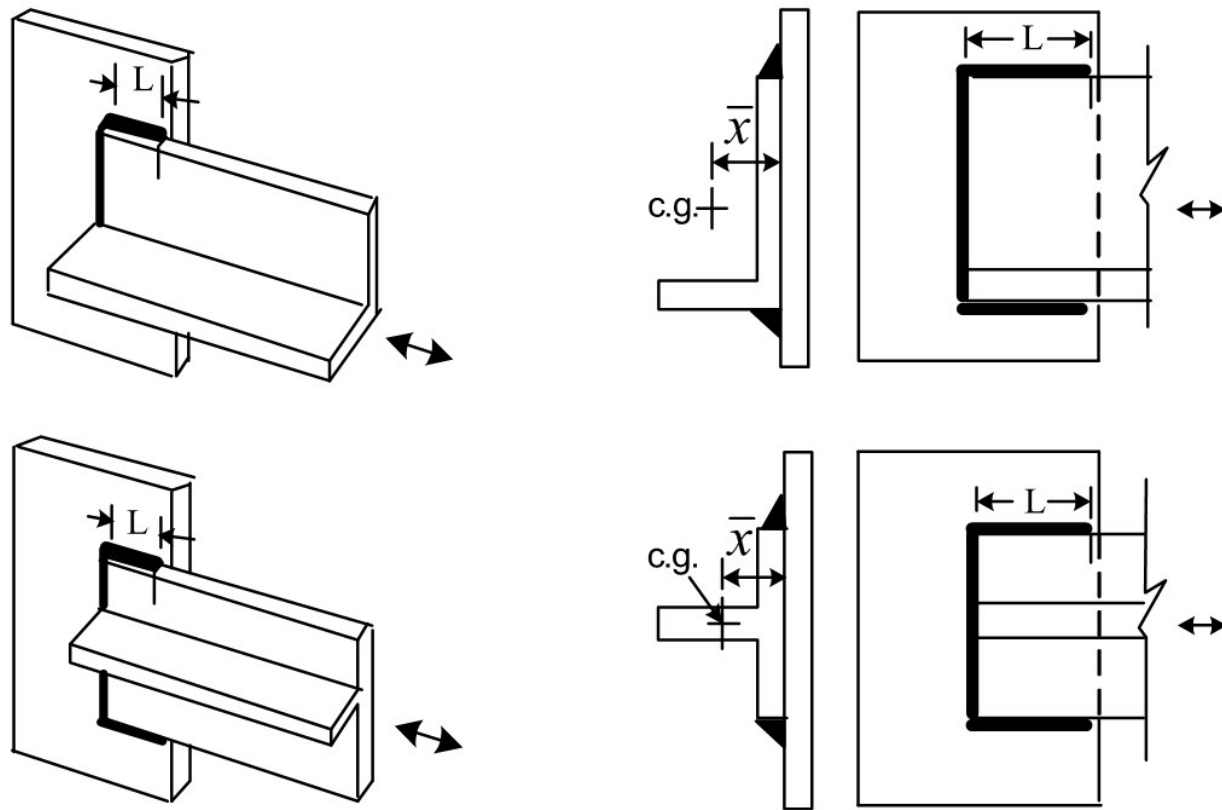


Figure 6.3.6.1-2 Shear lag considerations for cross-frame member end connections.

For cases in which the ends of the cross-frame members are bolted, the fatigue stress range is also computed. When slip-critical connections are used, no deduction in member area is required for the presence of bolt holes and the shear lag reduction factor is applied to the gross member cross section. For cases in which slip-critical connections are not used, admittedly an unusual occurrence for diaphragm connections, the effective area must be corrected to the net area.

6.3.6.2 Curved and Skewed Bridges

Curved and skewed bridges are unique from conventional straight and non-skewed steel bridges in that they are subject to primary bending moments as well as lateral bending moments arising from the effects of torsion and skew. As these bridges are loaded, torsion from curvature and unequal deflection due to skew causes the cross-frames to become loaded. Although this unequal deflection can also occur in straight non-skewed bridges, the phenomenon of differential deflection is exacerbated in curved and moderately to sharply skewed bridges (i.e., those whose skew angle exceeds 20 degrees from a square condition). The force transfer from the cross-frames to the girders results in lateral forces being exerted on the flanges and therefore lateral flange bending moments and stresses. These lateral bending moments and stresses can be significant, and their presence reduces the girders' ability to resist primary bending. Although it is likely that the live load placement causing the maximum in-plane stress is not necessarily at the same position as that causing the maximum lateral flange bending (unless the results from a refined analysis model provide concurrent force effects), it is acceptable and conservative to use the envelope values. An example is provided in Figure 6.3.6.2-1 to demonstrate the application of *AASHTO LRFD* to a bottom flange connection plate in a curved bridge.

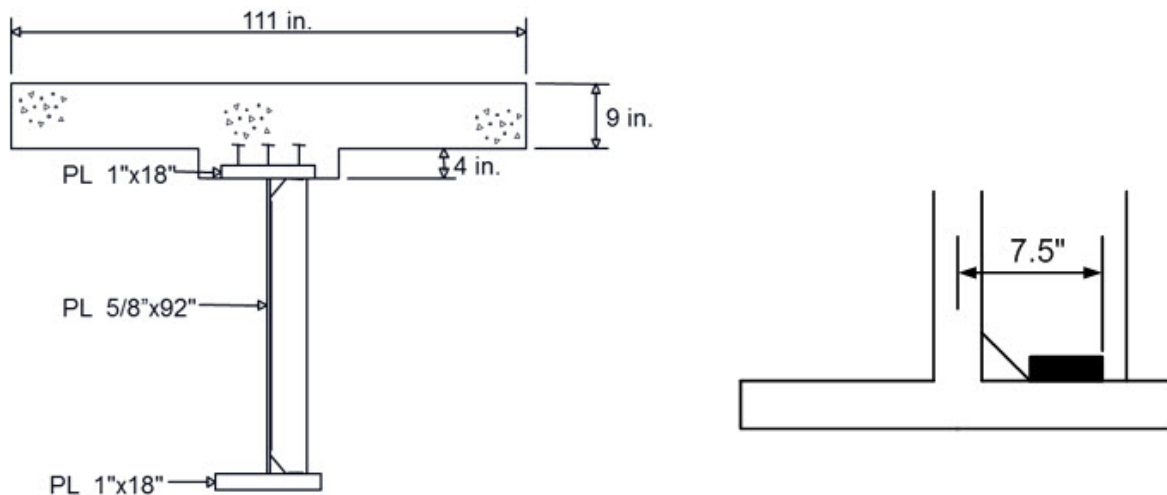


Figure 6.3.6.2-1 Bottom flange weld subject to in-plane and lateral flange bending.

Due to the effects of primary bending, the Fatigue I load combination in-plane bending stress at the intersection of the connection plate and the inside of the bottom flange is calculated to be 9 ksi. In addition, the lateral flange bending stress range from curvature and skew effects must be added to this. The detail of the weld connecting the stiffener to the bottom flange is provided, and the most highly stressed portion of the weld is located 7.5 inches from the centerline of the web. The range of lateral flange bending moments was computed to be 8 ft-kips. The flange measures 18 inches wide and 1 inch thick. The calculations for the lateral stress range are as follows:

$$I_{flange,lateral} = \frac{tb^3}{12} = \frac{(1)(18)^3}{12} = 486 \text{ inches}^4$$

Equation 6.3.6.2-1

$$f_{lateral} = \frac{1.5(8 \text{ ft} - \text{kips}) * 7.5 \text{ inches} * 12 \text{ inches/foot}}{486 \text{ inches}^4} = 2.2 \text{ ksi}$$

Equation 6.3.6.2-2

When added to the primary bending stress of 9 ksi, the combined stress range of 11.2 ksi is compared to the Detail Category C' infinite life resistance of 12 ksi and the detail satisfies the infinite life requirement. No further check for finite life is required.

6.3.6.3 Shear Studs

Headed shear studs are the most common form of providing composite action between concrete decks and steel beams. Attached by means of a “stud gun,” the process of welding a stud to a beam flange involves establishing an arc between the tip of the stud and the beam flange, creating a pool of molten steel, and then forcing the stud into the molten steel. This creates a full cross-sectional weld at the end of the stud.

The design of shear studs must satisfy requirements of the strength and fatigue limit states, and the latter are described herein. The design procedure defined in *AASHTO LRFD* Article 6.10.10 considers the force effects from straight, skewed, and curved bridges. Figure 6.3.6.3-1 depicts a beam cross section indicating the placement of the studs, demonstrates the horizontal shear loading to which they are subjected, and includes a photo of several steel beams after attachment of the studs. When loaded in fatigue until failure, the failure of a welded stud is characterized by one of the three failure surfaces in Figure 6.3.6.3-2.

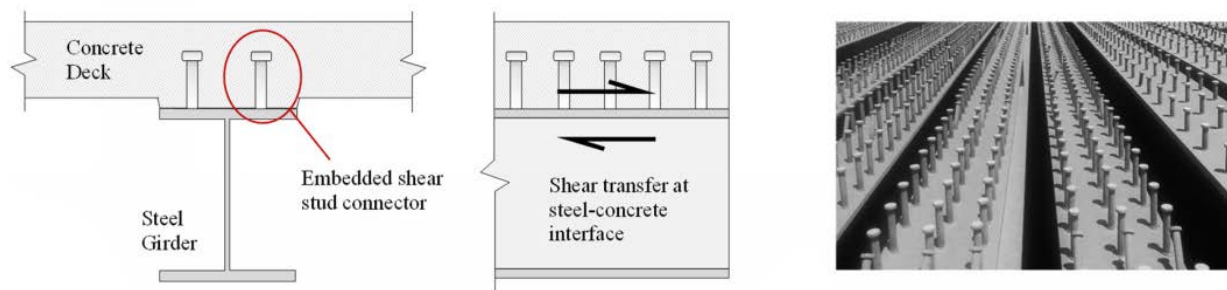


Figure 6.3.6.3-1 Shear stud connection to beam flange and force transfer mechanism.

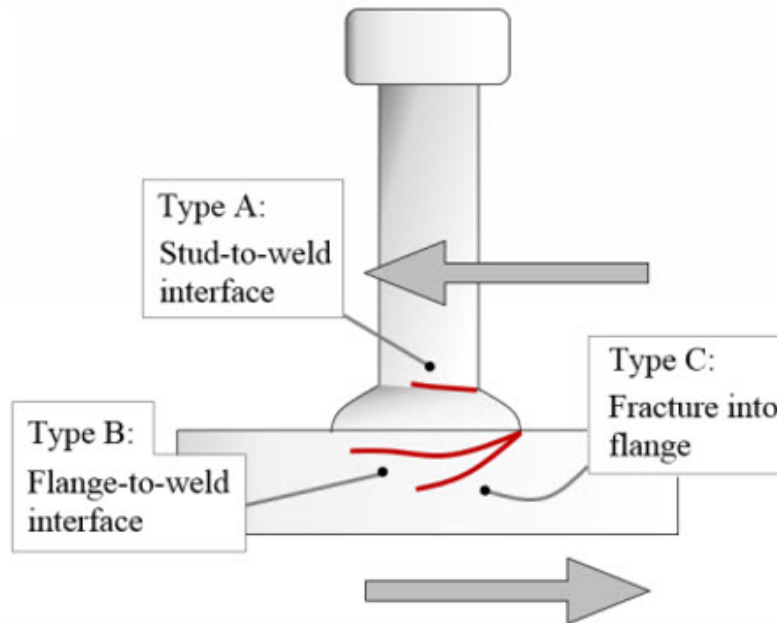


Figure 6.3.6.3-2 Shear stud failure mechanisms.

Since the role of the shear stud is to join the concrete deck to the steel beam, the composite action is enforced through resistance to the horizontal shear flow across the slab-to-beam interface. The flow of shear comes from two sources, that due to conventional flexure and shear, V_{fat} , as well as a lateral component from skew and curvature, F_{fat} .

The horizontal shear flow from applied vertical shear forces in the beam is modeled using a traditional equation:

$$V_{fat} = \frac{V_f Q}{I}$$

Equation 6.3.6.3-1

where:

- V_{fat} = fatigue shear range per unit length (kips/inch)
- V_f = vertical shear force range under the applicable fatigue load combination (kips)
- Q = first moment of the transformed short-term area of the concrete deck about the neutral axis of the short-term composite section (inches³)
- I = moment of inertia of the short-term composite section (inches⁴)

This is a conventional application of a shear flow equation from strength of materials where the force computed by the term V_{fat} represents the range of longitudinal force per unit inch to resist the shear flow between the deck and the top of the steel beam using the fatigue truck to compute the range of vertical shear force, V_f .

In addition, lateral shearing forces due to curvature and skew may also be present.

In the case of curvature, the force on the shear connectors is taken as the larger of an inferred force due to curvature, F_{fat1} , and that due to direct application of cross-frame forces, F_{fat2} , as might be obtained from a refined analysis.

First, for estimated force effects from curvature, the following equation is provided, as illustrated in Figure 6.3.6.3-3.

$$F_{fat1} = \frac{A_{bot}\sigma_{flg}l}{wR}$$

Equation 6.3.6.3-2

where:

- A_{bot} = area of bottom flange (in²)
- σ_{flg} = range of longitudinal fatigue stress in the bottom flange without consideration of flange lateral bending (ksi)
- l = distance between brace points (feet)
- w = effective length of deck (inches) takes as 48 inches except at end supports where w may be taken as 24 inches
- R = minimum girder radius within panel (feet)

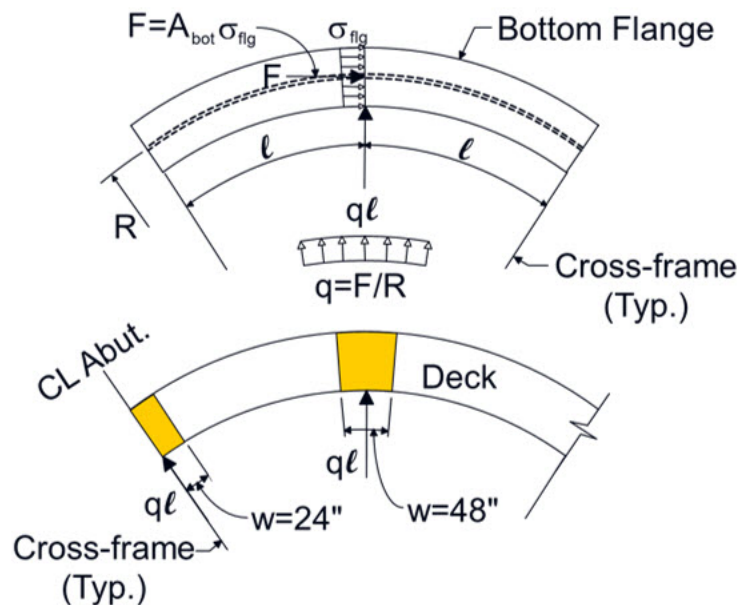


Figure 6.3.6.3-3 Analysis model for lateral loading of shear stud groups.

In the equation for F_{fat1} , the force in the bottom flange is used as an indicator of the range of longitudinal force acting along the interface between the beam and slab. It is important to clarify this point since the equation references stresses and forces in a flange which in fact does not have

studs attached to it. The longitudinal force obtained by multiplying the stress and flange area together, $\sigma_{flg}A_{bot}$, is divided by the radius, R , to create an equivalent radial load. This load, shown as q in Figure 6.3.6.3-3, is then accumulated between cross-frames spaced a distance apart equal to l . This is the total radial load acting between cross-frames. It is assumed that this entire load must be resolved “near” a cross-frame, and the 24- and 48-inch limits for w apply accordingly. This method is simply a way of estimating the total radial force demand between cross-frames and apportioning the load to a local region surrounding each frame.

An alternate source of lateral load is the range of force introduced by the cross-frames themselves. An analysis model for net range of force at the top flange from cross-frames is presented in Figure 6.3.6.3-4.

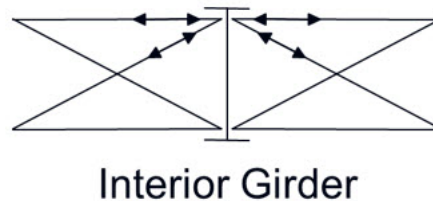


Figure 6.3.6.3-4 Analysis model for net range of force at top flange from cross-frames.

$$F_{fat2} = \frac{F_{rc}}{w}$$

Equation 6.3.6.3-3

where:

F_{rc} = net range of cross-frame or diaphragm force at the top flange (kip)

Using the greater lateral force contribution from considerations of curvature, F_{fat1} , or from direct use of the local cross-frame forces, F_{fat2} , the resultant shear demand on the stud is computed as a vector sum as follows:

$$V_{sr} = \sqrt{(V_{fat})^2 + (F_{fat})^2}$$

Equation 6.3.6.3-4

where:

V_{sr} = horizontal shear range per unit length (kips/inch)

Having determined the shear flow or force per unit length, V_{sr} , the designer solves for a theoretical pitch for a chosen number of studs per group and performs the layout of the studs. Commonly this is done at even intervals along the length of the beam such as tenth points. The pitch is found using the strength of an individual stud or groups of studs and is predicted as follows:

$$p \leq \frac{nZ_r}{V_{sr}}$$

Equation 6.3.6.3-5

where:

- n = number of shear connectors in a cross section
 Z_r = shear fatigue resistance of an individual shear connector

The resistance of a shear connector, Z_r , is, like other fatigue details, a function of the number of cycles in the finite life region and also has a constant amplitude fatigue threshold limit for higher cycle designs. The resistance of shear connectors in *AASHTO LRFD* is based on work by Slutter and Fisher (1966). Their work included unidirectional and reverse loading push-out tests of shear studs embedded in a concrete slab. Both 3/4-inch and 7/8-inch diameter studs were tested. A total of 35 specimens using 3/4-inch diameter studs were tested along with nine additional specimens tested with 7/8-inch diameter studs.

In the region of finite life, the resistance of an individual welded shear stud connector is given in *AASHTO LRFD* Article 6.10.10.2 as

$$Z_r = \alpha d^2 \qquad \alpha = 34.5 - 4.28 \log N$$

Equation 6.3.6.3-6

where:

- α (alpha) = finite life resistance of the shear stud in ksi; is dependent on the number of design cycles, N
 d = diameter of the shear stud in inches

In Figure 6.3.6.3-5, taken from Slutter and Fisher (1966), the line labeled “Eq. 2” is given as $\log N = 8.072 - 0.1753S_r$. The variable S_r is the range of horizontal shear stress and is related to the value alpha used in *AASHTO LRFD* by the relationship shown in the equation below.

$$\alpha = S_r * \pi/4$$

Thus the Slutter and Fisher equation can be related to that given in *AASHTO LRFD* with the appropriate substitution. The *AASHTO LRFD* equation for finite life is unlike other fatigue life equations in that it represents the mean strength from laboratory tests. Most fatigue life equations are based on the mean minus two standard deviations, or a 97.5 percent confidence that the provided life will exceed the predicted life. Slutter and Fisher defend using the mean life since their regression analysis neglected test results from studs tested in reversal which demonstrated much higher strengths. Also given the redundancy of shear studs with many hundreds applied to typical beams, isolated failures of a few studs will not change the overall system behavior and is considered acceptable.

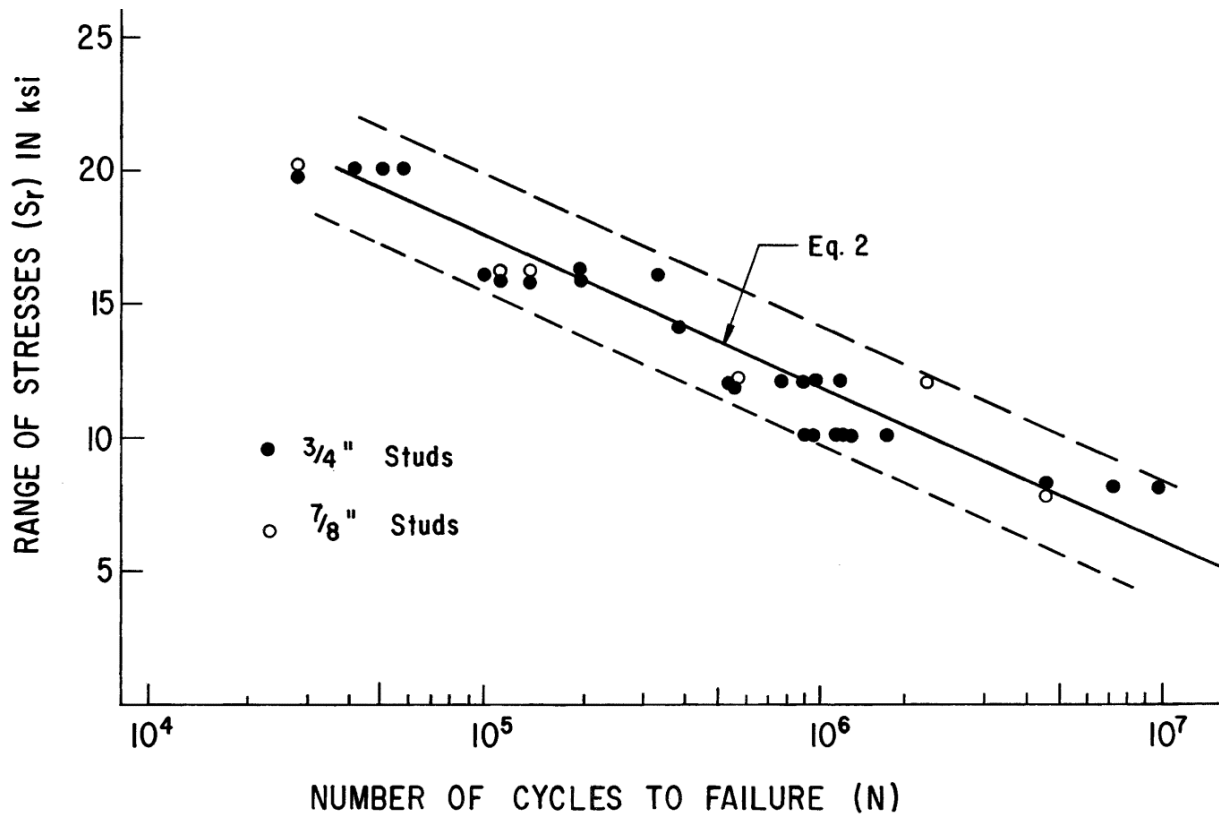


Figure 6.3.6.3-5 Shear stud push-out test results.

For infinite life, the strength of the shear stud is specified as $5.5d^2$. The value of 5.5 used for alpha is a derived value. It comes from the CAFT for average shear stress between the slab and flange of 7 ksi multiplied by the value of $\pi/4$ (i.e., 5.5). The CAFT value of 7 ksi leading to the alpha value of 5.5 ksi was somewhat arbitrarily but conservatively chosen since limited data existed regarding infinite life at the time. Recent research by Ovuoba and Prinz (2015) includes testing six additional push-out test specimens with applied average shear stress ranges between 30 and 60 MPa (4.35 and 8.7 ksi). These tests were conducted near the current AASHTO CAFT limit to add additional data points in this area where henceforth there was little information. Their work suggests a CAFT value for shear stress of 6.5 ksi, not unlike the implied value of 7 ksi assumed in the derivation of alpha equals 5.5 in the infinite life AASHTO LRFD equations. No changes to the specifications are expected as a result of these slight changes in the CAFT values.

6.3.6.4 Expansion Joints

Of the various types of joints used to accommodate expansion and contraction of bridges (steel and concrete), modular bridge expansion joints are among the most complex. They rely on a series of interconnected steel elements, welded and bolted, to allow for movements in the bridge due to thermal expansion and contraction and from other sources such as creep and shrinkage, deflection under high winds, and longitudinal movement due to braking in bridges with flexible substructures.

The design requirements for modular bridge expansion joints are provided in *AASHTO LRFD* Article 14.5.6.9 and follow the procedures first outlined in NCHRP Report 402, *Fatigue Design of Modular Bridge Expansion Joints* (Dexter, Connor, and Kaczinski, 1997). Additionally, fatigue and overall durability testing requirements are found in the *AASHTO LRFD Bridge Construction Specifications* (AASHTO, 2015a) and follow the guidance found in NCHRP Report 467, *Performance Testing for Modular Bridge Joint Systems* (Dexter, Mutziger, and Osberg, 2002).

Although the discussion below focuses on the design of Modular Bridge Joint Systems (MBJS), it is rare for an engineer involved in the design of a bridge to design the joint components. They are typically chosen as engineered systems from vendors who manufacture and market such devices. The engineer will typically only size the joint from a movement perspective and detail its connection to the structure via a blockout to accommodate the joint as shown in the accompanying photographs in Figure 6.3.6.4-1 and Figure 6.3.6.4-2. The design guidance in *AASHTO LRFD* is used to proportion joint elements, but their acceptance is only confirmed after passing the acceptance test criteria in the *AASHTO LRFD Bridge Construction Specifications*.



Figure 6.3.6.4-1 Modular joint installation.

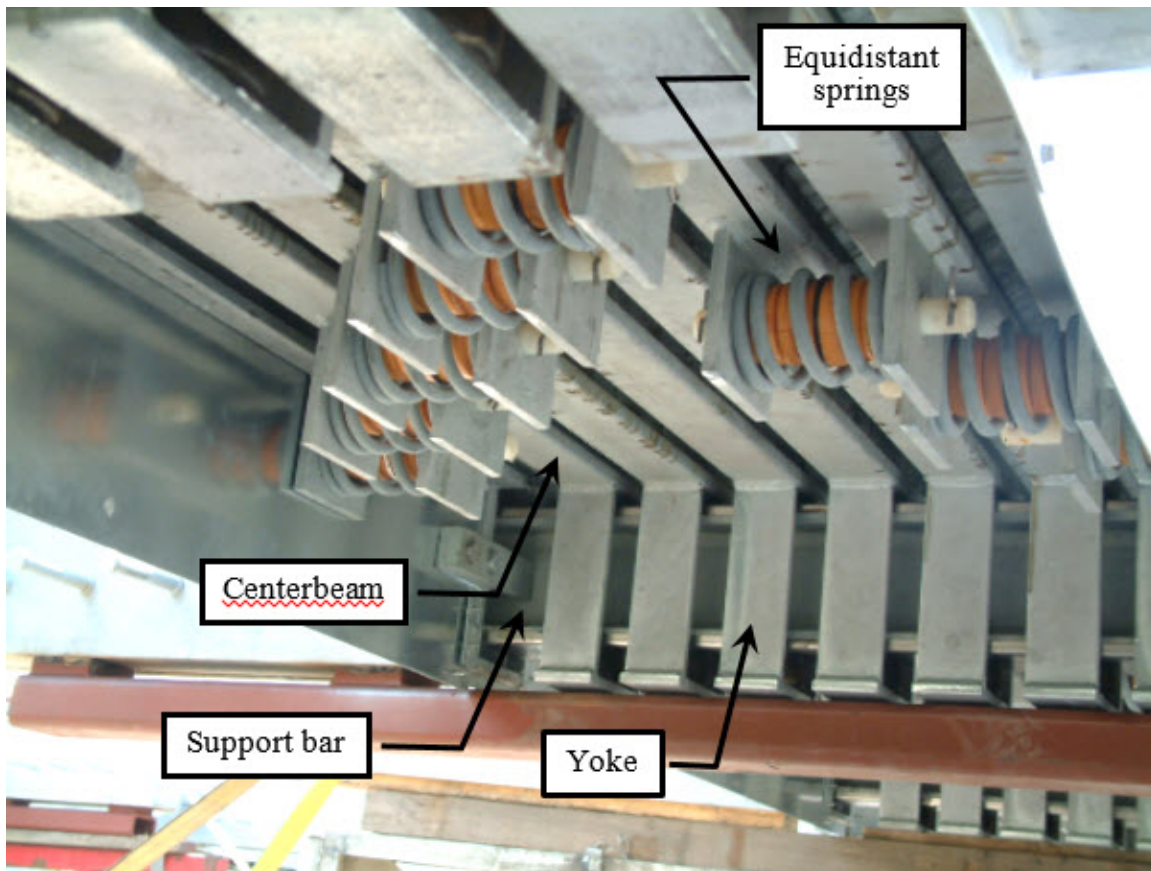


Figure 6.3.6.4-2 Underside of modular joint with details shown.

The design of expansion joint components must meet the requirements of the strength and fatigue limit states. Only the fatigue design considerations are discussed herein. The joints are proportioned assuming that the conventional 32-kip axle of the fatigue design truck is replaced by two 16-kip axles, and these loads are transmitted to the joint as two 8-kip wheel loads. A high impact value of 75 percent is used for fatigue design due to the rapid loading and unloading of joints. This value represents the downward effects of load application, rebound, and dynamic load effects. The 75 percent value was confirmed through field testing of modular joints in Europe and in the United States.

Since joints are subjected to multiple cycles per truck passage over many years, the designs must satisfy infinite life requirements of the Fatigue I load combination. Due to the effects of vertical grade and braking, a horizontal force component is applied. A common value of 20 percent is used for the horizontal force range as a fraction of the vertical force range, assumed to be evenly distributed as 10 percent forward and 10 percent backward. This is to be increased for bridges on vertical grades in excess of five percent.

The structural members of an MBJS must meet fracture toughness requirements and must be designed for infinite life, as mentioned previously. Their design is frequently governed by limiting the fatigue stress range at critical details, though numerous strength limit state checks are required as well. Multiple fatigue sensitive details may be present, including the connection

between center beams and support bars. These may be welded or connected through a mechanical yoke system. Other fatigue sensitive details include attachments to the center beams and support bars such as to support the equidistant springs and shop or field splices that may be required for wide joints or joints installed as part of phased construction.

AASHTO LRFD Article 14.5.6.9.7 outlines the fatigue design approach for MBS elements. For the determination of the stress range in primary load-carrying elements, several simplified analytical models are provided for computing forces and stresses in single- and multiple-support bar systems. The influence of bolted splices which create hinges and thus higher stress ranges in the center beams is discussed. The need to check other details such as welded attachments to the support bars and center beams is discussed in the commentary to the design specification.

Due to the inherent difficulty in predicting the stresses in MBS assemblies, their performance is judged after the static design process by fatigue testing using the Opening Movement Vibration Test outlined in the *AASHTO LRFD Bridge Construction Specifications* (AASHTO, 2015a). The test is used to demonstrate the performance of center beam to support bar connections, connections of attachments to the center beams, and the performance requirements for shop or field splices in the center beams. The design of anchors connecting the joint system to the concrete deck (i.e., anchor shear studs and edge beams) may be exempted from testing and design, provided certain minimum member size and anchor spacing requirements of the design specifications are met.

6.3.6.5 Orthotropic Steel Decks

Orthotropic steel decks represent a deck type used on some long span steel structures to provide weight reduction, rapid construction, and long life. They are generally applicable on high volume, long span, or otherwise critical structures. Having first been used in Europe in the 1930's, these deck types, though infrequently used, have certain advantages as mentioned above.

Orthotropic steel decks are unique in that the steel deck plate serves to receive the direct loading from traffic and at the same time serves as a top flange to the longitudinal main girders, as well as the transverse floorbeams (see Figure 6.3.6.5-1). Stiffened by ribs and floorbeams, the deck system is subject to a complex stress distribution and the direct effects of local wheel loads, as well as global participation in the structural response. Orthotropic steel decks may be made integral with "I" and box-shaped girders or may be stand-alone deck systems used in structures such as suspension, arch, and other long-span structural forms. They have been used as integral parts of new construction, as well as to limit dead load in bridge rehabilitation and redecking projects such as the Bronx-Whitestone Bridge reconstruction project.

Orthotropic decks are characterized by common components. These include the steel deck plate, a series of ribs which stiffen the deck plate and themselves span between transverse floorbeams, and the transverse floorbeams which span to the main supporting members. Critical welded connections exist between the ribs and the deck, at the intersection of the ribs and floorbeams, and at the connection of the floorbeams to the main longitudinal spanning elements.

The FHWA *Manual for Design, Construction, and Maintenance of Orthotropic Steel Deck Bridges* (Connor et al., 2012) is the most recent comprehensive manual covering most aspects of

steel orthotropic decks. Only a brief description is provided herein, and the reader should consult Connor et al. (2012) for many additional details on analysis, design, detailing, and construction not addressed in this manual.

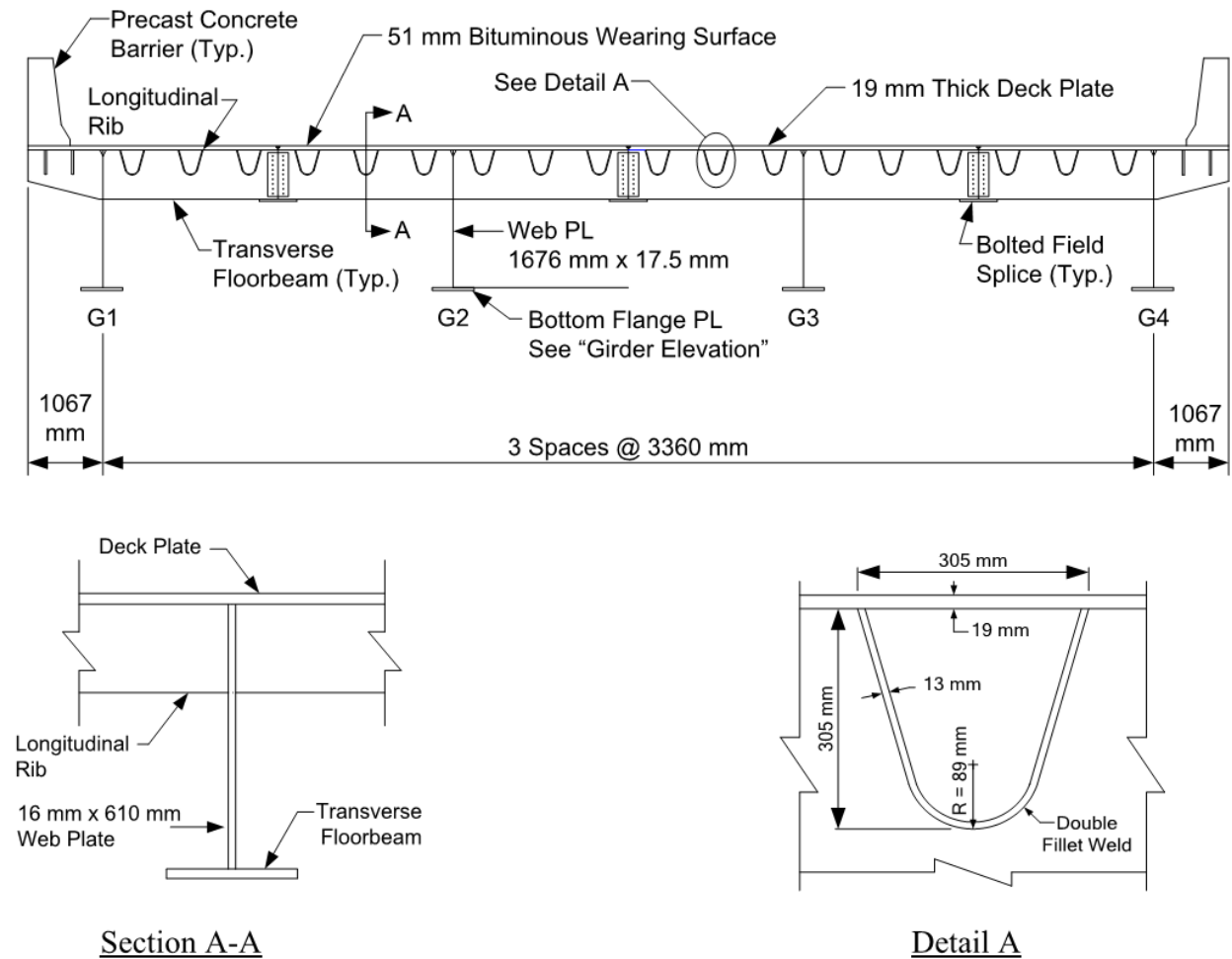


Figure 6.3.6.5-1 Orthotropic deck and I-beam steel bridge.

A schematic of the fabrication of an orthotropic steel deck is presented in Figure 6.3.6.5-2. Shown is an inverted deck as it would be fabricated consisting of a deck plate (the riding surface) and the supporting elements – the ribs and floorbeams. The ribs, commonly bent using a press break into a U-shaped closed section, are first welded to the underside of the deck plate. This is depicted on the left side of the figure. Then floorbeams are fabricated and cutouts are located so as to allow for the ribs to pass through each floorbeam and to control the local stresses that arise from floorbeam-to-rib interaction. The floorbeam is then fit around the ribs and is welded to the ribs and deck plate. A photo of the ribs passing through a floorbeam is provided in Figure 6.3.6.5-3. Figure 6.3.6.5-1 through Figure 6.3.6.5-3 are taken from Connor et al. (2012).

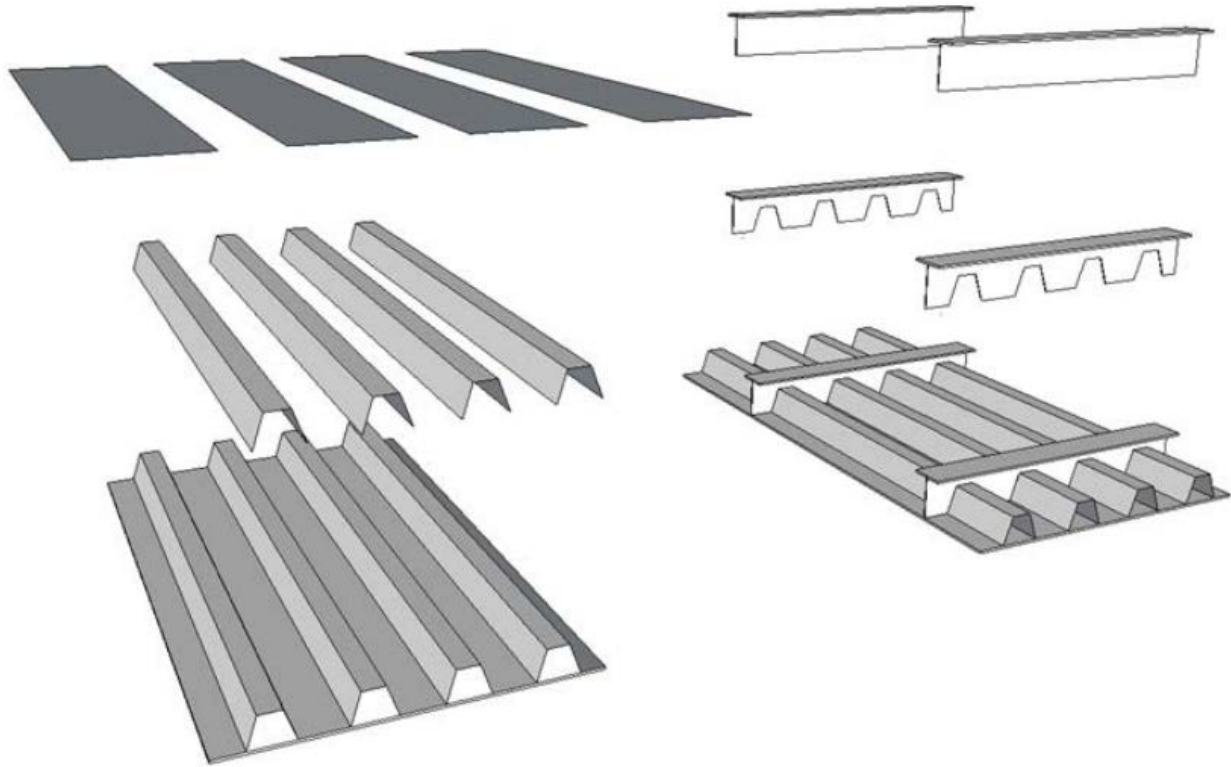


Figure 6.3.6.5-2 Fabrication schematic of orthotropic steel decks.



Figure 6.3.6.5-3 Orthotropic deck rib and floorbeam intersection.

AASHTO LRFD categorizes various common details found in orthotropic steel decks and assigns the standard *AASHTO* fatigue categories to those details. Included are fatigue strength categories for rib-to-deck welds, bolted and welded rib splices, deck plate splices, rib-to-floorbeam welds, floorbeam cutouts, and rib wall connections.

Because of the unique fatigue response characteristics of orthotropic decks, *AASHTO LRFD* provides a special load combination that increases the Fatigue I load factor to 2.25 when investigating fatigue at the welded rib-to-floorbeam cutout details and at the rib-to-deck welds. The increased load factor is cited in *AASHTO LRFD* as a result of prior investigations that found the basic load factor for live load is unconservative to provide infinite life for certain orthotropic steel deck details. This increased load factor is based on stress monitoring of orthotropic decks. The increase of the load factor for infinite life reflects a greater difference between the maximum stress range and effective stress range, as compared to standard girder design. Fatigue design of orthotropic decks is more highly dependent upon localized wheel loads as opposed to general truck weight distributions, and the load distribution and relative movement of orthotropic decks is significantly different than the load-induced fatigue behavior of steel girders.

For the evaluation of finite life using the Fatigue II load combination, the effect of local wheel crossings must also be considered. For orthotropic deck details connected directly to the deck plate (i.e., the rib-to-deck weld), partial cycles are created by the crossing of individual loads or a total of five partial cycles from the passage of a single truck. *AASHTO* suggests that the stress range can be conservatively taken as the worst case from the five wheels or that Miner's rule can be used to determine an effective stress range from a group of wheels. Five cycles of loading are to be used for every truck passage. This is described in *AASHTO LRFD* in greater detail.

Figure 6.3.6.5-4 presents a refined loading model whereby the standard fatigue truck axle loads are converted into equivalent rectangular patch loads in order to perform the local analysis of orthotropic decks. *AASHTO LRFD* Article 4.6.3.2.4 requires that the refined analysis of orthotropic decks be accomplished using a three-dimensional finite element model and describes some of the simplifying assumptions that can be used in the creation of the model.

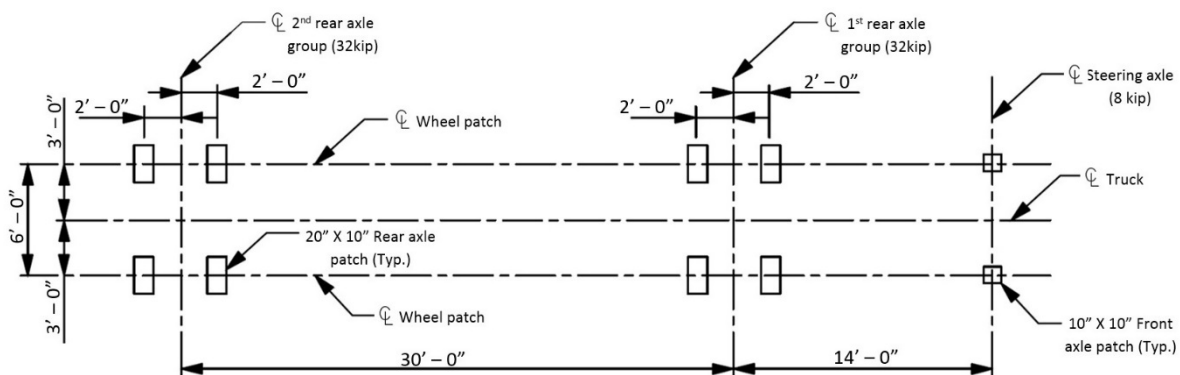


Figure 6.3.6.5-4 AASHTO orthotropic deck wheel patch loading.

6.3.6.6 Structural Supports for Highway Signs, Luminaires, and Traffic Signals

AASHTO publishes the *LRFD Specifications for Structural Supports for Highway Signs, Luminaires, and Traffic Signals* (AASHTO, 2015c), focusing specifically on the structural design aspects of those elements. Unlike a highway traffic bridge where the number of cycles of loading can be correlated to design traffic volumes and other structural parameters, the design of highway structures, light poles, traffic signals, and other appurtenances must consider the completely random nature of loading from wind, interactions with gust loading from vehicles, and the harmonic response of traffic structures mounted on bridges. Because of the inability to define a design number of cycles, the design of these types of structures is done exclusively with the goal of providing infinite life.

Highway traffic and lighting structures are commonly constructed of steel, though aluminum is also used. The AASHTO standard provides guidance for the design of both materials, and a specific chapter, Section 11, is devoted to fatigue design. The fatigue design for sign and lighting structures is based on specific loads that are unique to these types of structures and also includes an importance factor related to the risk of structural failure posing a hazard to the motoring public. Three importance categories are established, and different importance factors are assigned to each. Category 1 applies to long-span cantilever sign structures (greater than 50 ft.), high mast towers (greater than 100 ft. tall), large sign structures, and structures located in areas where wind-induced vibrations are known to occur. Category 3 applies to structures on roads with speed limits of 35 mph or less where structural failure would not affect traffic. Category 2 is defined as not falling in either Category 1 or 3, as previously defined.

Wind loads are provided as equivalent static loads acting on projecting areas of the various structures. The wind loads were selected so as to minimize the possibility of objectionable vibrations and deformations in service and to minimize the development of fatigue cracks in the various unique connections found in sign and lighting structures. The loadings specified are to be used to compute stress ranges in the vicinity of fatigue sensitive connection details using either standard, nominal stresses computed based on classical structural analysis or alternately by a method based on experimental testing or finite element analysis. The types of design loads considered for fatigue include:

- Galloping – An aeroelastic instability in which the wind causes an initial vibration of the structure, accompanied with continued coupling of the structural vibration, with the wind effects resulting in large amplitude vibration. Galloping results from the wind effects on attachments (e.g., signs and signal heads), not the structure itself (i.e., a structure with no attachments is not generally prone to galloping). AASHTO provides an equivalent pressure to be applied vertically to the projected area of the structure, though only over the length of the structure where there is an attachment.
- Vortex shedding – Another form of aeroelastic instability where the structure is a bluff body in the flow of wind. The flow of wind spins into vortices on the leeward side of the structure, and these shed on alternating sides of the structure. Each vortex causes an area of low pressure that pulls the cross section across the wind, and since the vortices alternate, so does the across-wind motion. However, the nature of the motion can also exacerbate the effects of the shedding, which is why it is an aeroelastic phenomenon. Vortex shedding occurs only at a critical wind velocity where the vortices are allowed to form and match the resonance of the structure itself; generally these are low wind velocities (i.e., less than 30 mph). Vortex shedding effects occur on the structure itself where there are no attachments, and attachments actually tend to disrupt the formation of vortices. Therefore, vortex shedding mostly occurs with high mast lighting structures. The AASHTO specification provides an equivalent static pressure based on the mean wind velocity at the site, and this is used in the computation of the nominal fatigue stresses.
- Natural wind gust – This is meant to capture the along-wind vibratory response of the structure from the wind blowing on and past the structure. All structures are susceptible to natural wind gust vibrations.
- Truck-induced gust – Cantilevered and non-cantilevered overhead sign and traffic signal support structures are to be designed to resist equivalent static truck gust pressures. Passage of trucks beneath the structures may induce vertical gust loads on horizontally projecting areas (e.g., variable message signs, the structure itself, and other attachments mounted along the horizontal span of the structure). The loads are specified to act in the vertical direction to the exposed area of horizontal supports, as well as in the horizontal plane of all signs, attachments, and other appurtenances. The pressures are assumed to act over a lateral distance of 12 feet, corresponding to the width of the standard traffic lane.

Figures illustrating galloping and vortex shedding (see Figure 6.3.6.6-1) and truck-induced gust (see Figure 6.3.6.6-2) are provided. Each of these is taken from FHWA-NHI-05-036, *Guidelines for the Installation, Inspection, Maintenance and Repair of Structural Supports for Highway Signs, Luminaries, and Traffic Signals* (Garlich and Thorkildsen, 2005).

The resistance to fatigue is the application of the CAFT rules for the various details commonly encountered in traffic lighting support structures. Covered by the specification are plain members, mechanically fastened connections, holes and cutouts, groove welded connections, fillet welded connections, and attachments. Guidance is provided for both steel and aluminum structures. Various unique details are commonly used in the fabrication and construction of lighting and support structures. The AASHTO specification provides sketches illustrating the

many unique connection types and provides the appropriate fatigue design guidance for each (AASHTO, 2015c). Examples of unique connections covered by the specifications include multiple examples of the connection of tubular members with the use of welded gusset plates, tube-to-plate connections, and the treatment of holes and access openings in structural members.

Figure 6.3.6.6-3, Figure 6.3.6.6-4, and Figure 6.3.6.6-5 depict finite element solutions and stress concentrations for certain common details found in sign and lighting structures, as well as representative sketches from the AASHTO specifications (AASHTO, 2015c). The finite element analysis models are from a presentation given of findings from NCHRP Project 10-70, *Cost-Effective Connection Details for Highway Sign, Luminaire and Traffic Signal Structures* (Roy et al., 2009).

Figure 6.3.6.6-6 and Figure 6.3.6.6-7 are from the State of Illinois, *Sign Structures Manual* (Bureau of Bridges and Structures, 2012) and depict a common overhead sign truss, as well as common bolted and welded details.

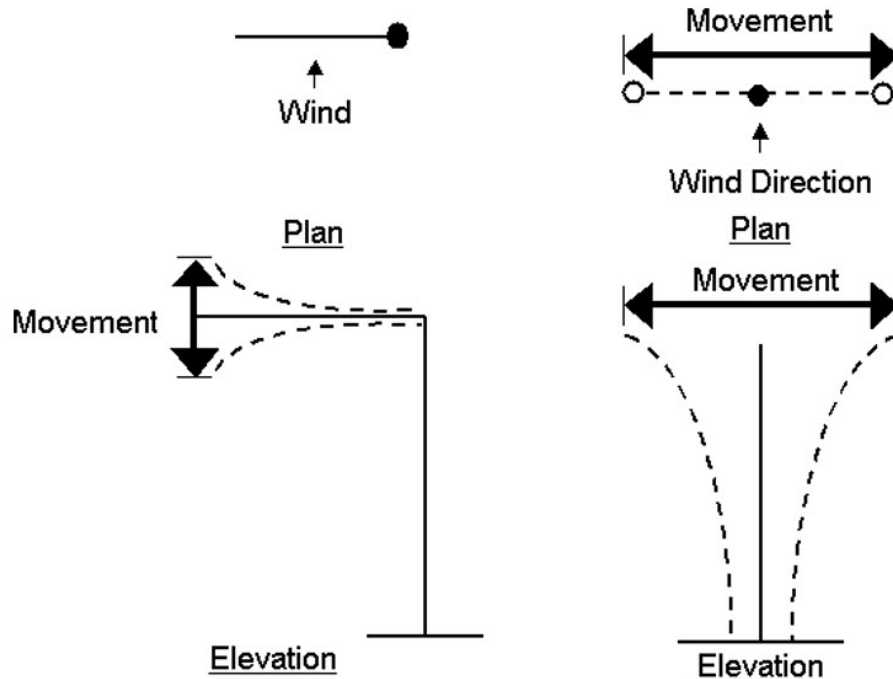


Figure 6.3.6.6-1 Galloping (left) and vortex shedding (right) behavior of cantilevered signs.



Figure 6.3.6.6-2 Truck-induced gust loading of overhead structures.

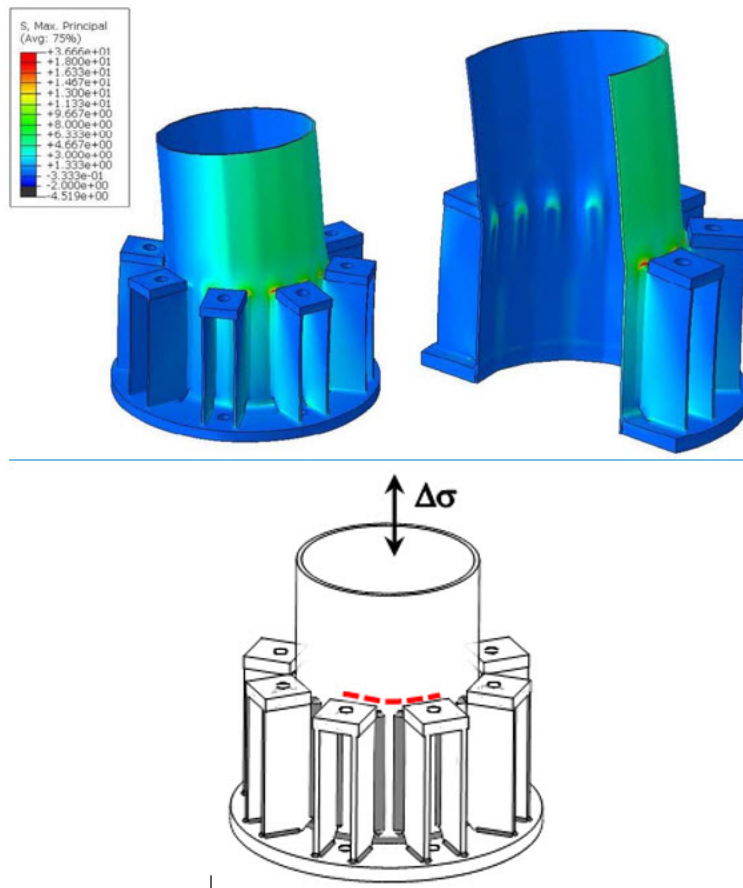


Figure 6.3.6.6-3 Fatigue cracking at a stool connection.

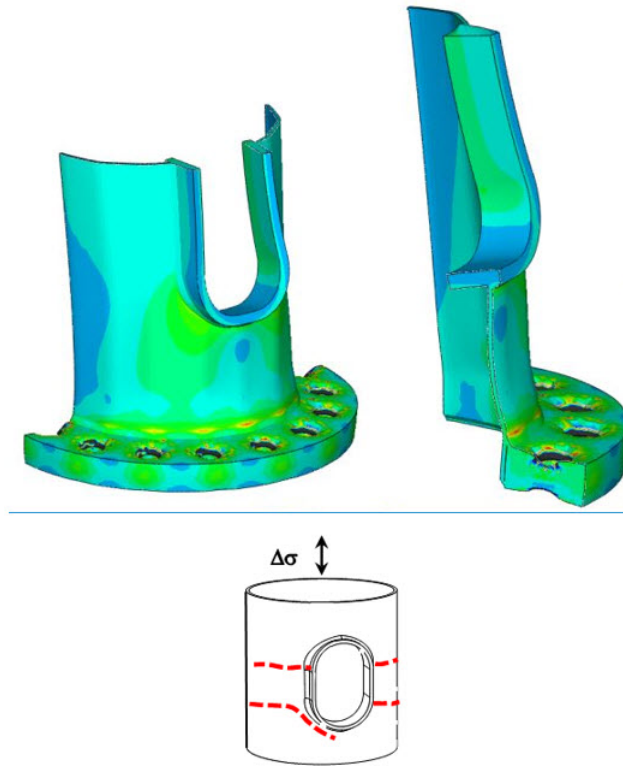


Figure 6.3.6.6-4 Fatigue cracking around reinforced access holes.

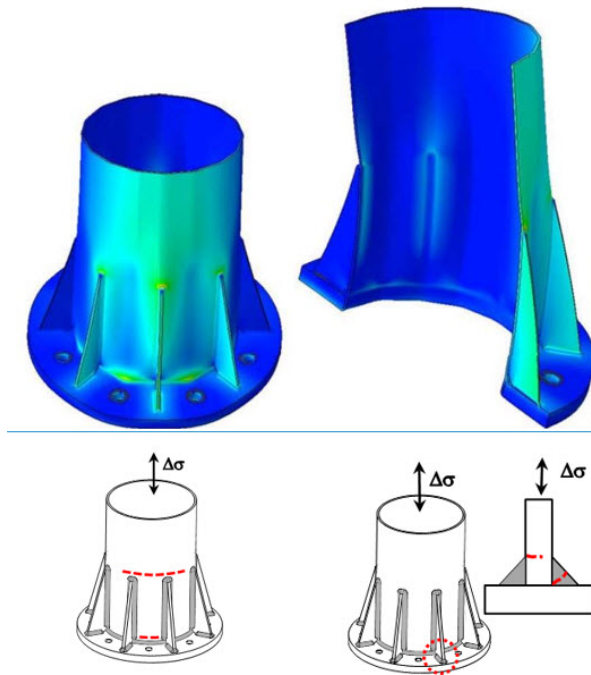


Figure 6.3.6.6-5 Fatigue cracking at tube base plate and stiffeners.

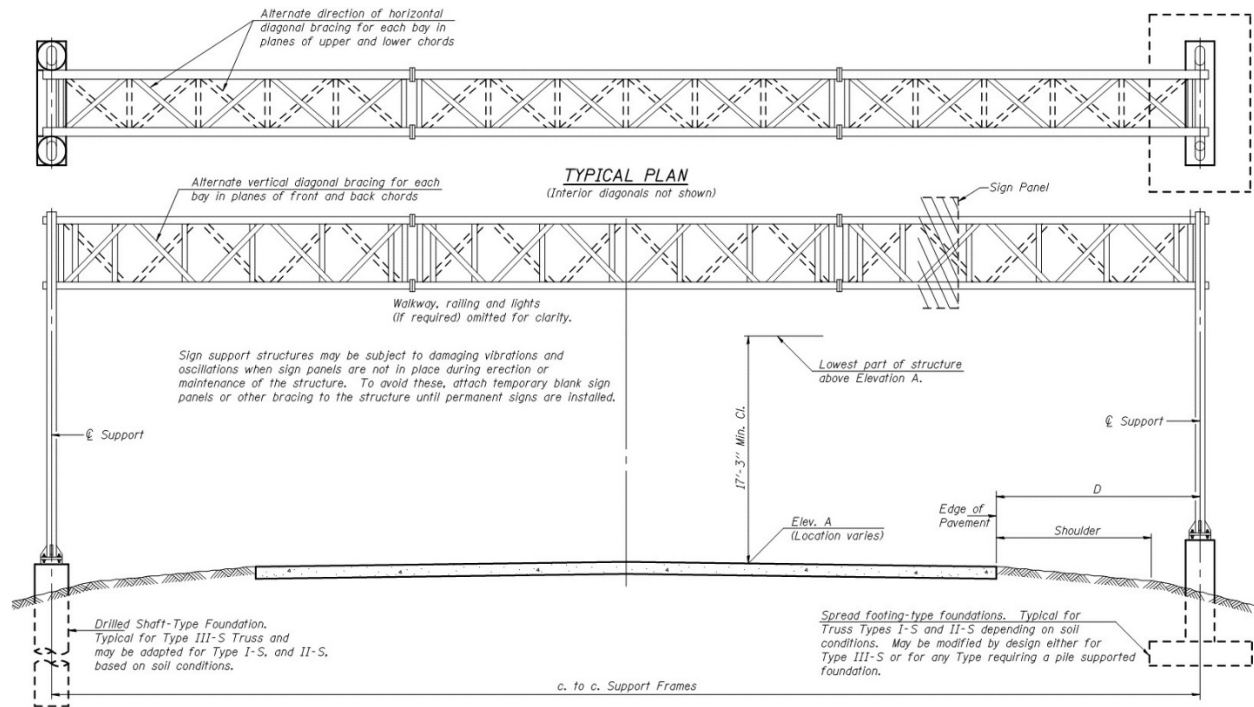


Figure 6.3.6.6 Standard Illinois DOT overhead sign truss schematic.

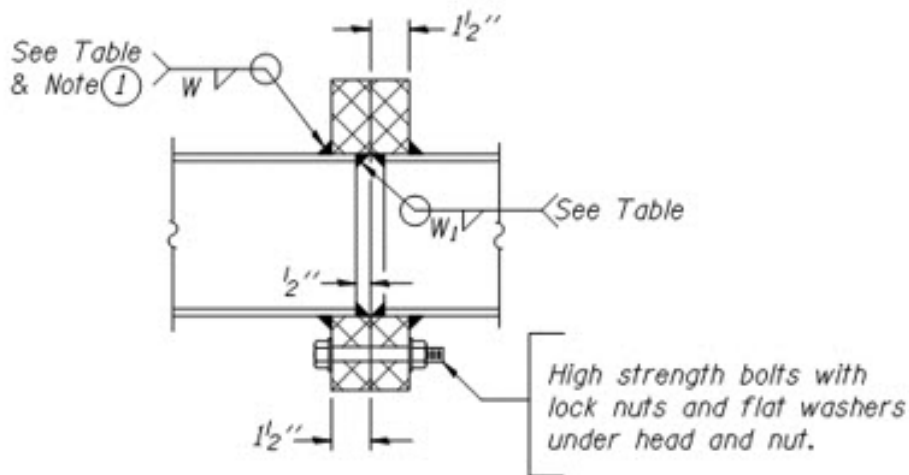
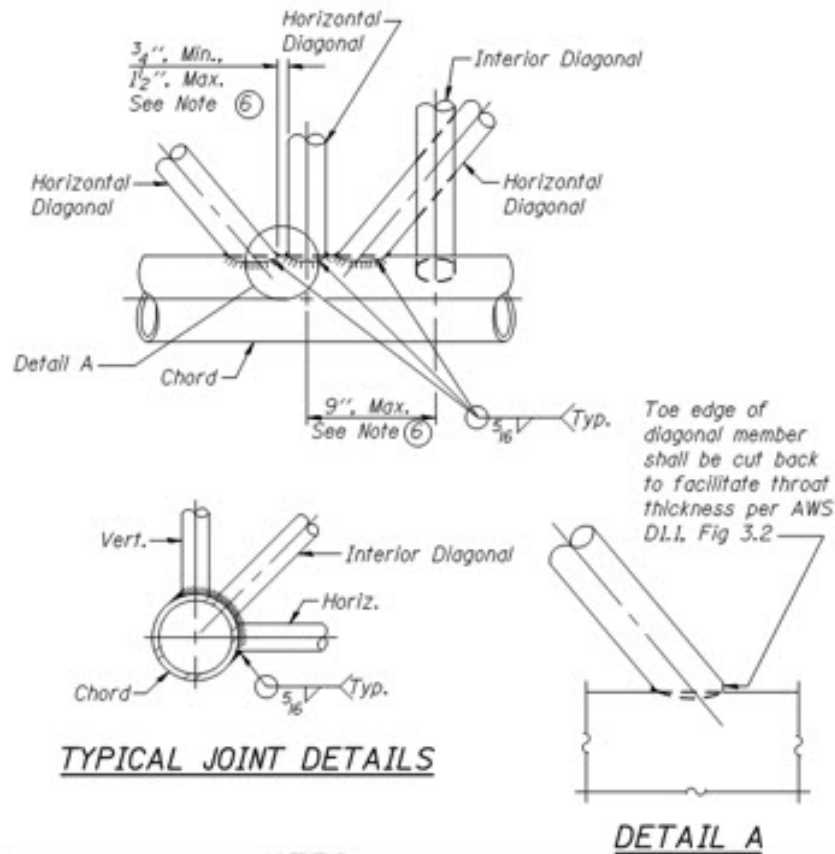


Figure 6.3.6.6-7 Welded truss joint details and bolted chord splice.

SECTION 6.4 DISTORTION-INDUCED FATIGUE

Transverse connection plates are used to connect elements such as diaphragms and cross-frames to longitudinal beams. Due to the differential displacement of the longitudinal elements, forces

are transferred between adjacent girders via the diaphragms or cross-frames. When this happens, lateral loads are imposed upon the transverse connection plate, the girder web, and the girder flanges. In many bridges of the past, engineers were concerned about transverse welds between connection plates and the flanges of the primary girders, creating a fracture concern.

For instance, the 1949 version of the AASHTO *Standard Specifications for Highway Bridges* specifically precluded transverse welds to a tension flange when the flange stress exceeded 75 percent of its capacity (AASHTO, 1949). So unless a member was purposely overdesigned just to allow welding to the tension flange, transverse welds between connection plates and tension flanges were omitted as a matter of standard practice. As a result, it was common to leave the connection plate unattached to the girder flange. Due to out-of-plane distortion, the resulting displacement and out-of-plane forces applied to the connection plate were not able to be resisted by the lateral stiffness of the flange but rather were transferred directly into the web and secondarily into the flange or slab. This out-of-plane force applied near the top and bottom of the web in the transverse direction resulted in displacements concentrated in a small web gap area and frequently resulted in cracks at the top or bottom of the stiffener or at the toe of the web-to-flange longitudinal weld. This is conceptually illustrated in Figure 6.4-1 and Figure 6.4-2.

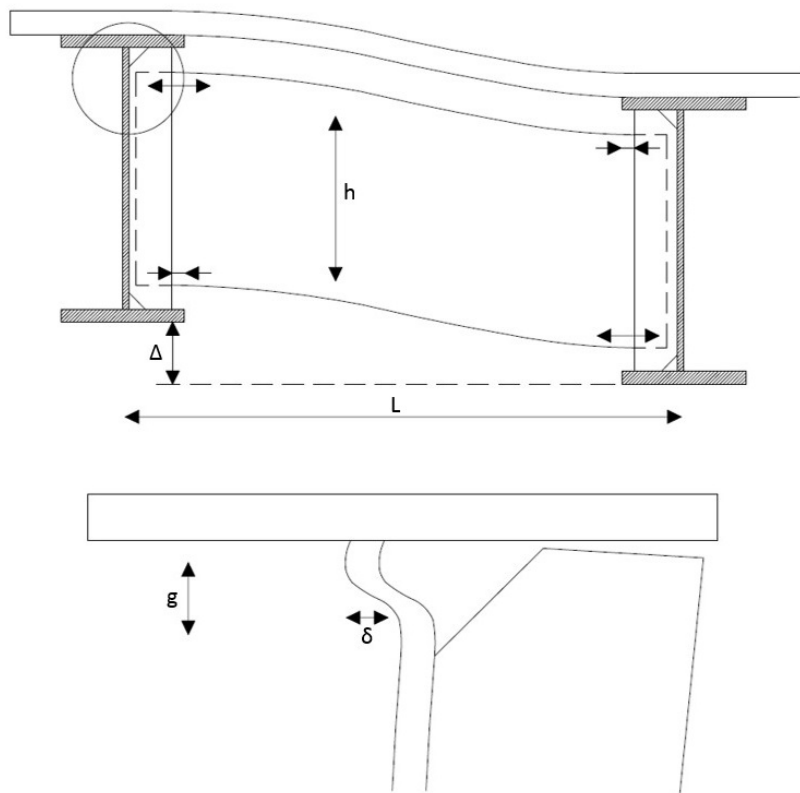


Figure 6.4-1 Distortion-induced fatigue loading of a diaphragm and girder.

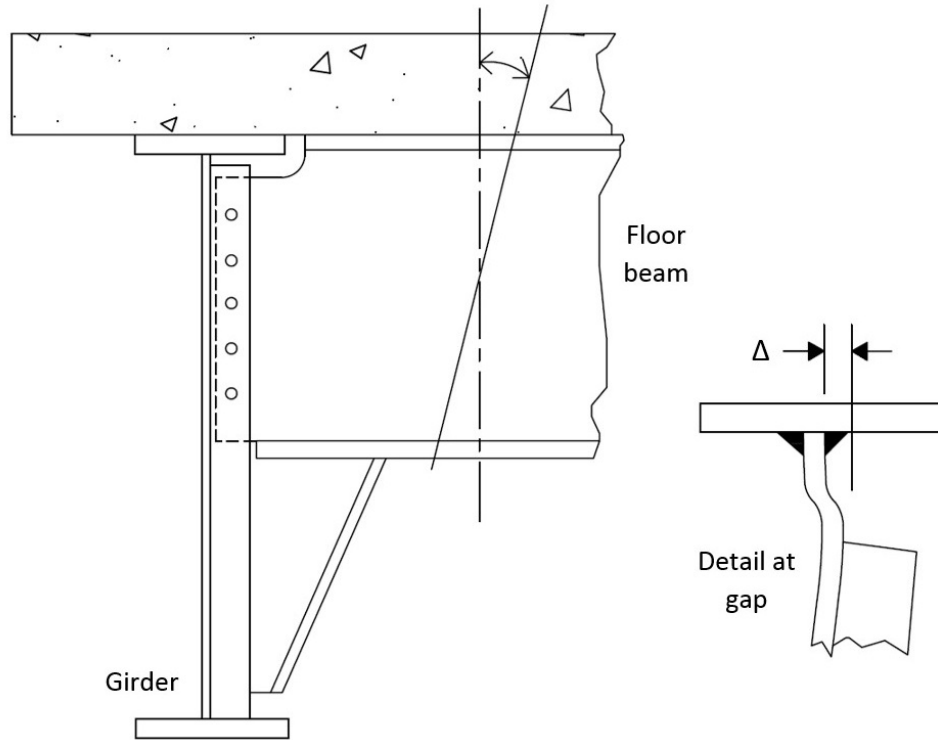


Figure 6.4-2 Web gap displacements in a girder-floorbeam steel bridge.

When a connection between the connection plate and girder flange is not provided, cracking such as that shown in Figure 6.4-3 has been noted. Although skew and curvature exacerbate the differential displacement effects, this type of cracking has been found in all bridge types. The bridge in Figure 6.4-3 is a non-skewed bridge with regularly spaced cross-frames and has significant cracking at many cross-frames throughout the bridge in positive and negative moment regions.



Figure 6.4-3 Distortion-induced fatigue cracking of a steel girder.

AASHTO LRFD Article 6.6.1.3.1 requires that, as a minimum, connection plates used to connect diaphragms and cross-frames, as well as those used to connect floorbeams, be welded or bolted to both the compression and tension flanges of the longitudinal beam. For bridges in which the force effects in the diaphragm and cross-frame are not directly computed (e.g., a straight or slightly skewed bridge), the specification requires that the connection between the transverse connection plate and the flanges be designed to resist a 20-kip transverse load. However, for bridges in which diaphragm, cross-frame, or floorbeam effects are computed by analysis, the forces resulting from that analysis are required to be transferred through this connection. Minor exceptions to these requirements are provided for rolled beam bridges that are straight and have composite reinforced concrete decks. The 20-kip provision is simply a rule of thumb that applies for straight, non-skewed bridges to detail the size of the weld. The intent of connecting to both flanges and providing a minimum strength connection is to provide a sufficient amount of stiffness to limit the amount of relative movement between the flange and web and to limit web lateral displacements. Because stiffness and not strength is the governing criteria behind the potential success of these connections, a welded attachment between the stiffener and flange is preferred, although a bolted connection is allowed. A bolted connection having the required stiffness of an equivalent welded connection is a more time-consuming, more costly, and less proven detail. It also does very little to alleviate the underlying fatigue concerns with welded connections because a similar fatigue detail exists where the transverse stiffener is welded to the girder web only several inches above or below the flange in question. Providing the bolted attachment to the flange does not change the underlying fatigue resistance of the girder as a practical matter. The practice is allowed but discouraged since it does not improve the overall fatigue resistance of a structure in any meaningful way.

It should be noted that transverse connection plates are distinguished from transverse stiffeners whose purpose is only to stiffen the web for shear resistance. A transverse stiffener provided simply to improve the shear resistance of the web does not require attachment to both flanges. *AASHTO LRFD* indicates that transverse shear stiffeners need not be in bearing or contact with the tension flange. At the compression flange, only a tight fit attachment is required, though a positive attachment is certainly permitted. The latitude to only tight fit the stiffener to the compression flange and leave it cut short from the tension flange greatly simplifies installation of the stiffeners, as they need not be in contact and connected to both flanges of the structure.

Another source of distortion-induced fatigue cracking is the attachment of lateral bracing connection plates to the webs of steel beams. Similar to the transverse connection plate, under the action of differential vertical displacement, forces are induced into lateral bracing systems that result in the diagonals of the lateral bracing being loaded alternately in tension and compression. The lateral bracing members therefore exert a potentially large lateral force on the webs of what are commonly plate girders. Given the relatively large forces that are introduced in the out-of-plane direction of the web, fatigue cracking has been documented in these connections due to the concentrated lateral displacement of the web between the lateral bracing connection plate and the nearest flange. The flange serves as a relatively stiff out-of-plane element and restrains the bottom of the web, or a concrete slab restrains the top of the web.

AASHTO LRFD Article 6.6.1.3.2 provides guidance on the attachment of lateral bracing plates to steel girders. It indicates that if it is not practical to attach the lateral bracing connection plate directly to the flange, then the connection plate may be attached to the web with the gusset plate

being separated from the flange by a distance of at least one half the width of the closest flange. The horizontal bracing connection plates must be at least 6 inches from the nearest flange as well. The stipulation of these minimum offset distances is so that the forces that are introduced into the lateral bracing connection plate are introduced at a distance far enough away from the nearest source of restraint, the nearest flange, so as to reasonably preclude the possibility of distortion-induced fatigue cracking. The requirement for locating the lateral connection plate on the web does not preclude other types of fatigue cracking that may result. These connection plates will still need to be evaluated for the appropriate load-induced fatigue detail used to attach them to the web of the beam.

SECTION 6.5 STEP-BY-STEP APPLICATION OF LRFD FATIGUE DESIGN

This section combines information from prior sections and demonstrates the practical application of *AASHTO LRFD* for fatigue design. A numerical example then follows. The use of the *AASHTO LRFD* specifications for fatigue design involves the application of the following steps:

- Step 1. Determine locations requiring fatigue limit state verification.
- Step 2. Compute force effects. This includes both the moving live load analysis and the calculation of distribution factors (or use of refined analysis methods) to compute forces in the individual members. For all force effects, apply the dynamic load allowance (impact), which is a required 15 percent increase in the force effects of the design truck.
- Step 3. Calculate stress ranges at fatigue details.
- Step 4. Calculate fatigue resistance of the specific details used on the structure and verify factored stress ranges are below the computed resistance.

6.5.1 Determine Locations Requiring Fatigue Limit State Verification (Step 1)

Fatigue must only be investigated when the detail is subjected to a net applied tensile stress. This is done by comparing the permanent compression, where it exists, to the maximum tensile stress produced by the Fatigue I load combination. Only when the tensile stress due to the Fatigue I load combination exceeds the unfactored permanent stress does fatigue need to be considered.

6.5.2 Compute Force Effects (Step 2)

AASHTO LRFD specifies that the loading to be applied is a single fatigue design truck placed in a single lane. This approach has been used since the introduction of LRFD, and its appropriateness was validated during the SHRP2 R19B research project. Additional information about the SHRP2 R19B study is provided in Appendix A. Examples of the determination of force effects for a common girder bridge and a more unique structure, a tied arch, are provided below.

6.5.2.1 Case Study – Force Effects for a Common Girder Bridge

Step 2.1 – Position the load longitudinally.

Using the principles of influence lines, position the fatigue truck at the longitudinal location which maximizes and minimizes the live load bending moment at the particular detail. For the common case of a continuous span bridge, this involves determining the peak ordinates of the influence line and placing the truck accordingly. Figure 6.5.2.1-1 demonstrates the two locations of the fatigue design truck that would be chosen to maximize the range of moments, and hence the range of stress, near midspan of Span 1 at a detail to be investigated. The loads are individually placed, once in Span 1 and once in Span 2, not simultaneously as the figure might suggest, and the moments are computed for each pseudo-static position.

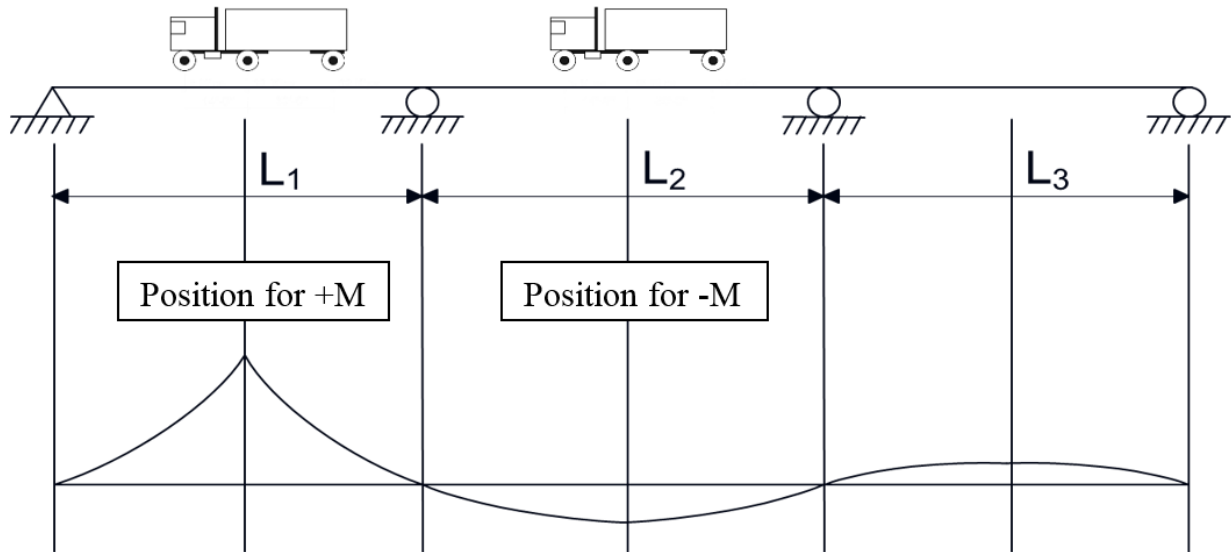


Figure 6.5.2.1-1 Influence line for bending moment for a three-span continuous bridge.

Step 2.2 – Apply impact.

The dynamic load allowance, commonly referred to as the impact factor, amplifies the static force effects due to contributing factors such as pavement roughness and vehicle / bridge dynamic characteristics. It is applied at the fatigue limit state as a 15 percent increase in the load effects computed from the moving load analysis.

Step 2.3 – Determine the fraction of bending moment resisted by a particular member.

For a traditional multi-girder bridge, the live load bending moments are first computed in the longitudinal direction and then distributed transversely. AASHTO provides empirical live load distribution factor equations to approximate the fraction of the total vehicle force effect that must be resisted by the most heavily loaded beam. The use of these empirical equations relieves the engineer from the difficulty of determining an exact transverse positioning of the vehicle. They are used in lieu of a refined analysis, such as a grid or 3-D finite element model, to determine individual member force effects. The concept of live load distribution factors is illustrated in Figure 6.5.2.1-2.

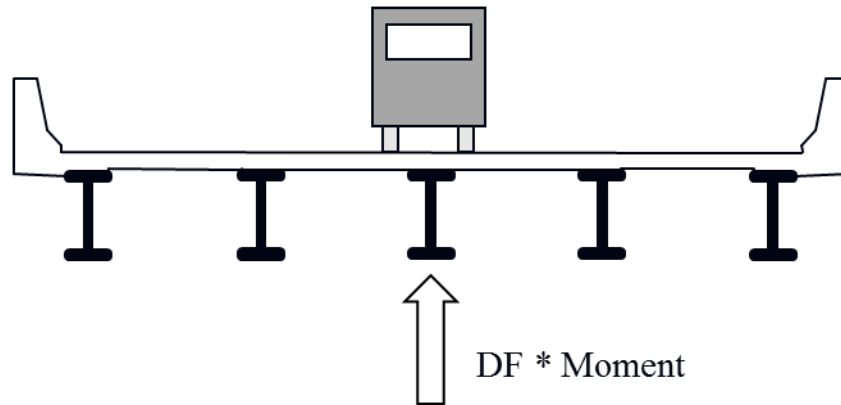


Figure 6.5.2.1-2 Distribution factor concept.

For a multi-beam steel bridge with a concrete slab, *AASHTO LRFD* provides the following equations for the case of a single lane loaded. It is important to recall that the fatigue limit state is based on a single truck in a single lane producing the stress ranges in question.

$$DF_{single\ lane} = 0.06 + \left(\frac{S}{14}\right)^{0.4} \left(\frac{S}{L}\right)^{0.3} \left(\frac{K_g}{12Lt_s^3}\right)^{0.1} \text{ Lanes}$$

Equation 6.5.2.1-1

To determine the moments in the beam, the force effects due to the entire vehicle on a per-lane basis (see Figure 6.5.2.1-1) are then multiplied by the distribution factor (DF) to determine the fraction of the force assigned to the most heavily loaded beam. The equation above must be modified, however, since included in this equation is the *AASHTO* multiple presence factor of 1.2 that was developed during the calibration of the strength limit state. The 1.2 multiple presence factor is included in the standard single-lane distribution factor equations to account for possible overloaded vehicles that produce force effects greater than those included in the live load calibration process. This occasional heavy weight vehicle that is important at the strength limit state is accounted for with the Fatigue I load combination instead and thus the additional 20 percent must be removed from the DF equations when designing for fatigue. Thus for fatigue, the DF equation results must be divided by 1.2 as shown below.

$$DF_{fatigue} = \frac{0.06 + \left(\frac{S}{14}\right)^{0.4} \left(\frac{S}{L}\right)^{0.3} \left(\frac{K_g}{12Lt_s^3}\right)^{0.1}}{1.2} \text{ Lanes}$$

Equation 6.5.2.1-2

AASHTO LRFD specifies that fatigue design be carried out using a single design vehicle placed in a single lane. The lanes are “design lanes” and do not correspond to the striped lane conditions since these are not guaranteed to be permanent. A “design lane” is hypothesized to be at any lateral location on the bridge. However, lane placement is not required when using the DF equations. For exterior beams, a check of the DF using the

“lever rule” model is required, and for that method, the loads are positioned manually by the engineer to determine the DF.

6.5.2.2 Case Study – Force Effects for a Tied Arch Bridge

For a more complex structure, the same principles apply to determining the live load effects (i.e., live loads must be placed longitudinally and transversely to determine the critical loadings). The example shown is the Kentucky Lake tied arch bridge (see Figure 6.5.2.2-1). The bridge was analyzed and designed using a three-dimensional finite element model. The influence lines for bending moment and axial load at a point of interest in the tie girder are plotted in Figure 6.5.2.2-2. Unlike the case of a girder bridge, which decouples the determination of bending moments and the distribution of forces to specific members, the finite element approach captures the effects of longitudinal and transverse positioning simultaneously. It incorporates the concept of “influence lines” and “load distribution factors” at the same time through a three-dimensional internal distribution of loading effects, commonly called an influence surface. Shown in Figure 6.5.2.2-2 are the axial load and primary bending moment influence lines for live loads traveling in a fixed transverse position (i.e., a longitudinal slice through the influence surface). Similar lines can be generated for other design or striped lanes.

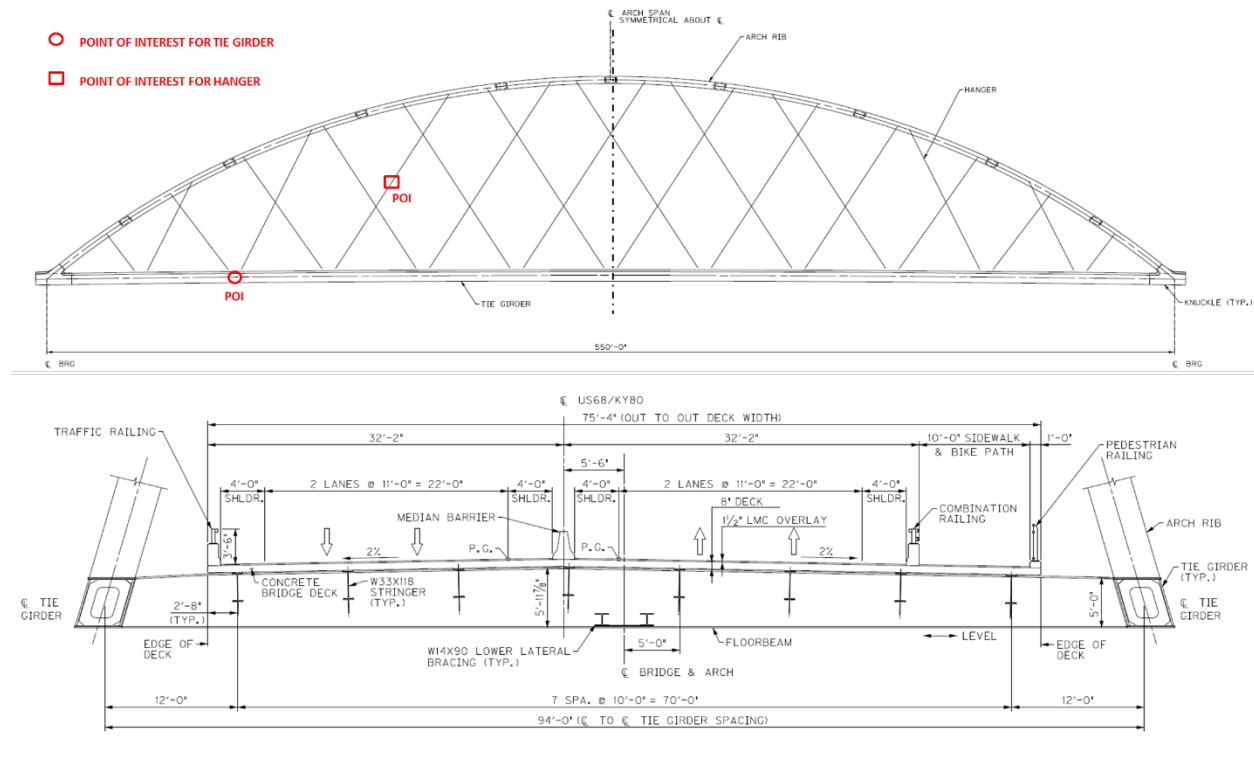


Figure 6.5.2.2-1 Kentucky Lake Bridge point of interest.

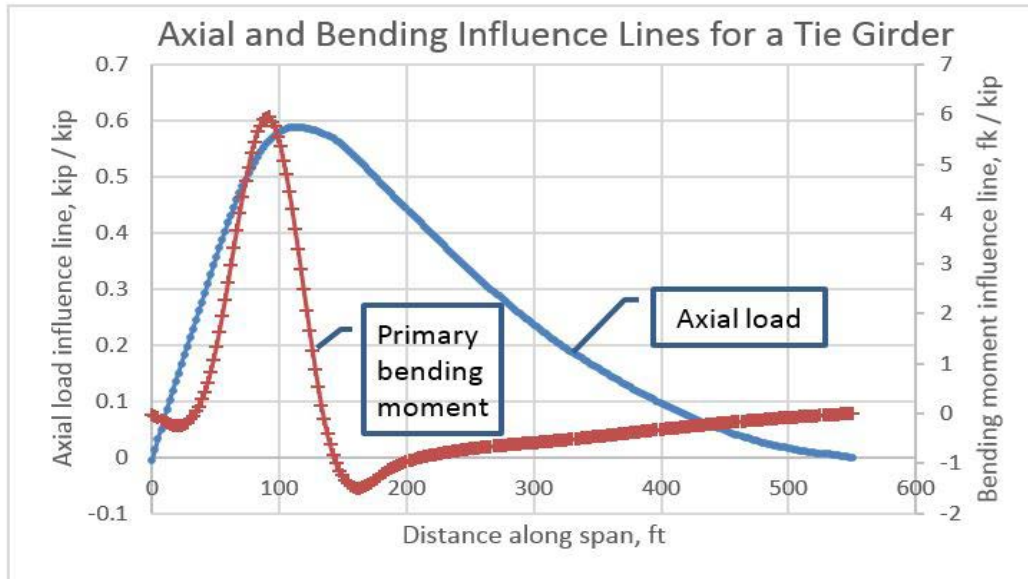


Figure 6.5.2.2-2 Kentucky Lake Bridge axial load and bending moment influence lines.

6.5.3 Calculate Stress Ranges at Fatigue Details (Step 3)

Once the detail is found to require investigation and the distributed live load forces are determined, the stresses due to the factored and distributed fatigue loads must be computed. For axially loaded members (e.g., truss members, the tie girder described previously, or members of a cross-frame), the steel section alone is used to resist the stresses.

For the case of flexural members, when shear connectors are provided over the entire length of the girder and the concrete deck slab meets the minimum area of reinforcing steel provisions of *AASHTO LRFD*, it is permitted to compute the flexural stresses using the short-term composite section of the steel girder and transformed concrete slab for both the positive and negative bending moments. Although the negative live load moments cause some tension in a composite concrete slab, the shear connectors and longitudinal slab steel result in a slab with only fine cracking, and the full composite section is maintained for the calculation of stresses.

The range of stress, Delta (Δ) f , at any detail is computed using the common formula for flexural stress:

$$\Delta f = \frac{\Delta M * y}{I_n}$$

Equation 6.5.3-1

where:

- ΔM = range of moment
- y = vertical distance from the neutral axis of the short-term composite section to the detail being evaluated
- I_n = moment of inertia of the short-term (n) composite section

Details that are furthest from the neutral axis are subjected to the highest stress range but may not be critical since the fatigue resistance of the detail is also important. For instance, in the accompanying Figure 6.5.3-1, numerous details were welded to a plate girder and tested.

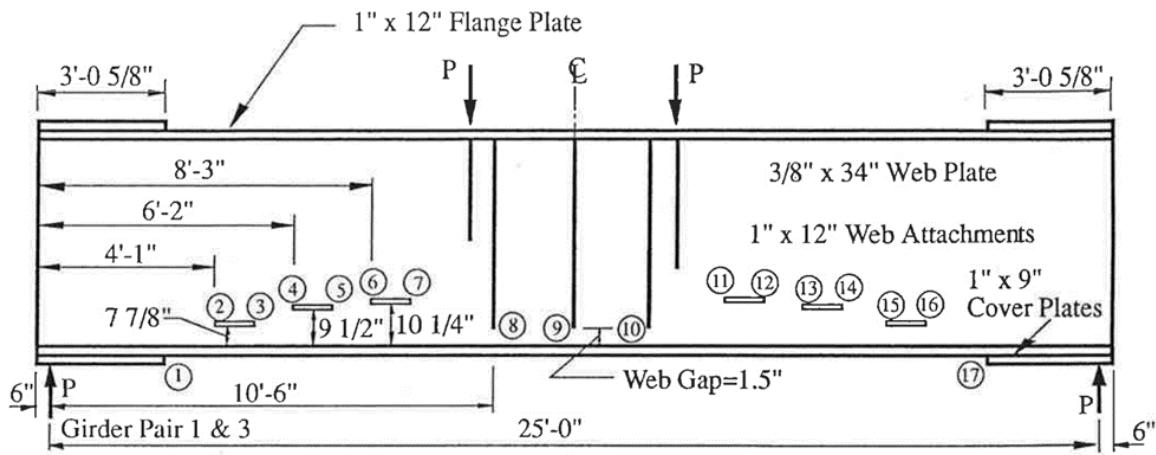


Figure 6.5.3-1 Multiple fatigue details on a plate girder.

Although the web-to-flange weld is furthest from the neutral axis of the section and is subjected to the highest stress range, it likely does not control the design due to the presence of more critical details. For instance, the transverse (vertical) stiffeners that are very near the bottom flange have essentially the same stress range as the web-to-flange weld but are a more severe fatigue detail category (C') as compared to the longitudinal weld (B), and thus will control. Also near the bottom flange are various longitudinal stiffeners, and these are generally more severe than the transverse stiffener, so it is likely that their lesser resistance will govern the fatigue design in regions of comparable stress range. The intent of this discussion is to demonstrate that some judgment can be used when evaluating fatigue in steel structures.

Details from an actual bridge are provided in Figure 6.5.3-2 to further illustrate this point and to show details from a composite bridge. The corner chamfer detail illustrates the minimum and maximum clearances used to locate the ends of fillet welds in a plate girder. For the two cross sections shown in the figure, a continuous fillet weld connects the web and flange but is not shown.

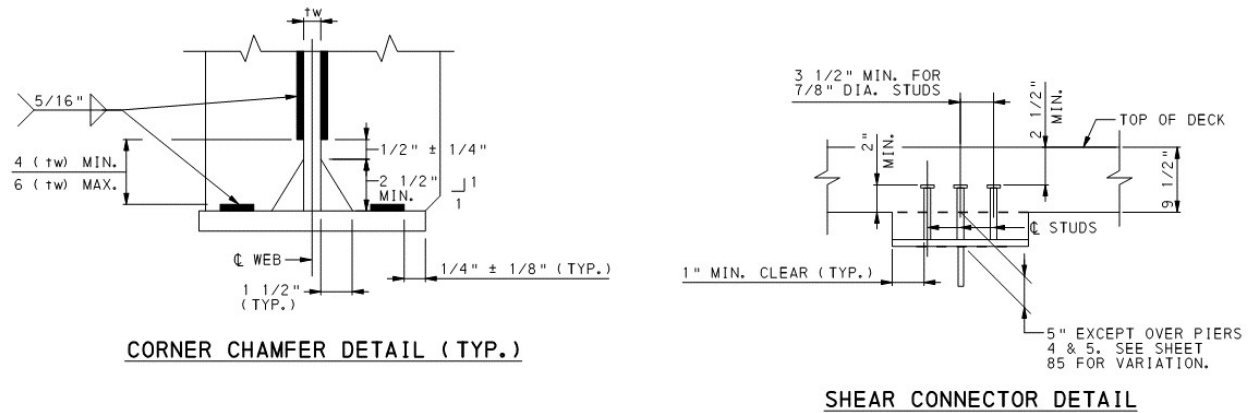


Figure 6.5.3-2 Common web-to-flange, connection plate, and shear stud welds.

At the elevation of the inside surface of the bottom flange, the web-to-flange weld is present along with the weld connecting the transverse stiffener to the flange. The web-to-flange weld (a continuous fillet weld) is a Detail Category B weld, while the transverse stiffener weld is a Detail Category C' weld. The Detail Category C' condition is more restrictive and thus the fatigue detail of the web-to-flange weld does not need to be checked.

At the top flange, several details are also present. These include the web-to-flange weld (again not shown in this detail), as well as the shear studs welded to the flange to create the composite condition. The shear studs welded to the outside of the flange are a Detail Category C detail, while the web-to-flange weld on the inside of the flange, where the stresses are marginally less, is a Detail Category B weld. Again, the web-to-flange weld is not the controlling detail. Shear studs must also be checked to ensure that their welds to the top flange do not fail in fatigue. This is described in *AASHTO LRFD* Article 6.10.10.

6.5.4 Calculate Fatigue Resistance (Step 4)

Much time has been spent detailing the development of the finite and infinite life resistance models for fatigue in this and other chapters. To apply these models in *AASHTO LRFD*, the following procedure is generally followed:

Step 4.1 – Categorize the details present on the member being investigated.

Categorize the details located on the member of interest and their location along its length. These include details such as mechanically fastened joints, welds joining components of built-up members, and welded attachments.

Step 4.2 – Classify the details according to AASHTO as Category A, B, B', C, C', D, E, or E'.

Step 4.3 – Determine the frequency of loading.

Step 4.4 – Determine the number of cycles per truck passage.

The current AASHTO recommended number of cycles per truck passage is presented in Table 6.3.4.2-3. However, it is likely that these recommendations will be replaced by the simpler approach in Table 6.3.5.1-1.

Step 4.5 – Determine the number of cycles over the 75-year design life.

For the investigation of the Fatigue II load combination, determine the number of design cycles using the equation $N = (365)(75)(n)(ADTT)_{SL}$.

Step 4.6 – Compute the infinite life resistance.

For the investigation of the Fatigue I load combination, the resistance is the CAFT value. Determine this value from *AASHTO LRFD* Table 6.6.1.2.5-3 or from Table 6.2.3.2-1 herein.

Step 4.7 – Determine if adequate infinite resistance is provided.

Compare the infinite life resistance with the fatigue demand. If the stress ranges are less than the fatigue resistance, then the design is adequate. However, if they are not, then the detail must be revised to comply with the *AASHTO LRFD* limits or a check of finite life (Step 4.8) must be performed.

Step 4.8 – If infinite life is not provided (see Step 4.7), compute the finite life resistance.

Use the following equation to determine the finite life fatigue resistance.

$$\Delta F_n = (A/N)^{1/3}$$

In cases where adequate infinite or finite life is not provided, in some cases, a detail can be relocated to improve its performance. For example, if the resistance is exceeded at a transverse stiffener or connection plate, the engineer can explore another arrangement of the connection plates so that the detail is located at a region of lower stress range. If the resistance is exceeded for a longitudinal stiffener termination, the termination can be moved to a region of lower stress range or to a zone of permanent compression, or the end of the detail can be improved by providing a radiused transition. In some cases, an increase in section modulus might be required, but only after exhausting these simpler and more cost effective changes first.

SECTION 6.6 EXAMPLE PROBLEM OF FATIGUE DESIGN

For the girder shown in Figure 6.6-1, the process described in Section 6.5 will be employed to determine the fatigue stresses and check a point 56 feet from the left abutment, the 0.4 point of the end span. An assumed cross-frame connection plate is at this location.

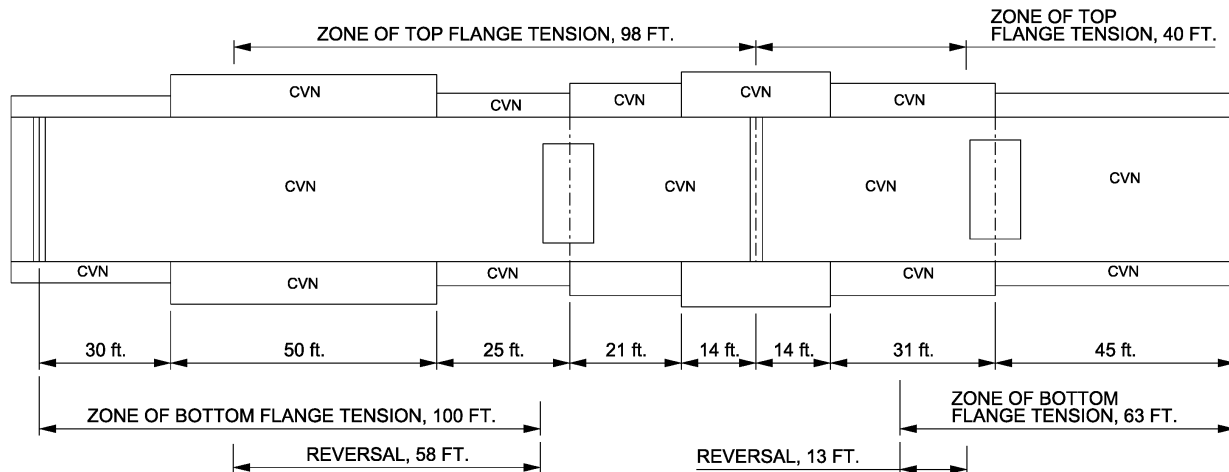


Figure 6.6-1 Girder elevation for sample fatigue calculations.

6.6.1 Determine Locations Requiring Fatigue Limit State Verification (Step 1)

Because the cross-frame connection being considered is welded to both flanges, and the bottom flange in particular is in flexural tension when dead load and live load are considered together, a fatigue check of the weld to the bottom flange is required.

6.6.2 Compute Force Effects (Step 2)

Step 2.1 – Position the load longitudinally.

A continuous beam analysis program was used to determine the maximum positive and negative live load moments due to the fatigue truck, prior to applying impact or distribution factors, at the point of interest. The results are:

Positive LL moment = 1,573 ft-kips
 Negative LL moment = -496 ft-kips

Step 2.2 – Apply impact.

An additional 15 percent is added to each of the above moments to reflect the impact value specified for use in the fatigue limit state.

Positive LL+I moment = $1.15 * 1,573 \text{ ft-kips} = 1,809 \text{ ft-kips}$
 Negative LL+I moment = $1.15 * -496 \text{ ft-kips} = -570 \text{ ft-kips}$

Step 2.3 – Determine the fraction of bending moment resisted by a particular member.

For the girder in question, an exterior beam, the live load distribution factor was determined using the lever rule and is 0.75 lanes. Therefore, the moments per girder are computed as follows:

Positive moment, including impact and distribution, $M(+) = 0.75 * 1,809 = 1,357$ ft-kips
 Negative moment, including impact and distribution, $M(-) = 0.75 * -570 = -428$ ft-kips

6.6.3 Calculate Stress Ranges at Fatigue Details (Step 3)

The range of stress is determined by applying the range of moments from above to the composite section of the slab and girder. The bridge being evaluated has shear studs between the girder and slab and meets all requirements to be considered fully composite for both signs of the bending moment.

The section modulus at the weld between the bottom of the web and flange was computed to be $2,661 \text{ in}^3$. This value is based on the uncracked composite section (using n).

Therefore the range of stress at the detail is computed as:

$$\Delta f = \Delta M / S_n$$

$$\Delta f = \frac{(1357 \text{ ft} - \text{kips} - (-428 \text{ ft} - \text{kips})) * 12}{2,661 \text{ in}^3} = 8.05 \text{ ksi}$$

For the evaluation of the Fatigue I load combination, a 1.75 load factor is applied, and for the Fatigue II load combination, a load factor of 0.8 is applied. Thus,

Factored stress range, Delta (Δ) f , for Fatigue I = $1.75 * 8.05 = 14.09$ ksi

Factored stress range, Delta (Δ) f , for Fatigue II = $0.8 * 8.05 = 6.44$ ksi

Now that the stresses have been computed, the resistance of the detail must be determined.

6.6.4 Calculate Fatigue Resistance (Step 4)

Step 4.1 – Categorize the details present on the member being investigated.

The detail being investigated is a welded connection plate attaching a cross-frame to the girder.

Step 4.2 – Classify the details according to AASHTO as Category A, B, B', C, C', D, E, or E'.

AASHTO LRFD classifies a welded connection between a connection plate and a girder flange as Category C'.

Step 4.3 – Determine the frequency of loading.

The average daily truck traffic in the most heavily traveled lane is estimated from the following equation:

$$\text{ADTT}_{\text{SL}} = p * \text{ADTT}$$

For this design, the ADTT value was provided by the traffic engineer as 675 trucks per day, and three lanes are available for truck traffic on the bridge. Therefore, AASHTO requires that the fraction of truck traffic assumed in the most heavily traveled lane be taken as 80 percent of the total volume. Thus,

$$\text{ADTT}_{\text{SL}} = 0.80 * 675 = 540 \text{ trucks per day}$$

Step 4.4 – Determine the number of cycles per truck passage.

For a point in the end span of this continuous beam bridge, one cycle per truck passage is produced.

Step 4.5 – Determine the number of cycles over the 75-year design life.

For the investigation of the Fatigue II load combination, determine the number of design cycles using the equation $N = (365)(75)(n)(\text{ADTT})_{\text{SL}}$.

$$N = 365 * 75 * 1 * 540 = 14,782,500 \text{ cycles}$$

Step 4.6 – Compute the infinite life resistance.

For the investigation of the Fatigue I load combination, the resistance is the CAFT value. For a Category C' detail, the threshold resistance is 12 ksi.

Step 4.7 – Determine if adequate infinite resistance is provided.

The first step is to determine if the design meets the infinite life requirements. The factored stress range from the Fatigue I load combination, 14.09 ksi, is compared to the constant amplitude fatigue threshold, 12 ksi. Since the computed stress range is greater than the threshold, infinite life is not provided. Therefore, further evaluation of this detail is required.

If the Fatigue I load combination check is satisfied (i.e., if the Fatigue I stress range is less than the CAFT), then the finite life resistance does not need to be compared to the Fatigue II load combination stress range to determine if the design is suitable. The second check shown below in Step 4.8 is not required for that situation.

Step 4.8 – If infinite life is not provided (see Step 4.7), compute the finite life resistance.

Use the following equation to determine the finite life fatigue resistance.

$$\Delta F_n = (A/N)^{1/3}$$

For a Category C' detail, the constant, A , is $44 \times 10^8 \text{ ksi}^3$. Therefore, the finite life resistance is:

$$\Delta F_n = \left(\frac{44 \times 10^8}{14,782,500} \right)^{1/3} = 6.68 \text{ ksi}$$

The factored stress range from the Fatigue II load combination, 6.44 ksi, is compared to the finite life resistance computed above, 6.68 ksi. Since the computed stress range is less than the finite life resistance, finite life is provided.

In the event that both infinite and finite life resistance are not sufficient, the Engineer must modify the design, including such options as moving the connection plate or revising the girder dimensions.

This page intentionally left blank

CHAPTER 7 FRACTURE CONTROL

SECTION 7.1 HISTORICAL DEVELOPMENT OF FRACTURE CONTROL PRACTICES

In the rare instances when the conditions are right for a fracture to occur, it is due to a critical combination of crack geometry, applied stress, temperature, and loading rate acting simultaneously on a member. The interrelationship of these factors was covered in Chapter 3, which describes the theoretical basis of brittle fracture in steel. Also covered in Chapter 3 are the background to material toughness requirements, the influence of crack size on element behavior, the influence of temperature and loading rate on the toughness requirements for bridge steels, and the theoretical use of fracture mechanics as a quantitative design or analysis tool. This chapter provides more complete coverage of the development of a comprehensive approach in which design, fabrication, and inspection requirements each have an important role in fracture control.

The concept of a bridge-specific approach to fracture control traces its origins to the collapse of the Point Pleasant Bridge (also known as the Silver Bridge) in West Virginia in December 1967 (see Figure 7.1-1). The collapse of the bridge was from the brittle fracture of an eyebar originating from a very small crack that was of an undetectable size. This collapse raised awareness on two fronts. First, there was no understanding at the time as to how many other bridges with similar brittle material were in the nation's inventory. As it turns out, only one bridge with similar eyebar material was located. A hanger detail of the same material was used in the Carquinez Truss Bridge, and the applicable eyebars were replaced. This event provided impetus for the creation of what are now called the National Bridge Inspection Standards (NBIS) and the National Bridge Inventory (NBI) in 1971. Second, it was the beginning of a national dialogue about the prevention of brittle fracture and defined bridge inspection procedures, frequency, inspector qualifications, and reporting requirements.



Figure 7.1-1 Point Pleasant Bridge before and after its collapse.

Over the next few years, other significant cracking events occurred on bridge structures. The fracture of the Bryte Bend Bridge during construction, which was fabricated with acceptable

steel, heightened the concern about the need for fracture toughness requirements for bridge steels.

Concurrent with some of these notable cracking events, a series of efforts were underway that would forever change elements of steel bridge design, fabrication, and inspection. As described below, there were numerous incremental changes to AASHTO, American Society for Testing and Materials (ASTM), American Welding Society (AWS), Federal Highway Administration (FHWA), and State design, fabrication, and inspection practices throughout the 1970's and 1980's. At about the same time, the American Society for Nondestructive Testing (ASNT) was developing and refining the requirements to qualify shop inspectors through its *Recommended Practice No. SNT-TC-1A, Personnel Qualification and Certification in Nondestructive Testing* (ASNT, 1966).

The first fracture-related provisions for bridges were formalized in 1973 and 1974. Included were material-only changes to the ASTM A709 specification and numerous AASHTO "M" specifications. The use of Charpy V-notch (CVN) testing was introduced as a supplemental requirement. The CVN testing supplemental requirements applied only to base metals, while the treatment of weld metals was ambiguous. During this same time, in 1974, AASHTO introduced the *Standard Specifications for Welding of Structural Steel Highway Bridges* as a supplement to AWS D1.1 (AASHTO, 1974b). This was a precursor to the AASHTO/AWS D1.5 *Bridge Welding Code* published in 1988. This marked the first time a national welding specification for steel bridges was put forth. Some states had developed their own welding specification, but this was the first national specification.

Also in 1974, AASHTO introduced the fatigue design details¹ and categories that are still used for the most part in the current *AASHTO LRFD* specifications. Enhancements for nondestructive testing were added to the *Standard Specifications for Welding of Structural Steel Highway Bridges* in 1975 (AASHTO, 1975).

In 1976, the first CVN requirements were added to the AASHTO design specifications, the *Standard Specifications for Highway Bridges*, with the understanding that they were to relate to design considerations rather than material specifications. The burden was thus placed on the designer to have a role in fracture prevention with the understanding that decreasing the possibility of fatigue crack formation and growth is an effective means to fracture prevention.

With the 1977 interims to the aforementioned design specifications, the first discussion of redundancy was added to the bridge design specifications, and nonredundant members were treated as more conservatively designed than redundant members by imposing a one category shift in the allowable fatigue stresses. The intent again was to discourage the use of fatigue sensitive details on nonredundant members through the lessening of the fatigue resistance. Also in 1977, AASHTO published the first M270 material standard and toughness testing, and minimum standards became a mandatory requirement unless specifically exempted by the owner.

¹ AASHTO first introduced fatigue design provisions in 1965, though as described in Chapter 1, they were fundamentally different than the stress-range concept and detail categories introduced in 1974.

Therefore, as described above, there were incremental advancements in bridge design, material specification, and fabrication requirements throughout much of the 1970's. The culmination of all of this was brought forth in 1978 when AASHTO released the *Guide Specifications for Fracture Critical Non-Redundant Steel Bridge Members* (AASHTO, 1978). This was when the term “fracture critical” first became widely used to describe members whose failure would cause collapse of the bridge, and this was also when more stringent base metal requirements, introduction of weld metal toughness requirements, increased shop inspection requirements, and requirements of inspector certification were added to standard practice. In addition, fracture critical welds were required to be inspected by both ultrasonic testing (UT) and radiographic testing (RT) methods. Those requirements were collectively referred to as the AASHTO Fracture Control Plan (AASHTO FCP).

The collapse of the Mianus River Bridge in 1983 (see Figure 7.1-2) led to changes in the federal bridge inspection standards. This bridge was designed prior to the establishment of the AASHTO FCP, but the collapse did not occur from a brittle fracture that the AASHTO FCP could have prevented. Rather it was the result of a pin-and-hanger failure from a combination of corrosion and fatigue. This accident highlighted the need for more in-depth inspection requirements for Fracture Critical Members (FCM's), and this was the nexus of changes to the NBIS that now require hands-on inspection of FCM's. Therefore, the nation's fracture control approach now includes the AASHTO FCP requirement that had oversight on the design and fabrication of a bridge and a federal oversight component throughout the life of the bridge.



Figure 7.1-2 Collapse of the Mianus River Bridge.

Even with the AASHTO FCP and the creation of a combined AWS D1.1 document for buildings and bridges in 1972, it was identified that bridge welding had more specialized requirements than buildings, and there was a need for a bridge-specific welding code. In 1982, a subcommittee was formed with AASHTO and AWS representatives to begin work on such a document. This resulted in the creation of AASHTO/AWS D1.5 *Bridge Welding Code*, first published in 1988 (AASHTO/AWS, 1988). In 1995, the *Bridge Welding Code* was amended with Clause 12, named the “AASHTO/AWS Fracture Control Plan (FCP) for Nonredundant Members,”

containing the various materials and workmanship provisions from the AASHTO FCP. By this point, other design and material specific requirements from the AASHTO FCP had been integrated into the AASHTO *Standard Specifications for Highway Bridges* and ASTM A709/AASHTO M270, and the *Guide Specifications for Fracture Critical Non-Redundant Steel Bridge Members* were withdrawn in 1989.

Collectively, the enhancement of design and materials specifications, fabrication and shop inspection (AASHTO/AWS FCP), and field inspection requirements (23 CFR 650) form the proverbial “three-legged-stool” that is deemed the Total Fracture Control Plan (TFCP) in this document (see Figure 7.1-3). This chapter describes each leg of the TFCP, presented in sequence of the normal life cycle for a bridge – first material and design, then fabrication and shop inspection, and finally field inspection. It is important to note that with the implementation of the requirements of the TFCP, there have been no noted brittle fractures of “modern” steel bridges (i.e., those designed and fabricated based on the various improvements detailed herein). More importantly, bridge collapse from fracture has not occurred.

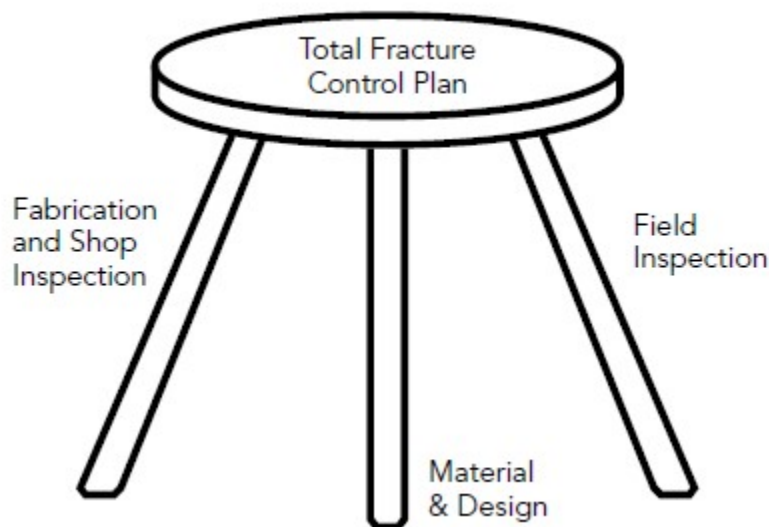


Figure 7.1-3 Three legs of the Total Fracture Control Plan (TFCP).

SECTION 7.2 FRACTURE CONTROL BY DESIGN

The first leg of the “three-legged-stool” Total FCP is the actions taken during the type selection and design of a steel bridge structure. Throughout design development, the engineer must make a series of choices regarding structure type (e.g., girder, truss, arch), member type (e.g., I-beam, box beam, welded, mechanically built-up), material selection (e.g., grade and characteristics of steel), and detailing that have an influence on fracture resistance. Each of these decisions made during the design phase has a subsequent influence on fabrication, inspection, and future maintenance.

AASHTO LRFD Article 1.3.2.3 states that “the fracture limit state shall be taken as a set of material toughness requirements of the AASHTO Materials Specifications.” Although the limit state is narrowly defined as only a series of material requirements, the various choices described above regarding structure type and member type all play a role in determining how fracture control will be addressed during design. Unlike the strength, service, extreme event, and fatigue limit states which require the computation of forces and stresses and a comparison to a resistance value, fracture is unique in that this limit state is generally not addressed via calculations but rather through the use of well-understood materials, by enforcing workmanship requirements, and through the choice of structure and member type. In this chapter, the treatment of fracture as a design consideration will focus on:

- Identifying fracture critical members
- Selecting appropriate materials
- Detailing structures to minimize the possibility of fracture

When fracture is rigorously considered computationally (and it rarely is in the bridge engineering profession), the process is complex. A fracture mechanics approach requires input parameters, such as material properties, anticipated service temperature, loading rate, plate thickness, and crack geometry, in order to compute common crack characterizing parameters (i.e., K or J), which are then compared to the expected fracture toughness to determine the susceptibility of a particular assumed condition. These calculations are difficult to perform accurately in practice because many engineering problems do not fit nicely into cracked section models which presume idealized conditions. Thus the use of fracture mechanics analysis methods is not common, and no such calculations are required of the bridge design engineer when using LRFD. Instead, engineers specify materials with a desired level of toughness and choose details that are known to provide good long-term behavior as a means of fracture prevention for new steel structures. A background on fracture mechanics for bridge design is presented in Chapter 3. Other references that discuss the application of fracture mechanics to bridge design include Barsom and Rolfe (1999), Fisher, Kulak, and Smith (1998), and Keating, Kulicki, Mertz, and Hess (1990).

7.2.1 Charpy V-Notch Requirements for Primary Members

A primary member is defined by AASHTO as “a member designed to carry the loads applied to the structure as determined from an analysis.” AASHTO LRFD Article 6.6.2 states that all primary longitudinal steel members, their connections, and transverse floorbeams shall meet mandatory Charpy V-notch (CVN) requirements when subjected to computed tensile stresses at the Strength I load combination. Elements such as the tension chord of a truss, the tie girder of a tied arch bridge, or flanges and webs of beams in bending are examples of members or components of a member that can experience tension.

In AASHTO LRFD Article 6.7.4.1, diaphragms and cross-frames in curved steel bridges are additionally defined as primary members implying similar CVN requirements as for the main girders. Though these members certainly carry computed dead and live load forces, they are not generally considered as critical as the main girders. A proposal is pending to AASHTO Subcommittee T-14 for 2016 consideration for the primary member designation to be struck from cross-frames and diaphragms so as to exempt them from the CVN test requirements.

However, in all cases it is the responsibility of the engineer to properly identify primary steel members subjected to tensile stress so that the CVN requirements can be applied during their fabrication. These primary member CVN requirements are the first and most basic requirement for fracture control. *AASHTO LRFD* Article 6.6.2 specifically exempts the following bridge items from CVN requirements unless required by the engineer: splice plates and filler plates in bolted splices connected in double shear; intermediate transverse web stiffeners not serving as connection plates; bearings, sole plates, and masonry plates; expansion dams; and drainage material.

An example that demonstrates the application of the AASHTO requirements for CVN designation is provided in Figure 7.2.1-1 and Figure 7.2.1-2.

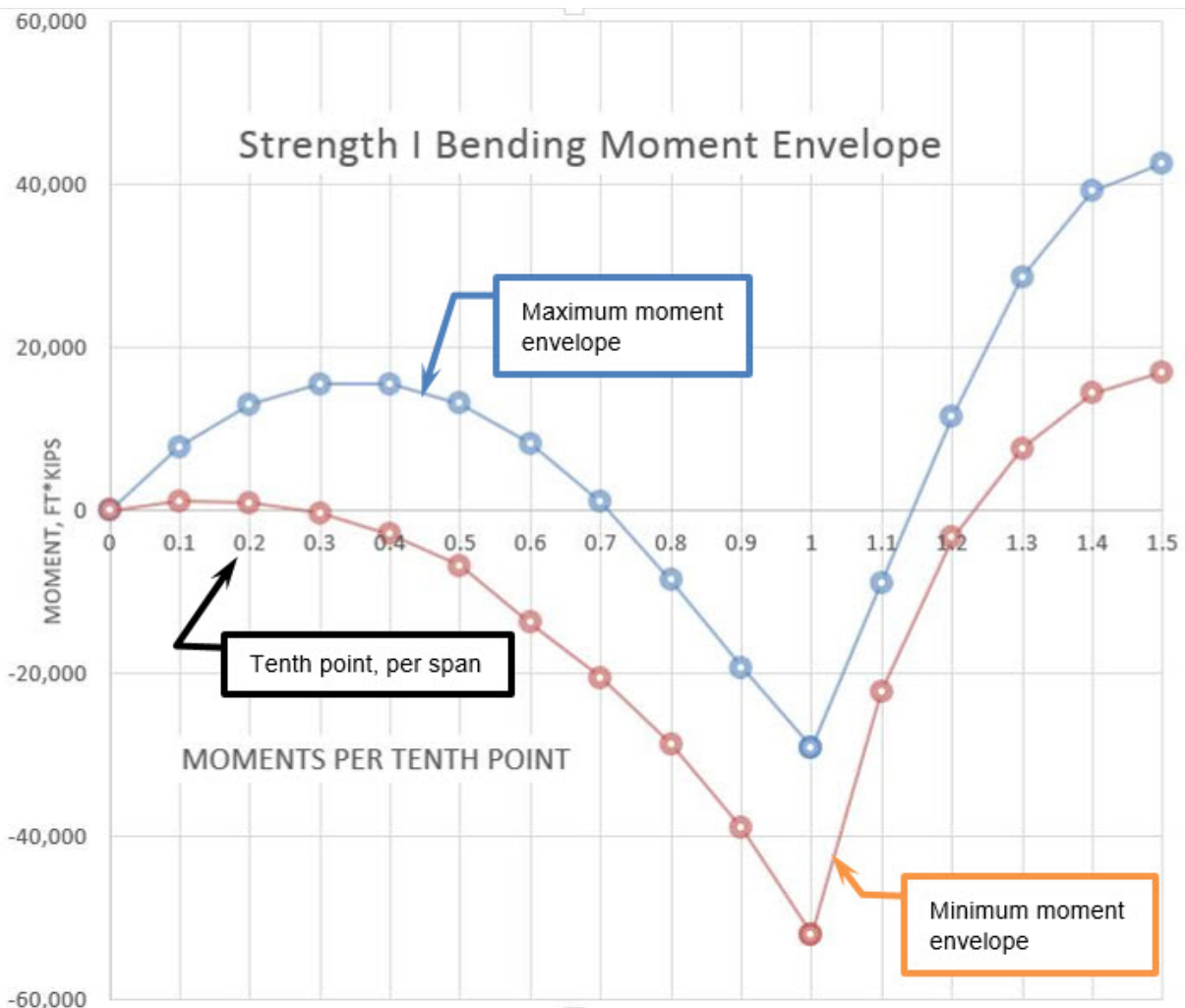


Figure 7.2.1-1 Strength I bending moment envelope for a three-span continuous beam (only half of diagram shown).

As previously described, the Strength I load combination is used to define members or regions of members for which the mandatory CVN requirements apply. The Strength I load combination bending moment envelope (factored dead and live loads are combined) for an example three-

span continuous bridge with spans of 140 ft. – 180 ft. – 140 ft. is provided in Figure 7.2.1-1. The example girder, for which half the total length is shown in Figure 7.2.1-2 owing to symmetry, is made up of various plates whose lengths are shown, connected with full penetration butt splices along with two field splices. In regions where the maximum moment envelope is positive, the bottom flange will experience tension. Similarly in other regions where the minimum moment envelope is negative, the top flange will experience tension. There are significant lengths where each of these conditions is met, meaning either flange could be in tension depending on live load position. It should be clarified that the designation of “tension zones” must be based on stresses. The use of moments in this example will reasonably define the limits of tension for purposes of discussion. However in reality, the ratio of non-composite and composite loads will slightly shift the true tension zones from those extrapolated solely from the use of bending moments.

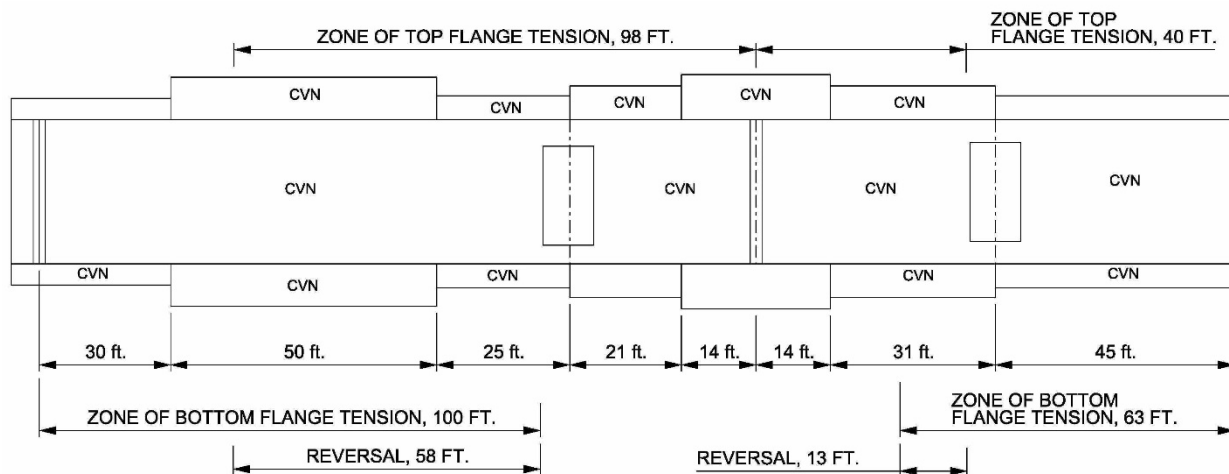


Figure 7.2.1-2 Tension zones and required CVN designation for a three-span continuous beam (only half of girder shown).

Figure 7.2.1-2 presents a common approach for designating the zones of tension on engineering plans. It is common to label, point to, or otherwise denote what elements of the girder are subject to the mandatory CVN requirements due to the presence of tensile stress. The limits of the tension regions correspond to the moment diagram provided in Figure 7.2.1-1. As is commonly the case for continuous beams, the majority of the plates in the example bridge can experience tension at one time or the other. The number of plates that will always be in compression is limited. In many bridges, there may be no plates at all that will be in permanent compression based on the way the engineer chooses to lay out the welded plate transitions and bolted field splice locations. Fabricators may need to, or choose to, introduce welded butt splices into the girder even when the plate size is not changed, perhaps due to plate-length limitations. For these reasons, it is useful to define the zones of tension using a linear dimension as in Figure 7.2.1-2 to explicitly define the regions of possible tension for each flange.

7.2.2 Fracture Critical Members

In addition to the primary member tension requirements, more stringent requirements apply to a special class of members known as Fracture Critical Members (FCM). A FCM is defined by

AASHTO as “a steel primary member or portion thereof subject to tension whose failure would probably cause a portion of or the entire bridge to collapse.” In other words, it is a nonredundant steel member subjected to tension, which will be explained in detail below. These members are subjected to specific and more stringent attention during design, fabrication, and both shop and in-service inspection. One requirement is that they be designed to satisfy the infinite life requirements of the Fatigue I load combination regardless of traffic volume on the bridge. They may also be subjected to an elevated design load if the owner decides to invoke the optional redundancy load modifiers presented in *AASHTO LRFD*, though many owners choose not to do so. The use of the redundancy load modifier, η_R , increases the total factored load by 5 percent to provide an additional margin of safety for nonredundant members. Additional details are provided in *AASHTO LRFD* Article 1.3.4.

The identification of FCMs revolves around three important questions:

1. Is the member made of steel?
2. Does the member ever experience tension?
3. Could the failure of the member cause collapse or loss of function of the bridge (i.e., is it nonredundant)?

If all of these conditions are met, then the member is deemed to be fracture critical. In order to answer these questions, the engineer must be able to identify members that meet the requirements listed above. It should be obvious if a member is made of steel, and somewhat obvious if the member experiences tension under loading, but the question of redundancy is often somewhat more difficult to answer.

7.2.2.1 Redundancy

AASHTO defines redundancy as “the quality of a bridge that enables it to perform its design function in a damaged state.” Redundancy is therefore related to the ability of a bridge to continue to carry dead and live load, without collapse, even in the presence of certain levels of damage.

The design of steel bridges today typically involves redundant structural systems. *AASHTO LRFD* Article 1.3.4 states “Multiple-load-path and continuous structures should be used unless there are compelling reasons not to use them.” A redundant bridge, such as a multi-beam steel bridge, has sufficient transverse and longitudinal load paths to ensure survival even in the unlikely loss of a member component or full member. The presence of multiple, parallel primary members spanning between supports, diaphragms or cross-frames, a concrete deck, and even the barrier rails, all form part of a redundant load path in the unlikely event of the loss of a primary member. In the design of redundant bridges, engineers are not required to quantify through analysis how load would be transferred in the unlikely event of a member loss. It usually amounts to a qualitative assessment of the bridge system based on engineering judgement.

Nonredundant members do not have alternate, secondary load paths to sustain a member loss and remain stable except occasionally only through load paths typically not accounted for in design. For instance, a statically determinate truss (without considering transverse members) has exactly the minimum number of primary members to be considered stable and determinate when

considered in two dimensions. Every primary member is needed to maintain the structure's stability, thus making them all equally critical. A failure of any primary member of a determinate truss leads to an unstable structure (on paper), and thus they all would be considered nonredundant. A certain number of these members are loaded in tension, making them not only nonredundant but fracture critical as well. It is important to be able to distinguish between redundant, nonredundant, and fracture critical primary members in a steel bridge. It is fundamental to understanding their behavior and identifying potential vulnerabilities, and it also impacts fabrication and in-service inspection, as will be discussed later in this chapter.

There are very rare instances in which nonredundant primary members in steel bridges have failed resulting in a collapse. The only known examples in the United States are the Silver Bridge at Point Pleasant, West Virginia (see Figure 7.1-1), the I-95 Bridge over the Mianus River in Connecticut (see Figure 7.1-2), the I-35W Mississippi River Bridge in Minnesota, and the I-5 Skagit River Bridge in Washington. The Silver Bridge was the only case directly caused by a brittle fracture. There are a greater number of cases where a failure of an individual member in an apparently nonredundant bridge has not led to the collapse of the structure. Examples where fracture occurred but did not cause collapse include the following:

- The 1976 full-depth fracture of the two-girder US-52 Lafayette Street Bridge over the Mississippi River in St. Paul, Minnesota (Fisher, 1984)
- The 1977 full-depth fracture of the two-girder I-79 bridge at Neville Island in Pittsburgh, Pennsylvania (Fisher et al., 1980a)
- The 2003 fracture of the two-girder US-422 Bridge near Pottstown, Pennsylvania (Kaufmann, Connor, and Fisher, 2004)
- The 2012 simulation of a lower chord fracture of the US-421 truss bridge over the Ohio River between Madison, Indiana and Milton, Kentucky (Connor, Digglemann, and Sherman, 2013)

These bridges did not collapse due to their ability to redistribute load in ways that are generally not captured by simple analyses. A conventional analysis, such as the planar analysis of a simply supported truss, does not capture the load redistribution benefits of elements such as lateral bracing systems, floor systems, decks, and barriers that can provide alternate load paths for certain primary members. The degree of redundancy of a particular structure is not always evident, and a detailed analysis of the load path and structural configuration is required to understand the load redistribution characteristics of the structure. However there are no standard rules and little guidance for this redundancy analysis. *AASHTO LRFD* discusses this in Article C6.6.2 where it indicates that a standard procedure for using analysis to determine what members are fracture critical (i.e., a redundancy analysis) is not yet available. This is due to a lack of consensus as to what load cases should be studied, what members should be considered failed, how to capture the dynamic effects of fracture, as well as many other issues such as how to account for the participation of bracing members and transverse members. The use of refined analysis to assess bridges is thus left by AASHTO to the discretion of an engineer and an owner to agree upon. This leaves a certain amount of ambiguity when engineers are designing or analyzing bridges with fracture critical members. Because of this ambiguity, FHWA instituted a policy addressing the design of FCM's. This policy is described in the following section.

7.2.2.2 FHWA Policy on Fracture Critical Members

In order to alleviate some of this ambiguity on how FCM's are to be identified and treated, FHWA issued its "Clarification of Requirements for Fracture Critical Members" in 2012 (FHWA, 2012b). The memo addresses the FHWA policy for classification of steel bridge members for design, fabrication, and inspection. It provides clarification on how various types of redundancy may be used during design, evaluation, and inspection. The following are definitions of the various types of redundancy discussed in the FHWA memo:

- Load Path Redundancy is the redundancy inherent to a system because of multiple longitudinal load paths between points of permanent support. An example of a bridge containing load path redundancy is a common multi-girder steel bridge. The FHWA memo does not prescribe the minimum number of required parallel girders such that sufficient load path redundancy is provided. There is no consensus among state agencies on this matter, with some accepting a three-girder bridge as redundant and others requiring four or more beam lines. In the case of the Hoan Bridge, two of the three main girders completely fractured, the third was cracked as well, yet the bridge did not collapse and carried some live load before the fracture was discovered. Load path redundancy is typically determined through qualitative assessment by engineering judgement and not calculations.
- Structural Redundancy is the redundancy in a system provided by structural continuity. In a hypothetical multi-span continuous beam or system, the fracture of a member within a span may not necessarily cause collapse if the damaged system has alternate load paths to carry load back to supports via longitudinal or transverse load redistribution. The sufficiency of this alternate load path however requires that the system be analyzed for potential failure scenarios to establish the demands on these backup load paths. Assessment of structural redundancy will typically require the use of a three-dimensional model of the bridge. In the design of a new bridge, structural redundancy may be leveraged for exemption from in-service fracture critical inspection requirements, but FHWA does not allow engineers to consider this to exempt the member from fracture critical fabrication requirements. This is discussed further as part of a new definition called a System Redundant Member, defined later in this section.
- Internal Redundancy is a design approach based on the requirement that the fracture of an individual component within a built-up member will not result in complete failure of the member. For instance, a member may consist of a section of many elements that are bolted or riveted together (e.g., plates and angles connected together to form a box for a tension tie or truss, or a built-up plate girder). The analysis typically involves a sectional stress check with one plate element removed. The premise of internal redundancy is that individual elements are not welded together. There is no continuous path that allows a crack in one element to propagate into an adjoining element. Because of questions surrounding issues such as energy dissipation during fracture, what constitutes effective isolation, how to ensure the capacity of the remaining member, and what load combinations should be evaluated for this extreme event scenario, the use of internal

redundancy as the only means to achieve redundancy for new bridge design is not allowed by FHWA.

Regarding the designation of FCM's, AASHTO states "*The Engineer shall have the responsibility for determining which, if any, component is a fracture-critical member (FCM). Unless a rigorous analysis with assumed hypothetical cracked components confirms the strength and stability of the hypothetically damaged structure, the location of all FCMs shall be clearly delineated on the contract plans.*" FHWA takes a similar position, but currently limits the analysis-based exemption to in-service inspection requirements, and not to fabrication requirements.

If a non-load path redundant member is fabricated to FCM standards and could be shown by some analysis to exhibit structural redundancy, the FHWA memo classifies this as a System Redundant Member (SRM). A SRM is a member that has been fabricated according to the AASHTO/AWS FCP, as one without load path redundancy, but does not need to be considered an FCM for purposes of in-service inspection. This is consistent with the aforementioned FHWA statement that analysis alone cannot exempt a member from FCM fabrication requirements. However, analysis can be used to eliminate certain members from FCM in-service inspection requirements. That is the crux of the SRM designation. Internal redundancy, though beneficial, is not deemed sufficient to eliminate a member's fracture critical designation for in-service inspection since a fracture could exist for some time undetected, and knowingly operating a bridge in this compromised condition is not acceptable to FHWA.

In summary, the key points of the FHWA policy clarification are as follows:

- A member is not fracture critical if either load path redundancy or structural redundancy is provided.
- In-service bridges built according to the FCP (post-1978) and new bridges can be evaluated using refined analysis to determine their sufficiency of structural redundancy.
- The FHWA memo introduced the new member classification, a System Redundant Member (SRM), which is a non-load path redundant member that gains its redundancy by system behavior.
- SRM's must still be fabricated according to the AASHTO/AWS FCP, but may be relieved from fracture critical in-service inspection requirements.
- Internal redundancy is not recognized to exempt the member from fracture critical classification. This may change as new research becomes available.

7.2.3 Selection of Materials

When selecting the specific materials for a bridge design, several factors are considered, including strength, toughness, weldability, corrosion protection, availability, and cost.

AASHTO LRFD Article 6.4 provides basic material requirements for steels that are recognized by the specifications. Included are various provisions for structural steels used in plates and shapes as well as other materials such as: pins and rollers; bolts, nuts, and washers; shear studs; weld metal; castings; and cables and strands.

The material properties for bridge steel are well defined for new structures. Historically many different types of steels, with widely varying chemistries and mechanical properties, have been used. These material properties influence the inherent tolerance of steels to fracture. *AASHTO LRFD* provides a table of minimum properties for steels commonly used for new bridge construction. This table is reproduced herein as Table 7.2.3-1.

Table 7.2.3-1 Minimum mechanical properties of structural steel by shape, strength, and thickness.

AASHTO Designation	M 270M/ M 270 Grade 36	M 270M/ M 270 Grade 50	M 270M/ M 270 Grade 50S	M 270M/ M 270 Grade 50W	M 270M/ M 270 Grade HPS 50W	M 270M/ M 270 Grade HPS 70W	M 270M/ M 270 Grade HPS 100W	
Equivalent ASTM Designation	A709/ A709M Grade 36	A709/ A709M Grade 50	A709/ A709M Grade 50S	A709/ A709M Grade 50W	A709/ A709M Grade HPS 50W	A709/ A709M Grade HPS 70W	A709/ A709M Grade HPS 100W	
Thickness of Plates (in.)	Up to 4.0 incl.	Up to 4.0 incl.	Not applicable	Up to 4.0 incl.	Up to 4.0 incl.	Up to 4.0 incl.	Up to 2.5 incl.	Over 2.5 to 4.0 incl.
Shapes	All groups	All groups	All groups	All groups	Not applicable	Not applicable	Not applicable	Not applicable
Minimum Tensile Strength, F_u (ksi)	58	65	65	70	70	85	110	100
Specified Minimum Yield Point or Specified Minimum Yield Strength, F_y (ksi)	36	50	50	50	50	70	100	90

By using materials from the AASHTO table of approved steels and the common requirements present in state construction specifications, there are multiple levels of control of basic material properties.

The plans and specifications must clearly indicate the grade of steel to be used and the temperature zone in which the bridge is to be constructed. The selection of steel for a particular application is left to the discretion of the designer and owner. Steels are generally selected for design considering the yield strength as the primary factor. Steels with yield points of 36, 50, and 70 ksi are the most common, and these values have been in use for many decades. Less common, though specified for some high demand applications, are steels with a 100 ksi yield strength. In Section 4.2.2, the yield strength of the steel was shown to not be a factor in fatigue life, and there are no advantages to using higher strength steels to control fatigue or fracture potential.

In order to provide materials with enhanced toughness, weldability, and enhanced atmospheric corrosion properties, high-performance steels (HPS) were introduced in the late 1990's. These plate steels are manufactured as either quenched and tempered (Q&T) or treated by thermomechanically controlled processing (TMCP) in order to achieve the higher toughness values. Thicker plates, those in the 1.5 inches to 2 inches range and up to a maximum of 4

inches, are required to be quenched and tempered in order to achieve the required mechanical properties. This Q&T operation effectively limits the plate lengths to 50 feet or less, thus increasing the costs of members fabricated with these plate length limits. For plates less than 1.5 inches to 2 inches thick, and this again depends on the mill, a TMCP plate is available that enables the mill to manufacture the plates “in-line” without additional treatment and provide the desired mechanical properties. The use of TMCP plates greatly expands the plate length limits and also includes wider slabs as well. As these rolling practices have evolved over time and as additional mills develop HPS rolling capabilities, no firm value is suggested as to what plates are available in HPS 50W, HPS 70W, and HPS 100W grades, and in specific lengths and widths. The engineer should check with fabricators at the time of design to determine what materials are available, as this might alter certain design decisions as to how long to make field sections and which size plates should be used.

Toughness requirements are achieved through CVN testing of base material as it comes from the production mill. The AASHTO requirements vary for fracture critical and non-fracture critical members as well as for grade of steel and plate thickness. The temperature zone for a specific bridge relates to the minimum service temperature and is usually specified by the owner. The CVN requirements from the AASHTO specifications are provided in Table 7.2.3-2.

Table 7.2.3-2 CVN impact energy requirements.

Grade (Y.P./Y.S.)	Thickness (in.)	Fracture Critical				Non-fracture Critical		
		Min. Test Value Energy (ft·lbs.)	Zone 1 (ft·lbs. @ °F)	Zone 2 (ft·lbs. @ °F)	Zone 3 (ft·lbs. @ °F)	Zone 1 (ft·lbs. @ °F)	Zone 2 (ft·lbs. @ °F)	Zone 3 (ft·lbs. @ °F)
36	$t \leq 4$	20	25 @ 70	25 @ 40	25 @ 10	15 @ 70	15 @ 40	15 @ 10
50/50S/50W	$t \leq 2$	20	25 @ 70	25 @ 40	25 @ 10	15 @ 70	15 @ 40	15 @ 10
	$2 < t \leq 4$	24	30 @ 70	30 @ 40	30 @ 10	20 @ 70	20 @ 40	20 @ 10
HPS 50W	$t \leq 4$	24	30 @ 10	30 @ 10	30 @ 10	20 @ 10	20 @ 10	20 @ 10
HPS 70W	$t \leq 4$	28	35 @ -10	35 @ -10	35 @ -10	25 @ -10	25 @ -10	25 @ -10
HPS 100W	$t \leq 2\frac{1}{2}$	28	35 @ -30	35 @ -30	35 @ -30	25 @ -30	25 @ -30	25 @ -30
	$2\frac{1}{2} < t \leq 4$	36	not permitted	not permitted	not permitted	35 @ -30	35 @ -30	35 @ -30

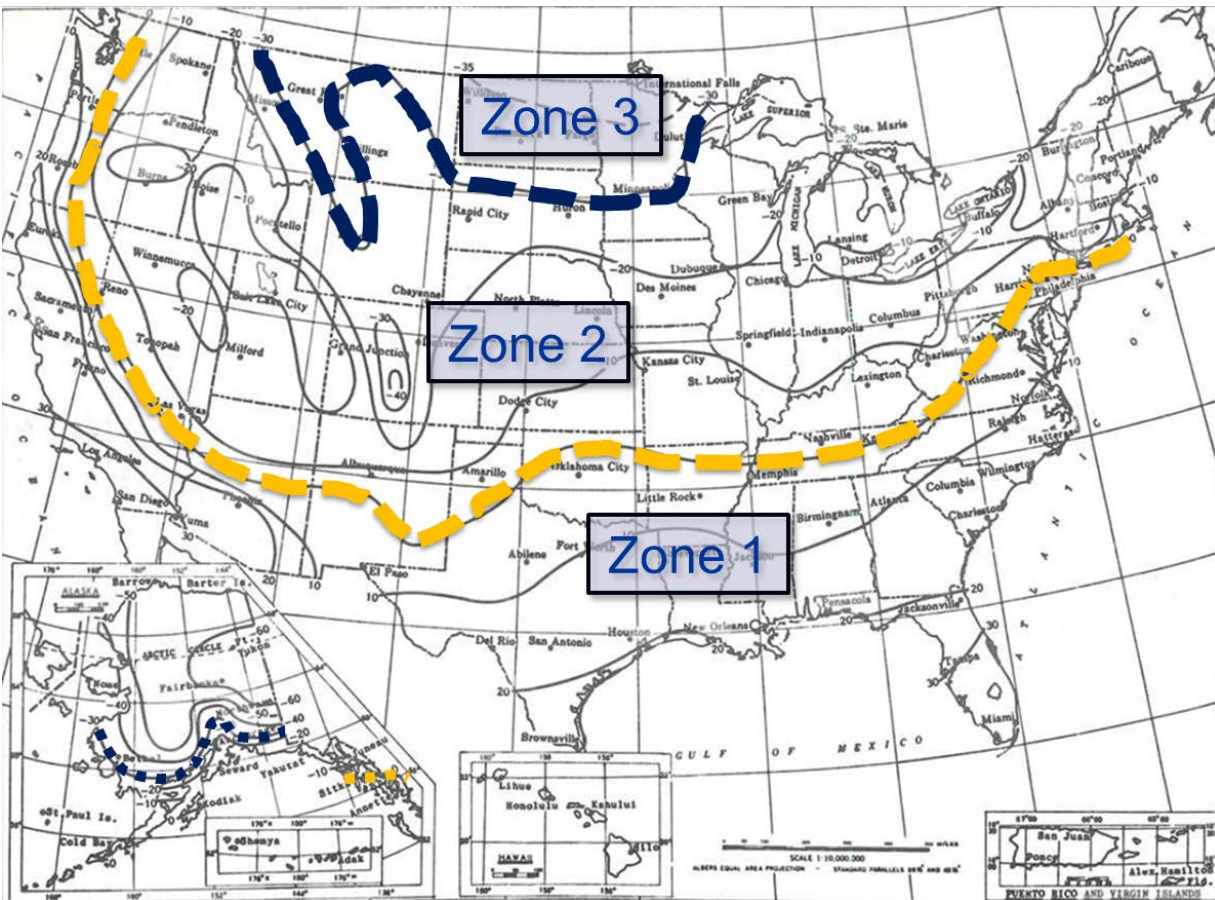
The aforementioned table distinguishes between fracture critical and non-fracture critical material requirements. AASHTO places the responsibility for determining whether members are fracture critical on the design engineer. Fracture critical members are subjected to more stringent CVN requirements, a key aspect in designing to prevent fracture in steel bridge members.

Depending on the minimum service temperature, the corresponding material performance requirements vary. AASHTO divides bridges into three zones depending on the minimum service temperature. The zones are described in Table 7.2.3-3. The importance of the temperature zone is that it defines the CVN requirements for particular grades of steel used in different temperature conditions.

Table 7.2.3-3 Temperature zone designations for Charpy V-notch requirements.

Minimum Service Temperature	Temperature Zone
0°F and above	1
-1°F to -30°F	2
-31°F to -60°F	3

There is often confusion about the “minimum service temperature” as required to implement the requirements of Table 7.2.3-3. AASHTO has no definition, yet a designation of one is needed for the specification of materials. In 1978, Hartbower proposed a temperature map for FCM’s that defined the lowest anticipated service temperature (LAST) based on an analysis of weather data from the period of 1950 through 1970 (see Figure 7.2.3-1). In the footnote to the temperature map in the source document is a note indicating that the contours are based on hourly readings with a 99 percent chance that the plotted values will not be exceeded (Hartbower, 1978). Though not adopted in specification form, this map is useful for engineers trying to understand the temperature zone designation and corresponding CVN requirements.

**Figure 7.2.3-1 Lowest anticipated service temperature (LAST).**

7.2.4 Detailing to Avoid Constraint

Fractures in steel girders have resulted from either the propagation of fatigue cracks to the point of fracture or as the result of large fabrication defects somehow undetected. When fracture following fatigue growth occurs, cracks are able to lengthen over time until such point that a component or an entire member is lost due to fracture of the remaining section. As mentioned in Chapter 4, however, visible cracking occurs very late in the life of a crack and indicates that most of the useful life of the detail has been exhausted. Fracture due to unstable crack propagation could occur soon after a crack is discovered. There are other instances, however, where the crack growth stage is not evident and fracture occurs under routine service conditions.

It is the responsibility of the design engineer is to choose details that are not susceptible to fracture due to excessive constraint. Two sources of constraint in welded steel structures will be described herein: that associated with elements joined with intersecting welds, and the constraint from thick plates and highly constrained joints.

7.2.4.1 *Constraint-Induced Fracture*

Constraint-induced fracture (CIF) is a type of fracture attributed to local constraint conditions in steel under tension, which may occur at details of certain geometries. It occurs due to the inability of steel to locally yield under a combined state of stress. One undesirable practice that is conducive to CIF occurrence is the intersection of multiple welds at a common location, as shown in Figure 7.2.4.1-1. Although the figure shows a longitudinal stiffener as the attachment, CIF is also possible with other types of attachments (e.g., a lateral bracing gusset plate) and has also been noted at bearing stiffener to flange connections as well.

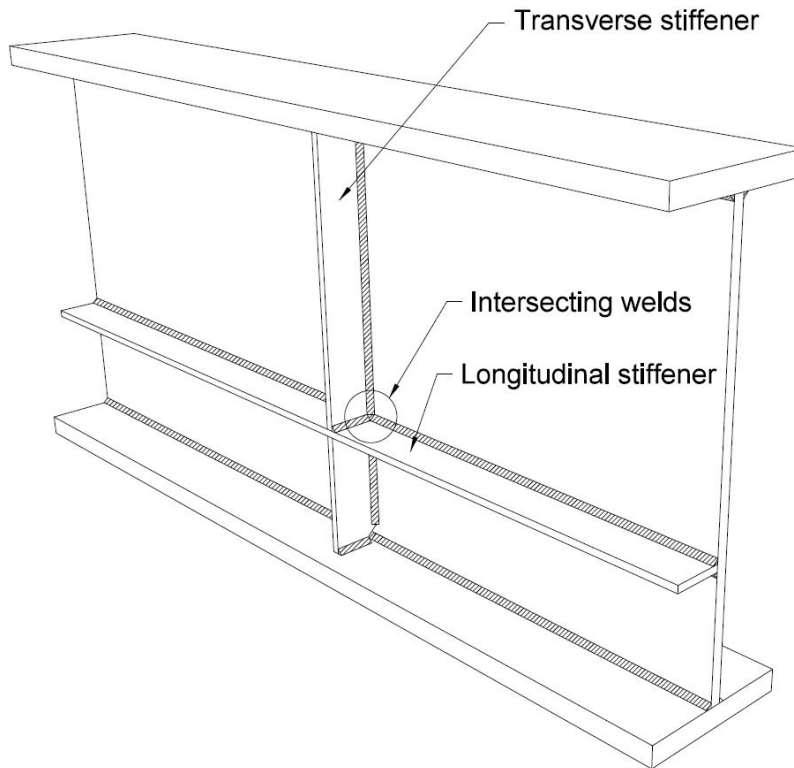


Figure 7.2.4.1-1 Example of improper stiffener detail with intersecting welds susceptible to CIF.

To understand the phenomenon of CIF in steel structures, an understanding of the behavior of steel in tension is important. Under tension, lateral contraction occurs due to Poisson's effect. For instance, in a steel tension test, elongation of the specimen occurs along with contraction in the lateral direction. In a steel I-beam, flexure of the section results in longitudinal tensile stresses developing in the web as well as in attachments parallel to the direction of loading. As the web and attachments elongate, the web contracts in the through thickness direction. This is illustrated in Figure 7.2.4.1-2 (Connor et al., 2007). Note that at the end of the longitudinal attachment, the web plate is in a state of plane stress and the out-of-plane stresses are zero.

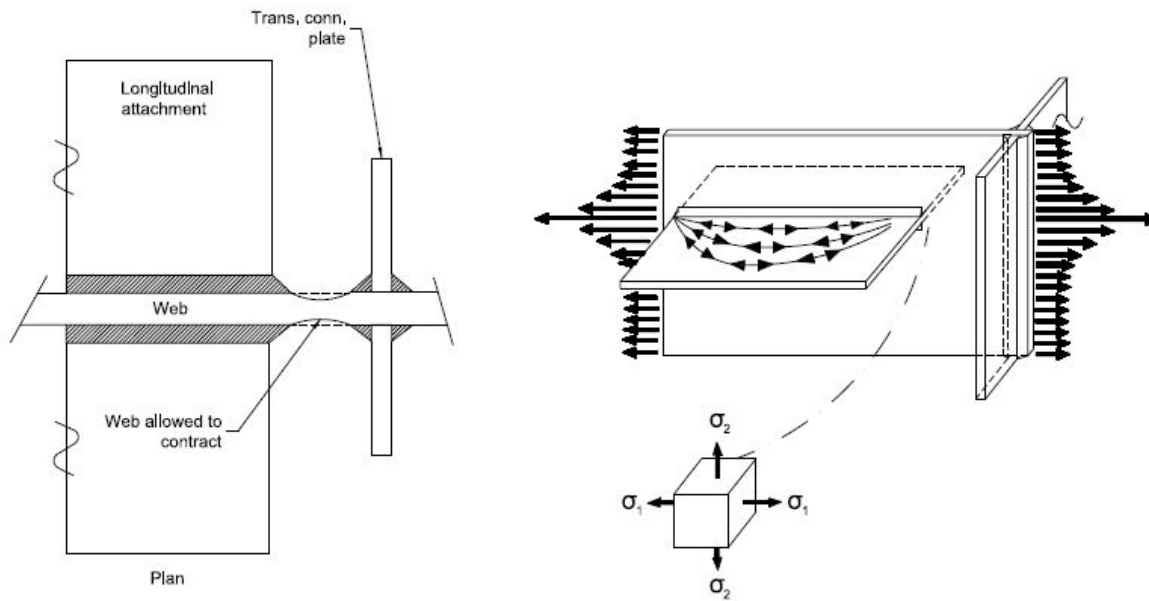


Figure 7.2.4.1-2 Illustration of local stress condition and natural deformations of girder web at stiffener termination when detailed correctly.

CIF can occur when the web gap area is not allowed to contract due to the proximity of the longitudinal and vertical stiffeners and their attaching welds. As flexural tension is applied to the girder web, its tendency to contract in the through thickness direction is highly restrained by the intersection of the longitudinal attachment, the transverse stiffener, and the multiple intersecting welds that all join at a common location. Under the actions of applied stress in the primary direction and the resulting restraint stresses in the through thickness direction, a more complex triaxial state of stress develops. Considering von Mises' yield criterion, this results in a combined state of stress that exceeds the uniaxial yield stress and greatly reduces the ductility of the material under the triaxial stress. The reduction in ductility can make the material behave in a brittle fashion.

An example of the local state of stresses in a highly constrained condition is shown in Figure 7.2.4.1-3 (Connor et al., 2007). Of note in this figure is how it differs from Figure 7.2.4.1-2. The longitudinal attachment, instead of stopping some distance away from the transverse connection plate, is now in contact with it, sometimes welded to it, and the longitudinal and vertical welds intersect. As a result, instead of the free lateral contraction of the web depicted in Figure 7.2.4.1-2, the web is now restrained in the through thickness direction and a stress, σ_3 , develops as a result. Due to the presence of the restraining stresses in the secondary direction, the material's ability to resist primary stress in the computed direction is diminished. When the degree of restraint is significant enough, constraint-induced fracture is possible.

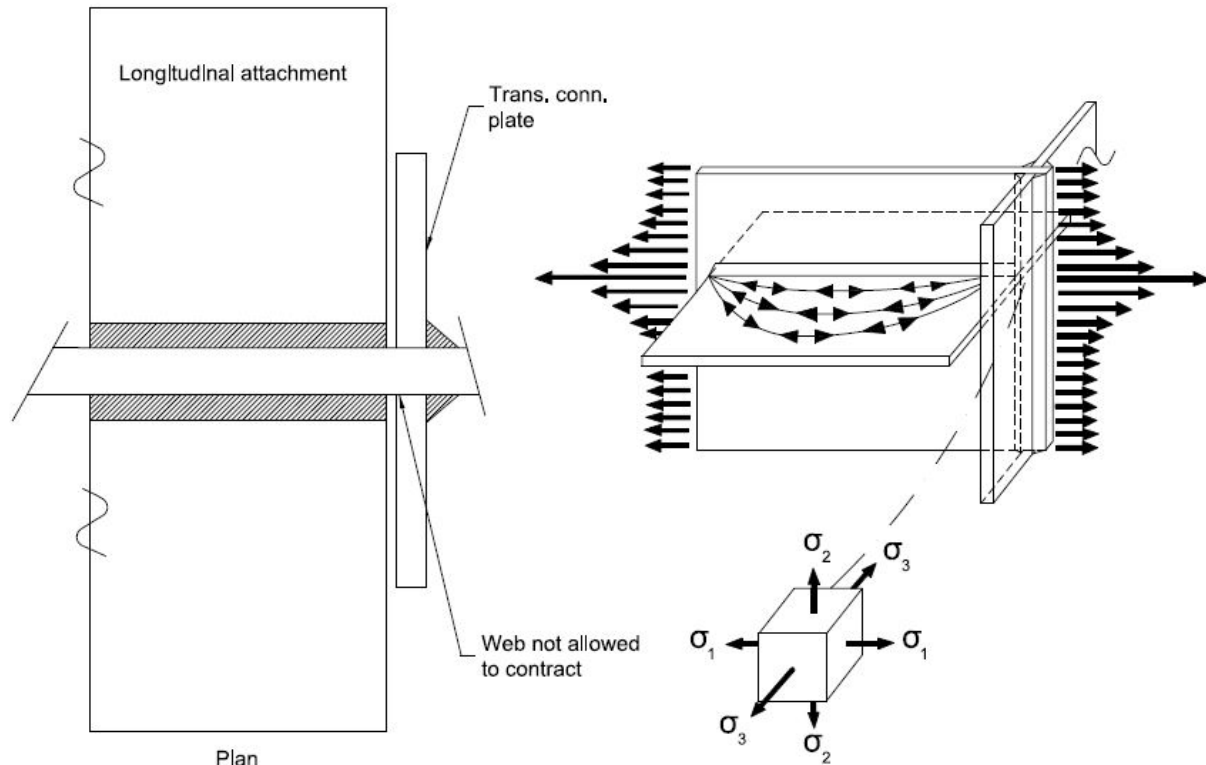


Figure 7.2.4.1-3 Illustration of triaxial stress state created in a highly constrained condition with insufficient gap.

Constraint-induced fractures have occurred on the I-794 Hoan Bridge in Milwaukee, Wisconsin (Fisher et al., 2001), the US 422 bridge in Pottstown, Pennsylvania (Kaufmann et al., 2004), the Diefenbaker Bridge in Saskatchewan (Ellis et al., 2013), and possibly other cases not identified as such at the time. In each of those bridges, premature fracture at a lateral gusset plate connection to a steel girder web occurred and is attributed to CIF. The welded details in which these fractures occurred are common and exist in many steel structures throughout the nation. In no case did the bridge collapse following the fractures, though each required closure for repair.

In the case of the December 2000 fracture of the I-794 Hoan Bridge, the failure was dramatic. The span in which fracture occurred was composed of three main girders with a floorbeam and stringer system supporting the deck. Gusset plates connecting the bottom lateral bracing system were fabricated with a slot to fit around and center on the transverse stiffener. When the girders were fabricated, the slot in the gusset plate was pushed tight against the transverse stiffener, and created a triaxial constraint condition that led to the fracture of two of the three main girders (Connor et al., 2007). Figure 7.2.4.1-4 depicts the condition of the bridge following the fracture along with a close-up of a similar lateral bracing gusset plate detail. There were several important findings and outcomes from the Hoan Bridge investigation, including the following (FHWA, 2001):

- The failure was confirmed through laboratory investigation as brittle fracture.
- There was no evidence of fatigue cracking prior to fracture initiation.

- The narrow gap between the gusset plate and transverse stiffener increased the local stiffness and prevented yielding and stress redistribution in the constrained area.
- Prior similar cracks were found several years earlier and were at the time assumed to be fatigue cracks. These prior cracks did not result in the chain reaction fracture of multiple elements of the bridge.
- The States were advised through a series of technical advisories and memos from the FHWA to identify bridges that might have similar details, conduct inspections, and implement selected retrofits as necessary.

In the case of the US 422 bridge, fracture occurred in the web at the intersection of welds connecting a lateral bracing gusset plate and a transverse connection plate, with the longitudinal and vertical welds intersecting at a common location several inches above the bottom flange. The fracture initiated in the web and propagated vertically until it was arrested by an internal discontinuity, and propagated downward resulting in fracture of the bottom flange. Figure 7.2.4.1-5 provides photographs of the bridge and fracture location. This fracture occurred in warm weather and was discovered only during a routine inspection in May 2003. There was no noticeable deformation of the bridge otherwise.

CIF cracks found in the Diefenbaker Bridge are also shown in Figure 7.2.4.1-6 to show the similar nature and extent of cracking in each of the three bridges.

In both the Hoan and the US 422 bridges, CIF fractures occurred in materials that otherwise met current material property requirements. In the case of the US 422 bridge, the tensile and CVN properties of the plate were obtained and compared to modern requirements. The yield and tensile strength of the web plate exceeded the requirements for ASTM A36. Although mandatory CVN testing was not required at the time this bridge was fabricated, the test results proved that the flange material met AASHTO Zone 2 fracture critical toughness requirements. The web and gusset plate had CVN results marginally less than that of the flange, but all were in general conformance with the AASHTO requirements. For the I-794 Hoan Bridge, material tests were conducted after the demolition of the approach spans. The complete toughness versus temperature transition curve was developed, and these results demonstrated that the fractured web plates satisfied the AASHTO Zone 2 requirements for fracture critical materials for the minimum service temperatures. For the Diefenbaker Bridge, the steel (ASTM A373-56T) was tested and it was determined that the yield, tensile, and CVN values were consistent with steels of the bridge's vintage but that the CVN results did not meet the requirement of ASTM A709. However, the below-standard CVN values were found not to be a contributing factor, nor was temperature as the fracture occurred in the summer.

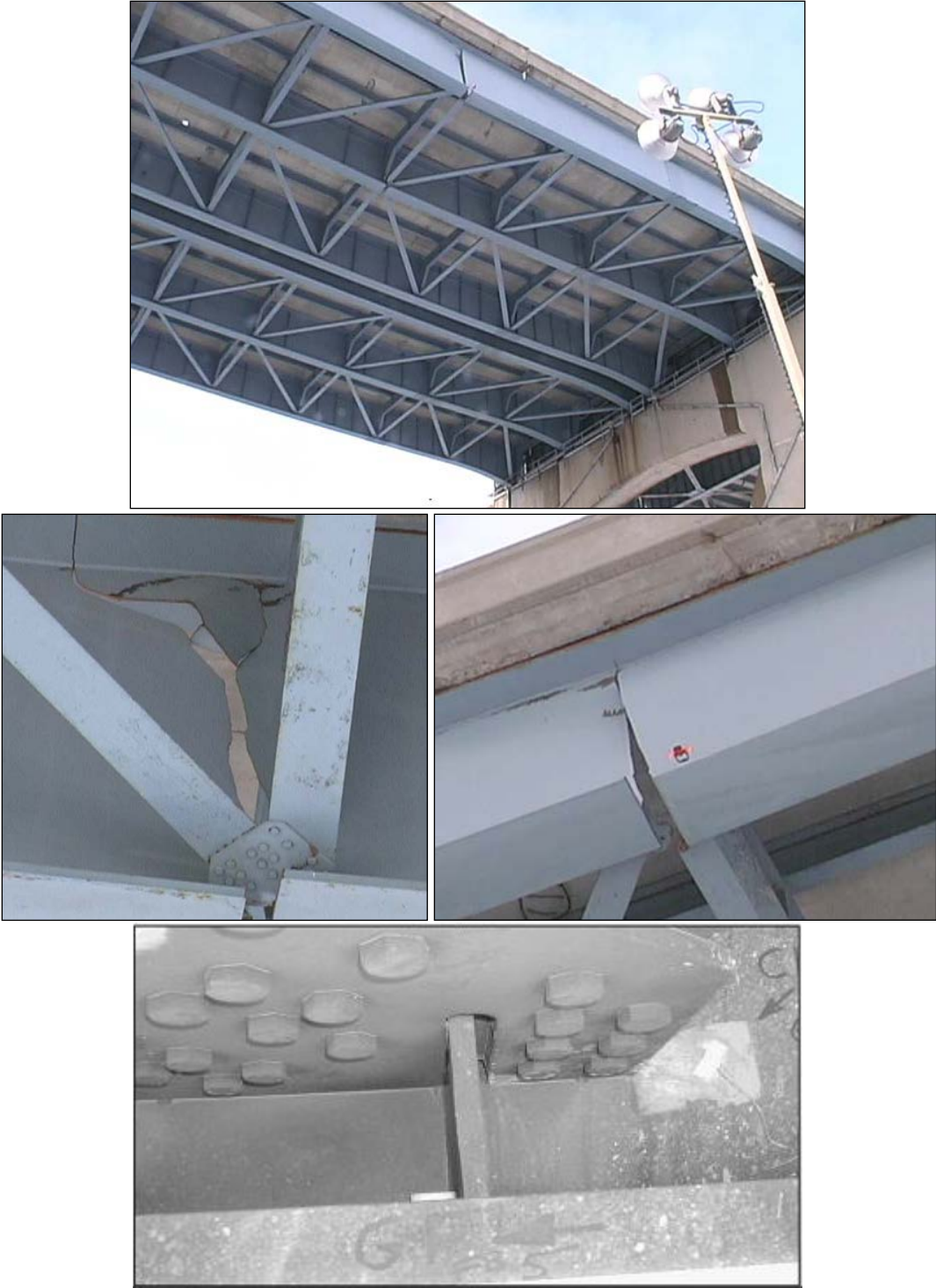


Figure 7.2.4.1-4 Hoan Bridge post-fracture photos and gusset plate detail.

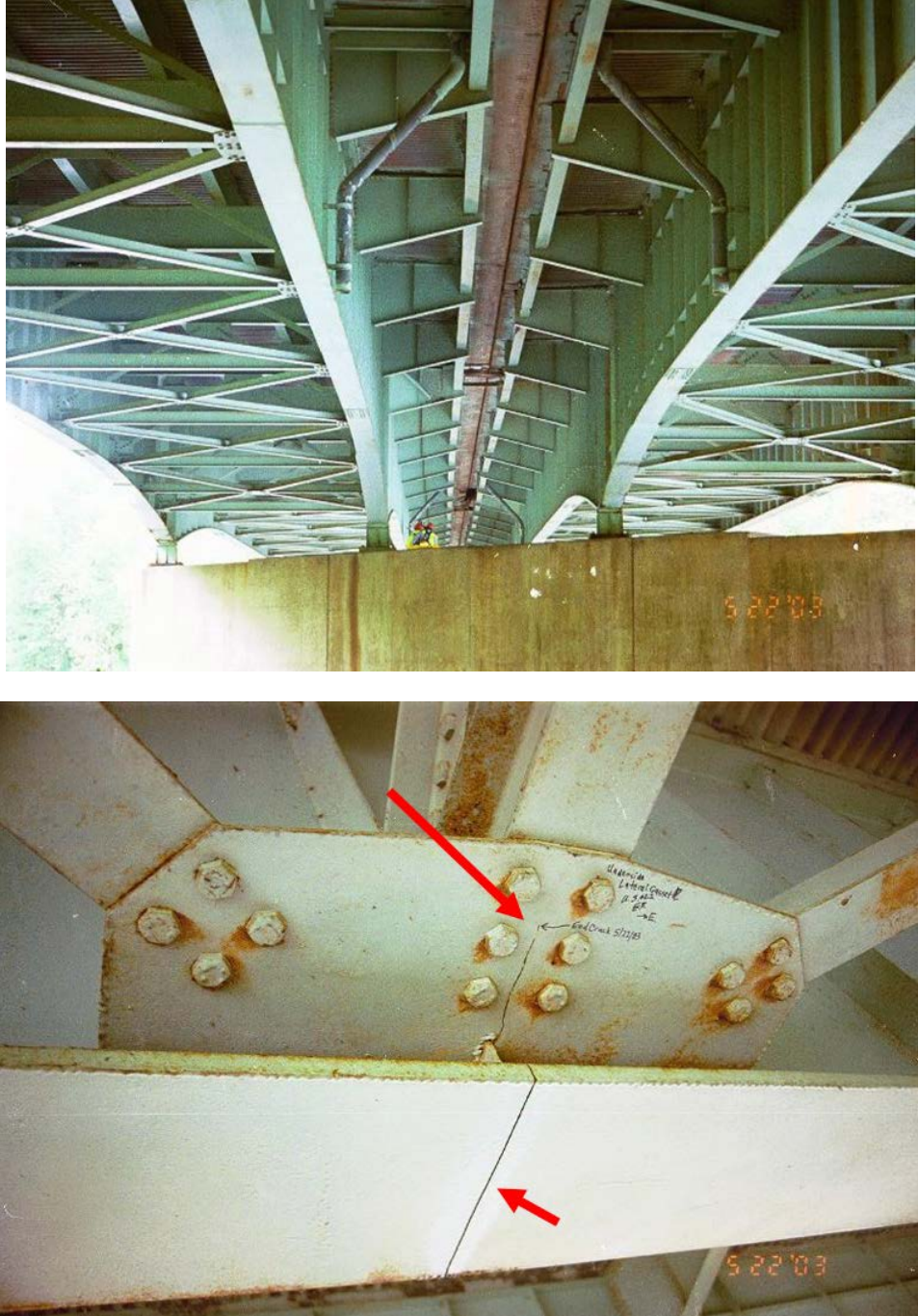


Figure 7.2.4.1-5 Fracture of the US 422 Bridge; lateral bracing configuration (top) and bottom view of fractured flange and gusset plate (bottom).



Figure 7.2.4.1-6 CIF cracks in the Diefenbaker Bridge.

To guard against CIF, AASHTO provides an approach for engineers to use in the design of new steel structures. They state:

“To the extent practical, welded structures shall be detailed to avoid conditions that create highly constrained joints and crack-like geometric discontinuities that are susceptible to constraint-induced fracture. Welds that are parallel to the primary stress but interrupted by intersecting members shall be detailed to allow a minimum gap of 1 inch between weld toes.”

This requirement focuses on the need to maintain a 1-inch separation between weld toes as the key practice to minimize the potential for CIF. This separation is depicted in Figure 7.2.4.1-7. The figure also depicts the preferred practice when longitudinal and transverse elements intersect. Depending on the specific location and detail, the preference is generally for the longitudinal attachment to be continuous while breaking the transverse stiffener. This provides the best flow of stress into and out of the longitudinal attachment.

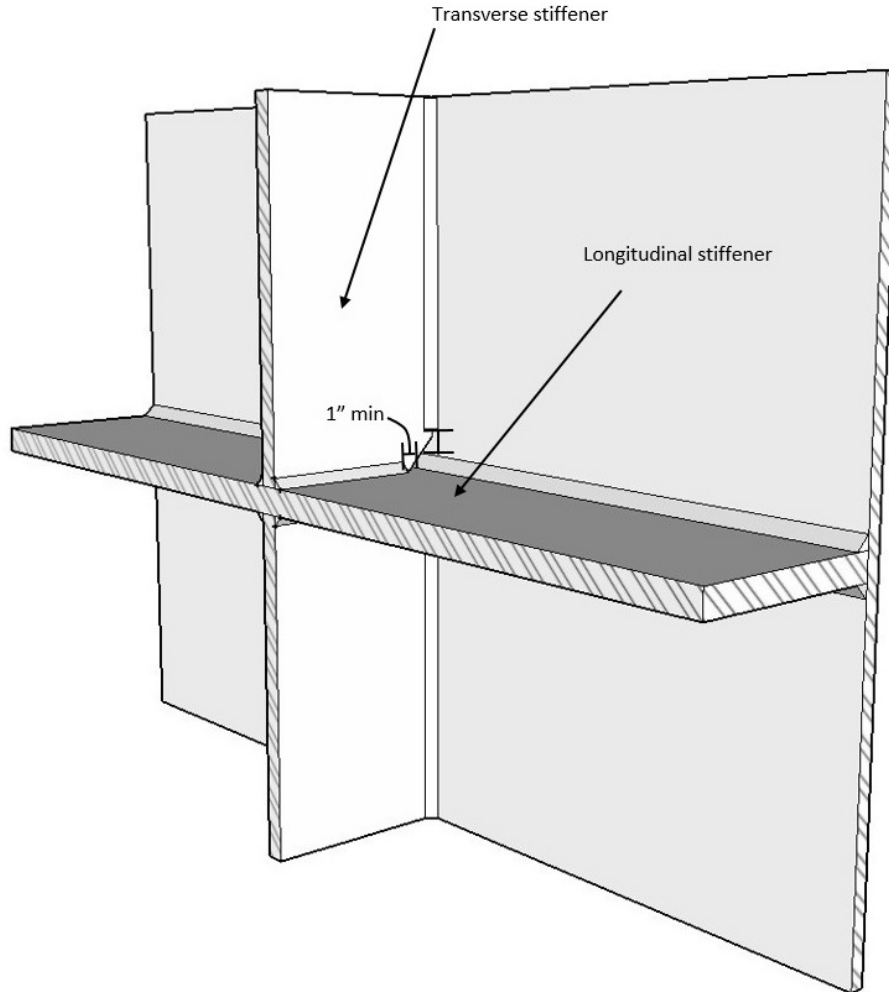


Figure 7.2.4.1-7 Weld detail where the longitudinal stiffener is continuous.

There are other details where CIF is possible. The following six figures (Figure 7.2.4.1-8 through Figure 7.2.4.1-13) provide illustrations which are followed by commentary on practices that are encouraged and discouraged with respect to CIF. These six figures and their accompanying commentary relate to Details A through F. In these six figures, arrows on both ends refers to stress reversal, whereas arrows on only one end refers to one-directional stress.

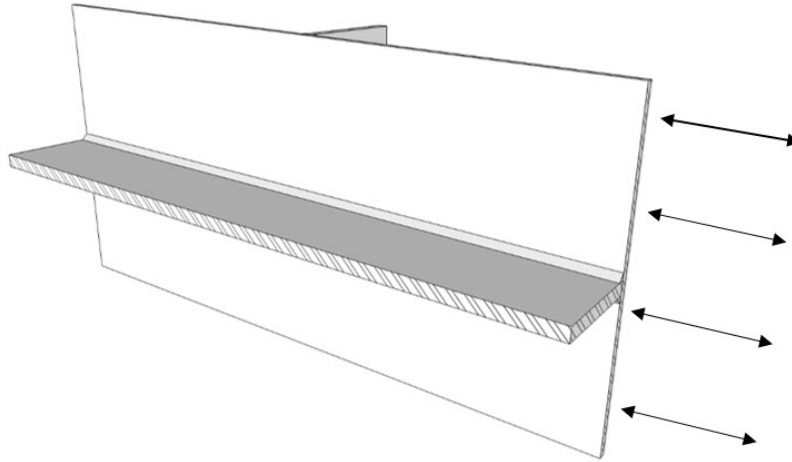


Figure 7.2.4.1-8 Detail A.

DETAIL A – When vertical and longitudinal stiffeners are required, it is preferred to have them on opposite sides of the web to preclude intersecting details. This detail is acceptable for webs in tension, compression, or reversal. However, frequently the length of the attachment is such that an interference is inevitable. See Detail B in Figure 7.2.4.1-9.

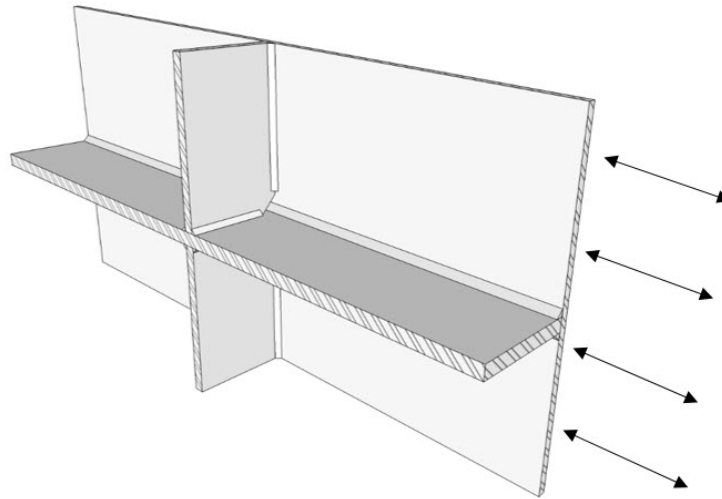


Figure 7.2.4.1-9 Detail B.

DETAIL B – When vertical and longitudinal stiffeners will intersect, make the longitudinal stiffener continuous and break the transverse stiffener, welding it to the top and bottom of the longitudinal stiffener with fillet welds. This detail is acceptable for webs in tension, compression, or reversal. Provide a 1-inch gap minimum between all weld toes.

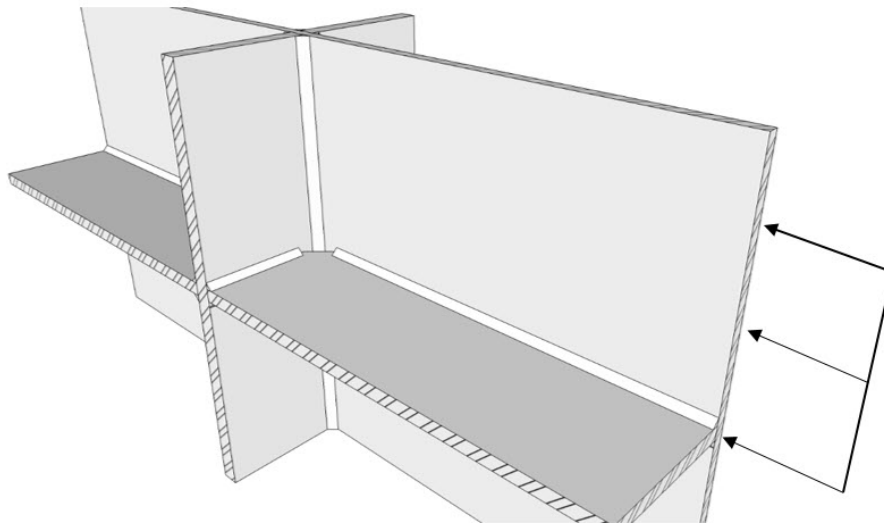


Figure 7.2.4.1-10 Detail C.

DETAIL C – When a longitudinal stiffener will intersect a bearing stiffener, provide full height bearing stiffeners and weld the longitudinal stiffener to the bearing stiffener with fillet welds. This detail is acceptable for webs in compression, which is where a longitudinal stiffener and bearing stiffener would generally intersect (e.g., a zone of flexural compression at the bottom of a web over a pier). Provide a 1-inch minimum gap between all weld toes.

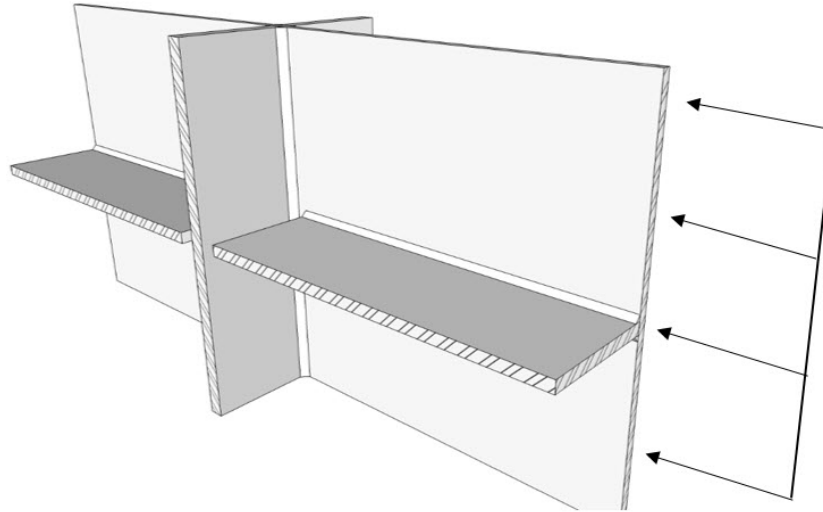


Figure 7.2.4.1-11 Detail D.

DETAIL D – Detail D, like Detail C above, has full height bearing stiffeners and longitudinal stiffeners. It is possible to discontinue the longitudinal stiffener near the bearing stiffener, leaving a minimum 1-inch gap but only when the web is loaded in compression and cannot experience tension at the Fatigue I load combination. This type of detail is discouraged, and Detail C is preferred.

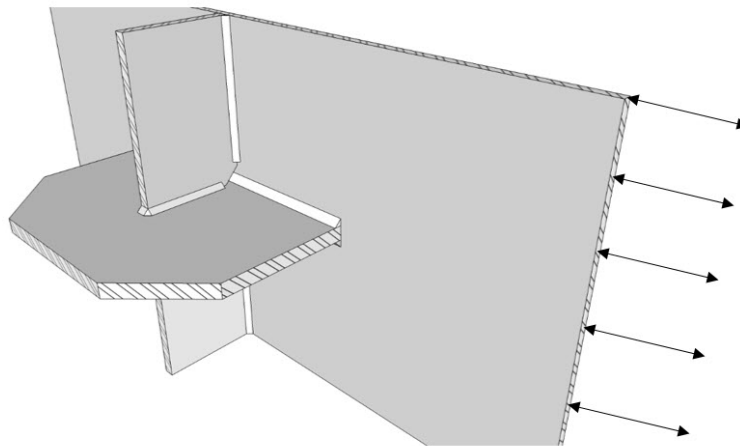


Figure 7.2.4.1-12 Detail E.

DETAIL E – When a vertical attachment, such as a diaphragm connection plate or shear stiffener, intersects a lateral gusset plate, and the girder web is loaded in tension, compression, or reversal, the preferred practice is to have the gusset plate be a continuous element, breaking the vertical stiffener and welding it with fillet welds to the gusset plate. Provide 1-inch minimum gaps between all weld toes.

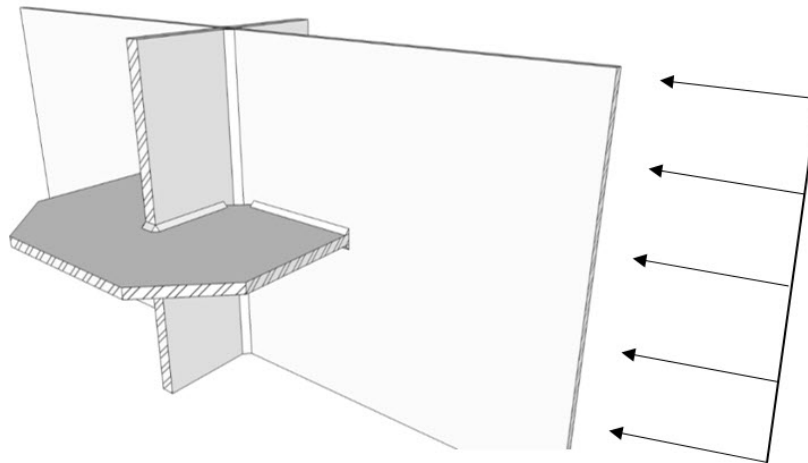


Figure 7.2.4.1-13 Detail F.

DETAIL F – When the web is loaded in compression only and a vertical attachment (e.g., a connection plate or shear stiffener) intersects a gusset plate, the preferred practice is to have the gusset plate be a continuous element, breaking the vertical stiffener and welding it with fillet welds to the gusset plate. The intersection must provide 1-inch minimum gaps between all weld toes. However, because the longitudinal stresses are entirely in compression, it is also acceptable to slot the gusset plate to fit around a continuous bearing stiffener, as shown in Figure 7.2.4.1-13. The gusset plate is then welded to the stiffener and the girder web, maintaining a 1-inch minimum gap between all weld toes.

Related to the AASHTO 1-inch weld gap requirement, research at Purdue University (DeLong and Bowman, 2010) also examined existing structures and the amount of web gap necessary to preclude CIF. Their research addressed the existing inventory of thousands of bridges with potential intersecting weld problems due to the presence of longitudinal stiffeners, gusset plates, and transverse stiffeners connected at common locations. Their concern was that just because a constraint-induced fracture occurred on several steel bridges, this should not lead to the general conclusion that it is likely on other existing bridges. The Purdue research confirmed the recommendations proposed by others (Mahmoud, Connor, and Fisher, 2005) with regard to the inspection of existing steel bridges, namely that a minimum observable gap in the field of 1/4 inch should provide for sufficient yielding and ductility so that CIF is unlikely. The research at Purdue also examined the influence of intersecting welds on the fatigue life of small gap details. They found that the presence of narrow web gaps did not seem to affect the fatigue life of such details, the fatigue life being governed by the toe at the outside end of a gusset plate and not by the toe nearer to the transverse connection plate. The test results for narrow web gaps where longitudinal stiffeners are terminated near transverse stiffeners was inconclusive.

7.2.4.2 Thick Plates

For a number of years, it has been known that welding thick components together in highly constrained joints can lead to fracture. This has been demonstrated in through thickness and lamellar tearing fractures in steel structures in the past. Lamellar tearing failures have been

reported where plates are welded at right angles to each other, resulting in through thickness stresses in one of the connected plates. Examples of these types of failures have been found in connections for rigid frames.

Brittle fractures have occurred during fabrication, immediately after fabrication, and shortly after an element has been placed into service. These early-age failures are not related to fatigue but rather to the unique condition present in complex joints or in joints and elements constructed with thick plates associated with large restraining forces which develop during differential cooling. Although it is generally desirable to avoid the angled connection of multiple thick plates and complex details, sometimes it is unavoidable. To minimize the potential for brittle fracture in thick joints, special precaution is required during fabrication, including the application of preheat, specific welding sequences, and robust nondestructive testing and inspection to provide the best possible performance.

Thick plate failures, known as lamellar tearing failures, have occurred beneath the weld metal in rolled steels with poor through-thickness ductility (see Figure 4.1.1-2). It is a failure type that occurs in tee and corner joints beneath the fusion boundary of the weld and the parent material. Failure is by tearing of the base metal in long parallel fibers at a location of inherently low ductility.

Failure is driven by either shrinkage strains at the time of fabrication or by high through thickness strains during service, additive to the strains due to residual stress. Thicker plates are generally more prone to lamellar tearing. In tee, corner, or other cruciform welds, those fabricated with full penetration butt welds are most susceptible.

Joint design and detailing have a significant influence on the susceptibility of lamellar tearing. Suggestions to improve the performance of thick joints include:

- Replacing full penetration welds with balanced fillet welds
- Replacing unbalanced welds with balanced welds
- Replacing large single-sided welds with balanced double-sided welds
- Beveling the fusion boundary of the susceptible plate to reduce the through thickness effects

These suggested improvements are depicted in Figure 7.2.4.2-1.

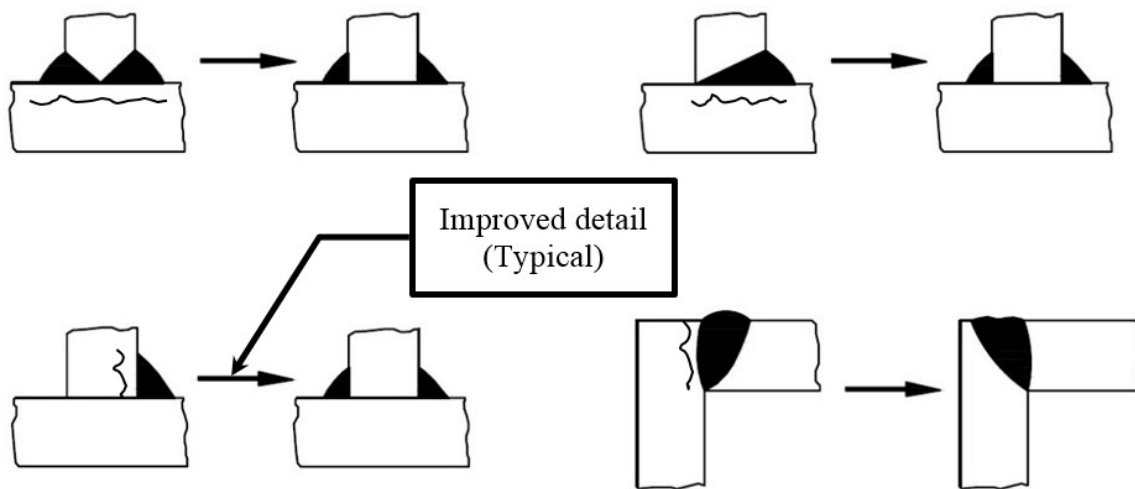


Figure 7.2.4.2-1 Recommended joint configurations to reduce the risk of lamellar tearing.

SECTION 7.3 FRACTURE CONTROL BY ENHANCED FABRICATION

The second leg of the “three-legged-stool” Total FCP is implementation of supplemental fabrication requirements as defined in Clause 12 of the AASHTO/AWS D1.5 *Bridge Welding Code* (AASHTO/AWS, 2010). Clause 12 provides supplemental requirements for materials, workmanship, and fabrication processes to provide structures with limited but acceptable discontinuities such that fracture is effectively prevented throughout the expected service life. The AASHTO/AWS Clause 12 FCP is structured in such a way that members fabricated to and meeting its requirements are not expected to suffer failure due to brittle fracture during their operating life.

As described in Section 2.2, there are steel manufacturing and fabrication processes such as rolling, cutting, welding, and drilling that result in the creation of discontinuities in all fabricated steel structures. Although known cracks are not allowed to remain in a fabricated element, some discontinuities are always present. The susceptibility to fatigue and fracture is a function of the severity of the discontinuities and their location relative to applied tensile stresses. The FCP attempts to limit the size, frequency, and severity of these discontinuities.

The fundamentals of fracture mechanics, previously discussed in Chapter 3, demonstrate that there is an interrelationship between a variety of factors including: material toughness; loading rate; in-service temperatures; the size, location, and orientation of discontinuities; and the levels of tensile stress that all combine to define regions of safe and unsafe behavior. The FCP recognizes this interrelationship and imposes minimum standards for materials and expectations on workmanship so that at the limits of each of these variables, a structure with a predictable and adequate reliability is provided.

The development of a fracture control plan, as well as national bridge inspection standards, can be traced to the collapse of the bridge at Point Pleasant, West Virginia (the Silver Bridge) in 1967 (see Figure 7.1-1). As a result, the 1970's saw rapid changes to engineering practice, including the introduction of CVN testing as a quality control measure for steel bridge fabrication and the introduction of modern fatigue design principles. The implementation of formal FCP's began in 1978 with the publication of the *Guide Specifications for Fracture Critical Non-Redundant Steel Bridge Members* (AASHTO, 1978). This formalized the requirements for testing of materials in FCM's as a quality control measure, and provided requirements for fabrication and shop inspection of FCM's as unique and requiring special attention as compared to redundant members. The AASHTO requirements are no longer maintained in the Guide Specification format; rather they have now been fully incorporated in the ASTM A709 standard, the *AASHTO LRFD Bridge Design Specifications*, and in the *AASHTO/AWS D1.5 Bridge Welding Code*, Clause 12, entitled "AASHTO/AWS Fracture Control Plan (FCP) for Nonredundant Members." The remainder of the *D1.5 Bridge Welding Code* focuses on requirements that apply equally for both fracture critical and non-fracture critical elements alike.

The provisions of the AASHTO/AWS FCP address items such as:

- Contract documents
- Base metal requirements
- Welding processes
- Consumable requirements
- Welding Procedure Specification (WPS)
- Certification and qualification
- As-received inspection of base metal
- Thermal cutting
- Repair of base metal
- Straightening, curving, and cambering
- Tack welds and temporary welds
- Preheat and interpass temperature control
- Post-weld thermal treatments
- Weld inspection
- Repair welding
- Attachments to FCM's

Guidance in these areas is not unique to FCM's; it applies to all steel structures. The purpose of AASHTO/AWS D1.5 Clause 12 is to provide more specific and/or stringent guidance in these areas for FCM's.

The design engineer is responsible to indicate the presence of FCM's in the contract documents, to specify the materials to be used in accordance with the agency policies, and is typically involved in the review and approval of shop drawings and associated fabrication procedures. The FCP provisions pertaining to material properties, fabrication, shop inspection requirements, and qualifications of shop personnel are typically addressed by owner / agency specifications. The

engineer must be familiar with these requirements and determine their suitability for a specific application. Occasionally, special provisions are required to amend an agency's typical requirements. The combination of agency materials and fabrication specifications, along with the input and approval of the engineer during all phases, is essential to control the fabrication of FCM's.

The AASHTO/AWS FCP also requires that FCM's be noted in the contract documents, most typically on the design plans, and that this designation is required prior to bidding. The designation of FCM's alerts all interested parties of the special attention required for certain elements of the structure. Prior to fabrication, it is common for shop drawings to be developed and reviewed. The shop drawings and supporting information regarding member fabrication will define: the materials chosen for member fabrication; specific welding processes; information on consumables to be used; and welding procedures. In addition, it may include information regarding the certification and qualification of specific individuals responsible for fabricating the FCM's; will identify cutting procedures; and may include pre-approval of repair procedures in advance. The obligation of the engineer is to ensure that the various procedures intended for the fabrication of the FCM's designated in the design documents are appropriate and allowed by the owner's policy.

7.3.1 Fabrication Controls

Fabrication of FCM's can only be done by shops possessing an intermediate or advanced certification through the *AISC Certification Program Requirements for Steel Bridge Fabricators* (AISC, 2011) and possessing the additional fracture critical endorsement. This is done to limit the fabrication of FCM's to those shops with the training and experience in fabricating FCM's and with the ability to meet the AASHTO/AWS D1.5 requirements.

FCM's are fabricated from base metals such as those previously referenced in Table 7.2.3-2 that adhere to toughness, heat treatment, and other mechanical properties as required by the FCP. An inspection of the base metal is required prior to member fabrication. The edges and ends of plates are required to be cut by thermal cutting. This includes edges that have previously been mechanically rolled or sheared. Inspection of the prepared edges is required. Visual discontinuities are to be inspected using magnetic particle testing. Specific repair processes are called for when the base metal contains rejectable discontinuities outside the limits of the specification. The repair procedures can include rotating the base metal so that the discontinuity no longer lies within a joint, by thermal cutting to adjust the length of a specific plate, with welding to repair a specific location of damage, or in the extreme case by replacement with equal or better material.

FCM's, like all welded steel members, are welded using only specifically approved welding processes, consumables, and in accordance with approved welding procedure specifications. The procedures for FCM's are more stringent than for non-fracture critical members. Quality assurance inspection of the fabrication process is required to ensure compliance with the FCP. However, this does not relieve the fabricator from the obligation to follow the plan in its entirety. Shop quality assurance inspectors are required to be familiar with the nature of work and have

the authority to accept or reject materials and workmanship. In addition to visual inspection, NDT technicians are also required and subject to the certification requirements of the FCP.

The use of repair welding on FCM's falls into two categories: noncritical and critical weld repairs based on the severity of the defect to be corrected. Repair welding to correct deficiencies in base metal or in previously deposited weld metal is permitted. The approval of repair procedures in advance is permitted before beginning the work in order to eliminate requiring specific approval at the time a particular discontinuity is discovered by inspection. Repair welding can also be used to build up previously deposited but insufficiently sized welds; to remove discontinuities, rollover, undercut, gouges, and laminar discontinuities; for the repair of base metal; and for other defects deemed noncritical. Whether noncritical or critical welding repair is performed, all repair welding is subject to inspection. Specific requirements are provided for the identification of unacceptable discontinuities, surface preparation, material and workmanship requirements, post-welding heat treatment, and final inspection and acceptance.

Procedures are specified for straightening, curving, and cambering fracture critical members. Cold bending of fracture critical members is allowed only with specific approval of the engineer.

SECTION 7.4 FRACTURE CONTROL BY IN-SERVICE INSPECTION

The third and final leg of the “three-legged-stool” Total FCP is provided by regular in-service inspections. Even if the design and fabrication requirements are followed and the bridge is performing as intended, there is always a chance that a crack could develop through fatigue or another anomalous scenario such as a truck impact or bearing freeze. In this case, we rely on the member to survive a short time until the next inspection occurs and the damage can be identified and repaired.

Modern standardized bridge inspection practices trace their origins to the Federal-Aid Highway Act of 1968. Following the collapse of the suspension bridge at Point Pleasant, West Virginia in 1967 (see Figure 7.1-1), the National Bridge Inspection Standards (NBIS) were established, and uniform rules for inspection, data collection, and reporting were developed and implemented in the coming years. Prior to 1968, there was no uniform standard for collecting and reporting bridge inspection data, though state initiated inspections were periodically performed. Subsequent legislation clarified what bridges were included in the inventory and have amended and made changes to the requirements periodically.

In 1983, the Mianus River Bridge collapsed, again focusing attention on bridges and their safety. This failure, related to corrosion and the eventual failure of a pin-and-hanger suspended span carrying I-95, triggered the requirement for hands-on inspection of fracture critical bridges as part of the Surface Transportation and Uniform Relocation Assistance Act of 1987.

While some cracks may be detected during routine inspections, fracture critical inspections are unique in that they require the inspection team to be close enough to the member for it to qualify as “hands-on”; that is, the team must be close enough to the fracture critical components and members to touch the elements. The inspection is at a minimum a visual inspection but

commonly uses other nondestructive techniques such as dye penetrant, magnetic particle, or ultrasonic testing to assess the condition of the members.

There are several requirements that are key to successfully inspecting bridges with FCM's. These are detailed below. These requirements share many features with the protocols for inspecting routine bridges. The requirements for the qualification of inspectors, record-keeping protocols, inspection intervals, etc. come from 23 CFR 650 Subpart C. They are additionally detailed in publications such as the *AASHTO Manual for Bridge Evaluation* (AASHTO, 2015d) and the *FHWA Bridge Inspector's Reference Manual* (FHWA, 2012a).

Understand Resource Requirements – A qualified team is required to administer and conduct the inspection. This includes staff working for the owner as a program manager as well as the field personnel. The program manager must have a Professional Engineer (PE) license or ten years of bridge experience and must have successfully completed a comprehensive bridge inspection course such as NHI “Safety Inspection of In-Service Bridges” (FHWA, 2012d) or equivalent.

Team leaders are the individuals responsible for planning and executing the inspection. There are multiple paths to attaining this status, including combinations of education, experience, and successful completion of NHI or equivalent inspection training courses. The team leader is assisted by qualified inspectors and NDE technicians as required.

The type of access must be considered. In order to meet the hands-on requirements, various types of access equipment might be required. These include various types of commercially available bucket trucks, ladders, ground mounted access, the use of rope access climbing, and frequently a combination of these techniques to access specific elements of a bridge. The type of access depends on the geometry of the bridge, the type of available access equipment, cost, impacts to traffic for inspection, and local factors that are unique to most bridges. The team leader must work with the entire inspection team to plan the inspection in advance, given the complications of access.

The need for specialty equipment must also be assessed. Many inspection teams have the ability to perform simple nondestructive tests such as dye penetrant or magnetic particle testing. However, for more complex testing such as ultrasonic testing or field x-ray (radiography), a sub-consultant and specialty testing firm are needed. This adds a level of coordination, cost, and complexity, but is sometimes required to determine the condition of certain FCM's, to verify the limits of observed cracks, to conduct pin integrity tests, and for other purposes.

FCM Identification – A copy of the design plans or as-built drawings should be available in the bridge inspection records. It is also helpful to have access to shop drawings to the extent that they are available. As part of planning the inspection, the team leader, with assistance from others, should review the design drawings, shop drawings, as-built plans, previous inspection reports, rehabilitation drawings, and any other pertinent information. All FCM's should be designated prior to inspection. Additionally, for each FCM, the team leader should locate all fatigue sensitive details associated with the individual members. For instance, this could include noting the presence of welded attachments on certain FCM's so they are specifically included in the field inspection. Specific attention should be paid to details categorized as AASHTO Detail

Category D or lower in resistance, since these are most likely to be limiting factors to the remaining fatigue life of a steel bridge.

Develop Inspection Procedure – There are various factors that can impact the success of a fracture critical inspection. For instance, accurately locating cracks in a heavily deteriorated steel member may be difficult. Knowing the expected condition of the materials is therefore critical to the potential success of the inspection effort. Bridges frequently carry attached utilities. These can interfere with a hands-on inspection of certain elements. Inspectors will frequently encounter environmental concerns, such as lead paint and confined spaces, and have to work in all weather and element conditions, all of which complicate the inspection process. Bridges are frequently dirty, laden with debris near expansion joints, and can contain contaminants, such as bird or animal excrement, all of which serve as health and access hazards. Bridges frequently cross other roads, railroads, streams, and rivers, which pose a challenge for access and safety that must be considered by the inspection team. The complexity of an individual bridge and site conditions will dictate the method of access, the time required to complete the inspection, and the relative complexity of the work. A pre-inspection meeting with the team leader and the inspection team should be held in order to go over safety requirements in advance, to assign staff to the individual inspection teams, to document the required tools and procedures to be used, to discuss any unique NDE requirements, and to discuss the project in general.

Prepare Follow-up Procedure – During or immediately following the inspection, the team leader should begin to identify any follow-up procedures based on the results of the inspection. These follow-up procedures could include a need for additional nondestructive testing, an updated load rating analysis, a remaining fatigue life analysis, the preparation of repair and rehabilitation plans, and in the most severe condition could result in recommendations to load restrict or permanently close a bridge. Any critical findings discovered during the inspection, or any inspection, must immediately be brought to the attention of the owner.

Quality Control/Quality Assurance – The team leader is responsible for quality control (QC) and quality assurance (QA) of the inspection. During the actual inspection, the team leader should perform routine QC checks on the inspection findings of other inspection team members. The team leader should also refine or update the inspection procedures as the field work progresses in order to address changed conditions in the field or as it is found that more or less scrutiny is required for certain details. It is not uncommon to find details and conditions in the field that differ from the plans and even the prior inspection report. The team leader's responsibility is to manage this change and properly document the updated conditions in the inspection report. The inspection team should observe and document how the conditions change from prior inspection cycles and based on a pattern of change predict the future maintenance and rehabilitation needs for the bridge. Examples of changed conditions could include crack growth from a prior cycle, new crack observations, assessment of the effectiveness of prior retrofits, and other similar observations that are related to the potential future life of the structure. It is not uncommon for changes to be made to structures that are not included on the design plans. Examples include utility attachments or field modifications that may negatively influence the fatigue or fracture characteristics of an existing steel structure. These should be noted in the field notes, photographed, sketched, and the bridge inspection and maintenance files updated accordingly.

Develop a Periodic Inspection Plan – Based on the findings of the inspection, the team leader should recommend an inspection interval for the structure. These intervals are frequently 24 months (the maximum allowed by 23 CFR without exemption), but it is also not uncommon to require more frequent inspection intervals, particularly as deterioration or member damage is noted on the bridge. Special inspections are sometimes required for specific elements of the bridge that require more frequent observation. There are advantages and disadvantages to the same inspection team conducting the inspection of a bridge repeatedly. The advantages of course are familiarity and first-hand knowledge of how conditions have changed over time. There is also a perceived disadvantage as well, that being a potential relaxed attitude toward the structure having seen it so many times. Each agency should consider these possible outcomes when planning and staffing bridge inspection projects.

Inspection Report – Following the completion of the inspection, a detailed inspection report is required. The inspection report generally contains four main components: a narrative, documentation support, an evaluation of the conditions, and recommendations.

The narrative describes the approach to the inspection, identifies the fracture critical members, details the inspection procedures, provides an overall description of the bridge, as well as a detailed description of the FCM's, and contains a summary and conclusions. The narrative frequently integrates other elements such as excerpts from the design drawings, photographs from the inspection, reports from nondestructive testing, sketches, and other field information or logs required to support the discussion in the project narrative. The narrative includes basic structure information such as overall photographs, information on the type of structure, the year it was built, the types of materials that were used to construct it, and any prior retrofit history. The narrative will frequently reference prior inspection reports and rehabilitation efforts. The individuals who perform the inspection, and their qualifications, will be detailed. A description of the scope of inspection, the means of access, and the types of routine and NDT equipment used should be provided.

Photographs and sketches should be used to highlight the fracture critical members of the bridge and to describe the details in the context of AASHTO fatigue categories. Reporting this information in a consistent manner over multiple inspection cycles promotes completeness and repeatability and allows the owner and future inspection teams to assess changes over time. It is important to document the condition of the FCM's and attached details. This is the fundamental reason for the detailed inspection.

An assessment of the overall condition of the structure should be provided with specific attention to how existing deficiencies affect the resistance or remaining life of the FCM's. The inspection report should document the impact of existing deficiencies and prioritize these for future rehabilitation work. If any critical findings are presented in the inspection report, recommendations must be made to minimize the risk. A critical finding is a structural or safety deficiency that requires immediate follow-up inspection or action. Based on the observations of the inspector, and in consultation with the owner, a critical finding could result in a recommendation for additional inspection, an updated load rating, load posting, partial or full closure of the bridge, and immediate or long-term repairs. The experience of the inspection team,

the team leader, and the owner are required to assess the critical finding and to determine an appropriate course of action.

CHAPTER 8 AASHTO FATIGUE-EVALUATION APPROACH

A methodology for fatigue evaluation of steel bridges is included in the *MBE* (AASHTO, 2015d). A fatigue evaluation is not routinely performed with each rating of a steel bridge; it is generally performed only when the remaining fatigue life of an uncracked bridge is desired as input into operating decisions. For example, if redecking of a cover-plated girder bridge is planned, a fatigue evaluation may suggest that the cover-plate ends should be retrofitted to match the service life extension of the bridge from the redecking.

The original fatigue-evaluation methodology as presented in the 1st Edition of the *MBE* included several levels of reliability of the evaluation: minimum, evaluation, and mean life. The first significant enhancements to this methodology are included in the 2015 Interim Revisions to the 2nd Edition. A second evaluation life and a methodology for low fatigue-life bridges accounting for past successful performance were added based upon NCHRP Report 721 (Bowman et al., 2012).

In this chapter, the methodology is examined and illustrated.

SECTION 8.1 IDENTIFYING THE NATURE OF CRACKING

As introduced in Chapter 4, fatigue damage is categorized as either load-induced or distortion-induced.

8.1.1 Load-Induced Fatigue

8.1.1.1 General

Load-induced fatigue is that due to the in-plane stresses in the steel plates that comprise bridge member cross sections. These in-plane stresses are those typically calculated by designers during bridge design or evaluation.

8.1.1.2 Determining Fatigue-Prone Details

Bridge details are only considered prone to load-induced fatigue damage if they experience a net tensile stress. Thus, fatigue damage need only be evaluated if, at the detail under evaluation:

$$2.2(\Delta f)_{tension} > f_{dead-load\ compression}$$

Equation 8.1.1.2-1

where:

$$\begin{aligned} (\Delta f)_{tension} &= \text{tensile portion of the effective stress range as specified in } MBE \\ &\text{Article 7.2.2 (discussed in detail in Section 8.2.1)} \\ f_{dead-load\ compression} &= \text{unfactored compressive stress at the detail due to dead load} \end{aligned}$$

8.1.2 Distortion-Induced Fatigue

Fatigue life is not evaluated for distortion-induced fatigue. Distortion-induced fatigue is that due to secondary stresses in the steel plates that comprise bridge member cross sections. These stresses can only be calculated with very refined methods of analysis, far beyond the scope of a typical bridge design or evaluation. These secondary stresses are minimized through proper detailing.

A distortion-induced crack propagating from the web gap at a transverse connection plate not positively attached to a longitudinal connection plate is illustrated in Figure 8.1.2-1.

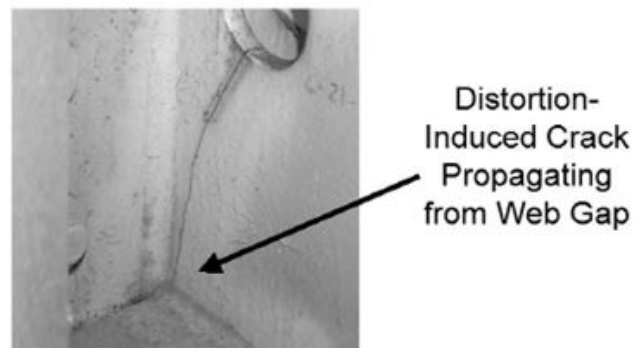


Figure 8.1.2-1 Typical distortion-induced fatigue crack.

In new design, the transverse connection plate should be welded or bolted to the longitudinal connection avoiding the web gap. Detailing to minimize the potential for distortion-induced fatigue, such as connecting transverse connection plates for diaphragms and floorbeams to both the compression and tension flanges of girders, is specified in *AASHTO LRFD* Article 6.6.1.3 (AASHTO, 2015b).

For existing bridges, the transverse connection plate should be connected to the longitudinal connection plate by adding connection angles to each side of the plate. (Field welding is an option, but bolting is preferred.)

SECTION 8.2 REMAINING FATIGUE LIFE EVALUATION

The evaluation methodology discussed herein is appropriate for bridges where fatigue cracking has not been visually detected.

If fatigue cracking has already been visually detected, a more complex fracture-mechanics approach, as discussed in Chapter 3, is appropriate instead of the methodology presented herein. Further, the expense and trouble of a fracture-mechanics analysis may not be warranted. Generally, upon visual detection of fatigue cracking, the majority of the fatigue life has been exhausted and retrofitting should be initiated.

8.2.1 Estimating the Stress Range

The stress range, either measured or calculated, is the stress range due to a single truck in a single lane on the bridge, as specified in *AASHTO LRFD* Article 3.6.1.4.3 (AASHTO, 2015b).

The stress range used for fatigue-life evaluation can be estimated in three ways:

1. Estimated from measured strains,
2. By direct application of *AASHTO LRFD* (AASHTO, 2015b), or
3. Estimated from a truck-weight survey.

8.2.1.1 Quantifying Uncertainty: Partial Load Factors

In determining the fatigue life, the uncertainty associated with the stress range, R_s , has two components:

- Uncertainty associated with analysis, represented by the analysis partial load factor, R_{sa}
- Uncertainty associated with assumed effective truck weight, represented by the truck-weight partial load factor, R_{st}

The product of these uncertainties is termed the stress-range estimate partial load factor, R_s .

The partial load factors were adapted from the *AASHTO Guide Specifications for Fatigue Evaluation of Existing Steel Bridges* (AASHTO, 1990) and are summarized in Table 8.2.1.1-1. As uncertainty is removed from the evaluation by more refined analysis or site-specific data, the increased certainty is reflected in lower partial load factors. Uncertainty decreases as one moves down the rows of the table. Simplified and refined analysis are as defined in *AASHTO LRFD* Articles 4.6.2 and 4.6.3 (AASHTO, 2015b), respectively.

Table 8.2.1.1-1 Partial load factors: R_{sa} , R_{st} , and R_s .

Stress-range Estimation Methods	Analysis Partial Load Factor, R_{sa}	Truck-Weight Partial Load Factor, R_{st}	Stress-Range Estimate Partial Load Factor, R_s
For Evaluation-1, Evaluation-2, or Minimum Fatigue Life			
Section 8.2.1.2 - simplified analysis, and truck weight per <i>AASHTO LRFD</i> Article 3.6.1.4	1.0	1.0	1.0
Section 8.2.1.3 – simplified analysis, and truck weight by truck survey or weigh-in-motion study	1.0	0.95	0.95
Section 8.2.1.2 - refined analysis, and truck weight per <i>AASHTO LRFD</i> Article 3.6.1.4	0.95	1.0	0.95
Section 8.2.1.3 - refined analysis, and truck weight by truck survey or weigh-in-motion study	0.95	0.95	0.90
Section 8.2.1.4 - field-measured strains	N/A	N/A	0.85
For Mean Fatigue Life			
All methods	N/A	N/A	1.00

8.2.1.2 Application of the *AASHTO LRFD* Specifications

The effective stress range shall be estimated as:

$$(\Delta f)_{eff} = R_p R_s \Delta f$$

Equation 8.2.1.2-1

where:

- R_p = multiple presence factor defined below
 R_s = stress-range estimate partial load factor specified in Table 8.2.1.1-1
 Δf = factored calculated stress range due to the passage of the fatigue truck as specified in *AASHTO LRFD* Article 3.6.1.4 for the Fatigue II load combination of *AASHTO LRFD* Table 3.4.1-1 (*AASHTO*, 2015b)

The multiple presence factor shall be calculated:

for longitudinal members, as:

$$R_p = 0.988 + 6.87 \times 10^{-5} L + 4.01 \times 10^{-6} (ADTT)_{PRESENT} + \frac{0.0107}{n_L}$$

Equation 8.2.1.2-2

and for transverse members, as:

$$R_p = 1.0$$

where:

L	=	span length (ft)
$(ADTT)_{PRESENT}$	=	present average daily truck traffic in both directions (trucks/day) (see Table 8.2.1.2-1)
n_L	=	number of striped lanes

The multiple presence factor was developed as discussed in NCHRP Report 721 (Bowman et al., 2012) for $2 \leq n_L \leq 4$ and $30 \text{ ft} \leq L \leq 220 \text{ ft}$ using the following assumptions.

Table 8.2.1.2-1 Assumed $(ADTT)_{PRESENT}$.

n_L	Assumed $(ADTT)_{PRESENT}$
2	8,000
3	11,000
4	13,000

The commentary to *MBE* Article 7.2.2.1 states that the use of the multiple presence factor “*may be justified outside of these ranges, but are not based on experimental evidence.*”

The stress range may be calculated using simplified or refined analysis, as defined in *AASHTO LRFD* Articles 4.6.2 and 4.6.3, respectively; and the fatigue truck is as specified in *AASHTO LRFD* Article 3.6.1.4 factored in accord with the Fatigue II load combination of *AASHTO LRFD* Table 3.4.1-1.

8.2.1.3 Truck-Weight Survey

The effective stress range shall be estimated as:

$$(\Delta f)_{eff} = R_p R_s (\Delta f)_{survey}$$

Equation 8.2.1.3-1

where:

R_p	=	multiple presence factor defined in Section 8.2.1.2
R_s	=	stress-range estimate partial load factor specified in Table 8.2.1.1-1
$(\Delta f)_{survey}$	=	calculated stress range due to the passage of a fatigue truck determined by a truck survey or weigh-in-motion (WIM) study

The stress range may be calculated using simplified or refined analysis, as defined in *AASHTO LRFD* Articles 4.6.2 and 4.6.3, respectively; and the fatigue truck is determined by a truck survey or WIM study factored in accord with the Fatigue II load combination of *AASHTO LRFD* Table 3.4.1-1.

8.2.1.4 Field-Measured Strains

The effective stress range may be estimated through field measurements of variable-amplitude strains at the fatigue-prone detail under consideration under typical traffic conditions. Field measurements of strains represent the most accurate means to estimate effective stress ranges at fatigue-prone details. Variable-amplitude stress-range behavior was previously discussed in Section 4.5.2.

The effective stress range, $(\Delta f)_{eff}$, shall be taken as the cube root of the weighted sum of the cubes of the variable-amplitude stress ranges from the measured strains, as given in:

$$(\Delta f)_{eff} = R_s \left(\sum \gamma_i \Delta f_i^3 \right)^{\frac{1}{3}}$$

Equation 8.2.1.4-1

where:

- R_s = the stress-range estimate partial load factor, calculated as $R_{sa}R_{st}$, unless otherwise specified
- γ_i = percentage of cycles at a particular stress range
- Δf_i = the particular stress range in a field-measured stress-range histogram greater than 45 percent (= 0.80/1.75) of the constant-amplitude fatigue threshold of the fatigue-prone detail

SECTION 8.3 ESTIMATING FATIGUE LIFE BY THE *MBE*

As introduced in Chapter 6, fatigue life is characterized as infinite or finite. The estimation of an existing bridge detail's fatigue life, infinite or finite, is reviewed in this section.

8.3.1 Infinite-Life Check

Theoretically, a fatigue-prone detail will experience little or no fatigue damage during its 75-year design life if all of the stress ranges experienced by the detail are less than the constant-amplitude fatigue threshold. Thus, the detail under evaluation is said to have infinite fatigue life.

If:

$$(\Delta f)_{\max} \leq (\Delta F)_{TH}$$

Equation 8.3.1-1

then the estimated fatigue life in years, Y , is infinite,

where:

$$\begin{aligned}
 (\Delta f)_{max} &= R_p \text{ times the factored calculated stress range due to the passage of the} \\
 &\quad \text{fatigue truck as specified in } AASHTO \text{ LRFD Article 3.6.1.4 for the Fatigue} \\
 &\quad \text{I load combination of } AASHTO \text{ LRFD Table 3.4.1-1, or} \\
 &= 2.2 (\Delta f)_{eff} \text{ when the effective stress range is calculated using a truck} \\
 &\quad \text{survey, WIM study, or measured strains with } R_s = 1.0 \\
 (\Delta F)_{TH} &= \text{constant-amplitude fatigue threshold given in } AASHTO \text{ LRFD Table} \\
 &\quad \text{6.6.1.2.5-3}
 \end{aligned}$$

AASHTO LRFD previously assumed that the maximum stress range was twice the effective stress range. Thus, a multiplier of 2.0 was previously used in the equation for $(\Delta f)_{max}$ above, representing the previous Fatigue I load factor of 1.5 divided by the previous Fatigue II load factor of 0.75.

The AASHTO Subcommittee on Bridges and Structures increased the Fatigue I and Fatigue II load factors to 1.75 and 0.8, respectively. Thus, the multiplier in the equation for $(\Delta f)_{max}$ above is 2.2, which equals 1.75 divided by 0.8. It is unlikely that the maximum stress range during the design life of the bridge will be captured during a limited field-testing session; therefore means to extrapolate from the measured effective stress range to the maximum stress range must be used. When measured values are used to evaluate fatigue life, the multiplier in the equation for $(\Delta f)_{max}$ should be reconsidered based upon the discussion of Section 8.1.1.

8.3.2 Finite Life

If the infinite-life check is not satisfied, the finite life of the detail may be estimated as described in this section.

Much scatter, or uncertainty, exists in experimentally derived fatigue resistance. For design, a conservative fatigue resistance is assumed at two standard deviations below the mean fatigue resistance or life. This corresponds to the minimum expected finite fatigue life for evaluation. Limiting actual usable fatigue life to this design life is very conservative and costly. As such, means of estimating evaluation fatigue lives and the mean finite fatigue life are also included in the *MBE* to aid the evaluator in the decision-making.

Four levels of fatigue life may be estimated:

1. Minimum life (very conservative design life)
2. Evaluation 1 life (a less conservative life)
3. Evaluation 2 life (an even less conservative life)
4. Mean life (most likely life)

The resistance factors for fatigue life, given in Table 8.3.2-1, represent the uncertainty of the fatigue life of the various detail categories, A through E'. As the stress-range estimate grows closer and closer to the actual value of stress range, the probability of occurrence associated with each level of fatigue life approaches the values given in Table 8.3.2-2.

Table 8.3.2-1 Resistance factor, R_R .

Detail Category as defined in <i>AASHTO LRFD</i> Table 6.6.1.2.3-1	Minimum Life R_R	Evaluation 1 Life R_R	Evaluation 2 Life R_R	Mean Life R_R
A	1.0	1.5	2.2	2.9
B	1.0	1.3	1.7	2.0
B'	1.0	1.3	1.6	1.9
C	1.0	1.3	1.7	2.1
C'	1.0	1.3	1.7	2.1
D	1.0	1.3	1.7	2.0
E	1.0	1.2	1.4	1.6
E'	1.0	1.3	1.6	1.9

Table 8.3.2-2 Probabilities of occurrence associated with levels of fatigue life.

Level of Fatigue Life	Probability of Occurrence
Minimum (Design) Life	98 percent
Evaluation 1 Life	84 percent
Evaluation 2 Life	67 percent
Mean Life	50 percent

MBE Article 7.2.5.1 gives an expression for estimating the total finite fatigue life of a fatigue-prone detail, in years, based upon the selected level of life:

$$Y = \frac{\log \left[\frac{R_R A}{365n[(ADTT)_{SL}]_{PRESENT} [(\Delta f)_{eff}]^3} g(1+g)^{a-1} + 1 \right]}{\log(1+g)}$$

Equation 8.3.2-1

where:

- R_R = resistance factor as given in Table 8.3.2-1
 A = detail category constant as specified in *AASHTO LRFD* Table 6.6.1.2.5-1
 n = number of stress-range cycles per truck passage
 g = estimated annual traffic-volume growth rate in percentage
 a = present age in years
 $[(ADTT)_{SL}]_{PRESENT}$ = present ADTT in a single lane
 $(\Delta f)_{eff}$ = effective stress range

In lieu of better information, *AASHTO LRFD* Table 6.6.1.2.5-2 may be used to determine the number of stress-range cycles, n . Otherwise, it may be determined from influence lines or field measurements.

8.3.3 Example

Determine the remaining fatigue life of the end weld of the cover plate of *MBE* Example A1 (AASHTO, 2015d). Consider the transverse welds connecting the cover plate ends to the flange. The flange thickness is 0.855 inches.

The cover plate end weld is Detail Category E' from *AASHTO LRFD* Table 6.6.1.2.3-1.

Check if $2.2(\Delta f)_{tension} > f_{dead-load\ compression}$

$$f_{dead-load\ compression} = 0$$

Therefore, fatigue must be considered, as shown in the following computations.

$$\Delta f_{LL+IM} = 4.56 \text{ ksi (unfactored)}$$

$$L = 65 \text{ ft and } n_L = 2 \text{ lanes}$$

$$(\text{ADTT})_{\text{PRESENT}} = 1,000 \text{ trucks/day}$$

$$R_p = 0.988 + 6.87(10)^{-5}(65) + 4.01(10)^{-6}(1,000) + 0.0107/2 = 1.0018$$

$$(\Delta f)_{\max} = R_p \gamma_{LL} (\Delta f_{LL+IM}) = (1.0018)(1.75)(4.56) = 7.99 \text{ ksi}$$

$$(\Delta F)_{TH} = 2.6 \text{ ksi from } AASHTO \text{ LRFD Table 6.6.1.2.5-3}$$

Therefore, since

$$(\Delta f)_{\max} = 7.99 > 2.6 = (\Delta F)_{TH}$$

the cover plate end weld does not have infinite life.

Now more data is required.

$$A = 3.9 \times 10^8 \text{ ksi}^3 \text{ from } AASHTO \text{ LRFD Table 6.6.1.2.5-1}$$

$$n = 1.0 \text{ for a simple span}$$

$$[(\text{ADTT})_{\text{SL}}]_{\text{PRESENT}} = 850 \text{ trucks/day from } AASHTO \text{ LRFD Table 3.6.1.4.2-1}$$

$$a = 48 \text{ years (1968 to 2016)}$$

Assume $g = 2$ percent

$$R_s = 1.0$$

$$(\Delta f)_{eff} = R_s R_p \gamma_{LL} (\Delta f_{LL+IM}) = (1.0)(1.0018)(0.8)(4.56) = 3.65 \text{ ksi}$$

$$Y = \frac{\log [1.31R_R + 1]}{\log (1.02)}$$

For Detail Category E' and:

$R_R = 1.0$, therefore Minimum Life = 42 years

$R_R = 1.3$, therefore Evaluation 1 Life = 50 years

$R_R = 1.6$, therefore Evaluation 2 Life = 57 years

$R_R = 1.9$, therefore Mean Life = 63 years

Since the age of the bridge is already 48 years, it appears that retrofit or more evaluation is required to assure sufficient remaining life. Such additional evaluation is explored in Section 8.4.

SECTION 8.4 REMAINING FATIGUE LIFE FOR “NEGATIVE REMAINING LIFE” BRIDGE DETAILS

8.4.1 General

Due to the conservative nature of fatigue design and evaluation, many times the calculated remaining fatigue life is determined to be negative, suggesting that the detail should have already cracked when it has not. The *MBE* addresses such cases through the Fatigue Serviceability Index, introduced with the 2015 interim revisions to the 2nd Edition of the *MBE*.

8.4.2 Fatigue Serviceability Index, Q

MBE Article 7.2.6 defines the Fatigue Serviceability Index, Q , as a dimensionless measure of the performance of a structural detail, at a particular location in the structure, with respect to the overall fatigue resistance of the member, calculated as:

$$Q = \left(\frac{Y - a}{N} \right) GRI$$

Equation 8.4.2-1

where:

Y	=	calculated fatigue life
a	=	present age of the detail, in years
N	=	greater of Y or 100 years
G	=	load path factor from Table 8.4.2-1

R = redundancy factor from Table 8.4.2-2
 I = importance factor from Table 8.4.2-3

Table 8.4.2-1 Load path factor, G .

Number of Load Path Members	G
1 or 2	0.8
3	0.9
4 or more	1.0

Table 8.4.2-2 Redundancy factor, R .

Type of Span	R
Simple	0.9
Continuous	1.0

Table 8.4.2-3 Importance factor, I .

Structure or Location	I
Interstate highways, major arterial state routes, or other critical routes	0.9
Secondary arterials or urban areas	0.95
Rural roads or low ADTT routes	1.0

The load path, redundancy, and importance factors reflect risk and modify the Fatigue Serviceability Index much as the load modifiers of *AASHTO LRFD* Article 1.3.2.1 modify loads.

MBE Article 7.2.6.2 suggests that the Fatigue Serviceability Index may be used as a guide for inspection or preservation actions but provides no guidance as to acceptable index values. The commentary to *MBE* Article 7.2.6 states that Q varies between 1.0 and 0.0. Clearly, a negative value of Q , suggesting a negative remaining fatigue life, is not acceptable.

The NCHRP project (Bowman et al., 2012) which originally proposed the Fatigue Serviceability Index as a guide for actions suggests the actions in Table 8.4.2-4 as a function of Q . This table was proposed to AASHTO, but not adopted. It is provided here only for guidance on acceptable index values from the researchers who developed the index, Q .

Table 8.4.2-4 Fatigue Serviceability Indices and suggested actions.

Fatigue Serviceability Index, Q	Suggested Action
1.0 to 0.2	Continue regular inspection
0.19 to 0.10	Increase inspection frequency
0.09 to 0.0	Assess frequently
< 0.0	Retrofit, replace, or reassess

8.4.3 Strategies to Increase the Fatigue Serviceability Index

8.4.3.1 General

The Fatigue Serviceability Index can be increased by rational modification of the factors included in its calculation or through retrofit of the detail.

8.4.3.2 Refined Calculation

8.4.3.2.1 Accepting Greater Risk

Traditionally, Evaluation 1 Life has been used in determining remaining fatigue life, with a probability of occurrence of 84 percent, as discussed in Section 8.3.2. If the detail under evaluation has already experienced a long successful fatigue life, bridge-specific factors such as a high degree of redundancy and/or a decreased inspection interval may suggest that the evaluator accept greater risk in the fatigue assessment. As such, the Evaluation 2 Life or Mean Life could be used in the determination of remaining life.

8.4.3.2.2 Using More Accurate Data

A more accurate estimate of the fatigue life refines the Fatigue-Serviceability-Index calculation. Sources of improvement of the fatigue-life estimate include:

- Field measurement of the stress ranges to determine the effective stress as discussed in Section 8.2.1.4,
- More refined analysis to determine the effective stress,
- Weigh-in-motion data to determine the fatigue truck as discussed in Section 8.2.1.3, or
- Site-specific ADTT counts.

8.4.3.2.3 Using a Truncated Distribution

In *MBE* Article 7.2.7.2.3, the *MBE* acknowledges a negative remaining fatigue life or Fatigue Serviceability Index. The equation below estimates the mean, evaluation, and minimum fatigue lives based upon truncating the distribution when no fatigue cracking is evident.

$$Y' = 2.19Y_{mean}e^{0.73\Phi^{-1}[x(1-P)+P]-0.27}$$

Equation 8.4.3.2.3-1

where:

Y_{mean}	=	mean fatigue life before updating
Φ^{-1}	=	inverse of the standard normal variable's cumulative probability function
x	=	variable based upon the fatigue life being updated

- = 0.039 for Minimum Life
 0.074 for Evaluation 1 Life
 0.12 for Evaluation 2 Life
 0.18 for Mean Life
- P = probability of fatigue life being shorter than current age before updating

$$P = \Phi \left[\frac{\ln \left(\frac{a}{2.19Y_{mean}} \right) + 0.27}{0.73} \right]$$

Equation 8.4.3.2.3-2

where:

- a = present age in years
 Φ = standard normal variable's cumulative probability function

The standard normal variable's cumulative probability function and the inverse of the standard normal variable's cumulative probability function are commonly included in commercial spreadsheets.

The fatigue life of a structural detail is typically characterized by a lognormal distribution, as shown in Figure 8.4.3.2.3-1. When the estimated life using Section 8.3.2 is smaller than the present age, the remaining life becomes negative as illustrated. In this situation, if field inspection reveals no cracking, the estimated life is overly conservative.

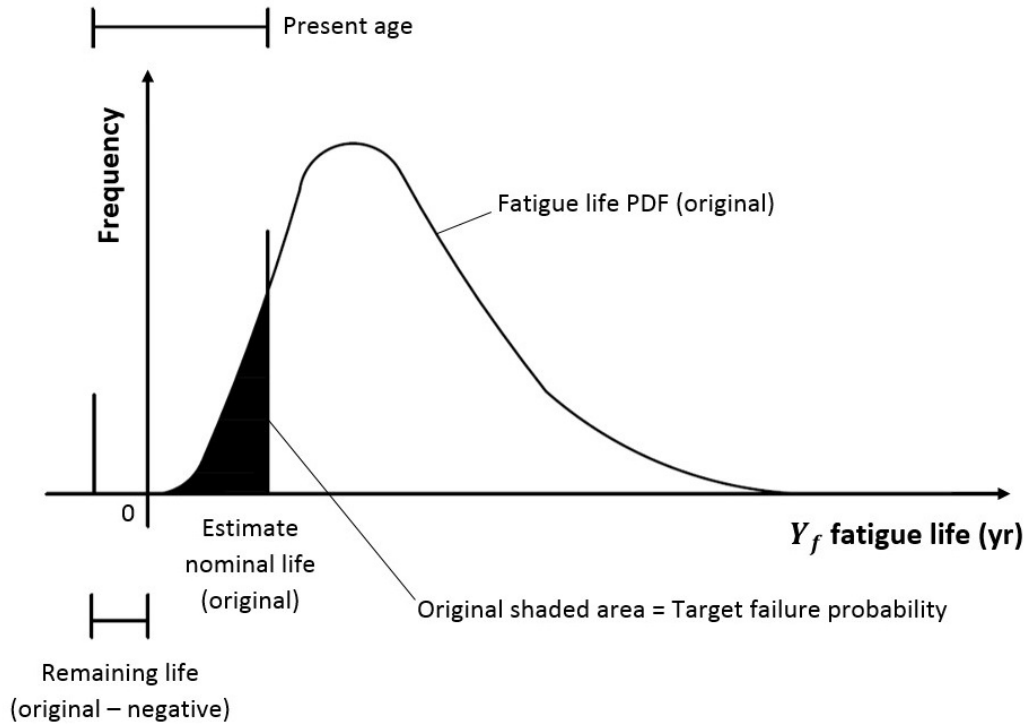


Figure 8.4.3.2.3-1 Probability density function of fatigue life and estimated life.

The equation for updated life is based upon:

- The lower tail of the total life distribution truncated up to the present life
- The eliminated probability P computed
- The resulting probability density function divided by $(1 - P)$ to ensure that the total probability under the distribution curve remains 1.0

Then the updated life is determined to maintain the same reliability level for fatigue life distribution as illustrated in Figure 8.4.3.2.3-2.

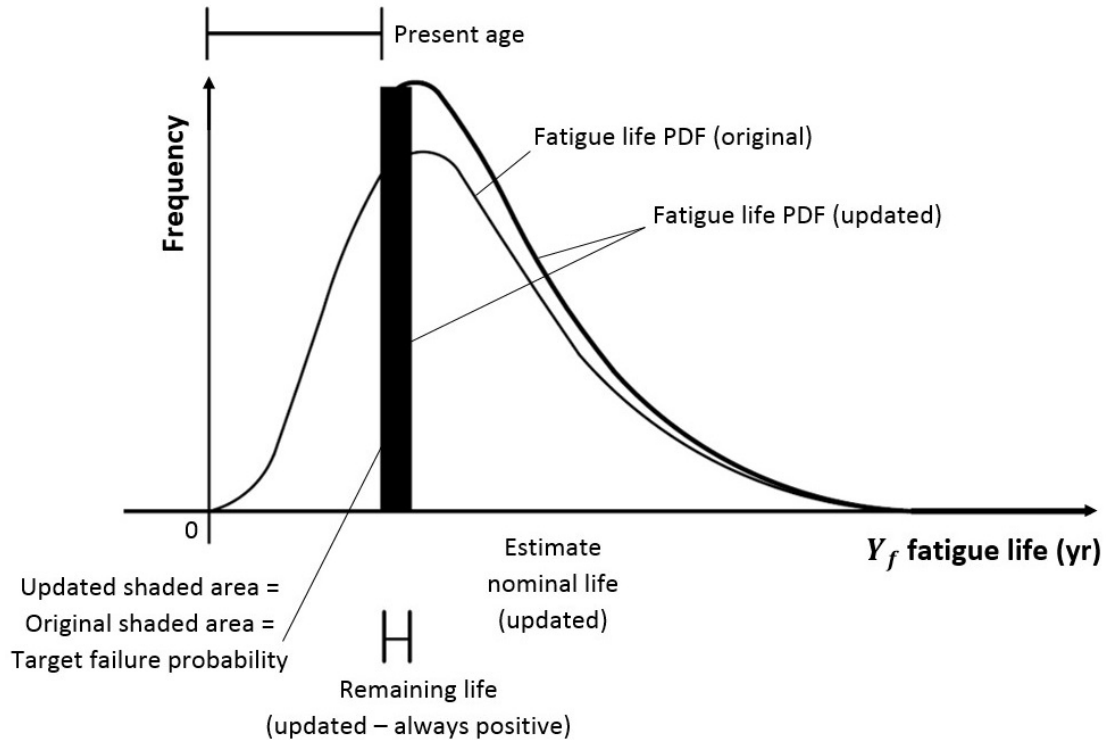


Figure 8.4.3.2.3-2 Truncated probability density function of fatigue life and updated life.

8.4.3.2.4 Example

Update the calculated remaining fatigue life of the end weld of the cover plate of the example in Section 8.3.3.

The cover plate end weld is Detail Category E' from *AASHTO LRFD* Table 6.6.1.2.3-1.

$$Y_{mean} = 63 \text{ years}$$

$$a = 48 \text{ years}$$

Calculate an updated Evaluation 2 Life.

$$Y' = 2.19 Y_{mean} e^{0.73 \Phi^{-1}[x(1-P)+P]-0.27}$$

$x = 0.12$ for Evaluation 2 Life

$$P = \Phi \left[\frac{\ln\left(\frac{a}{2.19 Y_{mean}}\right) + 0.27}{0.73} \right] = \Phi \left[\frac{\ln\left(\frac{48}{2.19 \times 63}\right) + 0.27}{0.73} \right] = 0.14$$

$$\begin{aligned} Y'_{Evaluation2} &= 2.19Y_{mean}e^{0.73\Phi^{-1}[x(1-P)+P]-0.27} = 2.19(63)e^{0.73\Phi^{-1}[0.12(1-0.14)+0.14]-0.27} \\ &= 64 \text{ years} \end{aligned}$$

The remaining life is now $64 - 48 = 16$ years.

8.4.3.3 Retrofit

If the updated Fatigue Serviceability Index is not acceptable, the fatigue life may be increased by retrofitting the critical detail to improve the detail category, as discussed in Chapter 9. This strategy increases the Fatigue Serviceability Index when further enhancement of the calculated Fatigue Serviceability Index, through more accurate estimates, is no longer possible or practical.

CHAPTER 9 ASSESSMENT, REPAIR, AND RETROFIT OF STRUCTURES

In addition to analyzing, designing, and evaluating for fatigue and fracture, it is often necessary to assess damage and provide repair and retrofit for steel bridge structures. This chapter provides a general summary of some common fatigue details (i.e., details for which care and assessment is required to ensure that the design satisfies fatigue requirements). It should be noted that more detailed information about the repair and retrofit of structures for fatigue and fracture is provided in the *Manual for Repair and Retrofit of Fatigue Cracks in Steel Bridges* (Dexter and Ocel, 2013). This reference provides a wealth of information that is not repeated in this chapter.

SECTION 9.1 COMMON FATIGUE DETAILS

Details that may be subject to fatigue cracking may exist on a variety of bridges, such as girder, frame, truss, or arch superstructure configurations. In addition, they may also exist on substructure components.

Fatigue details are most commonly encountered on older bridges that were constructed prior to the mid-1970's² and/or on bridges that lacked proper quality control (QC) measures. As described in Chapters 6 and 7, AASHTO provides design requirements for fatigue and fracture to prevent the problems described in this chapter. Therefore, steel bridges constructed in the modern era using AASHTO fatigue specifications and using proper QC generally do not exhibit these fatigue problems. However, since many pre-1970's bridges remain in service, the issues described in this chapter must still be considered when assessing older bridges.

The fatigue performance of steel bridges reveals that the majority of cases of fatigue damage which have been reported for highway and railway bridges are caused by secondary load effects not considered during design. In most cases, unforeseen interaction between different members and load-carrying systems in the bridge, often combined with details exhibiting low fatigue resistance, have been the cause of fatigue cracking in bridge details. In some cases, a complex stress state may also exist in structural details which is neglected in the traditional line-girder design method and which may have been considered by the designer. The basic mechanism behind most types of fatigue cracking caused by secondary effects is an applied out-of-plane distortion generated by the displacement compatibility of adjacent girders as the truck passes over the bridge, creating a cyclical stress.

A common feature in many details which have experienced fatigue cracking is that they incorporate an abrupt change in stiffness, frequently in unstiffened web gaps where the applied distortion is concentrated. This often results in high local stresses which might eventually lead to fatigue cracking in the detail. The most common types of distortion-induced fatigue damage can

² The fatigue provisions that are used in design today were largely adopted in 1974 and have been modified little since then, so an exact date cannot be defined because there is always a lag between AASHTO adoption and implementation by individual states. However, any bridge constructed in 1974 and before will have poor fatigue details, and bridges constructed between 1975 and 1979 may or may not have poor fatigue detailing.

be found in the connections between stringers and transverse elements, between transverse elements and longitudinal girders, and at the connections of diaphragms and cross-frames.

In addition to the details described above, low fatigue resistance can also be present in elements with coped ends (most significantly at copes with small radii) and cut-short flanges, at connections between girder welded splices, at repair plates that have been welded perpendicular to the primary live load stress, and in riveted structures that employed tack welds to hold plates in position during fabrication and erection. Each of these fatigue details is most prevalent in bridges constructed prior to the mid-1970's.

A few of the more common details and bridge elements requiring careful attention for fatigue are described in greater detail in the following sections. It should be noted that problems with these details are generally not encountered on bridges constructed in the modern era using proper QC measures.

9.1.1 Web Gaps Associated with Out-of-Plane Bending

Out-of-plane bending occurs when a member is loaded such that it twists about its longitudinal axis. Bridge members are normally designed to resist axial tension or compression, shear, or in-plane bending. However, when the bridge is loaded unsymmetrically about its longitudinal axis (e.g., due to a heavy truck in a curb lane), the girders do not deflect equally, and the bridge twists about its longitudinal axis. Local out-of-plane bending can occur at the connection of the cross-frames to the girders and at the unsupported web in the gap between the connection plate termination and the web-to-flange weld.

A common source of out-of-plane bending is the connection between transverse elements (e.g., floorbeams, cross-frames, or diaphragms) and the main longitudinal girders. When the transverse elements deflect or rotate, they cause out-of-plane bending and distortion in the main superstructure members, as illustrated in Figure 9.1.1-1. Rotation, θ , of the transverse elements causes out-of-plane bending in the longitudinal elements, which in turn results in a lateral shift, Δ , in the web gap when there is not a positive connection between the plate and the flange.

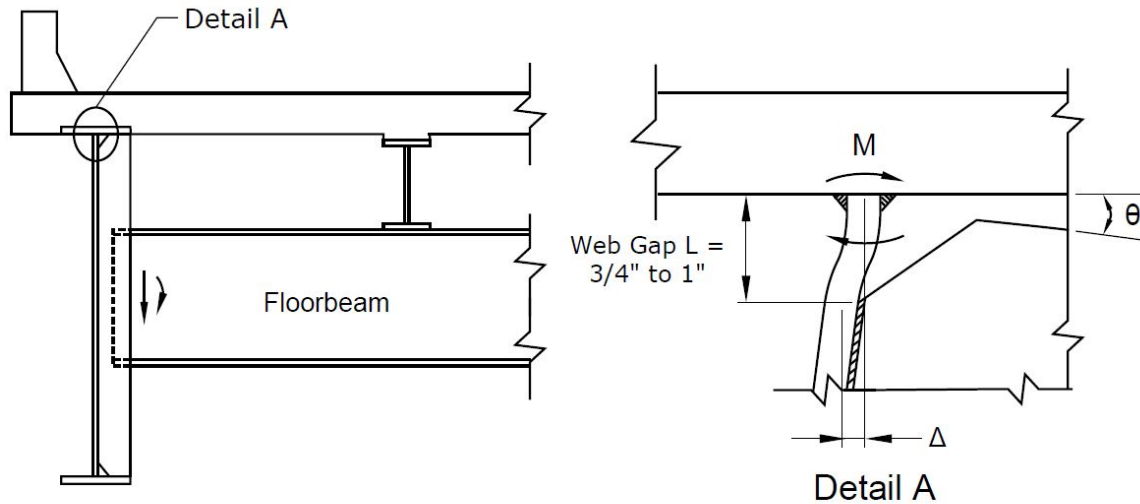


Figure 9.1.1-1 Out-of-plane bending at connection between floorbeam and girder.

The web at the end of the gap is restrained from rotating by the connection plate below the gap, as well as by the concrete deck holding the top flange in place above the gap. This semi-flexible connection is commonly referred to as a “web-gap” detail. As illustrated in Figure 9.1.1-1, the web gap is frequently in the range of $\frac{3}{4}$ to 1 inch between the end of the connection plate and the longitudinal element. The resulting out-of-plane bending is distortion-induced rather than load-induced, and it can occur in welded or riveted members. For a given rotation of the floorbeam, a smaller web gap results in larger web stresses.

Out-of-plane, lateral bending of the flanges occurs in skewed bridges with staggered floorbeams, diaphragms, and cross-frames due to the differential deflection between the girders, as illustrated in Figure 9.1.1-2. When contiguous cross-frames are used, flange deformations are reduced but cross-frame forces become greater. If a gap exists at the end of the stiffeners connecting the cross-frames to the girders and if the connection plate is not connected as required in the current specifications, the large cross-frame forces may introduce cracking in the web gap.

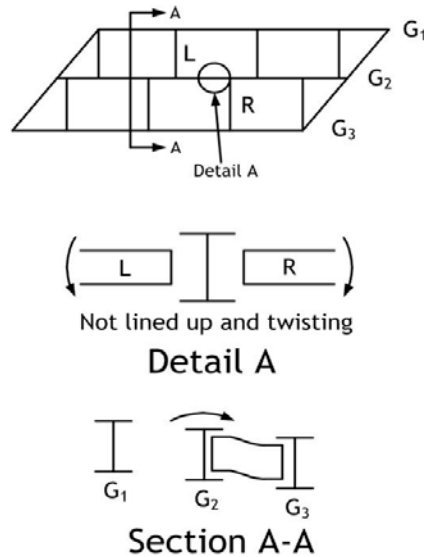


Figure 9.1.1-2 Out-of-plane bending due to differential deflection in skewed bridges.

Another common location for out-of-plane bending is at lateral bracing. For many years, lateral bracing was required by AASHTO and owners as a permanent wind bracing system for the bottom flange. Primary live loads from trucks cause the lateral bracing to vibrate up and down at its midpoint, as well as to lengthen and shorten as it participates in resisting live load forces. This combined movement due to vibration and lengthening bends the gusset plate about its mid-plane and alternately “pushes and pulls” on the web plate.

9.1.2 Fatigue Considerations for Welds

Welds on bridges that were designed after the mid-1970’s and that employed proper QC measures generally do not experience significant fatigue issues. However, older bridges with intersecting welds, longitudinal stiffener butt welds, field welds, or intermittent welds may be susceptible to fatigue cracking.

Intersecting welds are defined as welds that run through each other, overlap, touch, or have a gap between their toes of less than $\frac{1}{4}$ inch. A common location of intersecting welds is the detail where transverse stiffeners and longitudinal stiffeners intersect, as illustrated in Figure 9.1.2-1. Any narrow gap between the longitudinal plates and transverse plates is likely to have a high stress concentration. The intersections of horizontal and vertical weld attachments are fatigue details and can be the source of constraint-induced fracture.

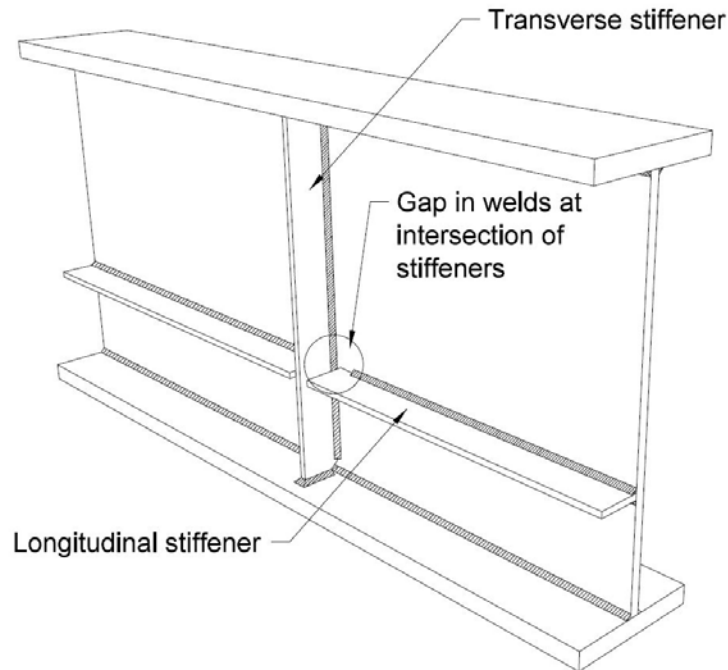


Figure 9.1.2-1 Gap in welds at intersection of transverse and longitudinal stiffeners.

A similar detail occurs at gusset plates for lateral bracing framing into the web at a transverse stiffener. The gusset plate conforms to the strain in the web and acts like a short flange connected to the web. If the gusset plate is interrupted at the transverse stiffener, a crack may form in the gap between the gusset plate and the stiffener, as shown in Figure 9.1.2-2. Modern bridge design requires that the lateral system is connected directly to the girder flange with bolts.

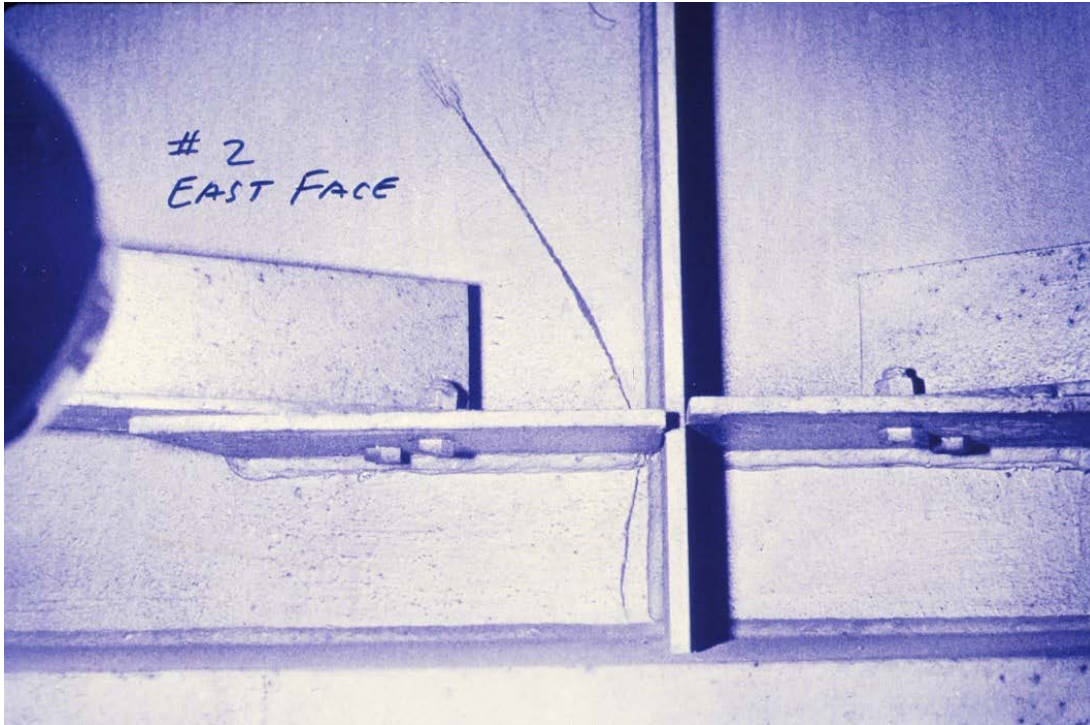


Figure 9.1.2-2 Crack at bottom lateral connection plate.

Another common fatigue detail is longitudinal stiffeners extended the full length of the bridge into tensile regions where they were not required for strength. These full-length longitudinal stiffeners were often butt spliced using welds with no preparation or quality control, often resulting in lack of fusion. Fatigue cracks propagated from the lack of fusion, severing the longitudinal stiffener and creating an edge crack into the web with a length equal to the stiffener width. Although the welded joints were located in regions of relatively low bending stress, large cracks developed after the stiffener weld fractured and propagated under relatively low stress ranges. Figure 9.1.2-3 shows an example of a fracture emanating from a stiffener butt joint.

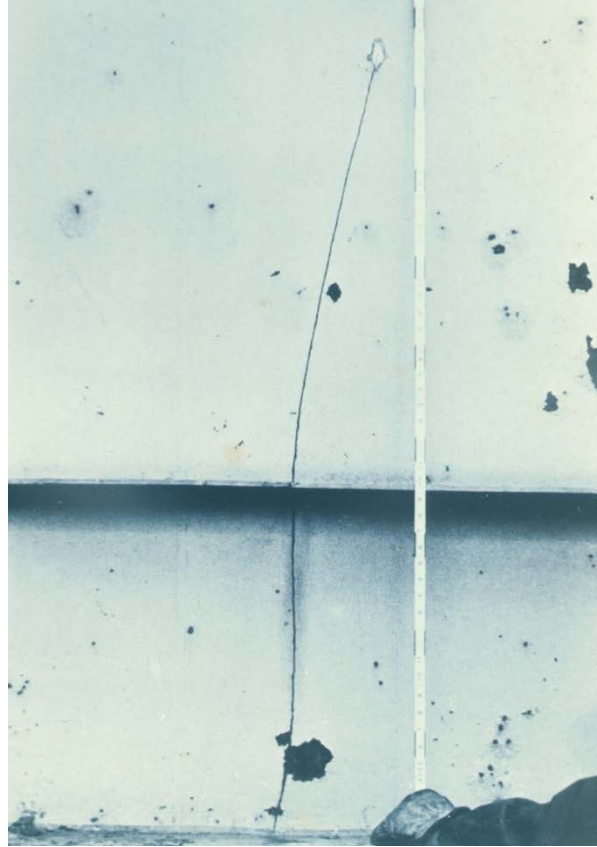


Figure 9.1.2-3 Fracture from longitudinal stiffener splice.

In addition to intersecting welds and longitudinal stiffener butt welds, field welds on older bridges must also be assessed for fatigue. Field welds are often used with patch plates or splice plates to repair corroded areas, to add strengthening components (e.g., to repair corrosion damage), and to correct fabrication errors. Sometimes steel patch plates or splice plates are field welded to those areas of reduced section to increase the total (or static) strength. However, these repairs can be ineffective since the welds may be perpendicular to primary stresses, creating Category D or E fatigue details with what used to just be base metal (a Category A detail). The chemistry of older steels used in riveted construction was often not suitable for welding, and this often led to welds and heat-affected zones with low toughness and fracture susceptibility.

Intermittent welds can also be fatigue details since they contain a series of partial length welds, and the start and finish of each partial weld can be considered as a fatigue initiation point. Between the late 1950's and the early 1970's, intermittent welding, or stitch welding, was often used to connect bridge members. Analysis showed that the stitch welds provided the required strength and that continuous fillet welds were not required. However, the intermittent weld ends resulted in multiple fatigue initiation locations, and the practice of stitch welding of bridge members was discontinued by the mid-1970's. Many bridges with intermittent welds, however, are still in service.

In addition to the fatigue cracking in welds described above, Figure 9.1.2-4 shows a fatigue crack that initiated at a tack weld in a riveted structure. Tack welds were commonly used to hold

individual elements of a member together as final riveting was completed. Tack welds are common and were widely used for decades in the construction of riveted or bolted built-up members. A tack weld would be considered as a Category E detail if the provisions of the *AASHTO LRFD* specifications were used in their evaluation. However, many times tack welds are not significant enough to constitute structural welds. Given their widespread use in flexural and tension members alike, owners have been faced with the challenge of whether to remove what can be thousands of individual tack welds from a large structure in order to alleviate a potential crack initiation site. Research at Purdue University determined that tack welded riveted members, when tested, performed better than the Category C design curve. Therefore for evaluation, tack welds can be considered as a Category C detail. The prior Category E rating was considered too severe. Clarifying language has been provided in the *MBE*. The tack welds studied in the NCHRP 721 project varied but were in the range of 1 to 2 inches in total length (Bowman et al., 2012).



Figure 9.1.2-4 Fatigue crack at toe of tack weld.

Figure 9.1.2-5 shows a fracture that started at an incorrectly located hole that was welded. This resulted in a large lack of fusion and the resulting fracture. The modern remedy for this problem is to fill the hole with a properly tightened high-strength bolt, resulting in a hole with a fatigue resistance comparable to Category B.

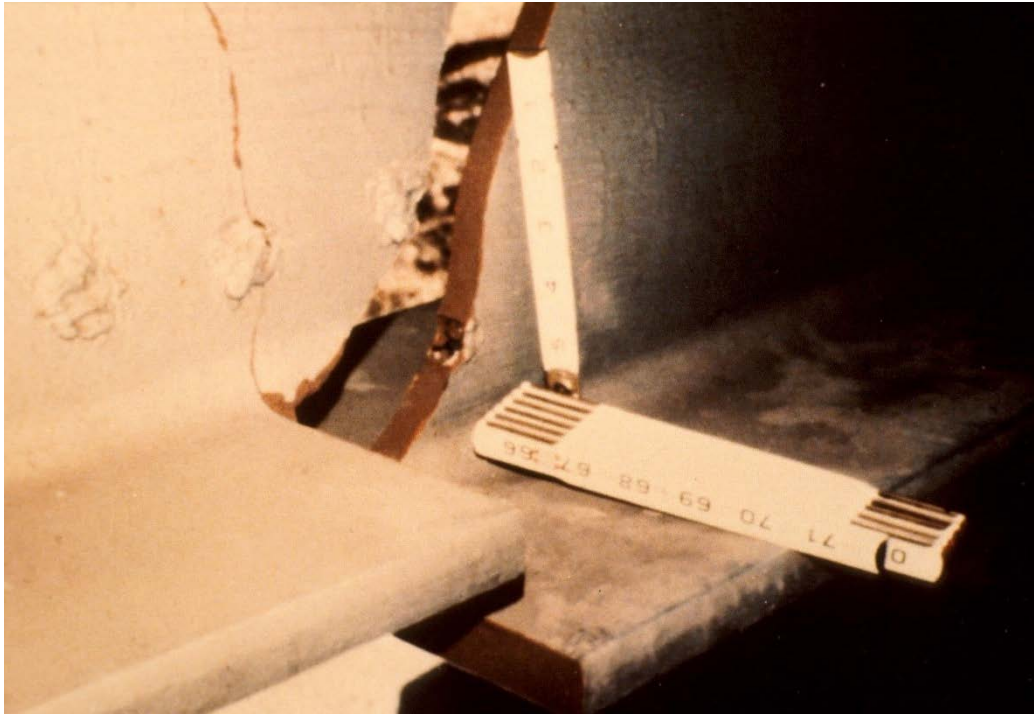


Figure 9.1.2-5 Fracture from welded hole.

9.1.3 Welded Cover Plates

A cover plate is defined as a welded plate generally used in conjunction with a rolled structural shape that increases the shape's flexural resistance by providing additional flange section. Cover plates usually extend over a limited length of a beam, as shown in Figure 9.1.3-1. The use of welded partial length cover plates on rolled beams was popular with designers in many states from 1940 to 1970, but they are seldom used in modern bridge designs. Partial length cover plates minimize the amount of structural steel required, since a simply supported steel beam experiences higher bending stresses at midspan where the plate is utilized. Partial length cover plates are also used in continuous spans in regions of maximum positive moment and maximum negative moment.

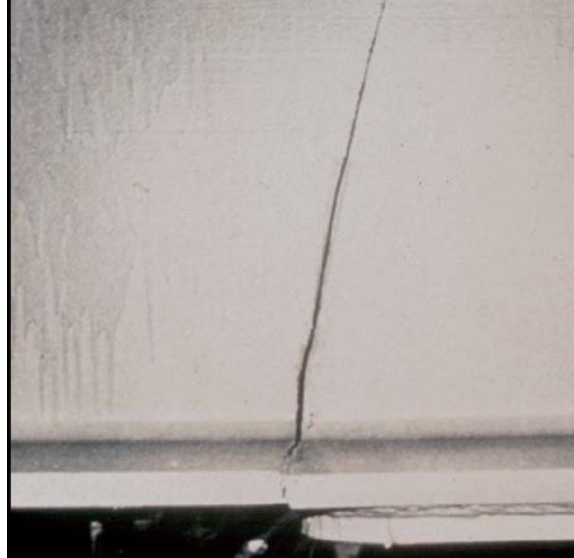


Figure 9.1.3-1 Fatigue crack at end of welded partial length cover plate.

After cover plates were in service and were inspected, it became apparent that the termination point of welded cover plates was a fatigue detail where cracks could initiate. The cracks occur because of fatigue problems associated with the stress concentration at a sudden change in section, combined with the inherent residual stresses at the end of a welded plate. Cover plates were fabricated and attached in a variety of styles, all of which have low fatigue resistance.

To improve this fatigue detail, several attempts were made to lessen the chance of crack propagations in partial length cover plates. For example, some cover plates were tapered or rounded to reduce stress risers. Others were widened to reduce stress risers. However, each of these conditions still resulted in low fatigue resistance. The only successful means of improving the fatigue resistance of cover plates was to terminate the cover plate with a bolted connection during fabrication. The current *AASHTO LRFD* specifications recognizes the superior fatigue resistance of end-bolted cover plates.

However, many existing bridges still have welded cover plates rather than end-bolted cover plates. On these bridges, fatigue cracks normally initiate at the weld toe and then propagate into the flange. The crack front develops a subsurface thumbnail or half penny shape as it propagates through the flange until reaching the inside surface. A fatigue crack at the end of a cover plate moving into the flange and web is shown in Figure 9.1.3-1 and is illustrated in Figure 9.1.3-2. When the fatigue crack has grown to a critical size and stress intensity, then fracture occurs.

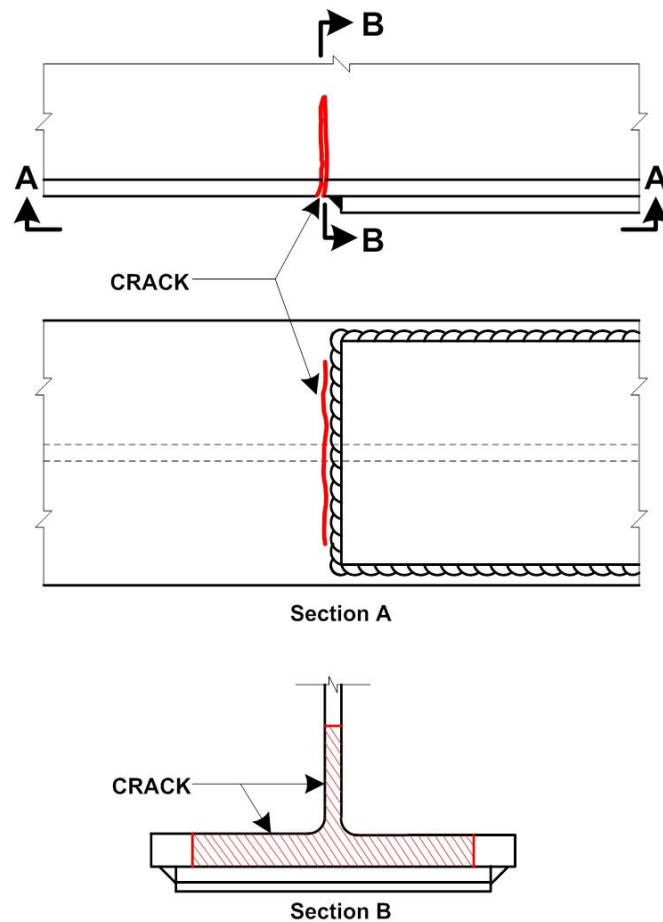


Figure 9.1.3-2 Crack at end of cover plate propagating through the flange and into the web.

The progression of a fatigue crack at a cover plate without an end weld is shown in Figure 9.1.3-3. The crack initiates at the termination of the weld and grows into the flange as an elliptical-shaped crack. Once the crack propagates through the flange, it grows as a two-end crack and then finally as a single-ended crack when the crack reaches the flange tip. The roughness of the fracture surface is an indication of the crack propagation rate. The greater the surface roughness, the faster the crack is propagating. After the crack reaches the flange tip and becomes single-ended, the stress intensity at the crack tip more than doubles, causing the increase in propagation rate.

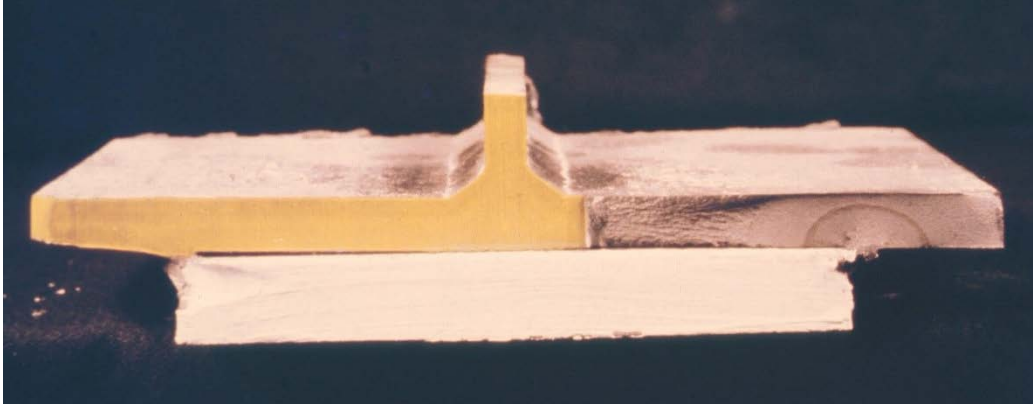


Figure 9.1.3-3 Crack at end of cover plate without an end weld.

It should be noted that many of the fatigue details described above are no longer commonly used in bridge design. However, they may still be present on existing bridges designed prior to the mid-1970's and must therefore be considered when assessing bridges for fatigue issues.

SECTION 9.2 REPAIR STRATEGIES

If fatigue-related problems are encountered in the field (most commonly on older bridges), then a repair strategy must be employed to rectify the problem and to help prevent additional problems. While the specifics of the repair strategy are dependent upon the specific nature of the detail and problem, there are several general repair and retrofit strategies that are common for most fatigue details. These general strategies are described in the following sections.

9.2.1 Understand the Source of Cracking

Before designing any repairs or retrofits, the first step must always be to understand the source of the crack. Without such an understanding, the proper repair or retrofit cannot be determined with any degree of certainty that it will successfully solve the problem. In addition, without such an understanding, any unsuitable repairs or retrofits may result in even worse problems. Therefore, it is essential that repairs and retrofits are not pursued until there is an understanding of why, how, and when the crack formed.

9.2.1.1 Assessment of Fatigue-Driven or Fracture-Driven

A first step in understanding the source of cracking is to assess whether the cracks are driven by fatigue or fracture. In some cases, this can be accomplished visually based on the detailing and crack path. In other situations, however, the crack must be cored to assess the presence of fatigue striations or cleavage fracture. A memorandum issued by the Federal Highway Administration (FHWA) on July 10, 2001 suggests that, for some details in tension zones that are found to be cracked based on inspection, the cracks should not be assumed to be fatigue-related, and cores of the fracture surface should be removed and analyzed for evidence of brittle fracture (FHWA, 2001).

If the crack is determined to be fracture-driven, then a bolted repair is typically used. All similar details that may also be susceptible to cracking must also be assessed. If the cracks are identified to be formed in a brittle mode, then an immediate safety evaluation of the structure should be performed and the potential need for bridge closure should be assessed. In addition, the urgency of this evaluation increases during periods of cold service temperatures.

If the crack is determined to be fatigue-driven, then the next step is to assess whether the crack is load-induced or displacement-induced. Such an assessment is critical in evaluating the suitability of drilling a hole in the crack tip. Drilling of holes should not be considered a universal solution to repair of fatigue cracks.

9.2.1.2 Assessment of Load-Induced or Displacement-Induced

Several strategies can be employed when seeking to understand if the crack is load-induced or displacement-induced. A first step, if it has not already been completed, is to inspect the bridge, focusing on fatigue details and locating any fatigue cracks. If one particular detail has cracked, it is highly likely that other similar details may have also cracked. A keen eye can be the best tool in finding fatigue cracks, looking either for open cracks or for rust staining or discoloration as evidence that oxidized material is bleeding from an existing crack. In addition, two common nondestructive techniques used to expose cracks are dye penetrant and magnetic particle inspection. When fatigue cracks are encountered, the crack should be carefully measured and the specific detail should be thoroughly documented.

In addition, another important step in determining the source of cracking is to understand the geometry of the bridge and how it affects system behavior of the bridge. In some cases, a computer model of the entire bridge may need to be created to better understand the global behavior of the bridge. This is especially applicable for skewed and/or curved steel bridges.

A common strategy for understanding the source of cracking is to apply instrumentation to common details in the bridge. Strain gauges provide an effective way to measure stress ranges on steel bridges, and they can be applied to a variety of structural components, including girder webs and flanges. Weldable strain gauges are shown in Figure 9.2.1.2-1. These strain measurements should be compared with the calculated stresses to evaluate if the analytical model can be used to predict further cracking at the measured location and at similar locations on the bridge.

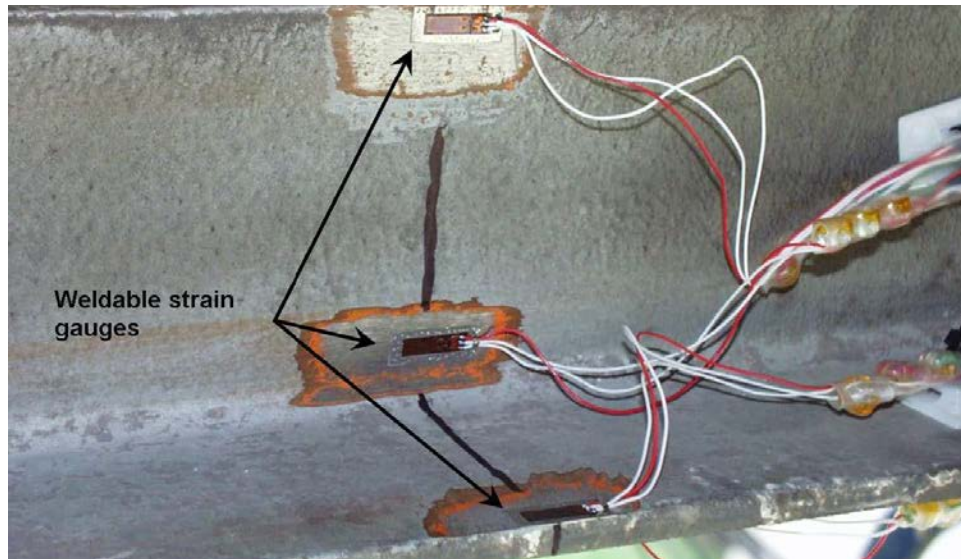


Figure 9.2.1.2-1 Weldable strain gauges applied to a steel bridge member.

As an alternative, displacement measurements can provide a quick and cost-effective strategy in many instances, primarily for benchmarking displacements to a computer model, or assessing the effectiveness of a stiffening retrofit for distortion-induced cracking. Displacement measurements can be obtained using either dial gauges or linear variable differential transformers (LVDT).

In conjunction with instrumentation, load tests can be performed with heavily loaded trucks of a specified weight and axle configuration. The trucks cross the bridge at a slow rate, patterning the truck locations to obtain the worst effect, and the resulting stress ranges are documented and compared with the fatigue limits for the various details being investigated. It should be noted that the fatigue stress ranges and thresholds presented in *AASHTO LRFD* are based on nominal stresses at the detail. If strain gauges are placed near the weld, the local stress concentration will increase the stress above the nominal value, leading to a conservative estimate of fatigue resistance.

The assessments described in this section can be used not only to determine the source of existing cracks but also to predict the remaining life until cracks may develop at other locations.

9.2.2 Design Repair Detail

After the source of the fatigue crack has been determined, the repair detail can be designed. The selected repair detail is a direct function of the specific fatigue detail, the fatigue crack source, and the crack length.

Various repair and retrofit methods are described in considerable detail in the *Manual for Repair and Retrofit of Fatigue Cracks in Steel Bridges* (Dexter and Ocel, 2013). For guidance in determining the most suitable repair detail and understanding the various requirements of each repair detail, this reference provides a wealth of information that is not repeated in this chapter.

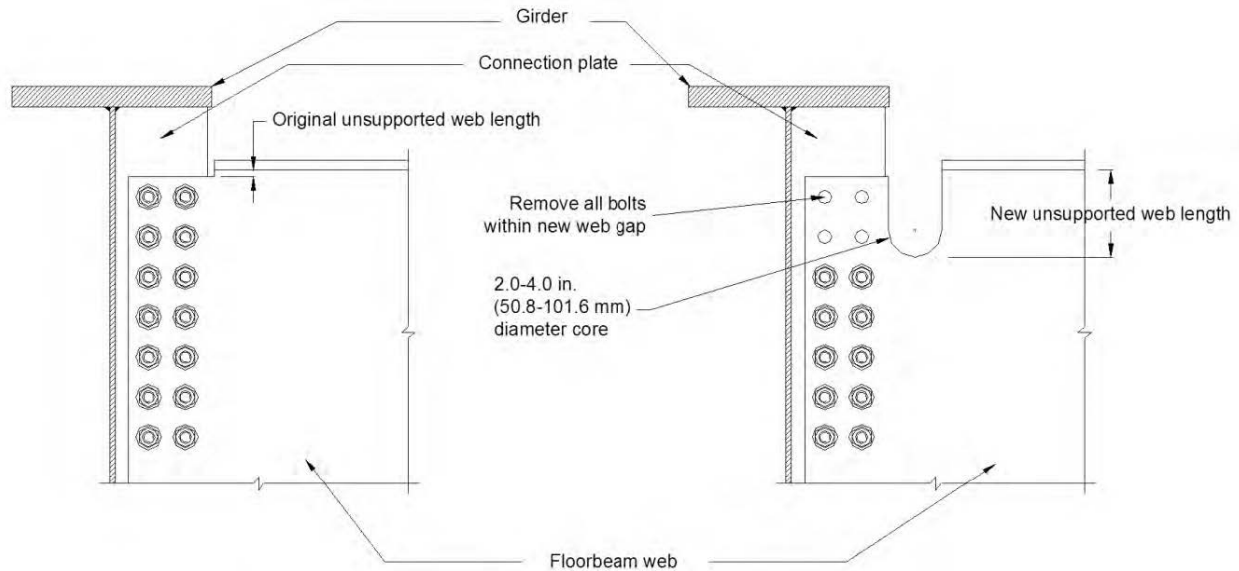
For example, for surface treatments of weld toes with shallow cracks originating from the surface, the following fatigue mitigation methods are available:

- Grinding (disc grinding or burr grinding)
- Gas tungsten arc (GTA) remelting
- Air hammer peening
- Ultrasonic impact treatment (UIT)

Similarly, for out-of-plane distortion, the following repair methods are available:

- Hole drilling
- Diaphragm or cross-frame removal
- Diaphragm repositioning
- Bolt loosening
- Web-gap stiffening (welded attachment, bolted connections, hybrid connections, adhesives, or nails)
- Web-gap softening (gross material removal or large hole retrofit)

For each repair and retrofit method, it is important to understand the limitations of application, the required equipment, the various procedures, and any follow-up recommendations. A work plan should be developed for each repair detail, as illustrated in Figure 9.2.2-1, before commencing any field work.



Procedure

1. Determine the new web-gap length. One recommendation is to increase the length by 10-20 times the original web-gap length. This may be controlled by the number of bolts that can be removed. The shear resistance of the connection cannot be reduced below the loads applied within the connection.
2. Core a 2.0-4.0 in. (50.8-101.6 mm) diameter hole through the floorbeam web, close to the connection plate, but avoid removing material from the connection plate. The placement of this hole will determine the new web-gap length.
3. Flame or plasma cut away the portion of the floorbeam remaining, making the cut tangent to the core.
4. Grind the flame-cut surfaces smooth to remove future crack initiation sites.
5. Prime and paint all bare steel to prevent corrosion.

Figure 9.2.2-1 Work plan to retrofit tie girder/floorbeam connection cracking.

Depending on the complexity and cost of the specific retrofit, it may be appropriate to apply the retrofit method to all similar details with similar loading on a bridge, even if they do not exhibit any fatigue cracks. This may prevent future problems with similar details. However, if the analytical model indicates the stress ranges at the other locations are below the threshold for crack extension, it may be appropriate to do nothing in terms of repair or retrofit.

9.2.3 Validate Repair Detail

The repair process is not complete until the repair detail has been validated. This step is essential, regardless of whether the repair detail is being applied to all similar details on a bridge or whether a decision has been made to do nothing in terms of retrofit. Either way, validating that the correct action was taken is essential.

Two key components of this final step are ongoing inspections and instrumentation. After the work on the bridge has been completed, the details that were repaired or retrofitted should be inspected to verify that the work was accomplished successfully and to note any changes in the

fatigue crack. In addition, a plan should be established for future inspections of the repair or retrofit. This plan should include a prescribed frequency of inspection, drawings showing the specific locations of the repair details, a detailed procedure for inspecting the repair details, and an ongoing log of field measurements associated with the specific fatigue crack or fatigue detail.

In addition, after the work on the bridge has been completed, the instrumentation that was performed to assess the most appropriate repair detail should be repeated. The various strain and displacement values that were documented before the repair should be documented once again after the repair has been completed to help validate the success of the specific repair and to establish a benchmark for future documentation of instrumentation findings. A plan should also be established for future instrumentation. This plan should include a prescribed frequency of instrumentation, drawings showing the specific types and locations of instrumentation, a detailed procedure for instrumentation, and an ongoing log of instrumentation findings. Significant changes in the instrumentation findings should trigger a more in-depth assessment of the repair details.

SECTION 9.3 SPECIAL TOPICS

9.3.1 Constraint-Induced Fracture

In Section 7.1.4.1, the concept of constraint-induced fracture (CIF) is illustrated, specifically with reference to the Hoan Bridge that fractured in 2001. In response to that fracture, FHWA issued a memorandum on July 10, 2001 to the states to highlight the problem and to suggest some remediation measures (FHWA, 2001). Since this memorandum was published, AASHTO has taken action to include CIF as a design consideration in *AASHTO LRFD*. Specifically, welds should be spaced with a minimum 1-inch gap so as not to intersect. While this may be appropriate for new design, research after 2001 has found that the critical distance for causing CIF is when the welds come within 0.25 inches or less, as described in Section 7.1.4.1. Therefore, for the assessment of existing bridges, the 0.25-inch rule may be used, as this is not outlined in the 2001 FHWA memorandum nor published in the *MBE*.

Possible corrective measures may include grinding or drilling away welds to remove the intersecting condition to at least meet the 0.25-inch criterion. Additionally, holes can be drilled above and below the intersecting weld that would effectively capture any fracture between the holes if it were to form.

9.3.2 Over-Height Vehicle Collisions

In addition to the fatigue details previously described in Section 9.1, a vehicle or vessel collision with a steel girder superstructure could also cause significant damage to a bridge (see Figure 9.3.2-1). Overpass bridges which cross over an interstate, for example, can be subjected to over-height vehicle collisions. Special loads or oversized loads may exceed the provided vertical clearance, and similarly, a bridge over a navigable waterway could also be hit (Chavel and Yadlosky, 2011).



Figure 9.3.2-1 Damage to a steel bridge girder due to an over-height vehicle collision.

A common method of repair for over-height vehicle collisions is heat straightening. Repair and retrofit using heat straightening is described in considerable detail in *Heat Straightening Repairs of Damaged Steel Bridges, A Technical Guide and Manual of Practice* (Avent and Mukai, 1998). As described in this reference, primary keys to a successful repair are: (1) selecting the heating patterns and sequences, (2) controlling the heating temperature and rate, and (3) controlling the applied restraining forces during repair.

Similar to the steps described in Section 9.2, repair and retrofit for over-height vehicle damage should generally include assessment of the degree of damage (particularly an examination of cracking at the collision location and at the toes of adjacent attachments such as cross-frames) and review of heating patterns, temperature control, and any jacking plans submitted by the repair contractor. In addition, the supervision of repairs should include monitoring the temperature, controlling the restraining forces, reviewing the proposed heating patterns, and checking geometric tolerances after straightening is completed.

Based on research from NCHRP Report 604 (Connor et al., 2008), it is recommended that the number of heat straightening repairs at a specific location be limited to two. Research has demonstrated that, after the third damage and repair cycle, there is a substantial decrease in the fatigue life at some details, along with a decrease in the base metal fracture toughness where the impact occurred.

Lastly, it is often found that impact damage may cause actual brittle fractures in the vicinity of the impact location. Generally, this does not mean the base metal is inadequate, but it is due to dynamic loading produced during the vehicle impact. Chapter 2 explained that the fracture toughness of steel is related to loading rate and temperature. Additionally, the AASHTO Charpy V-notch (CVN) requirements were established based on a temperature shift concept that equates the results from a dynamic Charpy impact toughness to that of a static fracture toughness at an intermediate loading rate since bridges are typically not loaded at true dynamic rates. When a bridge is struck by an over-height vehicle, this assumption is no longer valid because the bridge is being impacted at a true dynamic rate. Therefore, the AASHTO CVN toughness requirements would not be sufficient to prevent brittle fractures from an over-height vehicle impact, and finding brittle fractures after these events should not be surprising.

9.3.3 Fitness-for-Service Analysis

A fitness-for-service (FFS) analysis is a quantitative engineering evaluation that is performed to demonstrate the structural integrity of an in-service component that may contain a flaw or damage (API, 2007). More specifically, FFS is a methodology that accounts for actual service stresses, flaw or damage zone sizes, as-built material properties, and operating environment to determine the actual safety or reliability of a structure in its present condition or its expected future state. FFS provides a common sense engineering approach to evaluating the suitability of a structure for its intended service. Practical benefits of FFS include a foundation for establishing the remaining life of a structure, as well as a basis for making capital-based decisions for repair or replacement.

FFS is applied most extensively to steel structures, since steel is widely used in many different types of structures and can be readily fabricated by welding. Welded joints inherently contain discontinuities or stress concentrations, and traditional design of steel structures accounts for these discontinuities and stress concentrations by conservatively limiting the size of discontinuities permitted in fabricated joints and by applying cautious factors of safety to joint stresses. In effect, traditional design assumes that no significant discontinuities or service-induced damage (e.g., fatigue cracking, corrosion, or distortion from collision) exists in the structure.

In contrast, FFS acknowledges the presence of discontinuities, stress concentrations, and service-induced damage and assesses the structure in its existing or anticipated condition. Therefore, FFS provides a quantitative assessment that is based on rational evaluation of stresses, material properties, nondestructive examination, and fracture mechanics (Vecchio, 2006).

An FFS assessment generally includes the following procedure:

- Review original design and operating history – may include required safety margins, test results, material certificates, repair records, and remaining fatigue life requirements
- Assess any flaws and/or damage – quantify nature and extent of existing damage
- Perform stress analyses – strain gauge analyses are most beneficial since they provide actual service loading data, but finite element analyses can also be used
- Determine critical damage size and/or remaining life – often the most important part of an FFS assessment since it establishes the need for repair or replacement
- Design repairs or replacement, as needed – must address any critical damage size and/or remaining life requirements
- Perform in-service monitoring – regardless of the outcome of the FFS analysis, ongoing monitoring is essential to ensure the continual proper functioning of the structure

FFS is never pursued during design, and it is generally considered only as a last resort for evaluation. It requires a very accurate representation of the flaw size and shape, an accurate state of stress, and considerable material testing to understand the fracture toughness. Therefore large amounts of data and input are needed, and it often requires many assumptions as well. FFS can be quite complex and challenging in many cases.

Due to its complexities and its unique application to each situation, FFS cannot be covered extensively in this Manual. More information is available in specifications such as *Fitness-For-Service* (API, 2007) and *Guide to Methods for Assessing the Acceptability of Flaws in Metallic Structures* (BS 7910) (British Standards Institute, 2015).

9.3.3.1 Fitness-for-Service Case Study

A fitness-for-service evaluation was performed on the electro-slag welds (ESW) of the west Fremont Bridge approach superstructures in Portland, Oregon, as requested by FHWA. The approach superstructure, fabricated in 1970, consists of two trapezoidal steel box girders connected by rolled steel crossbeams and a reinforced concrete deck continuously composite with the box girder and crossbeam top flanges. A photo of the bridge is presented in Figure 9.3.3.1-1, and a typical section is shown in Figure 9.3.3.1-2.



Figure 9.3.3.1-1 Fremont Bridge in Portland, Oregon.

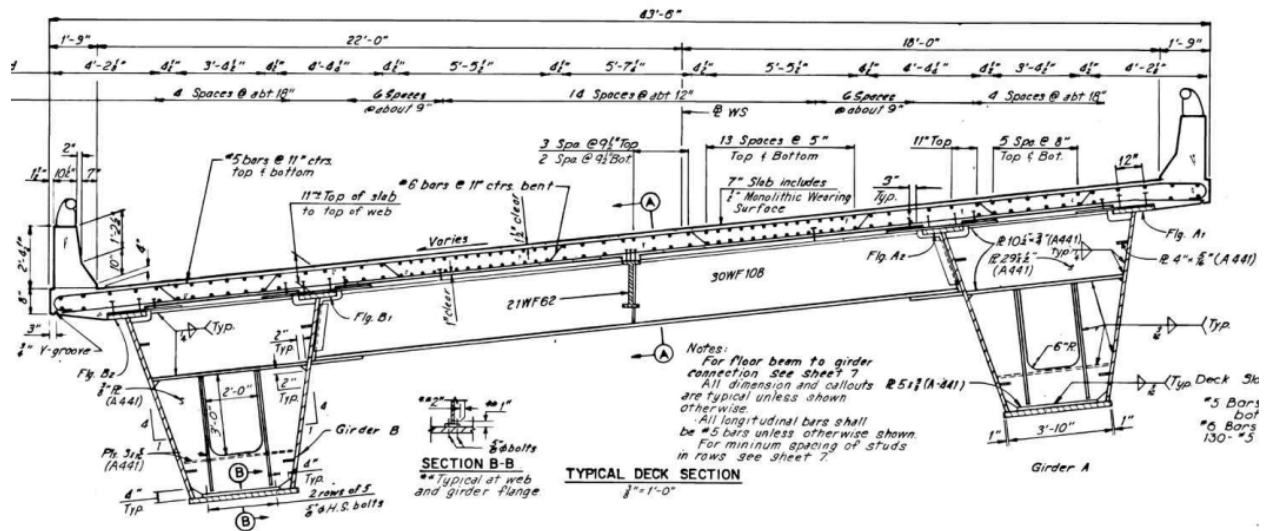


Figure 9.3.3.1-2 Typical cross section of Fremont Bridge based on original drawings.

This evaluation required gathering knowledge of the service loads, fabrication stresses, material properties, non-destructive testing, and failure analysis pertaining to the weldments in question, as described below. The serviceability of the weldments was assessed based on the fatigue and fracture performance. This FFS evaluation facilitated the development of repair or inspection requirements to assure public safety. A comprehensive report of the FFS findings is presented in *A Fitness-for-Purpose Evaluation of Fracture Critical Electro-Slag Welds* (Lovejoy, 2009). The following is a general overview of the primary findings and conclusions.

SERVICE LOADS – The first FFS evaluation involved service loads. No formal load rating or seismic analysis was performed. However, it was determined that the maximum design stress for the box girder flange plates was less than or equal to 55 percent of the minimum yield stress of the base metal, or 27.5 ksi. In addition, structural load testing concluded that the maximum thermal stress range was approximately 3.0 ksi, the maximum single event live load was less than 6 ksi, and the root-mean-cube effective stress range was less than 2.0 ksi.

FABRICATION STRESSES – Residual stresses from the welding process were shown by previous studies to have a core of triaxial tension and a compressive outer shell surrounding the weld region. The magnitude of these stresses was near the yield strength of the weld metal.

MATERIAL PROPERTIES – The tensile, toughness, and crack growth threshold properties of the base heat affected zones (HAZ) and weld metals were quantified. The lowest measured fracture toughness, as defined by the small scale yielding criteria applied to ASTM E 1820 test data, was found to be 97 ksi-in^{1/2} in the weld metal at 0°F. The minimum fatigue crack growth threshold measured, as defined by ASTM E 647, was 8.4 ksi-in^{1/2} in the weld metal and 7.1 ksi-in^{1/2} in the base metal. A sample curve showing Charpy V-notch data in a heat affected zone is presented in Figure 9.3.3.1-3.

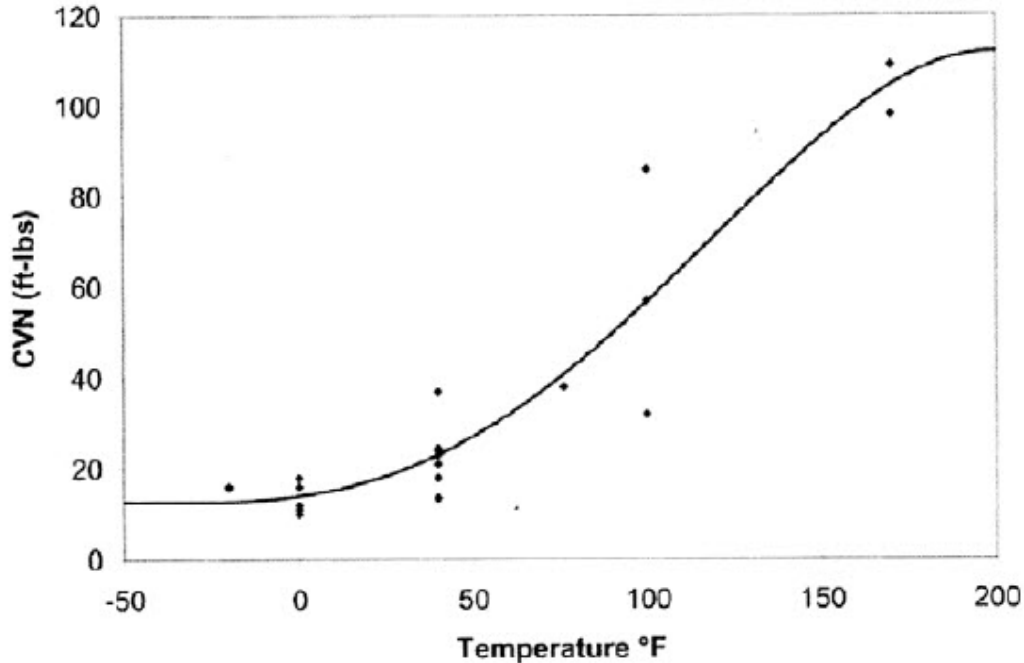


Figure 9.3.3.1-3 Charpy V-notch data in heat affected zone.

NON-DESTRUCTIVE TESTING – Based on the original fabrication inspection documents and previous weld testing, the most likely size of weld defects to escape inspection was found to be less than $\frac{1}{4}$ inch in maximum dimension. The largest flaw anticipated to escape detection is $\frac{1}{2}$ inch in minimum dimension. Two of the 20 fracture critical electro-slag welds inspected contained rejectable defects based on the AASHTO/AWS D1.5 *Bridge Welding Code*. One of these welds with ultrasonic testing rejectable defect indications was inspected with radiographic testing, and no defects were identified. Based on radiographic testing and detailed analysis of the ultrasonic testing results, these defect indications were not considered to be problematic. A photograph of ultrasonic testing of the electro-slag welds is presented in Figure 9.3.3.1-4, and fusion lines in the electro-slag welds are shown in Figure 9.3.3.1-5.



Figure 9.3.3.1-4 Ultrasonic testing of electro-slag welds.



Figure 9.3.3.1-5 Fusion lines in electro-slag welds.

FAILURE ANALYSIS – Based on the quantified data previously described, a failure assessment was made considering two modes of failure – brittle and ductile. Based on the strip yield theory of combined failure modes, the electro-slag welds were found to be very unlikely to fail under even the most extreme combination of service loads and relatively low material crack tolerance. Critical crack dimensions were on the order of four inches for an assumed through-thickness crack in a finite width plate. Given the maximum crack size to escape non-destructive testing, the fatigue crack growth threshold, and the service loads, fatigue crack growth under live load was not anticipated for the service life of this structure. From a traditional Stress Life (S-N) approach, infinite fatigue life was predicted based on comparison with fatigue testing of similar electro-slag welds.

As a direct result of the fitness-for-service evaluations on this bridge, it was concluded that the welds have sufficient toughness and fatigue resistance to remain in-service with no retrofiting. More specifically, the FFS evaluations led to the following conclusions:

- The electro-slag weld metal had equal strength but slightly less ductility than the base metal.
- The toughness was substantially lower than the base metal, but it was adequate to sustain anticipated service conditions.
- The fatigue crack growth threshold indicated that fatigue crack growth was very unlikely under service loads.
- The fabrication and inspection quality of these welds was very good. A flaw larger than $\frac{1}{2}$ inch is unlikely to exist in any of the electro-slag welds, and they are probably less than $\frac{1}{4}$ inch.
- The bottom flange welds experienced higher fatigue stress ranges than the upper flange welds.
- From a conventional S-N approach, the electro-slag welds are expected to have an infinite fatigue life.
- Retrofitting of the electro-slag welds is not necessary nor is it recommended.
- A rigorous yet reasonable non-destructive testing program can ensure public safety.

CHAPTER 10 NON-WELDED COMPONENTS

Although fatigue and fracture are generally associated with welded construction, other structural elements can also be subject to the effects of fatigue or fracture, including riveted or bolted members, reinforcing or prestressing steel, cable hangers, tendons, and cable stays. This chapter focuses on the fatigue and fracture characteristics of non-welded components.

SECTION 10.1 BUILT-UP MEMBERS

10.1.1 Behavior of Riveted and Bolted Connections

The fatigue behavior of mechanically fastened connections is an important part of the design of new high strength bolted connections, as well as the assessment of existing riveted and bolted members. Mechanically fastened connections are used in many applications, such as bolted field splices of girder and truss members, for the connection of bracing elements, and as part of riveted or bolted built-up-member construction. In general, mechanically connected details have a better fatigue life than equivalent welded details. They do not introduce the same types of internal discontinuities, stress concentrations, or residual stresses associated with welding and tend to distribute connection forces over a larger portion of the connected element.

The introduction of holes into a structural member does however cause its own form of stress concentration. The presence of the hole interrupts the uniform flow of stress across the width of the element. For the simple case of an infinitely wide plate with a central hole, the stress at the edge of the hole, parallel to the stress field, is three times as large as the nominal stress on the net section. This is known as the stress concentration factor, as it relates the true stress in the presence of the discontinuity to a reference or nominal stress on the gross or net section. Figure 10.1.1-1 depicts this general case showing the elevated stress condition near the edge of the hole.

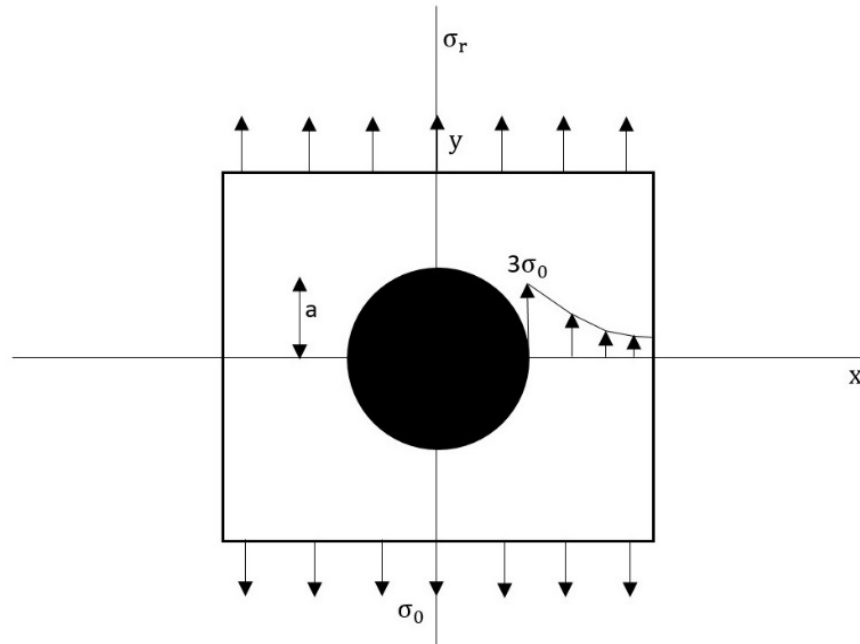


Figure 10.1.1-1 Stress concentration caused by central hole.

Structures however are not composed of infinitely wide plates but rather elements of finite thickness in which the holes generally occupy a portion of the cross-sectional area. Application of the load through fasteners in bearing against the edge of the hole increases the stress concentration effects as compared to uniform stress applied to the entire width of the plates that would be assumed when load is transferred by friction and clamping force. These stress concentrations in bearing connections are understood and documented through many full-scale tests of bolted and riveted members. The presence of these holes and edge bearing loading conditions are accounted for in the *AASHTO LRFD* specifications through the specific details and categories used for mechanically fastened joints.

Although mechanical connections are not as fatigue sensitive as welded connections, the fatigue strength of riveted or bolted built-up sections is a more severe fatigue condition than base metal of basic rolled shapes and plates due to the stress concentration effects discussed above. The presence of punched or drilled holes provides a reduction in fatigue life compared with the plain member. Punched holes create a less desirable fatigue condition because the act of punching results in damage and permanent imperfections around the edge of the hole. For holes that are drilled full size, sub-punched, or sub-drilled and reamed to the proper size, the edge condition of the holes is improved and the fatigue resistance is enhanced. These different hole conditions are treated with different fatigue categories in *AASHTO LRFD*.

10.1.2 Bolted Connections with Bolts Loaded in Shear

High-strength bolted connections are commonly used in steel structures. Bolts are typically used to connect distinct elements of the structure together in the field. The most common use of bolts is in shear type connections. These include common connections such as flange butt splices, the

connection of diaphragms and cross-frames to transverse connection plates, and for the assembly of large elements such as truss members, tie girders, and edge girders in long-span structures. Most commonly, high-strength bolts are installed in a pretensioned condition, creating a clamping force between the elements.

In connections that transmit load by shear, the load transfer can occur by some combination of friction between the plies created by the bolt clamping force or by bearing of the bolt against the edge of the connected material. It is likely that in a bolted connection, a certain number of bolts are in bearing at any one time, so the true nature of load transfer is difficult to ascertain. Kulak, Fisher, and Struik (2001) discuss the behavior of high strength bolted friction connections as an example of load transfer and fatigue.

In the simple butt splice connection shown in Figure 10.1.2-1, assuming that all of the load transfer is by friction, there is a significant discontinuity in strain between the main plate and the upper and lower splice connection plates. At one point, the main plate carries 100 percent of the applied load and is fully strained. At the same point, the connected plate is clamped to the main plate yet carries no load. Under the action of cyclic loading, a small amount of slip occurs at this location causing cracks to form from the plates rubbing against each other. This is the cause of fretting fatigue. Numerous tests have demonstrated that the cracks initiate in the faying surface near the end of the splice plates resulting in gross section failures of the main plate. Because the pretensioning forces from bolting do not uniformly compress the lap splice to the main plate, slip or fretting can occur in the main plate between the end of the splice plates and the first line of bolts.

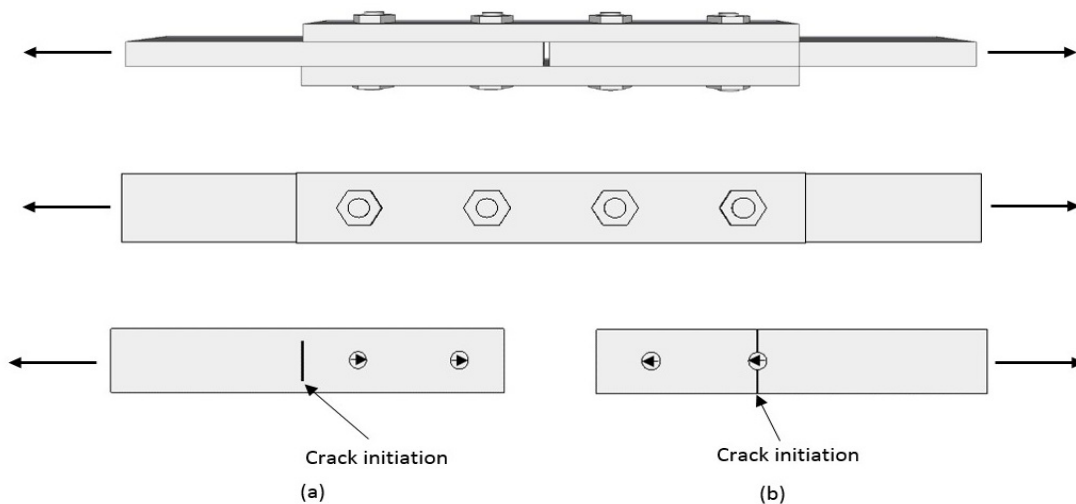


Figure 10.1.2-1 Basic failure modes (a) gross section failure and (b) net section failure.

The other type of fatigue failure that can occur is crack initiation and propagation from the edge of the bolt hole. In this type of failure, cracks initiate at the edge of the hole and grow across the

net section of the member. These types of cracks are more likely to form in structures where the slip resistance of the connection has been exceeded, or where the bolts are in bearing against the edge of the hole. The “pin type” loading of the bolt against the edge of the hole results in a significant stress concentration along the lateral edges of the hole. Eventual failure is by fracture of the net section.

In either case of fretting or net section failures, the fatigue failure is always known to occur in the connected material and not in the bolt itself. Results from hundreds of fatigue tests on high-strength pretensioned bolted connections are presented by Kulak, Fisher, and Struik (2001).

As shown in Figure 10.1.2-2, the test data indicate that Detail Category B is a conservative and reliable estimate of the expected fatigue resistance of high-strength bolted splices. Although the Detail Category B classification was originally developed from tests conducted on plain welded beams, this detail category constituted a reasonable lower bound to the test data for bolted joints. The use of this 97.5 percent survival value for evaluating the fatigue resistance of bolted connections is expected to be conservative, especially for joints subject to reversal loading, since the compression portion of the load cycle is not expected to contribute significantly to crack growth.

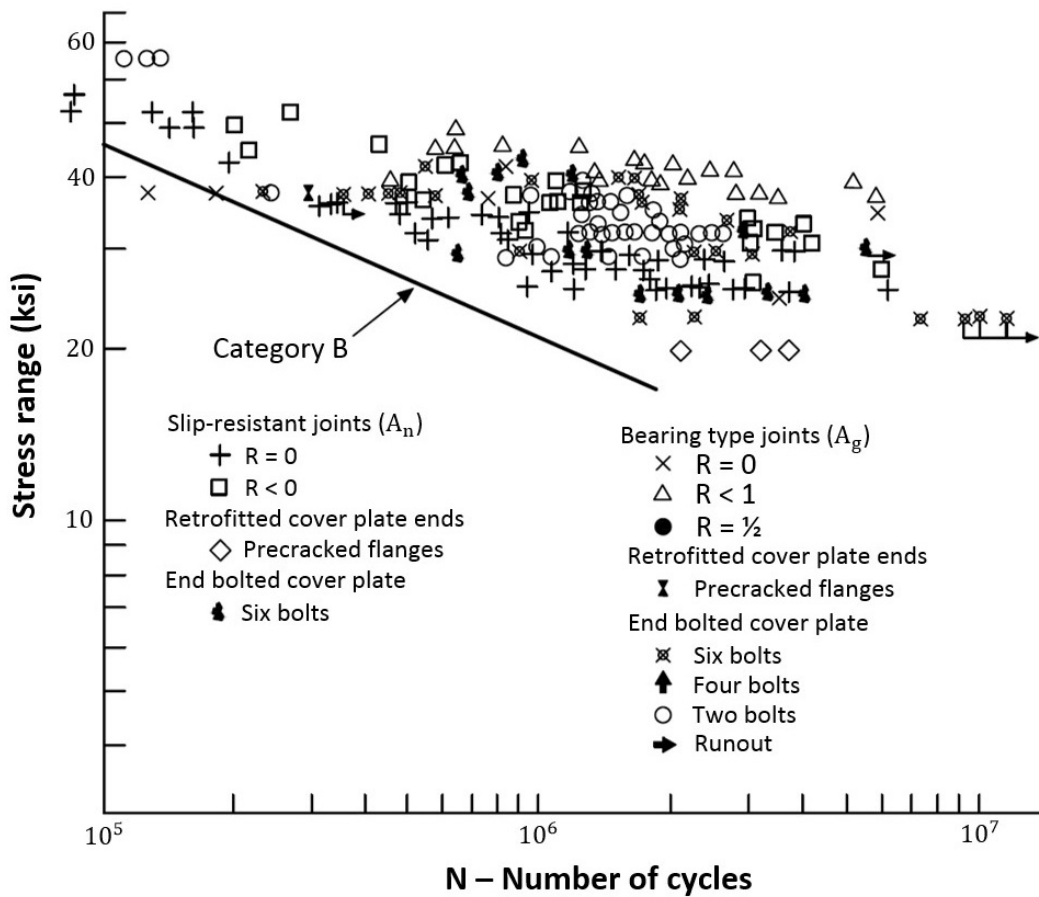


Figure 10.1.2-2 Results of fatigue tests on high strength bolts.

When compared to the test data from welded details, the scatter of bolted shear splice test data is much greater. This is due to several sources. First, the test data were compiled from a wide variety of sources and various different types of details that were tested. This explains some of the scatter. In addition, welded details have a pre-existing tensile residual stress that results in the entire stress range causing damage during the test. The bolted connections do not include the same level of residual stress, and therefore every cycle is not as likely to cause damage especially for those details tested in reversal.

For design of bolted connections for fatigue, *AASHTO LRFD* provides four approaches:

1. For high strength bolted joints designed as slip-critical and using pretensioned bolts installed in holes drilled full size or sub-punched and reamed to full size, stresses are to be computed based on the gross section and Detail Category B applies.
2. For high strength bolted joints designed as bearing connections but with pretensioned bolts installed in holes drilled full size or sub-punched and reamed to full size, stresses are to be computed based on the net section and Detail Category B applies.
3. For evaluating the gross and net section stress in members with pretensioned bolts installed in holes punched full size or for evaluating the net section stress in members connected with non-pretensioned bolts, Detail Category D applies.
4. For connections between angles or tee members to gusset plates, an additional correction is required to reduce the member effective area due to the effects of shear lag. The fatigue categories remain the same as above, but the member area is reduced.

In Cases 1 and 2 above, the holes are fabricated in such a way that damage is minimized and high strength tensioned bolts are used in the connections. This is the most favorable condition. The distinction between the gross section (for slip critical connections) and net section (for bearing connections with tensioned bolts) reflects the severity of the local stress condition around the holes in each type of connection. (It should be noted that each type of connection is Category B, but the method of calculating the stress is different. For pretensioned connections, the gross section is used, but for bearing connections, the net section is used. Therefore, the stress on the net section can be viewed as more severe than the stress on the gross section.) Case 3 includes a series of less favorable conditions. Holes punched full size contain crack initiation sites in the final member. Connections using non-tensioned bolts are prone to slip and stress concentration at the hole edges under repeated loading. For each of these conditions, Detail Category D applies.

10.1.3 Bolted Connections with Bolts Loaded in Tension

The less commonly used joint configuration in bridges is one in which bolts are loaded in direct tension or direct tension and the additional effects of prying action. Prying action effects are possible when connected elements try to separate under the application of the applied tensile load. These tensile loads can come from direct tension (i.e., the true hanger type connection) or as a result of end restraint of moment in deep framed connections. As the connected elements separate, the high-strength bolt is subjected to an additional prying force due to the flexibility of the outstanding leg of the connected element. The bolt is subjected to tension as well as a certain

amount of bending, as shown in Figure 10.1.3-1, and the cyclic effects of the prying force can cause crack growth in the threaded portion of the bolt with cracks initiating at the thread root.

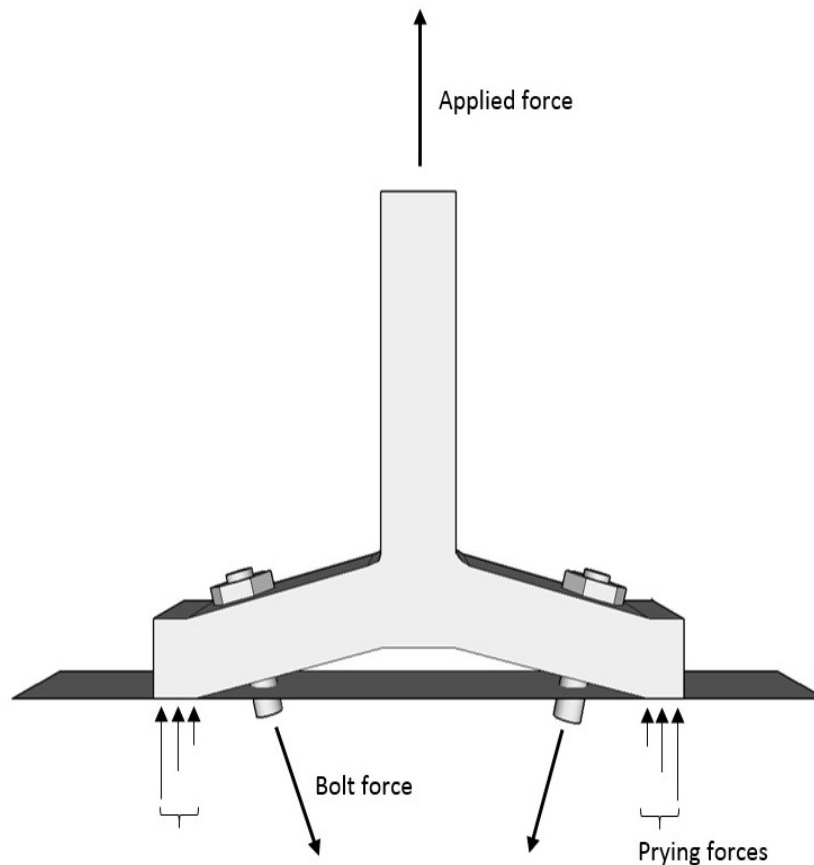


Figure 10.1.3-1 Prying forces acting on bolted connection.

The amount of prying action the bolt will experience in a connection is strongly influenced by the amount of preload in the bolt. Properly tensioned bolts in a very stiff connection will experience very little prying action under cyclic loading. Conversely, in a flexible connection, significant prying forces in the bolt are present, and if the bolt preload is low, separation of the connected parts is likely. This leads to large increases in bolt tension, yielding of the bolt is possible resulting in even greater elongations, and fatigue failures have occurred.

AASHTO LRFD requires that high-strength bolts in axial tension satisfy the fatigue requirements considering the effects of direct tension plus the effects due to prying action. As a safeguard against fatigue failure, the calculated prying forces are limited to 30 percent of the externally applied direct tension. The specification also prohibits the use of ASTM A307 bolts in connections subjected to fatigue. *AASHTO LRFD* provides an approach to compute the load effects due to prying action and flexible connections. This approach can be universally applied to loads of any limit state, including strength, service, and fatigue.

For mechanically fastened web angle connections, a combination of larger gage length and reduced angle thickness (as permitted by the beam end shear design) is required both for preventing angle cracking and for preventing fastener failure, and both for repair and for new design.

10.1.4 Riveted Members and Connections

Prior published reports, such as Fisher, Kulak, and Smith (1998) and Kulak, Fisher, and Struik (2001), comment that the experimental evidence demonstrates that the fatigue cracking in riveted connections and built-up riveted members originates from the connected material and not from a failure of the rivet itself. The fatigue resistance is related to the characteristics of the connected part such as the size and condition of the hole, the method of hole forming, the bearing conditions of the rivet against the edge of the hole, and the clamping force provided in the connection. They comment that the influence of clamping force, bearing condition, and method of hole formation have not been assessed in a rigorous way. Although these factors may have an influence on fatigue resistance, their individual contribution has not been studied. Rather, the fatigue resistance of built-up riveted members has been established by tests of full-size or near full-size members loaded in tension or bending. The members were frequently removed from in-service bridges and were deemed to be undamaged from a fatigue perspective at the time of testing. A plot of the available test data, presented in Figure 10.1.4-1, shows a significant amount of scatter in the available fatigue life in the members that were tested. Most of these members were made from mild steel, but several tests of wrought iron members are also included in the test data. The results primarily include riveted built-up flexural members, with a more limited number of direct tension fatigue tests of truss members.

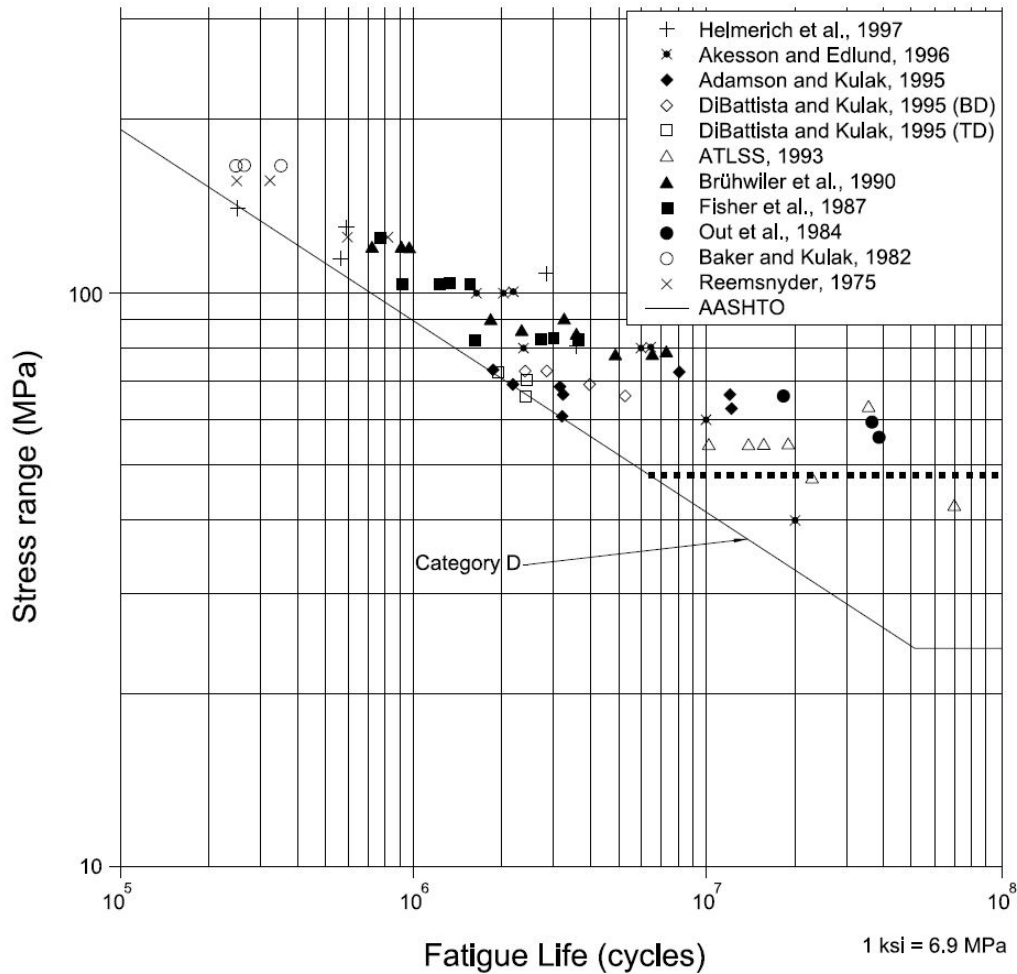


Figure 10.1.4-1 Fatigue performance of riveted built-up members.

Isolated failures of riveted truss members due to fatigue have been reported in the literature. These in-service failures typically occurred at the connection between truss members and gusset plates. The failures were shown to occur where the member initially connects to the gusset plate, through failure of the net section of the member, or occasionally at the end of the member where the gusset plate is most heavily loaded. A combination of stress concentration, initial flaw conditions at the hole edges, and shear lag or nonuniform loading of the gusset plate are responsible for fatigue cracking in all cases. The stress concentration effects from the connection of built-up or rolled shape members is expected to be more severe than would be found in the butt splices of a flange plate. This is due to a concentration of force effects due to shear lag and eccentricity. The fatigue resistance of riveted connections is reduced because the pretensioning force is not as great nor as reliable and a greater amount of bearing load transfer occurs. Load distribution in riveted truss connections is unequal and can result in a larger portion of the total member load being delivered by a smaller fraction of the total number of fasteners in the connection. Although this is not likely to affect the static resistance of the connection, the uneven distribution may affect the fatigue resistance.

AASHTO LRFD does not specifically address the fatigue category for riveted connections, as they are not commonly used in new construction. The closest analogy to the performance of a riveted connection is Detail 2.3 in the *AASHTO LRFD* specifications which references the performance of mechanically fastened joints using non-pretensioned fasteners.

When it comes to bridge evaluation, the *MBE* indicates that the base metal at the net section of riveted connections is to be evaluated as a Detail Category C detail. The *MBE* commentary indicates that the Detail Category D classification used for new designs with non-tensioned fasteners is used to represent the first cracking of a built-up member. The Detail Category C classification better represents the expected life of a detail when the initial discontinuity has grown to a critical size. It is deemed to better represent the critical stage of fatigue crack growth for members with a high degree of internal redundancy. The *MBE* goes on to state however that once cracks are visually detected, a more complex fracture mechanics approach should be used in lieu of the stress range approach. Research at Purdue University suggests that, for riveted members in poor condition with loose or missing rivets or with obvious signs of damage from hole punching, the engineer should revert back to the standard Category D designation, much like an open hole (Bowman et al., 2012).

Another aspect of fatigue and fracture for riveted members is the treatment of tack welds (see Figure 10.1.4-2). Tack welds are generally associated with non-welded components such as built-up members. They were commonly used to hold individual elements of a member together as final riveting was completed. Tack welds are common and were widely used for decades in the construction of riveted or bolted built-up members.



Figure 10.1.4-2 Tack weld detail.

A tack weld would be considered as a Category E detail if the provisions of the *AASHTO LRFD* specifications were used in their evaluation. However, many times tack welds are not significant enough to constitute structural welds. Given their widespread use in flexural and tension members alike, owners have been faced with the challenge of whether to remove what can be thousands of individual tack welds from a large structure in order to alleviate a potential crack initiation site. Research at Purdue determined that tack welded riveted members, when tested, performed better than the Category C design curve. Therefore for evaluation, tack welds can be

considered as a Category C detail. The prior Category E rating was considered too severe. Clarifying language has been provided in the *MBE*. The tack welds studied in the NCHRP 721 project varied but were in the range of 1 to 2 inches in total length (Bowman et al., 2012).

SECTION 10.2 ANCHOR RODS

10.2.1 Fatigue Considerations for Anchor Rods

Anchor rods, or anchor bolts, are the most common means of attaching structures such as overhead signs, traffic signals, high mast poles, and other similar structures to concrete foundations. They consist of fully threaded bars embedded into the concrete, to which the overhead structure is eventually connected with nuts. Due primarily to the action of wind, but also due to forces such as gust induced loading on cantilever and overhead sign structures, these anchor rods are subjected to high cycles of variable amplitude tensile loading which can make them prone to fatigue.

Two common types of anchor bolt connections are used: single nut and double nut varieties. A single nut connection is typically used when the underside of the base plate rests on a leveling grout pad. The double nut connection is used when the base plate is otherwise unsupported. Illustrations of each of these conditions are provided in Figure 10.2.1-1 and Figure 10.2.1-2.

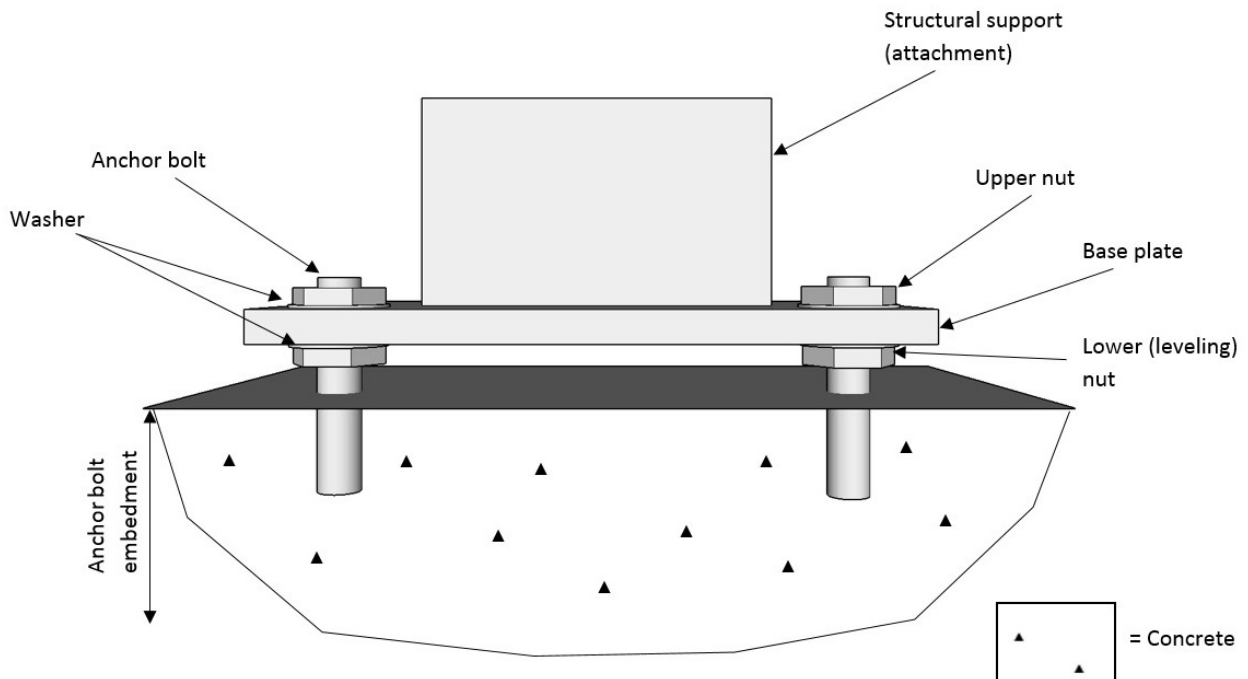


Figure 10.2.1-1 Typical double nut connection.

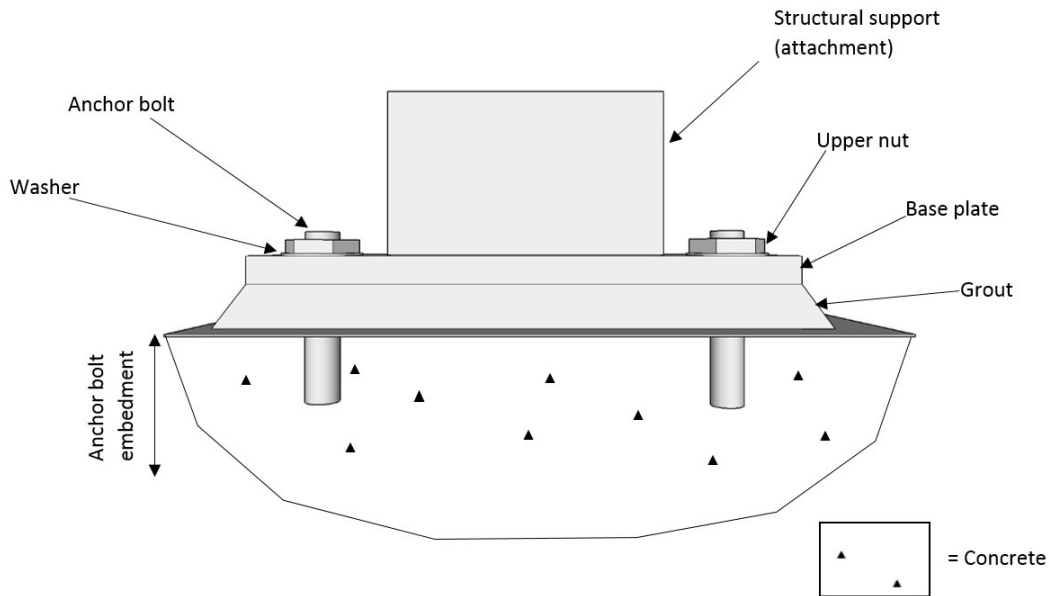


Figure 10.2.1-2 Typical single nut connection.

Research conducted at the University of Texas at Austin examined the fatigue behavior of steel anchor bolts (Frank, 1978). The study investigated the contribution of various parameters including: the strength of steel, thread size and pitch, bolt diameter, the method of forming threads (rolled or cut), the influence of galvanizing, and the effect of double nuts. Also studied was the stress corrosion behavior of anchor bolts. The report included an assessment of the results of testing by others as well. The summary of the fatigue testing indicated the type of steel, thread size, diameter, effect of galvanizing, and method of the forming of threads were not significant for design. The lower bound fatigue life for anchor bolts with single nuts and anchor bolts with loose double nuts was consistent with Detail Category E. Pretensioned anchor bolts, those with double nuts tightened one third of a turn past snug tight, had improved fatigue lives. Although no evidence of stress corrosion cracking was found in the test bolts, Frank recommended that the maximum yield strength for anchor bolts be limited to 125 ksi. This is consistent with modern practices that limit the yield strength of anchor bolt material.

Fisher, Kulak, and Smith (1998) also discussed and summarized the history of fatigue test data for threaded rods. They reported that most threaded rod fatigue tests were conducted under constant amplitude fatigue loading and that many of the tests were conducted in a double nut configuration in order to pre-stress a short section of the anchor bolt. A small amount of vertical misalignment was also included in some tests. The fatigue test data included threaded rods tested without preload, rods preloaded to a snug tight level, and rods preloaded by one third turn of the nut past the snug tight condition. Figure 10.2.1-3 presents results of fatigue tests on threaded rods.

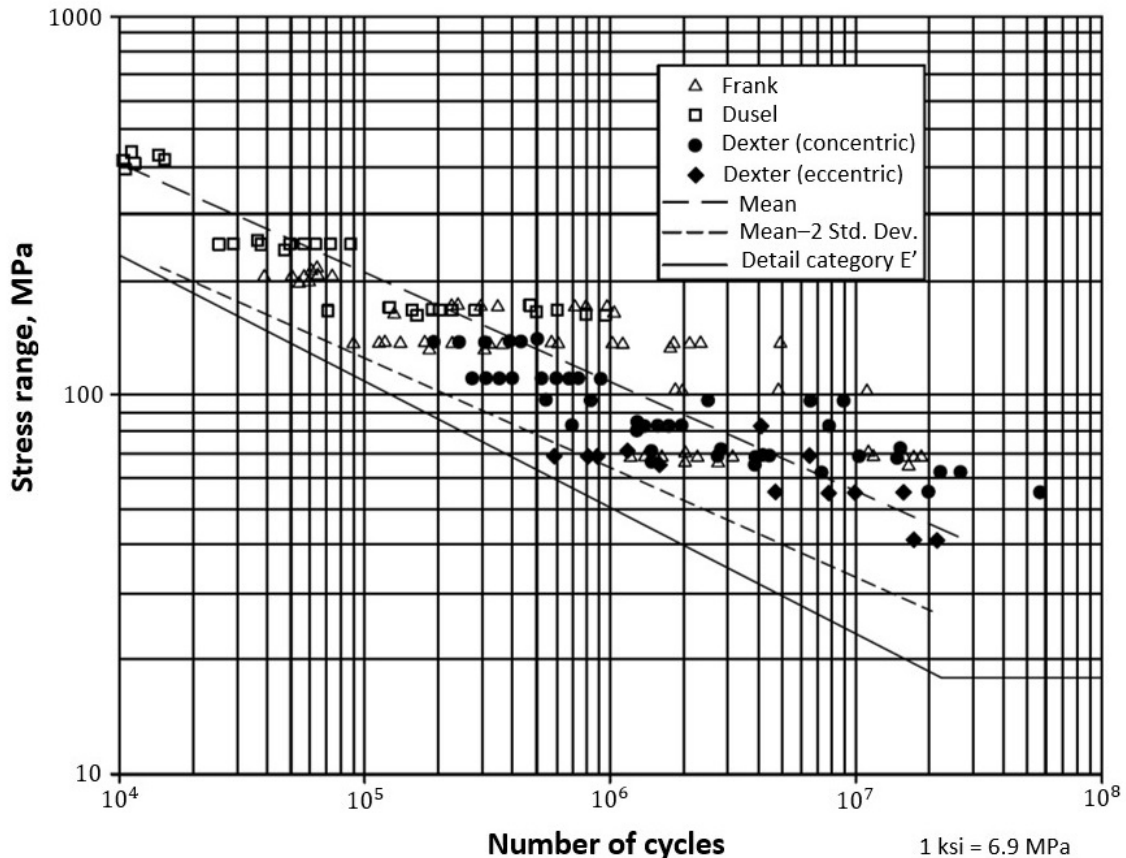


Figure 10.2.1-3 Results of fatigue tests on threaded rods.

Fisher, Kulak, and Smith (1998) comment that although there is considerable scatter in the results, the evidence suggests that anchor bolts loaded in fatigue have poor resistance. Included in the test data shown are anchor bolts of various grades, thread sizes, methods of forming, and bolt diameters, none of which were statistically significant to the fatigue life. The bolts tested with a vertical misalignment, as much as 1:40, did not have a significantly reduced fatigue life. Therefore *AASHTO LRFD* maintains this plumbness requirement for anchor bolts since there is insufficient evidence as to the fatigue resistance of anchor bolts with greater misalignments.

NCHRP Report 412 (Kaczinski et al., 1998) provides the most current information on the behavior of anchor bolts in fatigue. Although prior research indicated that Detail Category E' was a reasonable lower bound for anchor bolts tested in the finite life region, and Detail Category E appeared to be a reasonable design curve for infinite life, no testing of anchor bolts below a stress range of 10 ksi was available to verify the existence of a constant amplitude fatigue threshold (CAFT). Additionally, the behavior of anchor bolts was thought to potentially be different than the E and E' Detail Categories since these categories were developed for welded details with high tensile residual stress distributions and stress concentrations.

Anchor bolt fatigue originates at the thread root, and the residual stress distribution is possibly even compressive in these regions. Given the nature of fatigue design in light and sign structures,

the behavior in the finite life region is of limited use since the design of new structures is predicated on providing an infinite life detail. Thus an accurate determination of the CAFT was needed. The NCHRP 412 report determined the strength of double-nut anchor bolts tightened to a snug tight condition evaluating the effects of mean stress, yield strength, bolt pretension, thread forming method, and misalignment. Their conclusions are as follows and form the basis of the current AASHTO design approach:

- In the region of finite life, snug tight bolts should be designed to satisfy the Category E' requirements.
- In the region of infinite life, the CAFT limit for Detail Category D (7 ksi) is applicable to both snug tight and fully tensioned anchor bolts.
- Although no benefit is derived when installing bolts in a fully tightened condition (i.e., one third of a turn beyond snug tight), doing so prevents the possibility of a nut becoming loose in service.
- Misalignment need not be considered when limited to a maximum value of 1:40. Bending from prying action must be controlled through selection of a base plate having adequate thickness.
- The above recommendations assume a maximum total stress of approximately 60 percent of the anchor bolt yield stress, as the level of maximum stress strongly influenced the fatigue strength (characteristically different than welded details in which only stress range is of concern).

Design of anchor bolts for fatigue is covered in the AASHTO *LRFD Specifications for Structural Supports for Highway Signs, Luminaires, and Traffic Signals* (AASHTO, 2015c) and is based on satisfying the 7 ksi limit for infinite life. The specification indicates that mandatory Charpy V-notch testing is not required for anchor bolt material since anchor bolts conforming to the F1554 specification (ASTM, 2015) have generally been found to have adequate toughness. Due to the use of anchor bolts in an environment in which they are subjected to fatigue as well as an aggressive environmental exposure, and due to the fact that there have been anchor bolt failures in structures in the past, a minimum of eight bolts are required for base connections of high-level (pole type) luminaire towers. The commentary (AASHTO, 2015c) indicates as many as 12 anchor bolts may be required when fatigue governs the design.

10.2.2 Stress Corrosion Cracking / Hydrogen Embrittlement

Stress corrosion cracking is generally associated with anchor rods or bolts. Stress corrosion is a term that has traditionally been used to describe the effects of hydrogen embrittlement. However, to aid in the understanding of the mechanisms causing the crack, stress corrosion and hydrogen embrittlement must be separated. Both mechanisms produce failure through crack extension under static steady loading. Both also normally exhibit a threshold stress which is dependent upon the material properties and the environment. Once a threshold stress is exceeded, failure may occur within hours or it may take months for the crack to extend to failure.

The most prevalent form of cracking in the relatively low strength steels used in bridges and in a relatively benign environment is hydrogen assisted cracking. The hydrogen atom and ion are very small and can migrate through the crystal lattice to locations of high stress. The hydrogen

causes separation of the material along grain boundaries. The hydrogen can come from internal sources such as hydrogen trapped in the steel during the steel-making process or introduced during the welding process from contaminated welding consumables. External hydrogen embrittlement is typically the result of a cathodic reaction at the surface of the steel, which can be exacerbated by a sacrificial zinc coating. A small crack in the coating tends to focus the evolution of the hydrogen on the crack surface and tip, leading to hydrogen induced cracking (Townsend, 1975; Brahim, 2007).

Hydrogen induced cracking in bridge steels occurs due to hydrogen introduced during the welding process either from the consumables, surface moisture, or paint. Higher strength steels are more sensitive and require more stringent limits on hydrogen. Fluxes and coated welding rods are normally supplied in sealed containers which then must be stored after opening at an elevated temperature to prevent moisture absorption from the ambient air. The AWS specifications spell out the requirements for preheating, as well as diffusible hydrogen limits for the electrodes and fluxes. The ultrasonic, magnetic particle, and final visual inspection of fracture critical welds cannot be done for at least 24 hours and up to 72 hours for thick high strength steels. The intent of the delayed inspection is to ensure delayed cracking caused by hydrogen, if it occurs, is found during the inspection.

High strength bolts are susceptible to delayed hydrogen assisted cracking. A490 bolts are not allowed to be zinc coated due to problems first found with the fracture of galvanized A490 bolts (Townsend, 1975; Brahim, 2007). The lower strength A325 bolts are commonly galvanized without problems. Both the A490 and the A325 specifications have maximum hardness values to ensure the bolts will not exhibit delayed cracking. Bolts which exceed these hardness values have failed after installation. The use of galvanized A354 Grade BD bolts should be avoided. The hardness of these bolts is allowed to be higher than the A490 limit. Often the A354 bolt has been specified for high strength large diameter rods. These large diameter rods are difficult to through-harden due to the relatively lean alloys employed by the manufacturer. Due to their large cross section, the outer surface of the bolt cools the quickest in the quenching process, producing a bolt with high hardness on the outer portion and a lower strength core. The critical root of the thread is located in this outer band of high hardness material, though the surface hardness is measured at one quarter of the bolt diameter. This is a concern for fracture, and thus the use of the A354 Grade BD galvanized bolts is discouraged for tensioned applications.

SECTION 10.3 REINFORCEMENT OF CONCRETE

Concrete is commonly reinforced by one of two methods: internal mild reinforcing and internal prestressed reinforcing. In a conventional reinforced concrete structure, the structure is assumed to crack under service with the reinforcing steel being required to carry the tensile forces associated with bending and shear. In a prestressed concrete structure, members are most commonly designed to remain uncracked under specified service conditions. As such, the entire transformed section of the concrete and prestressing steel is effective at resisting the applied bending moments. The result of this uncracked condition is that a very large section is available to resist the external forces.

It is not common for the fatigue limit state to govern the design of structural concrete. For reinforced concrete elements, there are design checks provided in *AASHTO LRFD* related to maximum fatigue stress range allowed in reinforcing steel. *AASHTO LRFD* also addresses the design of prestressed concrete elements, though fatigue rarely governs the design of such elements.

10.3.1 Reinforcing Bars

Reinforced concrete, which cracks under the application of service loads, resists the externally applied forces through an internal force couple of reinforcing steel tension and concrete compression, as illustrated in Figure 10.3.1-1. The concrete portion of the member is used to resist the internal compressive forces, and internal reinforcing steel is used to resist the tensile forces. Because the internal reinforcing steel is subjected to tension, and this tension fluctuates due to the application of live load, fatigue is one of the limit states that must be satisfied in the design of a reinforced concrete element. Therefore the passage of routine traffic creates stress cycles throughout the life of the bridge, and they in turn load the reinforcing steel in fatigue.

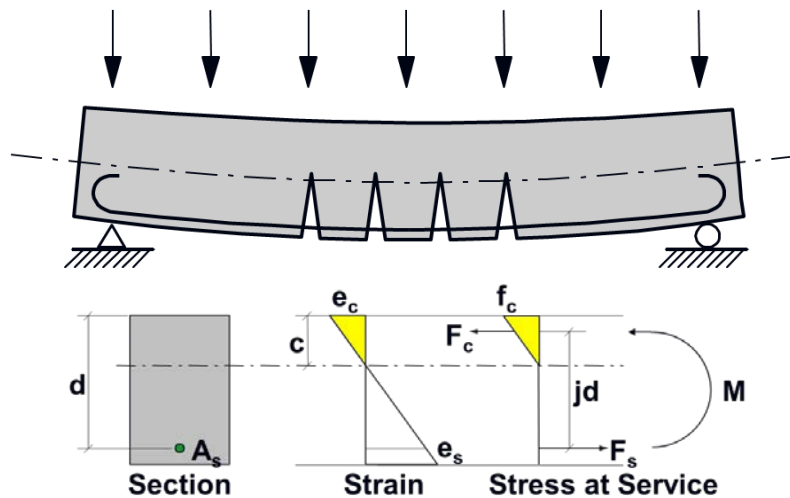


Figure 10.3.1-1 Resultant forces on beam subject to distributed load.

The fatigue of reinforcing steel is a possibility in reinforced concrete structures. For instance, structures such as a longitudinally reinforced concrete slab bridge, of which there are many thousands throughout the United States, are subjected to many fatigue cycles throughout their life. Other examples include reinforced concrete caps in substructures which are constantly loaded and unloaded as vehicles traverse the bridge and load is transferred to the bearings. Because of the many cycles of fatigue loading that can be applied to a cracked reinforced concrete section, *AASHTO LRFD* requires that the computed stress ranges in the reinforcing steel be less than the CAFT. The requirement is expressed as:

$$\gamma(\Delta f) \leq (\Delta F)_{TH}$$

Equation 10.3.1-1

with the stress range being taken as that corresponding to the Fatigue I load combination and the constant amplitude fatigue threshold provided by an equation presented below. There are no provisions in *AASHTO LRFD* for the finite life evaluation of a reinforcing bar.

The *AASHTO LRFD* constant amplitude fatigue threshold for straight reinforcement bars is given as:

$$\Delta F_{th} = 24 - 0.33 f_{min}$$

Equation 10.3.1-2

expressed in units of ksi. The variable f_{min} is the minimum live load stress resulting from the Fatigue I load combination, combined with the more severe stress from either the permanent loads or the permanent loads, shrinkage, and creep-induced external loads. In other words, it is a total minimum stress including the effects of permanent and transient loads at the same time. The *AASHTO* relationship was established by enveloping the results of many fatigue studies considering a range of bar sizes and reinforcing steel grades. Its accuracy as a true constant amplitude fatigue threshold was studied and is described later in this section.

The *AASHTO* equations are derived from an NCHRP research project by Hanson et al. (1976). Their study focused primarily on Grade 60, #8 reinforcing bars, though other sizes and grades were also tested. Hanson's equation for fatigue life is the one used in *AASHTO LRFD* with a slight simplification. Hanson's research comprised 353 concrete beams, most of which were tested in the finite life region. The conclusion of the research was that the fatigue limit of reinforcing steel was not sensitive to concrete beam dimensions, material properties, reinforcing bar size, steel grade, or metallurgy (Amorn et al., 2007). The original work of the NCHRP study concluded that the maximum stress and the minimum stress (i.e., the stress range) was a dominant parameter along with a factor related to the geometry of the rolled ribs and lugs of the reinforcing. These deformations, essential to bond of the reinforcing steel to the concrete, influence the fatigue life of the reinforcing steel because they serve as crack initiation sites.

Tilly (1979) provides a thorough synopsis of the various factors that influence the fatigue of reinforcing bars. One of the challenges associated with the fatigue analysis of concrete structures is determining how to correlate the performance of bars tested in air with those embedded in concrete. The difficulty of knowing how to accurately compute the stress in the reinforced concrete element poses a fundamental challenge when trying to apply the free length bar test data to the performance of bars embedded in concrete and loaded in flexure.

The simplest types of tests to conduct are of course axial fatigue tests of free length bars. These tests can be conducted quickly and without ambiguity as to the magnitude of the stress range and the fatigue life of the specimen. These tests are not without their challenges, specifically trying to overcome the premature failures that commonly occur where the bars are gripped in the test machine. However many years of testing have developed standardized approaches and methods of testing in order to develop reliable fatigue test results.

Somewhat more difficult but of greater similarity to actual in-service conditions are bending tests on reinforced concrete beams. Although these tests bear a greater resemblance to actual service

conditions, they introduce an additional complication and that is the determination of the fatigue stress range in the reinforcing steel in a section that is cracked under service load. Tilly comments that the results of bending tests have typically shown greater lives than axial “in air” loading, but the differences are not very significant. Tilly cites work consistent with findings of others that the fatigue life of smaller bars is somewhat better than larger bars. It is hypothesized that the lower fatigue life for larger bars is potentially due to the fact that a larger bar is more likely to have a defect than is a smaller bar. The influence of corrosion on fatigue life of reinforcing steel was also discussed. Tilly comments that corrosion not only reduces the cross section of the bar, therefore increasing its stress, but in and of itself creates pitting and as a result decreases the remaining fatigue life of the reinforcing steel even further. This is a significant observation for bridge evaluation and remaining fatigue life determination.

Equation 10.3.1-2 was recently evaluated as part of the fatigue limit state calibration conducted as part of the SHRP2 Project R19B, *Bridges for Service Life Beyond 100 Years: Service Limit State Design* (Modjeski and Masters, 2015). Regarding the AASHTO limits, the R19B report offers the following:

ACI Committee report ACI 215R-74(92) and the supporting literature indicate that nonprestressed reinforcement exhibits a constant amplitude fatigue threshold, yet it is unclear that these equations are in fact the threshold values. ACI 215R-74(92) suggests that the resistances are “a conservative lower bound of all available test results.” In other words, a horizontal constant amplitude fatigue threshold has been drawn beneath all the curves.

Therefore the “limit” was arbitrary, and its reliability was unknown. In the calibration of the limit state, an assumed Fatigue I load factor of 2.0 was chosen based on calibration of the limit state for steel structures. When this load factor was applied to the evaluation of concrete reinforcing bars in tension, it was determined that the AASHTO approach would provide a level of reliability substantially higher than for the fatigue of steel structures. An initial suggestion was that a resistance factor, ϕ , could be taken as 1.25. This is unusual and inconsistent with other fatigue design approaches. In lieu of the higher load factor, the R19B researchers instead suggested simply raising the nominal resistance equation to the following value:

$$\Delta F_{th} = 30 - 25 \frac{f_{min}}{F_y}$$

Equation 10.3.1-3

As discussed in Chapter 6, the Fatigue I load factor is currently 1.75. This results in a change of the nominal resistance equation by the ratio of 1.75/2.0.

10.3.2 Prestressing Strands

The fatigue behavior of prestressing strands and the fatigue behavior of prestressed concrete elements has been a focus of research since the material was first widely introduced into practice in the 1950’s. At the time, researchers were wrestling with not only the determination of strand fatigue properties but also with the basic problems of how to develop test methods and fixtures to

accurately determine the characteristics of strands. Data on the fatigue performance of prestressing strand has been gathered by numerous investigators through the years, as well as by various industry groups including manufacturers. The results of prestressing strand fatigue data testing have not always been presented in a consistent manner nor do they reflect tests that have been conducted under similar conditions. The fatigue performance of strands has been assessed both by flexural testing of small-scale and full-size elements, as well as by many tests of strands in air. The conclusions of these two types of testing have also not always been consistent.

In a study for the Texas Department of Transportation (Paulson et al., 1983), researchers synthesized several decades of prestressing strand fatigue behavior and supplemented historical information with additional testing. Their findings were corroborated by others including Heller (2003). The 1983 report by Paulson et al reviews the results of over 700 individual specimens of seven-wire prestressing strand tested in fatigue. This included test results from the United States as well as Europe. The early researchers noted a clear trend: beams that remained uncracked performed well, whereas beams that cracked during loading were susceptible to fatigue failure with little to no impending warning. Paulson reviewed the results of the various tests and performed a regression analysis on the fatigue test data. In Figure 10.3.2-1, the solid line represents the mean result and the dashed line represents the 97.5 percent survival limit. It is notable that the performance of prestressing strand tested in air follows the same logarithmic behavior as for other structural steel elements discussed previously.

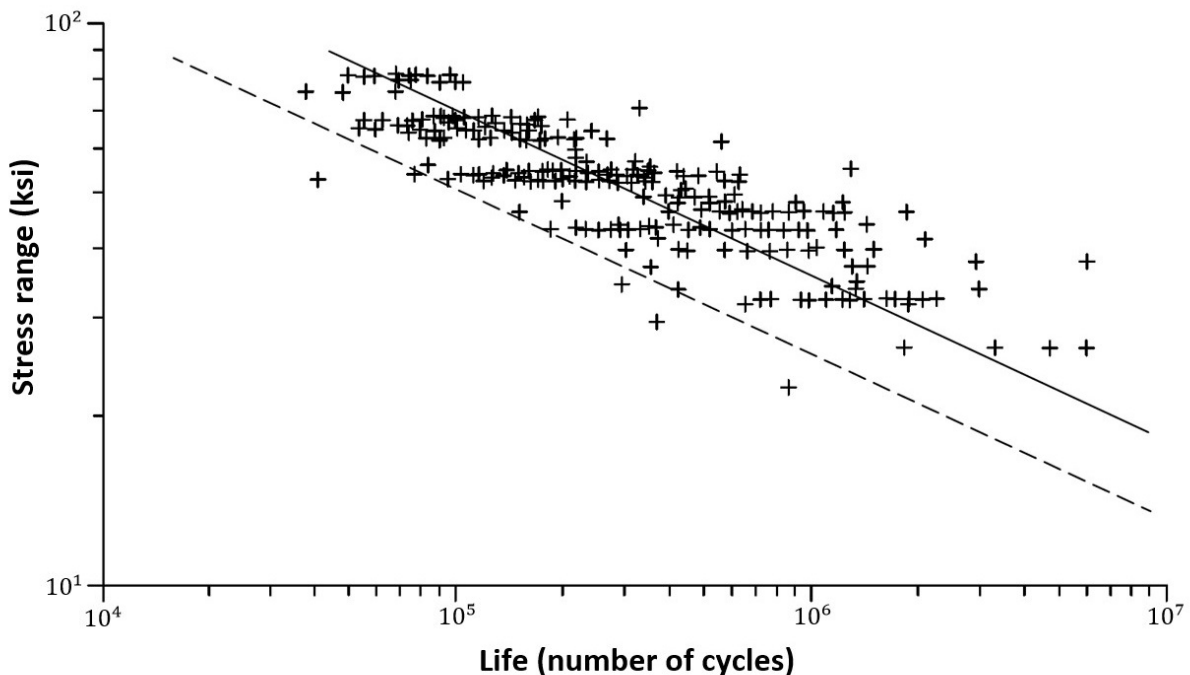


Figure 10.3.2-1 Results of prestressing strand tests.

Although prestressing strand obeys the same general behaviors as other steel elements when subjected to fatigue loading, the design process for prestressed concrete is characteristically different than for steel structures. For a prestressed concrete structure, the designer is not

concerned with fatigue life estimation but rather the design approach is generally to take steps to avoid the chance of fatigue failure. The Paulson research suggested a fatigue limit of 20 ksi as a reasonable endurance limit for strands.

One fundamental problem with the fatigue behavior of cracked sections is coming up with a model that consistently predicts the range of stress in the strands in the vicinity of the crack. Until an accurate estimate of the stress range can be made, there is no reasonable way to create a reliable fatigue model. Paulson suggests that the fatigue test data summarized in his report is also applicable for elements such as hangers, stay cables, and other elements where the loading in direct tension most directly corresponds to the nature of most laboratory fatigue tests. Regarding pretensioned concrete girders, they divided their recommendations into two cases: uncracked girders and cracked girders. Paulson suggests that for uncracked girders, the behavior of the strand in fatigue is very similar to the fatigue of strand when treated as an isolated element. However for cracked girders, the situation is more complex. At the time of Paulson's work, no code recommendations were available related to fatigue of prestressing strand. Their work suggested a logarithmic fatigue life equation similar to those used currently for structural steel. Modern practice has replaced their suggested equations with a series of limiting stress values for uncracked and cracked sections alike.

Heller states, in follow-up work to the original Paulson study, that *“The published literature does not include a single case of a strand fatigue failure in an uncracked prestressed concrete beam. It is not considered possible to design a prestressed concrete beam such that the stress range in the strand is sufficiently large to cause a fatigue failure without cracking the concrete first. With this in mind, it is rational to specify that the fatigue capacity of the pretensioned concrete beam is satisfactory if the extreme concrete tensile stress is limited such that no cracking can occur.”* This is fundamentally the approach taken in *AASHTO LRFD*.

AASHTO LRFD defines a constant amplitude fatigue threshold for prestressing tendons. For tendons having a radius of curvature in excess of 30 feet, the limit is 18 ksi. For tendons having a radius of curvature less than 12 feet, the limit is 10 ksi. Engineers are allowed to interpolate linearly between the two radii. In post-tensioning applications, tendons are frequently deviated vertically and laterally using curved tendon profiles. The geometry of these ducts is related to the constant amplitude fatigue threshold value to be used in a particular design. In pretensioned applications, strands are also frequently held down, or deviated, in order to control stresses near the end of the beam, as well as to provide enhanced shear strength in the harped region. At the locations of the hold-down anchors, strands are bent sharply around a mechanical device, and this change in profile would also be considered a location of sharp curvature.

From a practical standpoint, the evaluation of prestressing strands for fatigue is not frequently performed. *AASHTO LRFD* states that fatigue of the reinforcement need not be checked for fully prestressed components designed to meet the tensile stress limitations of the Service III load combination. The vast majority of prestressed concrete structures are designed to satisfy this load combination and by default would be exempt from any fatigue checks. In the rare instances in which an owner would allow the computed tensile stresses to exceed the permissible values of *AASHTO LRFD*, the section should be assumed to be cracked under service load conditions, subjecting the reinforcing steel to a stress range that would need to be computed and checked against the fatigue resistance.

10.3.3 Post-Tensioning Tendons and Anchorages

Tendon anchorages are a critical component of any post-tensioning system and are usually based on proprietary designs by specialty hardware suppliers. The purpose of the anchor is to provide a common location at which post-tensioning tendons are terminated and their tensile force converted into compression acting on the concrete member. The performance of post-tensioning anchorage systems is typically established through a combination of detailed analysis and experimental testing. This testing includes static and fatigue testing in order to assess the performance of the complex anchoring system under static and fatigue loading.

Post-tensioning anchors can take several forms. These include an older style basic bearing plate and trumpet configuration, used for smaller tendons, as shown in Figure 10.3.3-1.

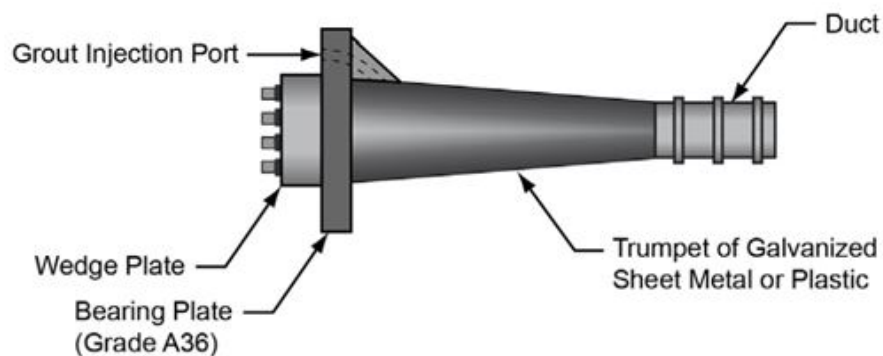


Figure 10.3.3-1 Post-tensioning anchor detail.

More commonly used are special cast anchors, known as multi-plane anchors, which deliver the high compression load they must resist into the concrete in a specially reinforced local zone at the end of the element. These areas require special reinforcement and confinement in order to resist the high static loads associated with anchorage of the tendon, as well as to resist the fluctuating loads associated with transient load effects. Figure 10.3.3-2 shows a multi-plane anchorage system.

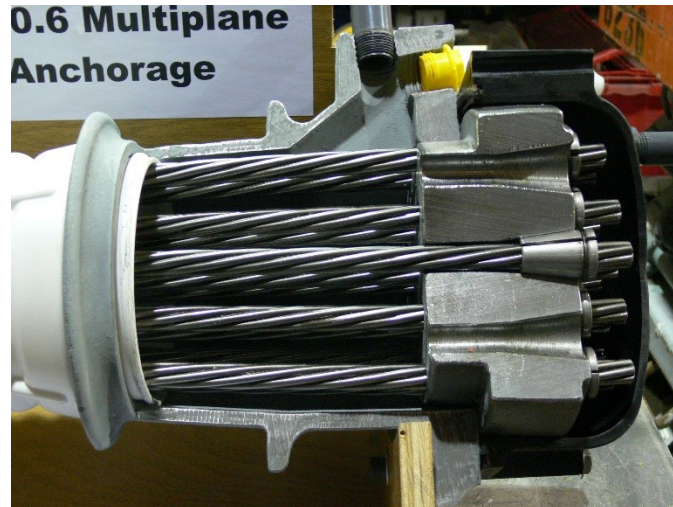


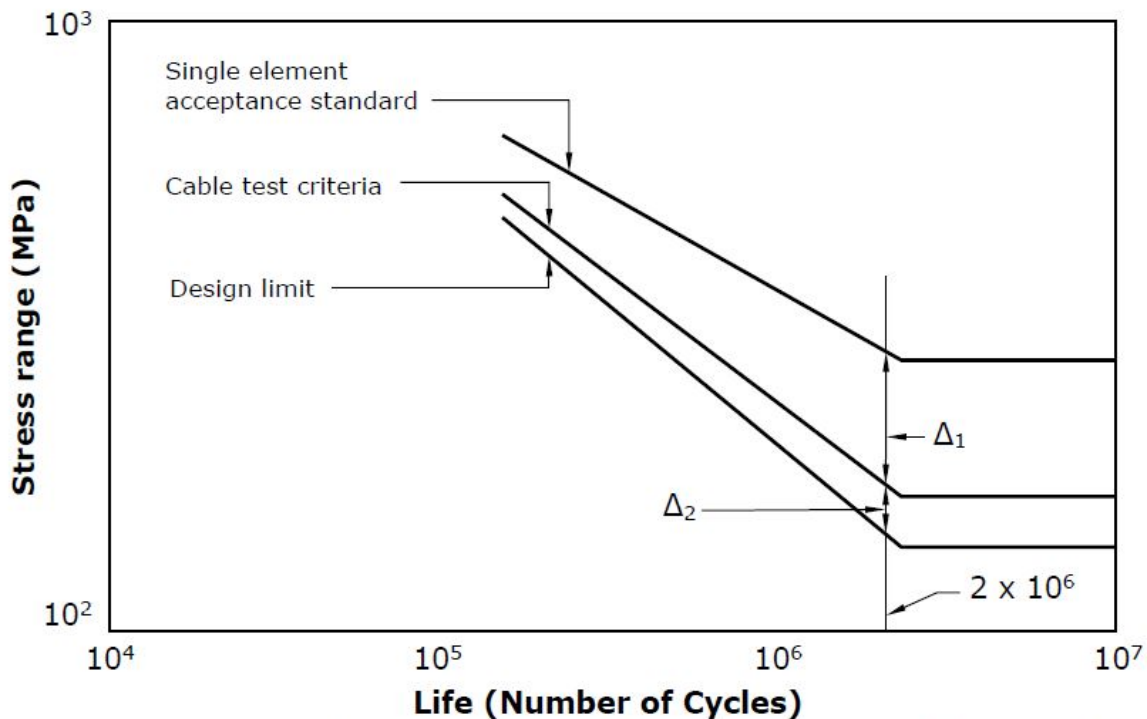
Figure 10.3.3-2 Multi-plane anchorage system.

The design and performance of these anchorages, as it relates to fatigue, is not something that the engineer of record is typically responsible for. Post-tensioning anchors and systems in general are typically subjected to prequalification testing by agencies and manufacturers in order to determine their suitability. Testing of anchorages usually involves static tests that determine the reliable anchorage of prestressing steel, tests to ensure the anchor can adequately deliver its force to the surrounding concrete, and special fatigue tests which assess the performance of the system under varying stress in the tendons. Other elements of the design of a post-tensioning anchor include the geometry of the trumpet and the ductwork. By providing a smooth transition from the wedge anchors into the duct, fatigue life performance and anchorage efficiency are increased.

10.3.4 Stay Cables

The requirements for the fatigue design of stay cables described herein come largely from the Post-Tensioning Institute *Recommendations for Stay Cable Design, Testing, and Installation* (PTI, 2012). The AASHTO specifications are largely silent in this area.

Within the PTI recommendations are guidance on quality control testing of stay cable materials as well as recommendations concerning the design of stay cable systems. The requirements for testing relate to the obligations of manufacturers and system vendors related to quality assurance and control in the manufacturing of strands, bars, wires, and couplers. Given that only isolated elements are generally tested, the acceptance standard for an element does not imply that a system should be designed to the same level. Rather the design limit of stress range for a given number of cycles is significantly less for an in-service structure as compared to the acceptance criteria for isolated elements. This is shown schematically in Figure 10.3.4-1.



Δ_1 = Quality assurance (17 MPa-coupled bar, 69 MPa strand and uncoupled bar, 103 MPa wire)
 Δ_2 = Length effect, anchorage stress riser, safety (34 MPa)

Figure 10.3.4-1 Fatigue safety philosophy.

Due to the unique characteristics of many stay cable systems, system qualification tests are required to demonstrate adequate performance. This includes both fatigue and static strength criteria. The PTI criteria define the acceptance testing of stay cables. The fatigue acceptance test criteria include specified test stress ranges, as well as an upper limit on the maximum cable stress. During testing of a completed cable mock-up, the failure of individual wires is limited to 2 percent of the total stay cross section. Any failure of a bar in a bar-type system will result in rejection of the test. Failures are not permitted in any component of the anchorage during testing. Failures of any anchor components constitute automatic rejection of the test.

The PTI commentary indicates that stay cable acceptance tests are to ensure that stay cable systems have uniform and high levels of quality and reliability. They also acknowledge that the fatigue loading ranges for stay cables computed by designers are subject to a high degree of uncertainty. The test criteria in the PTI recommendations are knowingly conservative to envelope the uncertainties of stay cable behavior and due to the importance of the stays themselves. Additionally, the acceptance test duration is very short and in no way mimics the time and environmental exposure of a real cable. Therefore a high standard for acceptance is required. At the conclusion of the fatigue testing, the specimens must be reloaded to a load of 95 percent of the minimum ultimate tensile strength of the cable to demonstrate adequate strength performance after the conclusion of the fatigue test. At the conclusion of the fatigue and static tests, test cable is required to be dissected and its components examined.

The fatigue design vehicle for cable-stayed bridges is the same as that used for the design of ordinary structures, the AASHTO fatigue loading placed in a single lane. However the computed load effect is multiplied by 1.4 in order to capture the effects of heavy trucks on longer spans placed in adjacent lanes. The standard dynamic load allowance of 15 percent is applied.

An additional fatigue concern for stay cables is the dynamic effects of wind loading and cable vibration. Some cable-stayed bridges have been subjected to undesirable wind-induced vibrations in the main cables. This cable vibration can be caused by turbulence present in the airflow (buffeting), vortex shedding, galloping, fluid structure interaction, wind and rain acting in combination, and a combination of these factors. Failures in cables and cable attachments due to each of these factors have occurred in the past. Recently the failure of a stay cable anchor in Minneapolis was attributed to cable vibration resulting in a connection plate between the cable and supporting tower exceeding its fatigue strength, breaking loose, and the cable falling onto the bridge deck (Wiss, Janney, Elstner Associates, Inc., 2012). The PTI recommendations provide guidance to help engineers develop a preliminary assessment of the susceptibility of cables to rain-wind induced vibrations, cable galloping, damping, the use of stabilizing cables, and the detailing of connections to minimize fatigue susceptibility of these critical elements.

For design at the fatigue limit state, both finite and infinite life design criteria are presented. The detail constants for finite life and the constant amplitude fatigue threshold limit for infinite life are provided. When comparing the computed stress to the fatigue limit, the computed stress range must be increased by 140 percent (a factor of 1.4) in order to account for the fatigue effects of long span, multi-lane loading. The suggested design life of 75 years is recommended for cable design, although the expected life of the bridge could be significantly longer.

An additional concern for stay cables is the interaction of the stay cable and the cable saddle. Minimum saddle radii are suggested for strands and bundled stays so that the effects of curvature and fretting on fatigue can be avoided.

The construction of cable-stayed bridges also involves operations that are fatigue and fracture sensitive. The PTI recommendations have various provisions that cover construction items such as the welding of steel pipe and weld inspection.

This page intentionally left blank

APPENDIX A

CALIBRATION OF THE FATIGUE I AND II LOAD COMBINATIONS

SECTION A.1 GENERAL

AASHTO LRFD introduced the concept of calibrated limit states to the practice of bridge engineering in the United States. Following their introduction in 1994, the design of structures has been based on satisfying the design requirements of the strength, service, extreme event, and fatigue and fracture limit states. One significant enhancement introduced with *AASHTO LRFD* was the introduction of calibrated loads, load factors, and load combinations to provide a more uniform level of safety and risk to various designs. Calibration is a process of selecting load and resistance factors and creating load combinations so that a targeted level of safety can be achieved. It requires that the uncertainties in the various inputs (i.e., the parameters on the load and resistance side) be known or able to be confidently estimated. The calibration of the *AASHTO LRFD* specifications was initially performed only to satisfy strength limit state criteria. The strength limit state statistics were produced through the NCHRP 12–33 project, documented in NCHRP Report 368 (Nowak, 1999) and in NCHRP 20-07/186 (Kulicki et al., 2007).

Fatigue, however, had been an uncalibrated limit state with an unknown, though deemed safe, level of safety. The limit state was based on testing to define safe design resistance values (see Section 4.4) and vehicle weight studies to establish load factors, but a statistical definition of safety was never fully established. The SHRP2 Project R19B – Bridges for Service Life Beyond 100 Years: Service Limit State Design (Modjeski and Masters, 2015) studied various aspects of the load and resistance models for the service and fatigue limit states in order to calibrate them. Unlike the current fatigue design principles which base their design vehicle, load factors, and distribution factor approach on studies from the 1960's and 1970's, the recent SHRP2 study relies on modern weigh-in-motion (WIM) data to investigate these various inputs. The R19B project relied on approximately 65 million individual vehicle records in a nationwide WIM database. Approximately 10 million of those vehicles were removed from the database because of perceived errors or lack of usefulness of the data. Additionally, for the calibration of the fatigue limit state, vehicles whose gross weight was less than 20 kips were also excluded since these cause no measurable fatigue damage.

After several rounds of filtering, approximately 8.7 million records remained and were used in the calibration of the fatigue limit state. As would be expected with data from many WIM sites throughout the United States, there is a significant scatter in the findings. For the 15 sets of WIM data provided by FHWA, the mean truck weight ranged from 20 to 65 kips with a maximum gross vehicle weight of approximately 202 kips. Because of the geographic diversity of the WIM sites, traffic volumes varied greatly. The lowest truck traffic volume expressed as the ADTT value was a site in Arizona with less than 100 trucks per day, while for a site in Arkansas, the ADTT was nearly 4,600 trucks per day.

SECTION A.2 FATIGUE LIMIT STATE CALIBRATION

The AASHTO formulation for the fatigue limit state requires that the stress range be less than the nominal resistance, expressed as follows:

$$\gamma(\Delta f) \leq (\Delta F)_n \quad \text{Equation A.2-1}$$

In the finite life region, the factored design stress must be below the finite life resistance:

$$\gamma(\Delta f) \leq (\Delta F)_n = \sqrt[3]{A/N} \quad \text{Equation A.2-2}$$

where the number of design cycles is given by the following equation:

$$N = (365)(75)n)(ADTT)_{sl} \quad \text{Equation A.2-3}$$

For the infinite life region, the factored design stress must be below the constant amplitude fatigue threshold (CAFT):

$$\gamma(\Delta f) \leq (\Delta F)_n = CAFT \quad \text{Equation A.2-4}$$

In order to calibrate the fatigue limit state, various inputs to this approach must be investigated. These include the load factors, γ , the number of cycles of loading per passage of the design truck, n , and the premise that the stress range, Delta (Δ) f , is related to the stresses produced by the design truck in a single lane only. These variables were investigated by the R19B team. Their findings and recommendations follow.

SECTION A.3 COMPONENTS OF THE FATIGUE LIMIT STATE

A.3.1 Multiple Presence

One of the assumptions of the AASHTO fatigue limit state is that structures need only be designed for the passage of the fatigue truck in a single lane. That is, there is no need to consider the simultaneous presence of trucks in adjacent lanes or trucks following each other in the same lane. The R19B team investigated the validity of this single truck, single lane design concept. The availability of the WIM data allowed researchers to filter the records and find times and speeds for occasions where similar weight trucks, with similar axle spacings, were crossing the bridge in the same lane or in adjacent lanes with the headway limited to less than 200 feet, as illustrated in Figure A.3.1-1.

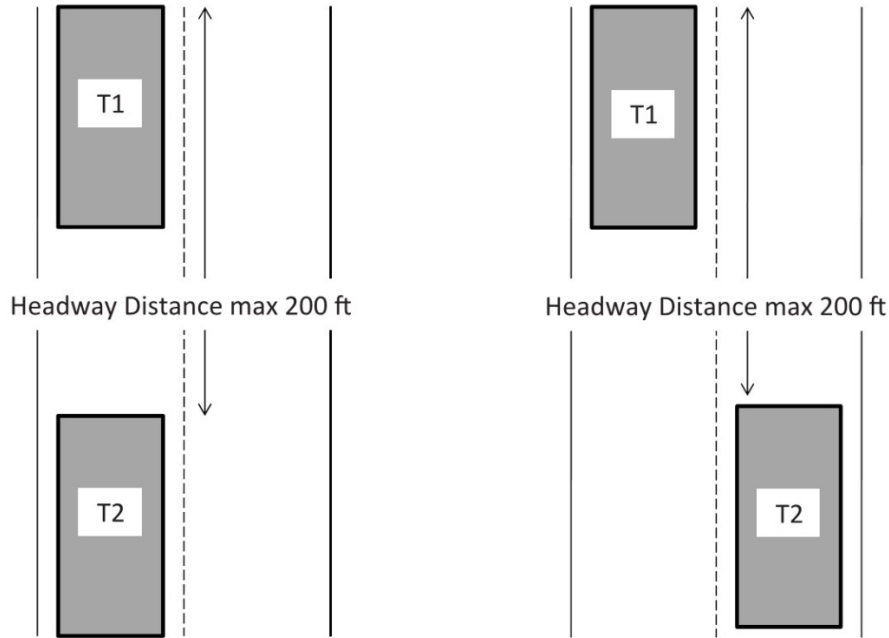


Figure A.3.1-1 Headway distance.

Using data from WIM sites in Florida and New York, the researchers concluded that there was a very low percentage of similar weight and configuration trucks traveling in adjacent lanes or trucks following one another in the same lane. On this basis, the researchers concluded that based on the low number of observed side-by-side and following occurrences, it is acceptable to consider only a single truck in a single lane for fatigue design. This confirms that a single lane live load model, as has been used in the past editions of *AASHTO LRFD*, is applicable for the load side of the limit state equations.

A.3.2 Cycle Counting / Cycles Per Passage

The calculation of an estimated number of design cycles is required for design for finite life. This is expressed by Equation A.2-3 and includes the effects of 75 years of truck traffic in the most heavily traveled lane. It is assumed to produce a certain number of cycles per truck passage, n . The *AASHTO LRFD* recommendations for the number of cycles per crossing are provided in Table A.3.2-1.

Table A.3.2-1 AASHTO cycles-per-passage.

Longitudinal Members		n	
		Span Length > 40 ft.	Span Length ≤ 40 ft.
Simple span girders		1.0	2.0
Continuous girders	Near interior support	1.5	2.0
	Elsewhere	1.0	2.0

The R19B team investigated the validity of these requirements using the WIM data. The WIM data was used to compute midspan moments for simply supported bridges, moments at the interior support of two-span continuous bridges, and moments at 0.4 of the end span of two-span continuous bridges for bridges of various lengths. To do this, measured vehicles were run as a simulated traffic stream across bridges from 30 ft. to 200 ft. in length (per span) to determine the number of cycles and magnitude of moment for various span lengths. A time history of bending moment was developed, as presented in Figure A.3.2-1.

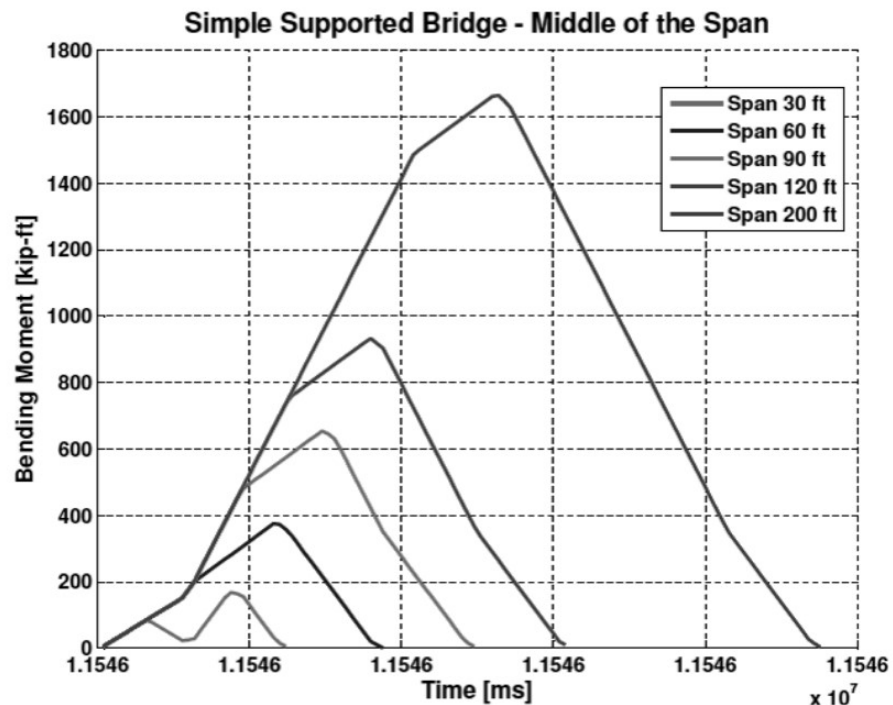


Figure A.3.2-1 Bending moment time history for a single truck passage on simple-supported bridges at midspan.

Figure A.3.2-1 demonstrates the variation in midspan bending moment for simply-supported bridges loaded by a particular vehicle chosen from the WIM data. It is useful to compare the behavior of the shortest span, 30 feet, and the longest span, 200 feet. For the longer span, a gradual increase-decrease in bending moment is apparent, and effectively one large cycle of moment is produced. For the shorter spans, the loading and unloading response of individual axles or axle groupings causes a greater number of smaller cycles for a single vehicle passage.

Figure A.3.2-2 shows a similar bending moment versus time plot for a family of two-span continuous bridges. The negative moment at the interior support is plotted. Again examining the longest bridge, the behavior is similar to what would be expected from the passage of a single point load. Moments increase to a peak, decrease as the vehicle crosses the pier, and follow a similar pattern in the second span. However, examining shorter spans, it is obvious that the moment at the pier fluctuates significantly due to the peak responses generated by multiple axles combining or interfering with each other. Using these time histories as an indication of the

fluctuation of stress, it is apparent that the definition of a cycle is more complex for the shorter spans.

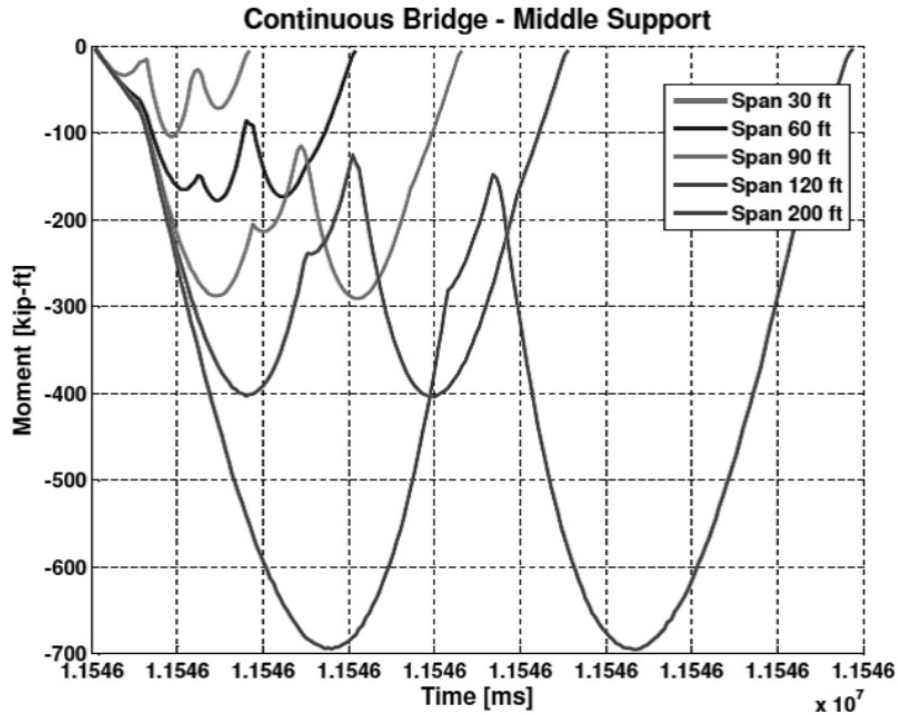


Figure A.3.2-2 Bending moment time history for a single truck passage on two-span continuous bridges at the pier support.

The rain flow counting algorithm is a method that accounts for the numerous partial cycles in the time history and was used by the R19B team to investigate the AASHTO approach to cycles-per-passage for the standard fatigue truck loading. In the rain flow method, time is plotted on the vertical axis with the origin being the earliest time. Stress is plotted on the horizontal axis, with tensile portions of stress (positive) being on the right and compressive stresses (negative) being plotted on the left. The rain flow method was envisioned to look like rain falling on the roof of a Japanese pagoda and falling from the tips of the roof either to the ground or to lower levels (Dowling, 1972).

Figure A.3.2-3 depicts the rain flow method of cycle counting for a portion of a stress time history. The rules for rain flow counting are as follows (Downing and Socie, 1982):

1. Rain begins at the beginning of the time history and at the inside of every peak.
2. Analysis of rain flow is first done by considering all of the flows that begin at a tensile peak (i.e., Points 2, 4, 6, etc.).
3. A half cycle is produced when rain terminates at a compressive peak opposite a more tensile peak than the point of origin (i.e., rain beginning at Point 2, flows to Point 3, and terminates since Point 3 is opposite (across the axis from) a “more tensile” Point 4 than the point of origin).

4. A half cycle is produced when rain falls off the time history (i.e., Path 4-5-7-9-11).
5. A half cycle is produced when rain merges with a flow that began at an earlier tensile peak (i.e., Path 6-6' or 8-8' or 10-10') or when it flows in the opposite direction of a tensile peak of greater magnitude (i.e., such as Path 5-6).
6. The process is then repeated for all rain that begins at the compressive peaks.
7. Each path is assigned a magnitude based on the value of stress at the start and end of the flow and these are deemed half cycles.
8. The number of half cycles of equal magnitude are added as a way of accounting for complete cycles. There are commonly some residual half cycles.

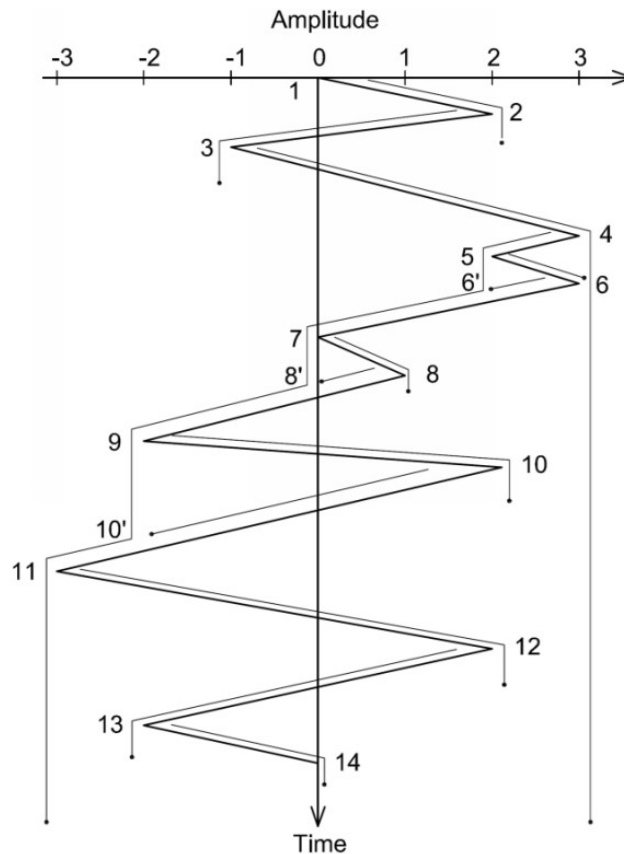


Figure A.3.2-3 Rain flow counting example.

Considering the time history shown in Figure A.3.2-3, the rain flow method would produce the half cycles and stress ranges presented in Table A.3.2-2.

Table A.3.2-2 Rain flow stress cycles for the example time history.

Positive Direction Half Cycles		Negative Direction Half Cycles	
Path	Amplitude	Path	Amplitude
1-2	2	2-3	3
3-4	4	4-5-7-9-11	6
5-6	1	6-6'	1
7-8	1	8-8'	1
9-10	4	10-10'	4
11-12	5	12-13	4
13-14	2		

The path from 4 to 11 involves three instances where the rain falls onto a lower roof and continues to flow until it leaves the time history at Point 11. Thus when rain is introduced to the roof at Point 6, 8, or 10, it encounters rain that was previously introduced at Point 4 and is therefore interrupted, creating a series of truncated cycles (i.e., 6-6', 8-8', and 10-10', as noted in Table A.3.2-2 and Figure A.3.2-3). The cycles are then grouped based on their common amplitudes, and the cycles are counted. This is shown in Table A.3.2-3.

Table A.3.2-3 Amplitude and cycle count for rain flow example.

Amplitude of Cycles	Number of Cycles and Paths
1	2 (4 – 1/2 cycles = Paths 5-6, 7-8, 6-6', 8-8')
2	1 (Paths 1-2, 13-14)
3	0.5 (Path 2-3)
4	2 (4 – 1/2 cycles = Paths 3-4, 9-10, 10-10', 12-13)
5	0.5 (Path 11-12)
6	0.5 (Path 4-11)

In a similar way that stress time histories can be counted, so can fluctuations in moment. After completing the truck crossing simulations, the total number of moment cycles found through the rain flow process was divided by the number of trucks processed in the database to compute an average number of cycles per truck passage. For simply-supported bridges, the number of cycles at midspan varied from 2 to 2.5 cycles per passage for short spans and decreased to one cycle per passage for spans of 100 feet or greater. For positive moment in the end spans of a continuous bridge, the number of cycles varied from 2.3 to 3.5 for short spans and dropped to 1 to 1.5 cycles for span lengths of 100 feet or greater. Finally, for negative moment over the interior support of a continuous bridge, there were 2.5 to 3.5 cycles per passage for short spans and about 2.5 cycles per passage for longer spans. As discussed previously, the greater number of cycles for short span bridges is attributed to the axle grouping effects as opposed to the effect of an entire vehicle.

Section 3.3 of this Manual, specifically Equation 3.3-8, discusses the development of an equivalent stress range concept, Miner's rule, which expresses an equivalency between a variable amplitude stress spectrum and one of constant amplitude and having the same life. The R19B research team extended this concept to the idea of an equivalent moment since the bridges being studied were those whose stress ranges were directly proportional to live load moment. In order

to develop an equivalent moment, the probability density functions for moment were developed for each WIM site and for various bridge lengths (simple and continuous), and thus an equivalent moment could be developed. An example of the moment probability for various simple spans is provided for one specific WIM site in Figure A.3.2-4.

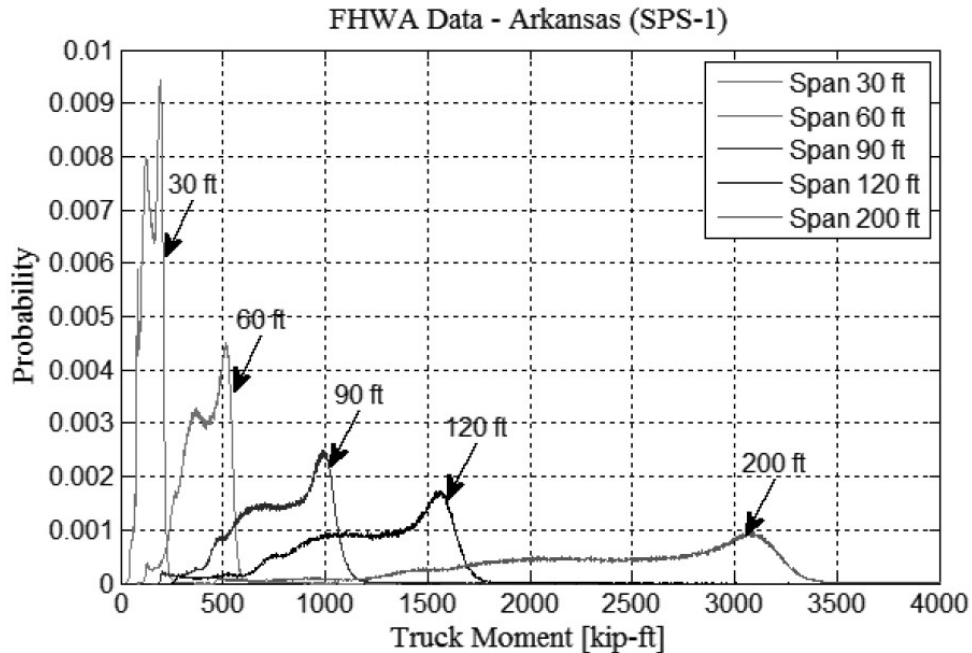


Figure A.3.2-4 Effective bending moment versus probability of occurrence.

Given the probability of certain moments being produced by the WIM trucks for various spans, the equivalent moments were computed using Miner's rule with the exponent, n , taken as 3, known as a root mean cube function.

$$M_{eq} = \sqrt[n]{\sum p_i M_i^n}$$

Equation A.3.2-1

These equivalent moments were compared to the *AASHTO LRFD* fatigue truck moments to determine how the measured trucks (producing simulated moments) compared to those expected from the LRFD fatigue truck loading.

Figure A.3.2-5 depicts the ratio of the equivalent moment compared to that predicted by the AASHTO fatigue truck. The ratio of the equivalent moment to the AASHTO moment is consistently lower for shorter spans. Although only the midspan, simple span plot is shown, the trend is similar for continuous spans as well.

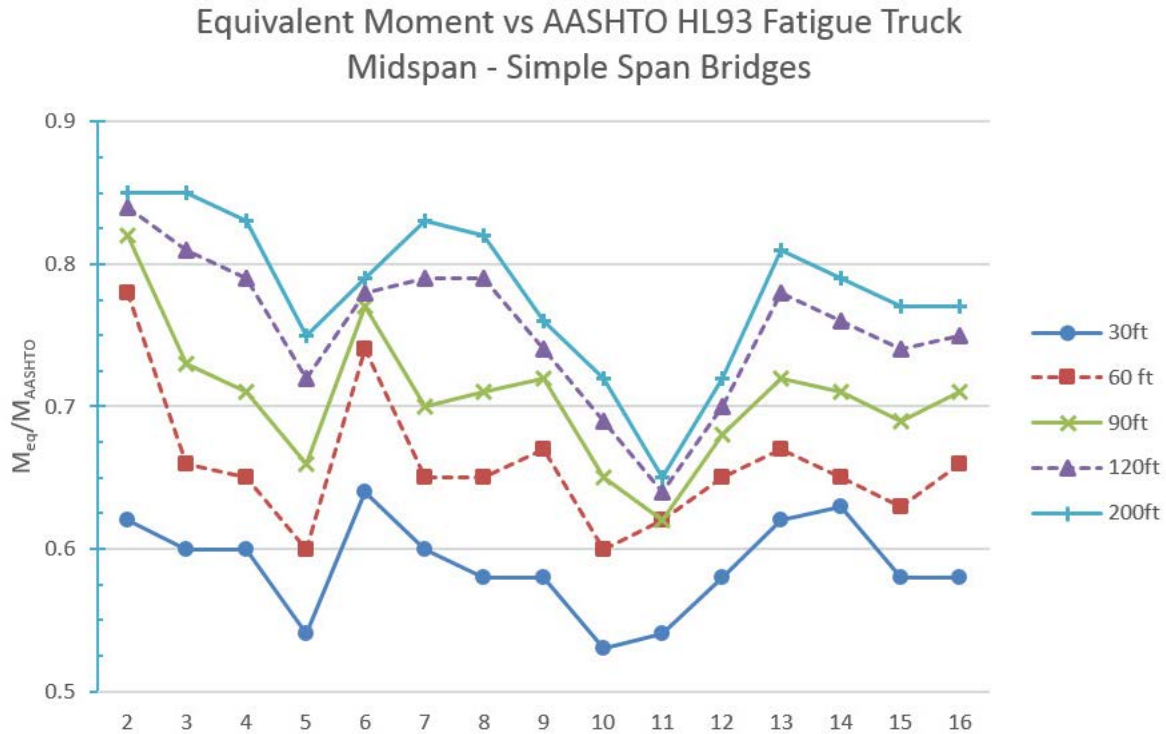


Figure A.3.2-5 Equivalent moment divided by AASHTO fatigue truck for 15 WIM sites.

The use of the equivalent moment was then extended to the computation of fatigue damage produced by the equivalent vehicles and that produced by the AASHTO vehicles as a means of also studying the influence of the cycles of loading term, n .

The boundary of actual fatigue damage is represented by the following equation:

$$\frac{M_{eq}}{S} = \sqrt[3]{\frac{A}{N_R}}$$

Equation A.3.2-2

Similarly, the boundary of code fatigue damage is represented by the following equation:

$$\frac{M}{S} = \sqrt[3]{\frac{A}{N}}$$

Equation A.3.2-3

where:

- M_{eq} = equivalent moment found by Miner's rule
- M = AASHTO fatigue truck moment
- A = AASHTO detail constant

- N_R = actual number of cycles
 N = AASHTO design number of cycles, $(365)(75)(n)(ADTT)_{SL}$, using the AASHTO “n” values

A parameter, λ , was developed to express the ratio of fatigue damage caused by the actual (WIM based) loads divided by the predicted damage caused by the AASHTO model.

$$\lambda = \sqrt[3]{\frac{N_R}{N} * \frac{M_{eq}}{M}}$$

Equation A.3.2-4

The ratio demonstrated that if the current AASHTO model is used, the damage was biased with shorter spans having less cumulative damage relative to the LRFD approach than longer spans. Although the short spans have a higher number of cycles than longer spans, the equivalent moments were also less than predicted by the standard AASHTO design vehicle. The bias in the λ values was proposed by the R19B researchers to be corrected by changing the cycles-per-passage approach and eliminating the under / over 40 foot span length distinction. The changes presented in Table A.3.2-4 were proposed to provide an equal bias to all span lengths and for simple and continuous span bridges.

Table A.3.2-4 Suggested cycles-per-passage factors.

Longitudinal Members		n
Simple span girders		1.0
Continuous girders	Near interior support	1.5
	Elsewhere	1.0

A.3.3 Selection of Fatigue Load Factors

Calibration of the Fatigue I load combination is based on continuing the philosophy that the limit state should have a probability of exceedance no more than 1:10,000. In terms of the bending moment (and hence stress) statistics, this exceedance can be determined by examining the cumulative distribution functions (CDF's) for a data set. The R19B report presents an example of the use of the CDF's to determine the 1:10,000 exceedance moment (see Figure A.3.3-1). For this particular WIM site, the simulated truck moments for 1:10,000 exceedance criteria are approximately 2,500 kip-ft. This exceedance moment was compared to the AASHTO design truck moments to normalize them for various bridges.

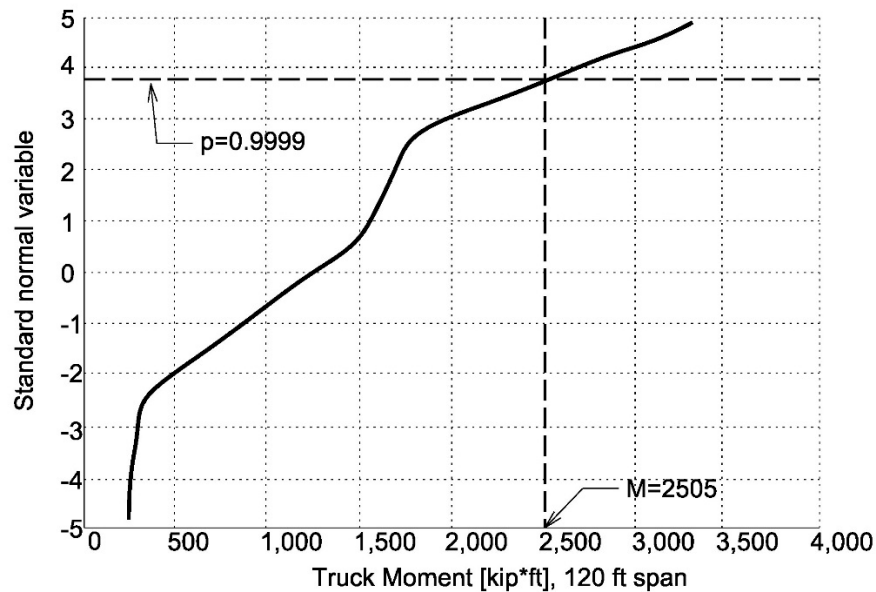


Figure A.3.3-1 1:10,000 probability of exceedance moments from a single WIM site.

The CDF's for the maximum moment ratios (Fatigue I) and the cumulative damage ratios (Fatigue II) were plotted and analyzed in order to calibrate the load factors for the fatigue load combinations (see Figure A.3.3-2 and Figure A.3.3-3). A straight line corresponding to a normal distribution was superimposed on the data plots, and from this, the mean, standard deviation, and variance were determined so that load factors could be determined. The research team determined that, for design, the mean design load should be taken as equal to the mean of the WIM data plus 1.5 standard deviations (i.e., $\mu+1.5\sigma$), which corresponds to a mean design value with an approximate 5 percent probability of exceedance.

Using the $\mu+1.5\sigma$ design mean to set the load factors, the range of load factors for the Fatigue I load combination was found to be between approximately 1.6 and 2.5. The R19B researchers recommended a value of 2.0 for the Fatigue I load combination. This was a change from the AASHTO value at the time of the research of 1.5. For the Fatigue II load combination, the range of calibrated load factors was found to be between approximately 0.75 and 0.87. The R19B researchers recommended a value of 0.8. This was a change from the AASHTO value at the time of the research of 0.75. Subsequent to the publication of the R19B report, and at the request of the AASHTO T14 Subcommittee, members of the R19B research team examined the statistical data for the Fatigue I load combination again, since this large change from 1.5 to 2.0 was perceived to be a major change for the fatigue design of steel bridges and one that could negatively impact the assessment of newer steel bridges designed using the previous 1.5 load factors. In August 2015, the R19B team presented revised recommendations to AASHTO to change the Fatigue I load factor to 1.75 while maintaining the recommended 0.8 value for the Fatigue II load combination. These changes were subsequently adopted by AASHTO.

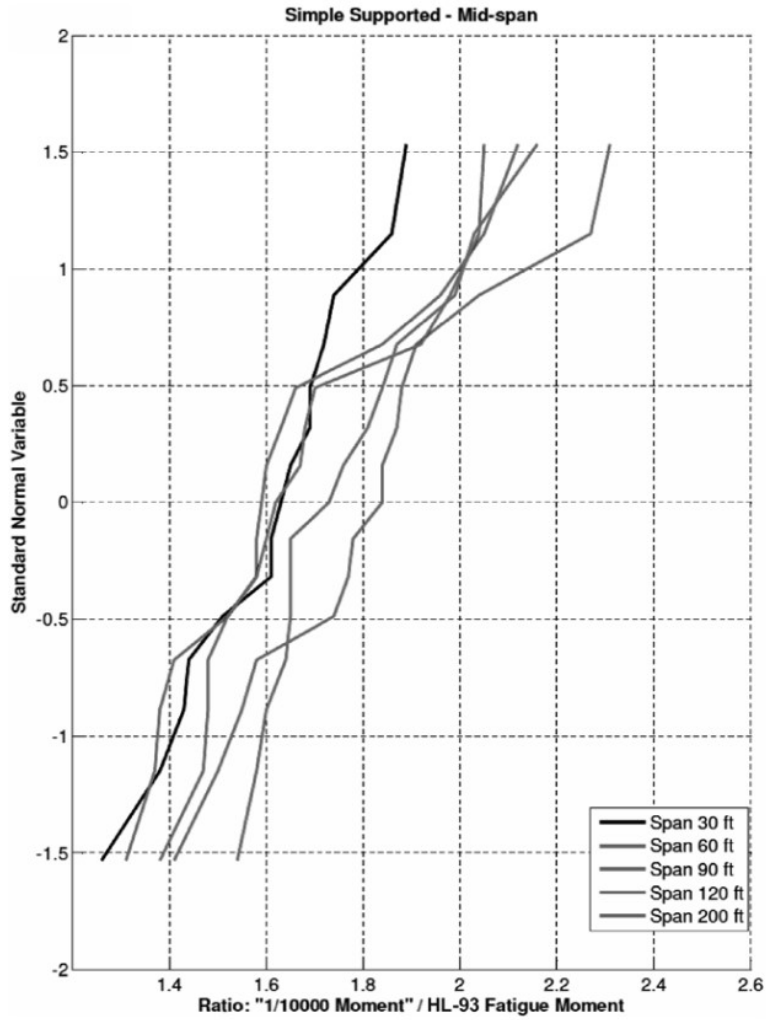


Figure A.3.3-2 Load factor versus standard normal variable curves for Fatigue I, simple span bridges.

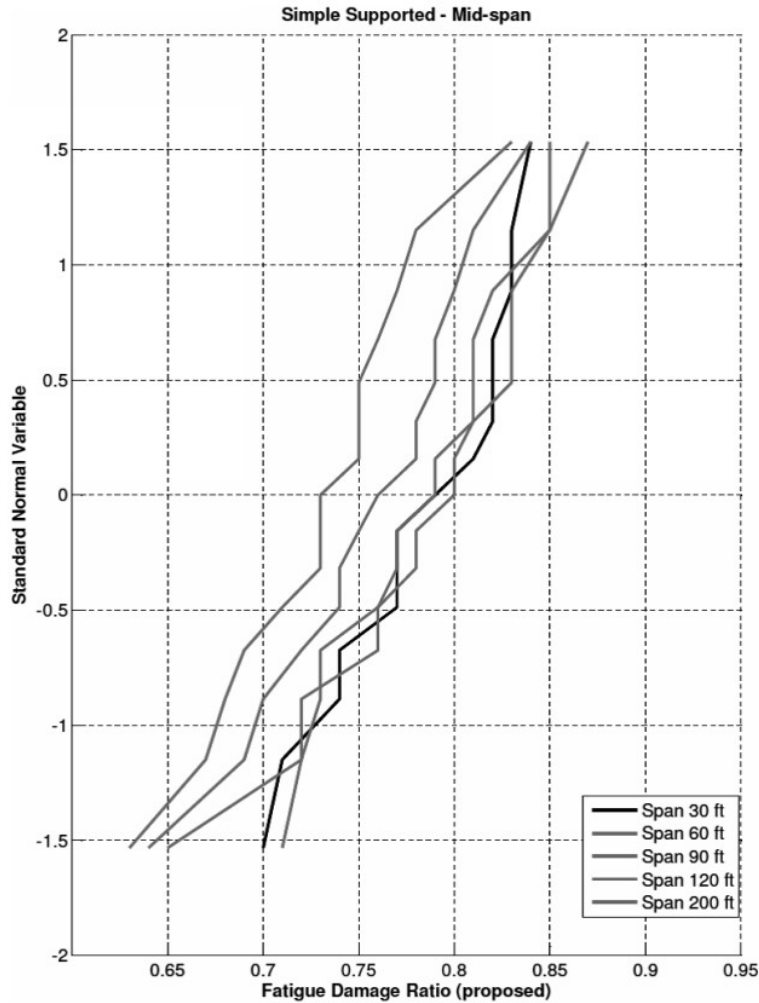


Figure A.3.3-3 Load factor versus standard normal variable curves for Fatigue II, simple span bridges.

SECTION A.4 CALIBRATION OF THE FATIGUE LIMIT STATE

In order to calibrate a limit state, the uncertainties on both the load and resistance side must first be quantified. Trial load factors were chosen as described previously. Calibration also requires characterization of the uncertainty of resistance as well as testing the trial load and resistance factors to determine if they provide the required degree of safety. The researchers made use of existing test data that have been used to develop the S-N curves found in the *AASHTO LRFD* specifications. These S-N curves, which follow a log-log relationship, or in exponential form as $N = AS_R^{-B}$, present a relationship between stress range and fatigue life in the finite life region. The regression analysis found values clustered around 3 for the term “*B*” in the exponential equation, so a coefficient of 3 was imposed for design purposes.

Similar to the approach taken in the investigation of load factors, the investigation of resistance required that the statistical parameters of the fatigue life test data be determined. For each of the eight detail categories in the *AASHTO LRFD* specifications, the available test data were plotted,

and the mean, standard deviation, and variance were computed. Having thus established the statistical characteristics of the resistance data and having previously chosen trial load factors, the research team performed a reliability analysis using a Monte Carlo simulation to verify the chosen load and resistance factors that would achieve a reliability close to the target value.

Selection of the target reliability index was performed by first determining the current reliability index for the Fatigue I and Fatigue II load combinations. The reliability index, called β , for the Fatigue I load combination varies from 0.9 for Category E to 2.0 for Category D. Both of these values are the extreme reliability indices. The other reliability indices lie between 1.1 and 1.5. For the Fatigue II load combination, the reliability index is in the range of 0.9 to 1.3, with extreme values of 0.7 for Category E and 1.4 for Category E'. The researchers settled on a proposed target reliability index, β , of 1.0, not unlike the existing level of reliability. Using the proposed load factors, the statistical characteristics of the resistance data, and an inherent resistance factor of 1.0, they computed β for the various AASHTO detail categories. The β for both the Fatigue I and Fatigue II load combinations vary from 0.9 to 1.2 and are tightly clustered around the target value of 1.0. This validates that the load factors chosen and the inherent resistance factor of 1.0, along with the suggested changes in the number of cycles to failure included in the finite life assessment, will produce the desired reliability.

A β of 1 suggests an 84 percent confidence in predicting that the detail will survive at least as long as the required design life. This chosen value of β is not significantly different than that inherent in structures designed using *AASHTO LRFD*, and researchers did not feel that there was excessive risk or conservatism in these older designs. As a comparison, the reliability index, β , chosen for the calibration of the strength limit state was 3.5. This implies that a structure designed to satisfy the strength limit state has an approximate 1:10,000 probability that the strength of the structure will be exceeded over the life of the bridge.

This last step, validating that the calibrated β is consistent with the target β , validates that the chosen load and resistance factors result in the desired level of safety being achieved and the fatigue limit state is deemed to be calibrated. Other subtle changes to the fatigue specifications were suggested by the R19B team, such as some adjustments to the detail constants, A , and minor adjustments to the constant amplitude fatigue threshold (CAFT) for certain details. These possible changes have already been evaluated by AASHTO, and it was determined that they will not be included in any update to the *AASHTO LRFD* specifications at this time.

GLOSSARY

The following terms are commonly used when considering design and evaluation of steel bridges for fatigue and fracture. (Many of the definitions presented below are as per AASHTO or FHWA.)

AASHTO—American Association of State Highway and Transportation Officials. AASHTO sets standards and publishes specifications, test protocols, and guidelines which are used in highway and bridge design and construction throughout the United States.

ADTT—Average Daily Truck Traffic. This value is used to compute the number of stress cycles to which a detail is subjected.

AWS—American Welding Society. AWS seeks to advance the science, technology, and application of welding and allied joining and cutting processes.

Brittle—Structural behavior that leads to sudden loss of load-carrying capacity immediately when the elastic limit is exceeded.

CAFT—Constant amplitude fatigue threshold.

Charpy V-Notch Impact Requirement—The minimum energy required to be absorbed in a Charpy V-notch test conducted at a specified temperature.

Charpy V-Notch Test—An impact test complying with AASHTO T 243M/T 243 (ASTM A673/A673M).

Constant Amplitude Fatigue Threshold—The nominal stress range below which a particular detail can withstand an infinite number of repetitions without fatigue failure.

Constraint-Induced Fracture—A form of brittle fracture that can occur at details characterized by highly constrained joints without any perceptible fatigue crack growth and, more importantly, without any warning.

CVN—Charpy V-notch.

Cyclical Stress—Stress that is not constant but rather is applied in cycles due to repeated loading, unloading, and subsequent reloading.

Design Cycles—The number of cycles of stress range for which a bridge component is designed.

Detail Category—A grouping of components and details having essentially the same fatigue resistance.

Discontinuity—An internal defect that is not observable by visual inspection. Discontinuities can generally be described as either volumetric defects that are three-dimensional (e.g., slag

inclusions and porosity) or planar defects that are essentially two-dimensional (e.g., cracks or lack of fusion). Discontinuities are inevitable byproducts of steel-making but must be controlled.

Distortion-Induced Fatigue—Fatigue effects due to secondary stresses not normally quantified in the typical analysis and design of a bridge.

Ductile—Structural behavior characterized by significant inelastic deformations before any loss of load-carrying capacity occurs. Ductile behavior provides warning of structural failure by large inelastic deformations.

Effective Stress Range—The assumed constant amplitude stress range produced by the Fatigue II load combination and used to determine if adequate finite life is provided.

Effective Truck—An assumed effective or statistically average weight truck that produces the stresses calculated using the Fatigue II load combination.

Evaluation—An assessment of the performance of an existing bridge.

Evaluation Fatigue Life—A level of fatigue life specified by AASHTO which equals a conservative fatigue life for evaluation (greater than the minimum fatigue life but less than the mean fatigue life).

Fatigue—The initiation and/or propagation of cracks due to a repeated variation of normal stress with a tensile component.

Fatigue Design Life—The number of years that a detail is expected to resist the assumed traffic loads without fatigue cracking. In the development of the *AASHTO LRFD Bridge Design Specifications*, it has been taken as 75 years.

Fatigue I Load Combination—A fatigue and fracture load combination related to infinite load-induced fatigue life.

Fatigue II Load Combination—A fatigue and fracture load combination related to finite load-induced fatigue life.

Fatigue Life—The number of repeated stress cycles that results in fatigue failure of a detail.

Fatigue Resistance—The maximum stress range that can be sustained without failure of the detail for a specified number of cycles.

FCM—Fracture-critical member.

FHWA—Federal Highway Administration. FHWA is an agency within the U.S. Department of Transportation that supports State and local governments in the design, construction, and maintenance of the Nation's highway system and various federally and tribal owned lands.

Finite Fatigue Life—The number of cycles to failure of a detail when the maximum probable stress range exceeds the constant amplitude fatigue threshold.

Fitness-for-Service Analysis—A quantitative engineering evaluation that is performed to demonstrate the structural integrity of an in-service component that may contain a flaw or damage.

Fracture—Rupture in tension or rapid extension of the fatigue crack, leading to gross deformation, loss of function or serviceability, or complete separation of the component.

Fracture Control Plan—A plan for non-redundant structures intended to provide a higher level of safety based on specific requirements for control of cracks (through detailing and enhanced fabrication inspection protocols) and specification of minimum material properties for steel and weld metal measured by CVN testing.

Fracture Critical Inspection—A FCM inspection must be at least a hands-on inspection of the fracture critical member or member component. The term hands-on means that the inspector must be close enough to place their hands on the fracture critical member or member component (tension area) being inspected. The inspection may also include non-destructive evaluation or non-destructive testing methods as determined by the Program Manager and outlined in the FCM inspection procedures.

Fracture-Critical Member—A steel primary member or portion thereof subject to tension whose failure would probably cause a portion of or the entire bridge to collapse.

Fracture Mechanics—The field of mechanics concerned with the study of the propagation of cracks in materials. It uses methods of analytical solid mechanics to calculate the driving force on a crack and those of experimental solid mechanics to characterize the material's resistance to fracture.

Fracture Toughness—A measure of the ability of a structural material or element to absorb energy without fracture. It is generally determined by the Charpy V-notch test.

Heat Straightening—A repair technique applied to bends and distortions in steel elements in order to restore them to their original shape.

Infinite Fatigue Life—The condition when the design stress range calculated using the Fatigue I load combination is less than the constant amplitude fatigue threshold.

Initiation—The portion of general crack growth in which existing discontinuities are sharpened into cracks.

Internal Redundancy—A form of redundancy that can be provided by built-up member detailing that provides mechanical separation of elements in an effort to limit fracture propagation across the entire member cross section. Internal redundancy is generally not considered for the purpose of identifying FCMs.

Limit State—A condition in which a component or structure becomes unfit for service and is judged either to be no longer useful for its intended function or to be unsafe. Limits of structural usefulness include brittle fracture and fatigue.

Load-Induced Fatigue—Fatigue effects due to the in-plane stresses for which components and details are explicitly designed.

Load Path Redundancy—A form of redundancy that is based on the number of main supporting members between points of support, usually parallel, such as girders or trusses. For the purpose of identifying FCMs, redundancy has been defined primarily based on conservative consideration of load path redundancy alone.

Maximum Stress Range—The assumed constant amplitude stress range produced by the Fatigue I load combination and used to determine if infinite life is provided.

Maximum Truck—An assumed maximum weight truck that produces the stresses calculated using the Fatigue I load combination.

Mean Fatigue Life—A level of fatigue life specified by AASHTO which equals the most likely fatigue life.

Minimum Fatigue Life—A level of fatigue life specified by AASHTO which equals the conservative design fatigue life.

National Bridge Inspection Standards—Federal regulations establishing requirements for inspection procedures, frequency of inspections, a bridge inspection organization, qualifications of personnel, inspection reports, and preparation and maintenance of bridge inventory records. The NBIS apply to all structures defined as highway bridges located on or over all public roads.

NBIS—National Bridge Inspection Standards.

Negative Remaining Life—The condition in which the calculated remaining fatigue life is determined to be negative, suggesting that the detail should have already cracked when it has not.

Nominal Resistance—Resistance of a component or connection to load effects, based on its geometry, permissible stresses, or specified strength of materials.

Out-of-Plane Distortion—Distortion arising from secondary stresses induced in bridge girders from displacement compatibility between the girders and the bracing elements.

Propagation—The portion of general crack growth that represents steady-state fatigue cracking that may occur when stresses above the threshold are applied.

Rain Flow Counting—A method of analysis of fatigue data used to reduce a spectrum of varying stress into a set of simple stress reversals.

Redundancy—The quality of a bridge that enables it to perform its design function in a damaged state.

Redundant Member—A member whose failure does not cause failure of the bridge.

Required Fatigue Life—A product of the single-lane average daily truck traffic, the number of cycles per truck passage, and the design life in days.

Residual Stress—The stresses that remain in an unloaded member or component after it has been formed into a finished product by cold bending, and/or cooling after rolling or welding.

Resistance Factor—A resistance multiplier accounting for the variability of material properties, structural dimensions and workmanship, and the uncertainty in the prediction of resistance.

Stress Concentration—A location in a bridge member where stress is concentrated. A steel member can fail, via a propagating crack, when a concentrated stress exceeds the material's resistance. Fatigue cracks generally begin at stress concentrations.

Stress Range—The algebraic difference between extreme stresses resulting from the passage of a load.

Structural Redundancy—A form of redundancy that can be provided by continuity in main members over interior supports or other three-dimensional mechanisms. Structural redundancy is generally not considered for the purpose of identifying FCMs.

System Redundant Members (SRM)—Members that are not designated as FCMs and do not necessarily require fracture critical inspection but that must be fabricated in accordance with AWS D1.5 Clause 12. The criteria, assumptions, and refined analysis used to determine the system redundancy condition must be retained to account for changes over the life of the structure.

Total Fracture Control Plan—A fracture control plan that incorporates specific fracture control requirements set forth by AASHTO, AWS, and FHWA.

Truncated Distribution—A conditional distribution used in statistics that results from restricting the domain of some other probability distribution. Truncated distribution can be used to estimate the fatigue life when the calculated remaining fatigue life is determined to be negative but no fatigue cracking is evident.

Web Gap—A small, unstiffened segment of a steel girder web created when a connection plate is not attached to the tension flange. Web gaps are often subjected to out-of-plane distortion when there is differential deflection between adjacent girders, leading to the creation of fatigue cracks.

This page intentionally left blank

REFERENCES

1. AASHTO. 1949. *Standard Specifications for Highway Bridges*, 5th Edition. Washington, DC: American Association of State Highway Officials.
2. AASHTO. 1957. *Standard Specifications for Highway Bridges*, 7th Edition. Washington, DC: American Association of State Highway Officials.
3. AASHTO. 1965. *Standard Specifications for Highway Bridges*, 9th Edition. Washington, DC: American Association of State Highway Officials.
4. AASHTO. 1969. *Standard Specifications for Highway Bridges*, 10th Edition. Washington, DC: American Association of State Highway Officials.
5. AASHTO. 1974a. *Standard Specifications for Highway Bridges*, 11th Edition (with Interim Specifications). Washington, DC: American Association of State Highway and Transportation Officials.
6. AASHTO. 1974b. *Standard Specifications for Welding of Structural Steel Highway Bridges*. Washington, DC: American Association of State Highway and Transportation Officials.
7. AASHTO. 1975. *Standard Specifications for Welding of Structural Steel Highway Bridges*. Washington, DC: American Association of State Highway and Transportation Officials.
8. AASHTO. 1978. *Guide Specifications for Fracture Critical Non-Redundant Steel Bridge Members*. Washington, DC: American Association of State Highway and Transportation Officials.
9. AASHTO. 1990. *Guide Specifications for Fatigue Evaluation of Existing Steel Bridges*. Washington, DC: American Association of State Highway and Transportation Officials.
10. AASHTO. 1994. *AASHTO LRFD Bridge Design Specifications*, 1st Edition. Washington, DC: American Association of State Highway and Transportation Officials.
11. AASHTO. 2015a. *AASHTO LRFD Bridge Construction Specifications*, 3rd Edition (with 2015 Interim Revisions). Washington, DC: American Association of State Highway and Transportation Officials.
12. AASHTO. 2015b. *AASHTO LRFD Bridge Design Specifications*, 7th Edition (with 2015 Interim Revisions). Washington, DC: American Association of State Highway and Transportation Officials.
13. AASHTO. 2015c. *LRFD Specifications for Structural Supports for Highway Signs, Luminaires, and Traffic Signals*, 1st Edition. Washington, DC: American Association of State Highway and Transportation Officials.

14. AASHTO. 2015d. *Manual for Bridge Evaluation*, 2nd Edition (with 2015 Interim Revisions). Washington, DC: American Association of State Highway and Transportation Officials.
15. AASHTO. 2015e. *Standard Specifications for Structural Supports for Highway Signs, Luminaires, and Traffic Signals*, 6th Edition (with 2015 Interim Revisions). Washington, DC: American Association of State Highway and Transportation Officials.
16. AASHTO/AWS. 1988. *Bridge Welding Code*. D1.5-88, Washington, DC: American Association of State Highway and Transportation Officials, and Miami, FL: American Welding Society.
17. AASHTO/AWS. 1995. *Bridge Welding Code*. D1.5-95, Washington, DC: American Association of State Highway and Transportation Officials, and Miami, FL: American Welding Society.
18. AASHTO/AWS. 2010. *Bridge Welding Code*, 6th Edition. D1.5M/D1.5, Washington, DC: American Association of State Highway and Transportation Officials, and Miami, FL: American Welding Society.
19. AISC. 2011. *AISC Certification Standard for Steel Bridge Fabricators*. Chicago: American Institute of Steel Construction.
20. Albrecht P., and A. Lenwari. 2008. "Fatigue Strength of Trolley Bridge Stringers Made of ASTM A7 Steel." *Journal of Bridge Engineering* 13, no. 1 (January).
21. Amorn, A., J. Bowers, A. Girgis, and M.K. Tadros. 2007. "Fatigue of Deformed Welded-Wire Reinforcement." *PCI Journal* 52, no. 1: 106-120.
22. API. 2007. *Fitness-For-Service*. API 579-1/ASME FFS-1, Washington, DC: American Petroleum Institute.
23. ASNT. 1966. *Recommended Practice No. SNT-TC-1A, Personnel Qualification and Certification in Nondestructive Testing*. Columbus, OH: American Society for Nondestructive Testing.
24. ASTM. 2012. "Standard Test Methods for Notched Bar Impact Testing of Metallic Materials." ASTM E23-12c, West Conshohocken, PA: ASTM International.
25. ASTM. 2013. "Standard Test Method for Measurement of Fracture Toughness." ASTM E1820-13, West Conshohocken, PA: ASTM International.
26. ASTM. 2014. "Standard Specification for General Requirements for Rolled Structural Steel Bars, Plates, Shapes, and Sheet Piling." ASTM A6 / A6M-14, West Conshohocken, PA: ASTM International.
27. ASTM. 2015. "Standard Specification for Anchor Bolts, Steel, 36, 55, and 105-ksi Yield Strength." ASTM F1554-07ae1, West Conshohocken, PA: ASTM International.

28. Avent, R.R., and D. Mukai. 1998. *Heat Straightening Repairs of Damaged Steel Bridges, A Technical Guide and Manual of Practice*. FHWA-IF-99-004, Washington, DC: Federal Highway Administration.
29. Avent, R.R., D.J. Mukai, and P.F. Robinson. 2000. "Effect of Heat Straightening on Material Properties of Steel." *Journal of Materials in Civil Engineering* 12, no. 3: 188-195.
30. AWS. 1936. *Specifications for Welded Highway and Railway Bridges, Design, Construction, and Repair*, 1st Edition. Miami, FL: American Welding Society.
31. AWS. 2010. *Structural Welding Code – Steel*. D1.1/D1.1M-10, Miami, FL: American Welding Society.
32. Barsom, J.M., and S.T. Rolfe. 1987. *Fracture and Fatigue Control in Structures*. Englewood Cliffs, NJ: Prentice-Hall, Inc.
33. Barsom, J.M., and S.T. Rolfe. 1999. *Fracture and Fatigue Control in Structures: Applications of Fracture Mechanics*, 3rd Edition. West Conshohocken, PA: American Society for Testing and Materials.
34. Bowman, M.D., G. Fu, Y.E. Zhou, R.J. Connor, and A.A. Godbole. 2012. *Fatigue Evaluation of Steel Bridges*. NCHRP Report 721, Washington, DC: Transportation Research Board.
35. Brahim, S. 2007. "Effect of Surface Processing Variables on Hydrogen Embrittlement of Steel Fasteners." Montreal, Canada: McGill University.
36. British Standards Institute. 1994. *Code of Practice for Fatigue Design and Assessment of Steel Structures* (BS 7608). London, UK: British Standards Institute.
37. British Standards Institute. 2015. *Guide to Methods for Assessing the Acceptability of Flaws in Metallic Structures* (BS 7910), 13th Edition. London, UK: British Standards Institute.
38. Broek, D. 1984. *Elementary Engineering Fracture Mechanics*. The Hague, Netherlands: Martinus Nijhoff.
39. Bureau of Bridges and Structures. 2012. *Sign Structures Manual*. Springfield, IL: Illinois Department of Transportation.
40. Chavel, B.W., and J.M. Yadlosky. 2011. *Framework for Improving Resilience of Bridge Design*. FHWA-IF-11-016, Washington, DC: Federal Highway Administration.
41. Code of Federal Regulation. 2013. 23 CFR 650C.
42. Connor, R., J. Fisher, W. Gatti, V. Gopalaratnam, B. Kozy, B. Leshko, D.L. McQuaid, R. Medlock, D. Mertz, T. Murphy, D. Paterson, O. Sorensen, and J. Yadlosky. 2012. *Manual*

- for Design, Construction, and Maintenance of Orthotropic Steel Deck Bridges*. FHWA-IF-12-027, Washington, DC: Federal Highway Administration.
43. Connor, R.J., and J.W. Fisher. 2006. "Identifying Effective and Ineffective Retrofits for Distortion Fatigue Cracking in Steel Bridges Using Field Instrumentation." *Journal of Bridge Engineering* 11, no. 6: 745–752.
 44. Connor, R.J., E.J. Kaufmann, J.W. Fisher, and W.J. Wright. 2007. "Prevention and Mitigation Strategies to Address Recent Brittle Fractures in Steel Bridges." *Journal of Bridge Engineering* 12, no. 2: 164-173.
 45. Connor, R.J., L. Digglemann, and R. Sherman. 2013. *Evaluation of Member and Load-Path Redundancy on the US-421 Bridge over the Ohio River*. FHWA-HRT-13-105, Washington, DC: Federal Highway Administration.
 46. Connor, R.J., M.J. Urban, and E.J. Kaufmann. 2008. *Heat-Straightening Repair of Damaged Steel Bridge Girders: Fatigue and Fracture Performance*. NCHRP Report 604, Washington, DC: Transportation Research Board.
 47. Connor, R.J., R. Dexter, and H. Mahmoud. 2005. *Inspection and Management of Bridges with Fracture-Critical Details*. NCHRP Synthesis 354, Washington, DC: Transportation Research Board.
 48. Daniels, J.H., and J.W. Fisher. 1968. *Fatigue Behavior of Continuous Composite Beams*. Fritz Engineering Laboratory Report 256, Bethlehem, PA: Lehigh University.
 49. Delong, D.T., and M.D. Bowman. 2010. *Fatigue Strength of Steel Bridge Members with Intersecting Welds*. FHWA/IN/JTRP-2009/19, Indianapolis, IN: Indiana Department of Transportation.
 50. Dexter, R.J., and J.M. Ocel. 2013. *Manual for Repair and Retrofit of Fatigue Cracks in Steel Bridges*. FHWA-IF-13-020, Washington, DC: Federal Highway Administration.
 51. Dexter, R.J., J.E. Tarquinio, and J.W. Fisher. 1994. "Application of Hot-Spot Stress Fatigue Analysis to Attachments on Flexible Plate." *Proceedings of the 13th International Conference on Offshore Mechanics and Arctic Engineering Conference*, Edited by Salama et al., 85-92.
 52. Dexter, R.J., M.J. Mutziger, and C.B. Osberg. 2002. *Performance Testing for Modular Bridge Joint Systems*. NCHRP Report 467, Washington, DC: Transportation Research Board.
 53. Dexter, R.J., R.J. Connor, and M.R. Kaczinski. 1997. *Fatigue Design of Modular Bridge Expansion Joints*. NCHRP Report 402, Washington, DC: Transportation Research Board.
 54. Dong, P., and J.K. Hong. 2006. "A Robust Structural Stress Parameter for Evaluation of Multiaxial Fatigue of Weldments." *Journal of ASTM International*. West Conshohocken, PA: ASTM International.

55. Dowling, N. 1972. "Fatigue Failure Predictions for Complicated Stress-Strain Histories." *Journal of Mechanics* 7, no. 1: 71-87.
56. Downing, S., and D. Socie. 1982. "Simple Rainflow Counting Algorithms." *International Journal of Fatigue* 4, no. 1: 31-40.
57. Ellis, R.M., R.J. Connor, M. Medhekar, D. MacLaggan, and M. Bialowas. 2013. "Investigation and Repair of the Diefenbaker Bridge Failure." *2013 Conference of the Transportation Association of Canada*. Winnipeg, Manitoba.
58. European Committee for Standardisation. 1992. "Eurocode 3: Design of Steel Structures." ENV 1993-1-1, Brussels, Belgium.
59. European Convention for Constructional Steelwork. 1985. "Recommendations for the Fatigue Design of Steel Structures." ECCS Technical Committee 6, Rotterdam, Netherlands.
60. FHWA. 2001. "Hoan Bridge Failure Investigation." memorandum issued July 10. Washington, DC: Federal Highway Administration.
61. FHWA. 2010. *Fracture Critical Inspection Techniques for Steel Bridges*. FHWA-NHI-10-014, Washington, DC: Federal Highway Administration.
62. FHWA. 2012a. *Bridge Inspector's Reference Manual*. Washington, DC: Federal Highway Administration.
63. FHWA. 2012b. "Clarification of Requirements for Fracture Critical Members." memorandum issued June 20. Washington, DC: Federal Highway Administration.
64. FHWA. 2012c. "Design for Fatigue." *Steel Bridge Design Handbook*. FHWA-IF-12-052, Vol. 12, Washington, DC: Federal Highway Administration.
65. FHWA. 2012d. "Safety Inspection of In-Service Bridges." FHWA-NHI-12-047, Washington, DC: Federal Highway Administration.
66. FHWA. 2013. *Manual for Repair and Retrofit of Fatigue Cracks in Steel Bridges*. FHWA-IF-13-020, Washington, DC: Federal Highway Administration.
67. Fish, P., C. Schroeder, R.J. Connor, and P. Sauser. 2015. *Fatigue and Fracture Library for the Inspection, Evaluation, and Repair of Vehicular Steel Bridges*. West Lafayette, IN: Purdue University.
68. Fisher, J.W. 1984. *Fatigue and Fracture of Steel Bridges: Case Studies*. New York: John Wiley & Sons.
69. Fisher, J.W., A. Nussbaumer, P.B. Keating, and B.T. Yen. 1993. *Resistance of Welded Details Under Variable Amplitude Long-Life Fatigue Loading*. NCHRP Report 354, Washington, DC: Transportation Research Board.

70. Fisher, J.W., A. Pense, J.D. Wood, J.H. Daniels, B.T. Yen, D.A. Thomas, H. Hausammann, W. Herbein, B. Somers, and H.T. Sutherland. 1980a. *An Evaluation of the Fracture of the I79 Back Channel Girder and the Electroslag Welds in the I79 Complex*. Fritz Engineering Laboratory Report 425-1(80), Bethlehem, PA: Lehigh University.
71. Fisher, J.W., B.M. Barthelemy, D.R. Mertz, and J.A. Edinger. 1980b. *Fatigue Behavior of Full-Scale Welded Bridge Attachments*. NCHRP Report 227, Washington, DC: Transportation Research Board.
72. Fisher, J.W., D.R. Mertz, and A. Zhong. 1983. *Steel Bridge Members Under Variable Amplitude Long Life Fatigue Loading*. NCHRP Report 267, Washington, DC: Transportation Research Board.
73. Fisher, J.W., E.J. Kaufmann, W. Wright, Z. Xi, H. Tjiang, B. Sivakumar, and W. Edberg. 2001. *Hoan Bridge Forensic Investigation Failure Analysis Final Report*. Madison, WI: Wisconsin Department of Transportation, and Washington, DC: Federal Highway Administration.
74. Fisher, J.W., G.L. Kulak, and I.F.C. Smith. 1998. *A Fatigue Primer for Structural Engineers*. Chicago: National Steel Bridge Alliance.
75. Fisher, J.W., K.H. Frank, M.A. Hirt, and B.M. McNamee. 1970. *Effect of Weldments on the Fatigue Strength of Steel Beams*. NCHRP Report 102, Washington, DC: Transportation Research Board.
76. Fisher, J.W., P.A. Albrecht, B.T. Yen, D.J. Klingerman, and B.M. McNamee. 1974. *Fatigue Strength of Steel Beams with Welded Stiffeners and Attachments*. NCHRP Report 147, Washington, DC: Transportation Research Board.
77. Frank, K.H. 1978. *Fatigue of Anchor Bolts*. FHWA/TX-78/05-172-2F, Austin, TX: Texas State Department of Highways and Public Transportation, Transportation Planning Division.
78. Garlich, M.J., and E.T. Thorkildsen. 2005. *Guidelines for the Installation, Inspection, Maintenance and Repair of Structural Supports for Highway Signs, Luminaires, and Traffic Signals*. FHWA-NHI 05-036, Washington, DC: Federal Highway Administration.
79. Griffith, A.A. 1921. "The Phenomena of Rupture and Flow in Solids." London: Phil. Trans. Royal Society (Series A) (221).
80. Hahin, C. 1994. *Effects of Corrosion and Fatigue on the Load Carrying Capacity of Structural and Reinforcing Steel*. Springfield, IL: Illinois Department of Transportation.
81. Hanson, J.M., N.F. Somes, T. Helgason, W.G. Corley, and E. Hognestad. 1976. *Fatigue Strength of High Yield Reinforcing Bars*. NCHRP Report 164, Washington, DC: Transportation Research Board.

82. Hartbower, C.E. 1978. *A Proposed Fracture Control Plan for New Bridges with Fracture Critical Members*. Structural Engineering Series No. 5 – Volume I, Washington, DC: Federal Highway Administration.
83. Heller, B.E. 2003. *Fatigue Response of Pretensioned Concrete Beams*. Austin, TX: University of Texas at Austin.
84. Hirt, M.A. 1971. *Effects of Weldments on the Fatigue Strength of Steel Beams*. Fritz Engineering Laboratory Report 325, Bethlehem, PA: Lehigh University.
85. Hobbacher, A. 2007. *Recommendations for Fatigue Design of Welded Joints and Components*. WRC Bulletin 520, Shaker Heights, OH: Welding Research Council.
86. IIW. 2007. *Recommendations for Fatigue Design of Welded Joints and Components*. IIW document XIII-2151-07 / XV-1254-07, Villepinte, France: International Institute of Welding.
87. Irwin, G.R., and R. de Wit. 1983. “A Summary of Fracture-Mechanics Concepts.” *J. Testing Evaluation* 11.
88. Kaczinski, M.R., R.J. Dexter, and J.P. Van Dien. 1998. *Fatigue Resistant Design of Cantilevered Signal, Sign and Light Supports*. NCHRP Report 412, Washington, DC: Transportation Research Board.
89. Kaufmann, E.J., R.J. Connor, and J.W. Fisher. 2004. *Failure Analysis of the US 422 Girder Fracture*. ATLSS Report No. 04-21, Bethlehem, PA: Lehigh University.
90. Keating, P.B., and J.W. Fisher. 1986. *Review of Fatigue Tests and Design Criteria on Welded Details*. Fritz Engineering Laboratory Report 488.1 (86), Bethlehem, PA: Lehigh University.
91. Keating, P.B., and L.C. Christian. 2012. *Effects of Bending and Heat on the Ductility and Fracture Toughness of Flange Plate*. FHWA/TX-10/0-4624-2, Austin, TX: Texas Department of Transportation.
92. Keating, P.B., J.M. Kulicki, D.R. Mertz, and C.R. Hess. 1990. *Economical and Fatigue Resistant Steel Bridge Details*. FHWA-HI-90-043, Washington, DC: Federal Highway Administration.
93. Kulak, G.L., J.W. Fisher, and J.H.A. Struik. 2001. *Guide to Design Criteria for Bolted and Riveted Joints*. Chicago: American Institute of Steel Construction.
94. Kulicki, J.M., Z. Prucz, C.M. Clancy, D.R. Mertz, and A.S. Nowak. 2007. *Updating the Calibration Report for the AASHTO LRFD Code*. NCHRP Report 20-07/186, Washington, DC: Transportation Research Board.
95. Lankford, J. 1985. “The Influence of Microstructure on the Growth of Small Fatigue Cracks.” *Fatigue Fracture Eng. Materials Struct.* 8.

96. Lovejoy, S. 2009. *A Fitness-for-Purpose Evaluation of Fracture Critical Electro-Slag Welds*. FHWA-OR-RD-09-13, Salem, OR: Oregon Department of Transportation.
97. Mahmoud, H.N., R.J. Connor, and J.W. Fisher. 2005. "Finite Element Investigation of the Fracture Potential of Highly Constrained Details in Steel Plate Members." *Computer-Aided Civil and Infrastructure Engineering* 20: 383-392.
98. Marshall, P.W. 1992. *Design of Welded Tubular Connections, Basis and Use of AWS Code Provisions*. Amsterdam, Netherlands: Elsevier Science Publications.
99. Miner, M.A. 1945. "Cumulative Damage in Fatigue." *Journal of Applied Mechanics* 67: A159-A164.
100. Modjeski and Masters. 2015. *Bridges for Service Life Beyond 100 Years: Service Limit State Design*. SHRP2 Report S2-R19B-RW-1, Washington, DC: Transportation Research Board.
101. Modjeski and Masters. 2016 (not yet published). *Manual of Refined Analysis*. Washington, DC: Federal Highway Administration.
102. Munse, W.H. 1964. *Fatigue of Welded Steel Structures*. New York: Welding Research Council.
103. Nowak, A.S. 1999. *Calibration of LRFD Bridge Design Code*. NCHRP Report 368, Washington, DC: Transportation Research Board.
104. NTSB. 1984. *Collapse of a Suspended Span of Route 95 Highway Bridge Over the Mianus River, Greenwich, Connecticut, June 28, 1983*. Report No. HAR-84/03, Washington, DC: National Transportation Safety Board.
105. Ovuoba, B., and G.S. Prinz. 2015. *On the Fatigue Capacity of Headed Shear Studs in Composite Bridge Girders*. Steel Structures Research Laboratory Report No. 2015-1, Fayetteville, AR: University of Arkansas.
106. Paris, P.C., M.P. Gomez, and W.E. Anderson. 1961. "A Rational Analytic Theory of Fatigue." *The Trend in Engineering* 13: 9-14.
107. Paulson, C., K.H. Frank, and J.E. Breen. 1983. *A Fatigue Study of Prestressing Strand*. FHWA/TX-82/54-300-1, Austin, TX: Texas State Department of Highways and Public Transportation, Transportation Planning Division.
108. Pellini, W.S. 1983. *Guidelines for Fracture-Safe and Fatigue-Reliable Design of Steel Structures*. Cambridge, UK: Welding Inst.
109. PTI. 2012. *Recommendations for Stay Cable Design, Testing, and Installation*. PTI DC45.1-12, Farmington Hills, MI: Post-Tensioning Institute.

110. Roark, R.J., W.C. Young, R.G. Budynas, and A.M. Sadegh. 2012. *Roark's Formulas for Stress and Strain*, 8th Edition. New York: McGraw-Hill.
111. Roberts, R., J.M. Barsom, S.T. Rolfe, and J.W. Fisher. 1977a. *Fracture Mechanics for Bridge Design*. FHWA-RD-78-68, Washington, DC: Federal Highway Administration.
112. Roberts, R., J.M. Barsom, S.T. Rolfe, and J.W. Fisher. 1977b. *Student Workbook – Fracture Mechanics for Bridge Design*. FHWA-RD-78-69, Washington, DC: Federal Highway Administration.
113. Roberts, R., J.W. Fisher, G.R. Irwin, K.D. Boyer, H. Hausammann, G.V. Krishna, V. Morf, and R.E. Slockbower. 1977c. *Determination of Tolerable Flaw Sizes in Full Size Welded Bridge Details*. FHWA-RD-77-170, Washington, DC: Federal Highway Administration.
114. Rolfe, S.T. 1983. “Fracture and Fatigue Control in Steel Structures.” *Eng. J. Am. Inst. Steel Constr.* 14.
115. Roy, S., R. Sause, J.W. Fisher, Y.C. Park, R.W. Thompson, E.J. Kaufmann, and B.T. Yen. 2009. “Cost-Effective Connection Details for Highway Sign, Luminaire and Traffic Signal Structures.” Bethlehem, PA: Lehigh University.
116. Shank, M.E. 1954. “A Critical Survey of Brittle Failure in Carbon Plate Steel Structures Other than Ships.” Washington, DC: National Research Council, Committee on Ship Structural Design.
117. Shank, M.E., ed. 1957. *Control of Steel Construction to Avoid Brittle Failure*. Shaker Heights, OH: Welding Research Council.
118. Signes, E.G. et al. 1967. “Factors Affecting the Fatigue Strength of Welded High Strength Steels.” *British Welding Journal* 14, no. 3.
119. Slutter, R.G., and J.W. Fisher. 1966. *Fatigue Strength of Shear Connectors*. Fritz Engineering Laboratory Report 316.2, Bethlehem, PA: Lehigh University.
120. Smith, R.A. 1978-79. “An Introduction to Fracture Mechanics for Engineers – Parts I, II, and III.” *International Journal of Materials in Engineering Applications* 1, nos. 2, 4, and 6.
121. Tada, H., P. Paris, and G. Irwin. 1985. *The Stress Analysis of Cracks Handbook*. St. Louis, MO: Paris Productions.
122. Tilly, G.P. 1979. “Fatigue of Steel Reinforcement Bars in Concrete: A Review.” *Fatigue and Fracture of Engineering Materials and Structures* 2, no. 3: 237-344.
123. Townsend, H.E. 1975. “Effect of Zinc Coatings on the Stress Corrosion Cracking and Hydrogen Embrittlement of Low-Alloy Steel.” *Metallurgical Transactions* 6A (April): 877-883.

124. Vecchio, R.S. 2006. "Condition Assessment of Steel Structures." *STRUCTURE magazine* (November): 52-56.
125. Wilson, W.M. 1940. *Design of Connection Angles for Stringers of Railway Bridges*. Urbana, IL: University of Illinois.
126. Wilson, W.M., and J.V. Coombe. 1939. *Fatigue Tests of Connection Angles*. Engineering Experiment Station Bulletin Series No. 317, Urbana, IL: University of Illinois.
127. Wiss, Janney, Elstner Associates, Inc. 2012. *Martin Olav Sabo Pedestrian Bridge Cable Diaphragm Plate Fracture Investigation*. Northbrook, IL.
128. Wöhler, A. 1870. "Über die Festigkeitsversuche mit Eisen and Stahl." *Zeitschrift für Bauwesen* 20.
129. Zhao, X.L. et al. 1999. *Design Guide for Circular and Rectangular Hollow Section Welded Joints under Fatigue Loading*. Edited by Comite International pour le Developpement et l'Etude de la Construction Tubulaire.

FIGURE AND TABLE CREDITS

- Figure 2.3-1 From *A Fatigue Primer for Structural Engineers*, by J.W. Fisher, G.L. Kulak, and I.F.C. Smith, 1998, Chicago, IL: National Steel Bridge Alliance. Copyright 1998 by the National Steel Bridge Alliance. Reprinted with permission.
- Figure 2.3.3-1 From *AASHTO LRFD Bridge Design Specifications*, 7th Edition (with 2015 Interim Revisions) (Figure 9.8.3.4.4-1), by the American Association of State Highway and Transportation Officials, 2015, Washington, DC: AASHTO. Copyright 2015 by AASHTO. Reprinted with permission.
- Figure 2.4.2-1 Adapted from *Fracture and Fatigue Control in Structures: Applications of Fracture Mechanics*, by J.M. Barsom and S.T. Rolfe, 1999, West Conshohocken, PA: American Society for Testing and Materials. Copyright 2008 by the American Society for Testing and Materials. Adapted with permission.
- Figure 3.2-1 From *A Fatigue Primer for Structural Engineers*, by J.W. Fisher, G.L. Kulak, and I.F.C. Smith, 1998, Chicago, IL: National Steel Bridge Alliance. Copyright 1998 by the National Steel Bridge Alliance. Reprinted with permission.
- Figure 3.2-2 From *A Fatigue Primer for Structural Engineers*, by J.W. Fisher, G.L. Kulak, and I.F.C. Smith, 1998, Chicago, IL: National Steel Bridge Alliance. Copyright 1998 by the National Steel Bridge Alliance. Reprinted with permission.
- Figure 4.2-2 From *Resistance of Welded Details Under Variable Amplitude Long-Life Fatigue Loading*, *NCHRP Report 354* (Figure 1), by J.W. Fisher, et. al., 1993, Washington, DC: Transportation Research Board. Copyright 1993 by the Transportation Research Board. Reprinted with permission.
- Figure 4.2.1-1 Adapted from *Effect of Weldments on the Fatigue Strength of Steel Beams*, *NCHRP Report 102* (Figure 33, pg. 25), by J.W. Fisher, et. al., 1970, Washington, DC: Transportation Research Board. Copyright 1970 by the Transportation Research Board. Adapted with permission.
- Figure 4.2.2-1 Adapted from *Effect of Weldments on the Fatigue Strength of Steel Beams*, *NCHRP Report 102* (Figure 36, pg. 28), by J.W. Fisher, et. al., 1970, Washington, DC: Transportation Research Board. Copyright 1970 by the Transportation Research Board. Adapted with permission.
- Figure 4.3.1-2 Adapted from “Fatigue Design: Its Past and What It Is Today” (PDF pg. 21), by John W. Fisher, Ph.D., [n.d.], (http://www.mceer.buffalo.edu/education/Bridge_Speaker_Series/2010-2011/presentations/Fisher_presentation.pdf). Copyright by John W. Fisher, Ph.D. Adapted with permission.
- Figure 4.3.1.1-1 From *Effects of Weldments on the Fatigue Strength of Steel Beams*, *Fritz Engineering Laboratory Report 325*, by M.A. Hirt, 1971, Bethlehem, PA: Fritz Engineering Laboratory, Lehigh University. Copyright 1971 by M.A. Hirt. Reprinted with permission.

- Figure 4.3.1.1-2 From *Effects of Weldments on the Fatigue Strength of Steel Beams*, Fritz Engineering Laboratory Report 325, by M.A. Hirt, 1971, Bethlehem, PA: Fritz Engineering Laboratory, Lehigh University. Copyright 1971 by M.A. Hirt. Reprinted with permission.
- Figure 4.4.1-1 From *A Fatigue Primer for Structural Engineers*, by J.W. Fisher, G.L. Kulak, and I.F.C. Smith, 1998, Chicago, IL: National Steel Bridge Alliance. Copyright 1998 by the National Steel Bridge Alliance. Reprinted with permission.
- Figure 4.4.2-3 From "Fatigue Strength of Trolley Bridge Stringers Made of ASTM A7 Steel," by P. Albrecht and A. Lenwari, 2008, *Journal of Bridge Engineering*, 13(1), p. 73. Copyright 2008 by the American Society of Civil Engineers. Reprinted with permission.
- Figure 5.3.1.1-1 From *AASHTO LRFD Bridge Design Specifications*, 7th Edition (with 2015 Interim Revisions) (Table 4.6.2.2.1-1), by the American Association of State Highway and Transportation Officials, 2015, Washington, DC: AASHTO. Copyright 2015 by AASHTO. Reprinted with permission.
- Figure 5.4.2.3-1 Adapted from *Recommendations for Fatigue Design of Welded Joints and Components*, by A. Hobbacher, 2007, Shaker Heights, OH: Welding Research Council. Copyright 2007 by the Welding Research Council. Adapted with permission.
- Figure 5.4.2.3-2 Adapted from *Recommendations for Fatigue Design of Welded Joints and Components*, by A. Hobbacher, 2007, Shaker Heights, OH: Welding Research Council. Copyright 2007 by the Welding Research Council. Adapted with permission.
- Table 5.4.2.3-1 Adapted from *Recommendations for Fatigue Design of Welded Joints and Components*, by A. Hobbacher, 2007, Shaker Heights, OH: Welding Research Council. Copyright 2007 by the Welding Research Council. Adapted with permission.
- Table 6.3.1.2-1 From *AASHTO LRFD Bridge Design Specifications*, 7th Edition (with 2015 Interim Revisions) (Table 6.6.1.2.3-1), by the American Association of State Highway and Transportation Officials, 2015, Washington, DC: AASHTO. Copyright 2015 by AASHTO. Reprinted with permission.
- Table 6.3.3.2-1 From *AASHTO LRFD Bridge Design Specifications*, 7th Edition (with 2015 Interim Revisions) (Table 6.6.1.2.5-3), by the American Association of State Highway and Transportation Officials, 2015, Washington, DC: AASHTO. Copyright 2015 by AASHTO. Reprinted with permission.
- Table 6.3.4.2-1 From *AASHTO LRFD Bridge Design Specifications*, 7th Edition (with 2015 Interim Revisions) (Table 6.6.1.2.5-1), by the American Association of State Highway and Transportation Officials, 2015, Washington, DC: AASHTO. Copyright 2015 by AASHTO. Reprinted with permission.
- Table 6.3.4.2-2 From *AASHTO LRFD Bridge Design Specifications*, 7th Edition (with 2015 Interim Revisions) (Table C3.6.1.4.2-1), by the American Association of State Highway and Transportation Officials, 2015, Washington, DC: AASHTO. Copyright 2015 by AASHTO. Reprinted with permission.

- Table 6.3.5.1-1 From *AASHTO LRFD Bridge Design Specifications*, 7th Edition (with 2015 Interim Revisions) (Table 6.6.1.2.5-2), by the American Association of State Highway and Transportation Officials, 2015, Washington, DC: AASHTO. Copyright 2015 by AASHTO. Reprinted with permission.
- Figure 6.3.6.3-1 From *On the Fatigue Capacity of Headed Shear Studs in Composite Bridge Girders* (Figure 1), by B. Ovuoba and G.S. Prinz, 2015, Fayetteville, AR: Steel Structures Research Laboratory, University of Arkansas. Copyright 2015 by the Steel Structures Research Laboratory, University of Arkansas. Reprinted with permission.
- Figure 6.3.6.3-2 From *On the Fatigue Capacity of Headed Shear Studs in Composite Bridge Girders* (Figure A-1), by B. Ovuoba and G.S. Prinz, 2015, Fayetteville, AR: Steel Structures Research Laboratory, University of Arkansas. Copyright 2015 by the Steel Structures Research Laboratory, University of Arkansas. Reprinted with permission.
- Figure 6.3.6.3-5 From *Fatigue Strength of Shear Connectors*, by R.G. Slutter and J.W. Fisher, 1966, Bethlehem, PA: Lehigh University. Copyright 1966 by J.W. Fisher. Reprinted with permission.
- Figure 6.3.6.4-1 From TechStar Inc., [n.d.], TechStar Inc.: Findlay, OH. Copyright by TechStar Inc. Reprinted with permission.
- Figure 6.3.6.4-2 Adapted from TechStar Inc., [n.d.], (<https://www.techstar-inc.com/projects/benicia-martinez/dscf0049.jpg>), TechStar Inc.: Findlay, OH. Copyright by TechStar Inc. Adapted with permission.
- Figure 6.3.6.5-4 From *AASHTO LRFD Bridge Design Specifications*, 7th Edition (with 2015 Interim Revisions) (Figure 3.6.1.4.1-1), by the American Association of State Highway and Transportation Officials, 2015, Washington, DC: AASHTO. Copyright 2015 by AASHTO. Reprinted with permission.
- Figure 6.3.6.6-3 From *Cost-Effective Connection Details for Highway Sign, Luminaire and Traffic Signal Structures*, by S. Roy, et. al., 2009, Bethlehem, PA: Lehigh University. Copyright 2009 by J.W. Fisher. Reprinted with permission.
- Figure 6.3.6.6-4 From *Cost-Effective Connection Details for Highway Sign, Luminaire and Traffic Signal Structures*, by S. Roy, et. al., 2009, Bethlehem, PA: Lehigh University. Copyright 2009 by J.W. Fisher. Reprinted with permission.
- Figure 6.3.6.6-5 From *Cost-Effective Connection Details for Highway Sign, Luminaire and Traffic Signal Structures*, by S. Roy, et. al., 2009, Bethlehem, PA: Lehigh University. Copyright 2009 by J.W. Fisher. Reprinted with permission.
- Figure 6.3.6.6-6 From *Sign Structures Manual (OS-A-1)*, by Bureau of Bridges and Structures, 2012, Springfield, IL: Illinois Department of Transportation. Copyright 2012 by the Illinois Department of Transportation. Reprinted with permission.
- Figure 6.3.6.6-7 From *Sign Structures Manual (OS-A-2 and OS4-A-2)*, by Bureau of Bridges and Structures, 2012, Springfield, IL: Illinois Department of Transportation. Copyright 2012 by the Illinois Department of Transportation. Reprinted with permission.

- Table 7.2.3-1 Adapted from *AASHTO LRFD Bridge Design Specifications*, 7th Edition (with 2015 Interim Revisions) (Table 6.4.1-1), by the American Association of State Highway and Transportation Officials, 2015, Washington, DC: AASHTO. Copyright 2015 by AASHTO. Adapted with permission.
- Table 7.2.3-2 Adapted from *AASHTO LRFD Bridge Design Specifications*, 7th Edition (with 2015 Interim Revisions) (Table 6.6.2-2), by the American Association of State Highway and Transportation Officials, 2015, Washington, DC: AASHTO. Copyright 2015 by AASHTO. Adapted with permission.
- Table 7.2.3-3 Adapted from *AASHTO LRFD Bridge Design Specifications*, 7th Edition (with 2015 Interim Revisions) (Table 6.6.2-1), by the American Association of State Highway and Transportation Officials, 2015, Washington, DC: AASHTO. Copyright 2015 by AASHTO. Adapted with permission.
- Figure 7.2.4.1-5 From Robert Connor, Ph.D., [n.d.], Copyright by Robert Connor, Ph.D. Reprinted with permission.
- Figure 7.2.4.1-6 From “Investigation and Repair of the Diefenbaker Bridge Failure” by R.M. Ellis, 2013, *2013 Conference of the Transportation Association of Canada*. Copyright 2013 by the Transportation Association of Canada. Reprinted with Permission.
- Table 8.2.1.1-1 From *Manual for Bridge Evaluation*, 2nd Edition (with 2015 Interim Revisions) (Table 7.2.2.1-1), by the American Association of State Highway and Transportation Officials, 2015, Washington, DC: AASHTO. Copyright 2015 by AASHTO. Reprinted with permission.
- Table 8.2.1.2-1 Adapted from *Fatigue Evaluation of Steel Bridges, NCHRP Report 721* (pgs. E-4, E-23), by M.D. Bowman, et. al., 2012, Washington, DC: Transportation Research Board. Copyright 2012 by the National Academies Press. Adapted with permission.
- Table 8.3.2-1 From *Manual for Bridge Evaluation*, 2nd Edition (with 2015 Interim Revisions) (Table 7.2.5.1-1), by the American Association of State Highway and Transportation Officials, 2015, Washington, DC: AASHTO. Copyright 2015 by AASHTO. Reprinted with permission.
- Table 8.4.2-1 From *Manual for Bridge Evaluation*, 2nd Edition (with 2015 Interim Revisions) (Table 7.2.6.1-1), by the American Association of State Highway and Transportation Officials, 2015, Washington, DC: AASHTO. Copyright 2015 by AASHTO. Reprinted with permission.
- Table 8.4.2-2 From *Manual for Bridge Evaluation*, 2nd Edition (with 2015 Interim Revisions) (Table 7.2.6.1-2), by the American Association of State Highway and Transportation Officials, 2015, Washington, DC: AASHTO. Copyright 2015 by AASHTO. Reprinted with permission.
- Table 8.4.2-3 From *Manual for Bridge Evaluation*, 2nd Edition (with 2015 Interim Revisions) (Table 7.2.6.1-3), by the American Association of State Highway and Transportation Officials, 2015, Washington, DC: AASHTO. Copyright 2015 by AASHTO. Reprinted with permission.
- Table 8.4.2-4 Adapted from *Fatigue Evaluation of Steel Bridges, NCHRP Report 721* (Table 13, pg. 35), by M.D. Bowman, et. al., 2012, Washington, DC:

- Transportation Research Board. Copyright 2012 by the National Academies Press. Adapted with permission.
- Figure 8.4.3.2.3-1 Adapted from *Fatigue Evaluation of Steel Bridges, NCHRP Report 721* (Figure C7.2.7.2.3-1, pgs. E-15, E-30), by M.D. Bowman, et. al., 2012, Washington, DC: Transportation Research Board. Copyright 2012 by the National Academies Press. Adapted with permission.
- Figure 8.4.3.2.3-2 From *Fatigue Evaluation of Steel Bridges, NCHRP Report 721* (Figure C7.2.7.2.3-1, pgs. E-15, E-30), by M.D. Bowman, et. al., 2012, Washington, DC: Transportation Research Board. Copyright 2012 by the National Academies Press. Reprinted with permission.
- Figure 10.1.2-2 Adapted from *Guide to Design Criteria for Bolted and Riveted Joints* (Figure 5.46), by Kulak, G.L., J.W. Fisher, and J.H.A. Struik, 2001. Chicago: American Institute of Steel Construction. Copyright 2001 by the Research Council on Structural Connections. Adapted with permission.
- Figure 10.1.4-1 From *Steel Design Guide 17: High Strength Bolts, a Primer for Structural Engineers* (Figure 7.1), by the American Institute of Steel Construction, 2002. Chicago: American Institute of Steel Construction. Copyright 2002 by the American Institute of Steel Construction. Reprinted with permission.
- Figure 10.2.1-3 Adapted from *A Fatigue Primer for Structural Engineers*, by J.W. Fisher, G.L. Kulak, and I.F.C. Smith, 1998, Chicago, IL: National Steel Bridge Alliance. Copyright 1998 by the National Steel Bridge Alliance. Adapted with permission.
- Figure 10.3.2-1 From *A Fatigue Study of Prestressing Strand*, by C. Paulson, K.H. Frank, and J.E. Breen, 1983, Austin, TX: Texas State Department of Highways and Public Transportation, Transportation Planning Division. Copyright 1983 by the Texas Department of Transportation. Reprinted with permission.
- Figure 10.3.3-2 From DYWIDAG-Systems International USA Inc., [n.d.], DYWIDAG-Systems International USA Inc.: Freedom, PA. Copyright by DYWIDAG-Systems International USA Inc. Reprinted with permission.
- Figure 10.3.4-1 From *Recommendations for Stay Cable Design, Testing, and Installation. PTI DC45.1-12*, by the Post-Tensioning Institute, 2012, Farmington Hills, MI: Post-Tensioning Institute. Copyright 2012 by the Post-Tensioning Institute. Reprinted with permission.
- Figure A.3.1-1 From *Bridges for Service Life Beyond 100 Years: Service Limit State Design* (Figure 5.17), by Modjeski and Masters, 2015, Washington, DC: Transportation Research Board. Copyright 2015 by the National Academies Press. Reprinted with permission.
- Table A.3.2-1 Adapted from *AASHTO LRFD Bridge Design Specifications, 7th Edition* (with 2015 Interim Revisions) (Table 6.6.1.2.5-2), by the American Association of State Highway and Transportation Officials, 2015, Washington, DC: AASHTO. Copyright 2015 by AASHTO. Adapted with permission.
- Figure A.3.2-1 From *Bridges for Service Life Beyond 100 Years: Service Limit State Design* (Figure 5.26), by Modjeski and Masters, 2015, Washington, DC:

- Transportation Research Board. Copyright 2015 by the National Academies Press. Reprinted with permission.
- Figure A.3.2-2 From *Bridges for Service Life Beyond 100 Years: Service Limit State Design* (Figure 5.27), by Modjeski and Masters, 2015, Washington, DC: Transportation Research Board. Copyright 2015 by the National Academies Press. Reprinted with permission.
- Figure A.3.2-3 Adapted from *Bridges for Service Life Beyond 100 Years: Service Limit State Design* (Figure 5.30), by Modjeski and Masters, 2015, Washington, DC: Transportation Research Board. Copyright 2015 by the National Academies Press. Adapted with permission.
- Table A.3.2-2 Adapted from *Bridges for Service Life Beyond 100 Years: Service Limit State Design* (Table 5.17), by Modjeski and Masters, 2015, Washington, DC: Transportation Research Board. Copyright 2015 by the National Academies Press. Adapted with permission.
- Table A.3.2-3 Adapted from *Bridges for Service Life Beyond 100 Years: Service Limit State Design* (Table 5.18), by Modjeski and Masters, 2015, Washington, DC: Transportation Research Board. Copyright 2015 by the National Academies Press. Adapted with permission.
- Figure A.3.2-4 From *Bridges for Service Life Beyond 100 Years: Service Limit State Design* (Figure 5.33), by Modjeski and Masters, 2015, Washington, DC: Transportation Research Board. Copyright 2015 by the National Academies Press. Reprinted with permission.
- Figure A.3.2-5 Adapted from *Bridges for Service Life Beyond 100 Years: Service Limit State Design* (Table 5.22), by Modjeski and Masters, 2015, Washington, DC: Transportation Research Board. Copyright 2015 by the National Academies Press. Adapted with permission.
- Table A.3.2-4 Adapted from *Bridges for Service Life Beyond 100 Years: Service Limit State Design* (Table 6.6.1.2.5-2), by Modjeski and Masters, 2015, Washington, DC: Transportation Research Board. Copyright 2015 by the National Academies Press. Adapted with permission.
- Figure A.3.3-1 From *Bridges for Service Life Beyond 100 Years: Service Limit State Design* (Figure 5.35), by Modjeski and Masters, 2015, Washington, DC: Transportation Research Board. Copyright 2015 by the National Academies Press. Reprinted with permission.
- Figure A.3.3-2 From *Bridges for Service Life Beyond 100 Years: Service Limit State Design* (Figure 5.36), by Modjeski and Masters, 2015, Washington, DC: Transportation Research Board. Copyright 2015 by the National Academies Press. Reprinted with permission.
- Figure A.3.3-3 Adapted from *Bridges for Service Life Beyond 100 Years: Service Limit State Design* (Figure 5.37), by Modjeski and Masters, 2015, Washington, DC: Transportation Research Board. Copyright 2015 by the National Academies Press. Adapted with permission.